

**Shape and growth of InAs quantum dots
on high-index GaAs(113)A, B and
GaAs(2 5 11)A, B substrates**

von

Dipl.-Phys. Yevgeniy Temko
aus Dniepropetrovsk (Ukraine)

Von der Fakultät II – Mathematik und Naturwissenschaften
der Technischen Universität Berlin
zur Erlangung des akademischen Grades
Doktor der Naturwissenschaften
genehmigte Dissertation

Berlin 2004

D 83

Promotionsausschuss:

Vorsitzender: Prof. Dr. Peter Zimmermann

Berichter: Prof. Dr. Karl Jacobi

Prof. Dr. Mario Dähne

Tag der mündlichen Prüfung: 1. April 2004

Abstract

The present thesis has been devoted to the investigation of self-organised InAs quantum dots (QD) on four high-index substrates: GaAs(113)A, B and GaAs(2 5 11)A, B. The samples were prepared by molecular beam epitaxy, and characterised by *in situ* scanning tunneling microscopy (STM), electron diffraction and photoluminescence (PL).

The Stranski-Krastanow (SK) growth mode occurs on all investigated surfaces. The symmetry of the QDs derives from the bulk-truncated substrate that proves epitaxial growth during and after the SK transition. The QD ensembles on the B faces exhibit a narrower size distribution (SD) and larger density than those on respective A faces.

InAs QDs on GaAs(113)A are given by $\{110\}$, (111)A and $\{2\ 5\ 11\}$ A bounding facets and a rounded region due to a stacking of vicinal (001) surfaces. Later in the growth this shape alters by an elongation with a size reduction of the (111)A facet, induced by the flattening of the rounded region with $\{113\}$ B facets. An undulating morphology of the bare GaAs(113)A and of the wetting layer (WL) accounts for a broad QD SD and low density.

InAs QDs on GaAs(113)B evolve with a central steep part sitting on a flat base. The shape of the central part is given by $\{110\}$ and (111)B bounding facets, and a $(00\bar{1})$ rounded region. High-index $\{135\}$ B and (112)B facets are derived for the flat base. The flat morphology of bare GaAs(113)B is retained in the InAs WL. The QDs grow simultaneously with an equal rate everywhere that results in a narrow SD and high density.

A remarkable feature of GaAs(2 5 11)A is the formation of GaAs(011) step bunches found on nominal and vicinal substrates. STM images from vicinal GaAs(2 5 11)A reveal 3D InAs islands, sitting on the step bunches with a very broad SD, that is believed to be characteristic for incoherent islands. It is confirmed by a low PL emission intensity. On nominal GaAs(2 5 11)A, the islands grow with narrow and broad SD. The latter stem from the islands appearing on the (011) step bunches. The narrow SD is ascribed to the coherent QDs which exhibit the same shape as those on GaAs(113)A except for a missing mirror symmetry. However, the PL shows similar spectra for vicinal and nominal GaAs(2 5 11)A.

The GaAs(2 5 11)B surface, which structure has been determined in this thesis for the first time, yields a uniform InAs QD ensemble with a high density. The shape of the QDs is mainly the same as that on GaAs(113)B, except for the missing mirror symmetry. The QD PL peak exhibits similar intensity as reference InAs QDs on GaAs(001), but with smaller energy and linewidth, indicating a smaller sized and more uniform QD ensemble. A red shift of the emission energy has been achieved by using a modified preparation.

Kurzzusammenfassung

Die vorliegende Dissertation ist der Untersuchung der selbst-organisierten InAs Quantenpunkte (QD) auf vier Substraten, GaAs(113)A, B und GaAs(2 5 11)A, B, gewidmet. Die Proben wurden mit Molekularstrahlepitaxie präpariert, und mit *in situ* Rastertunnelmikroskopie (STM), Elektronenbeugung und Photolumineszenz (PL) untersucht.

Der Stranski-Krastanow Wachstumsmodus tritt auf allen untersuchten Oberflächen auf. Die Symmetrie der QDs ergibt sich durch die Symmetrie des Substrates und beweist damit das epitaktische Wachstum. Die QD Ensembles auf B Flächen zeigen schmalere Grössenverteilungen (GV) und grössere Inseldichten als die QDs auf A Flächen.

InAs QDs auf GaAs(113)A werden durch $\{110\}$, (111)A und $\{2\ 5\ 11\}$ A Facetten und einen gerundeten (001) Bereich begrenzt. Diese Form wird später durch eine Verlängerung unter Reduzierung der (111)A Facette, verändert. Dabei tritt eine Abflachung des gerundeten Bereichs durch $\{113\}$ B-Facetten auf. Die wellige Morphologie von GaAs(113)A und von der InAs-Benetzungsschicht (WL) erklärt die breite GV und niedrige QD Inseldichte.

InAs QDs auf GaAs(113)B wachsen mit einem steileren zentralen Teil, der auf einem flachen Sockel sitzt. Die Form des steilen Teils wird durch $\{110\}$ und (111)B Facetten und einen $(00\bar{1})$ -vizinalen Bereich gegeben. Die $\{135\}$ B- und (112)B-Facetten rahmen den flachen Sockel ein. Die flache Morphologie von GaAs(113)B bleibt in der InAs WL erhalten. Deshalb wachsen die QDs überall gleichzeitig und erbringen eine schmale GV und hohe Inseldichte.

GaAs(2 5 11)A wächst unter Bildung von (011) Stufenbündeln. Nach Aufbringen von InAs zeigen STM Bilder von vizinalen GaAs(2 5 11)A Oberflächen 3D Inseln, die genau auf den (011)-Stufenbündeln sitzen. Ihre sehr breite GV ist typisch für die inkohärente Inseln und wird durch eine niedrige PL Intensität bestätigt. Auf dem nominalen Substrat zeigt die GV einen schmalen und einen breiten Anteil. Der letztere stammt von den Inseln auf den Stufenbündeln. Der schmale Anteil wird den kohärenten QDs zugeschrieben, die nahezu die gleiche Form wie die QDs auf GaAs(113)A aufweisen. Jedoch zeigt die PL ähnliche Spektren für vizinale und nominale InAs/GaAs(2 5 11)A Systeme.

Die GaAs(2 5 11)B-Oberfläche, deren atomare Struktur zum ersten Mal in dieser Arbeit bestimmt wurde, ergibt ein homogenes InAs QD Ensemble mit einer hohen Inseldichte. Die Form der QDs ist dieselbe wie für die QDs auf der GaAs(113)B Oberfläche bis auf die fehlende Symmetrie. Die PL Spektren von InAs QDs auf GaAs(2 5 11)B und GaAs(001) weisen ähnliche Intensitäten aber kleinere Werte für Emissionsenergie und Linienbreite für GaAs(2 5 11)B auf. Eine Rotverschiebung der Emission wurde durch geänderte Wachstumsparameter erzielt.

Contents

1 Introduction	8
2 Background	
2.1 Electron counting rule.....	12
2.2 Atomic structure of low-index GaAs surfaces	13
2.3 Step bunching	15
2.4 Growth modes	17
2.5 Coherent and incoherent islands	19
2.6 Experimental setup	23
2.7 STM	25
2.8 Photoluminescence of InAs QDs.....	28
2.9 Sample preparation	29
3 InAs quantum dots on GaAs(113)A	
3.1 Introduction.....	32
3.2 Geometry of the bulk-truncated GaAs(113)A surface.....	32
3.3 The reconstructed GaAs(113)A surface: a literature survey.....	33
3.4 The reconstructed GaAs(113)A surface: our own results.....	36
3.5 InAs (or $\text{In}_x\text{Ga}_{1-x}\text{As}$) QDs on GaAs(113)A grown by MBE: a literature survey.....	41
3.6 InAs QDs on GaAs(113)A: our own results.....	43
3.7 Conclusion.....	52
4 InAs quantum dots on GaAs(113)B	
4.1 Introduction.....	54
4.2 The bare GaAs(113)B surface and InAs (or $\text{In}_x\text{Ga}_{1-x}\text{As}$) QDs on it: a literature survey...54	
4.3 Shape, size, and number density of InAs QDs on the GaAs(113)B surface at different temperatures: our own results.....	57
4.4 Conclusion	70
5 InAs quantum dots on vicinal and nominal GaAs(2 5 11)A	
5.1 Introduction.....	71
5.2 Surface structure of GaAs(2 5 11)A.....	71

5.3 Step structure on the 1° vicinal GaAs(2 5 11)A surface.....	82
5.3.1 Steps along $[3\bar{1}1]$	85
5.3.2 Steps along $[4\bar{5}\bar{3}]$	90
5.3.3 Steps along $[2\bar{3}1]$	92
5.4 InAs islands on 1° vicinal GaAs(2 5 11)A.....	97
5.5 InAs islands on nominal GaAs(2 5 11)A.....	105
5.6 Conclusion.....	113
6 InAs quantum dots on nominal GaAs(2 5 11)B	
6.1 Introduction.....	115
6.2 Surface and step structure of the bare GaAs(2 5 11)B surface.....	115
6.3 Structural properties of InAs QDs on GaAs(2 5 11)B.....	122
6.4 Optical properties of InAs QDs on GaAs(2 5 11)B.....	126
6.5 Conclusion.....	130
7 General conclusions	132
Appendix 1.1	136
Appendix 1.2	137
Appendix 1.3	137
Bibliography	138
Our own papers	149
Thanks to...	150
Curriculum vitae	151

List of used acronyms

AFM	atomic force microscopy
BEP	beam equivalent pressure
DB	dangling bond
DFT	density-functional theory
ECR	electron counting rule
FWHM	full width at half maximum
HREM	high-resolution electron microscopy
HRTEM	high-resolution transmission electron microscopy
IBA	ion bombardment and annealing
LEED	low-energy electron diffraction
MBE	molecular beam epitaxy
ML	monolayer
MOCVD	metal-organic chemical vapor deposition
MOVPE	metal organic vapor phase epitaxy
PL	photoluminescence
PLE	photoluminescence excitation
QD	quantum dot
QW	quantum well
QWR	quantum wire
RHEED	reflection high-energy electron diffraction
SEM	scanning electron microscopy
SK	Stranski-Krastanow
STM	scanning tunneling microscopy
TEM	transmission electron microscopy
UHV	ultra-high vacuum
WL	wetting layer
3D, 2D, 1D or 0D	three, two, one, or zero-dimensional.

1 Introduction

Our nowadays life cannot be imagined without semiconductor devices that have solidly come to it since the beginning of the 1970s. Among all these devices, the semiconductor heterostructures play an important role. They are used in the medicine, natural and material sciences. But also in everyday life we are surrounded from them, hearing the music, working with a computer or just collecting our goods from the supermarket strip after a saleslady has read off the bar codes.

The principal advantage of application of semiconductor heterostructures originates from a quantum size effect: One creates a physical object with a size below the de Broglie wavelength for an electron in one, two, or three directions. One embeds epitaxial this object made up from a semiconductor with a low band gap (e.g., InAs) in a semiconductor with a larger band gap (e.g., GaAs). This leads to an electronic localisation, or “confinement”, producing quantised energy levels in these directions. Furthermore, the reduction of the dimensionality of the electron gas modifies the density of the energy levels, which moves from the square-root function for the bulk material to the δ -like function for the object with completely confined electrons. If object dimensions are about 10 nm in all three directions, one gets in principle a big “artificial” atom with confined electrons, quantised energy spectra and infinitely sharp energy levels. One creates a new physical object among the semiconductor heterostructures that is called quantum dot (QD). The QDs are very promising for the production of laser diodes, single electron transistors, or cellular automata. Electrons, excited in the QD, can loose their energy through a recombination process with holes and can emit photons with only one certain energy. Particularly important is to use the QDs as active media in injection lasers emitting light with a wavelength range of 1.28-1.32 μm for datacom applications, where the optimum transparency window for glass fibers is reached [Gru02]. Currently, two approaches are competing to cover this and a longer wavelength range: InGaAsN quantum wells and InAs QDs embedded in a GaAs matrix. We are working on fundamental aspects in the latter field.

In order to prepare a very tiny QD, different techniques have been employed [see, e.g., Bim99 and references therein]. In principle the lithographic patterning [Sch86, For88] widely used in the semiconductor industry or etching of quantum well structures [For88] allow the fabrication of small nanostructures that can confine the carriers in all three dimensions. However, the utilisation of these complex methods yields highly damaged

QDs with low density and many defects, which are seen by a small value of integrated photoluminescence (PL) intensity. Nowadays, a self-organisation concept is mainly employed, where nature governs the QD formation by itself. Due to the mismatch in lattice constants of about 7 % between InAs and GaAs, the former grows epitaxial on GaAs substrates (wafers) via a Stranski-Krastanow (SK) growth mode [Str37]: Firstly the layer-by-layer mode is realised, and then after the deposition of a certain InAs amount three-dimensional (3D) InAs islands suddenly appear on top of the 2D InAs layer (=wetting layer (WL)). The size of the islands is fortunately exactly the one required for the QDs applications, with the large separation of quantised energy levels that are not populated by electrons at room temperature. After an overgrowth of these InAs islands with the GaAs material, they become completely embedded in the larger band gap GaAs matrix, and can be used for several types of devices.

It is known that the reconstruction and orientation of the substrate play a key role in InAs/GaAs heteroepitaxy: QDs form by means of the SK growth mode on GaAs(001) [Leo94, Bim99], GaAs(113)A, B [Hen97, For98], and GaAs(114)A, B [For98], whereas InAs grows in the 2D layer-by-layer growth mode with introduction of dislocations on GaAs(110) [Bel97], GaAs(111)A [Yam96] and GaAs($\bar{1}\bar{1}\bar{1}$)B [Hoo93]*. The differences in growth mode have not been explained yet. Presumably, the atomic reconstruction of different substrates provides different chemical potentials for the deposited species and affects the kinetics of adsorption, migration, and desorption, producing specific QD sizes and size distributions [Hen97, San00]. Furthermore, the substrate orientation may induce certain bonding facets on the QDs and therefore, determine their shape [Mar01, Suz02]. One of the main points of the present thesis is to compare the formation and development of InAs islands on substrates of different orientations. Since on the low-index substrates InAs QDs grow only on GaAs(001), we have employed high-index substrates for the comparison, which all yield QD ensembles after the SK transition. In this work we investigate the InAs deposition on GaAs(113)A, B and GaAs(2 5 11)A, B surfaces. Their reconstructions exhibit many differences, e.g., they are As or Ga terminated, have one or zero symmetry plane, flat or undulating morphology, etc., and therefore, allow an extraction of substrate features affecting the QD evolving.

* To simplify matters we will call in the following the ($\bar{1}\bar{1}\bar{1}$)B surface (and all others B faces) as (111)B without indication of bars over the Miller index.

Another very important point for application of QDs is their shape. It is known from quantum mechanics, that the position of energy levels and therefore, the optical parameters are largely dependent on the spatial geometry of the material, which confines the charge carriers. In order to understand the growth process in more detail and to design the shape and size of QDs, a direct imaging of their atomic structure is required. The structural characterisation is usually performed from buried QDs, as they are used in optical devices. For this purpose the semiconductor substrate is cleaved perpendicular to the epitaxial layers and then the cleavage surface is imaged by high-resolution electron microscopy (HREM) or cross-section scanning tunneling microscopy (XSTM) [see, e.g., Gru02 and references therein]. These powerful techniques have achieved many exciting results, however, they are either very complex (XSTM) or yield ambiguous QD shapes because of a superposition of the lattice plane images with local strain contrast (HREM). Our way of approaching this problem is to interrupt the preparation process on GaAs surfaces after the SK transition and to look at the unburied InAs QDs *in situ* by top-view STM. Using this technique the bounding facets can be identified from the atomically resolved reconstruction on the facets and their geometrical orientation. Although it is likely that the QD shape alters during following overgrowth, our approach delivers structural information on islands evolving in the first step of self-organisation, that largely influences QD shape, size and size distribution.

It has been reported already that on GaAs(001) the shape of the InAs QDs exhibits two mirror symmetry planes which are the same as on the bulk-truncated (001) substrate. From reflection high-energy electron diffraction (RHEED) observations, (136) facets were proposed earlier [Lee98]. Later four (137) bounding facets were derived from scanning tunneling microscopy (STM) [Mar01]. These facets, which frame nearly the whole QD, grow with equal rates because of the same reconstruction and elastic energy density. On high-index substrates the symmetry is lower and, e.g., GaAs{113} surfaces exhibit only one symmetry plane normal to the surface. Therefore, only two planes are expected with equivalent indices and growth rates. As two planes alone cannot frame a 3D islands, other surfaces with different growth rate may develop. Thus, preferential migration of In atoms among the different bounding facets from the slower to the faster growing facets should be taken into account in order to understand the QD growth kinetics.

In this work self-organised InAs QDs are grown by molecular beam epitaxy (MBE) on four high-index substrates: GaAs(113)A, B and GaAs(2 5 11)A, B. The two latter substrates have been employed for heteroepitaxy for the first time. The structural

parameters like shape, size, and size distribution of the QD are determined on all surfaces. The development of the unburied InAs islands has been followed by means of the top-view STM technique from the atomic structure of the bare substrate through the InAs WL stage to the determination of the facets of 3D islands.

The thesis is organised in the following manner: After a short description of theoretical and experimental basics of the QD growth and used instruments in chapter 2, each next chapter is devoted to one of four InAs/GaAs systems. In chapter 3 we consider the InAs QDs on GaAs(113)A, starting from the unusual substrate morphology that significantly influences the onset of the SK transition and therefore, the QD size distribution. The QDs are found to be in different growth stages. This allows us to retrace their growth kinetics from the small nuclei to the mature elongated islands. The opposite side of the same (113) wafer i.e., GaAs(113)B surface, remains flat until the SK transition, as described in chapter 4. The InAs QDs appear on it with a narrow size distribution that is quite different from the GaAs(113)A case. As they start to grow simultaneously on the whole GaAs(113)B surface, the different growth shapes are not observed. Since the InAs/GaAs(113)B system is interesting for applications, we also present experiments on the influence of the sample temperature on the QD size and shape. We have also used the stable GaAs(2 5 11)A and B substrates located within the stereographic triangle and, therefore, exhibiting no mirror symmetry. The InAs islands grown on vicinal and nominal GaAs(2 5 11)A surface are described in chapter 5. The surface exhibits well-pronounced step bunches that reveal fairly large areas of the GaAs(011) surface. The InAs islands appear mostly on these step bunches presumably with incorporation of dislocations and, therefore, with a very broad size distribution. The incoherent nature is confirmed with PL spectra, which exhibit very low integrated intensity of the islands in the QD energy range. Finally, the atomic structure of the GaAs(2 5 11)B substrate is determined for the first time in this thesis and described in chapter 6. After InAs deposition the surface yields an ensemble of InAs QDs with a narrow size distribution and a completely asymmetrical shape. The GaAs(2 5 11)B PL spectra are found to be mainly identical to those on GaAs(001) except for the smaller linewidth on GaAs(2 5 11)B. A small red shift of the emission energy can be achieved by using some special tricks. Finally, chapter 7 contains the general conclusions, where the common and different points of QD evolving are extracted.

2 Background

2.1 Electron counting rule

In order to understand the influence of the GaAs substrates on the structural and optical properties of InAs QDs it is useful to give the main concepts, associated with the structural changes when a substrate surface forms. Compound semiconductors such as GaAs or InAs have a crystal structure, which is similar to that of diamond. However, their lattice contains two different types of atoms. This structure is referred to as zinc blende lattice, named after the zinc blende (ZnS), and belongs to the face centered cubic (fcc) lattices. Each atom in GaAs crystal is tetrahedral surrounded from four atoms of the other type and has four covalent bonds with them. Ga exhibits three valence electrons and gives 3/4 of electron per bond; As exhibits five valence electrons (5/4 of electron per bond). Therefore, each of four bonds is filled with two electrons.

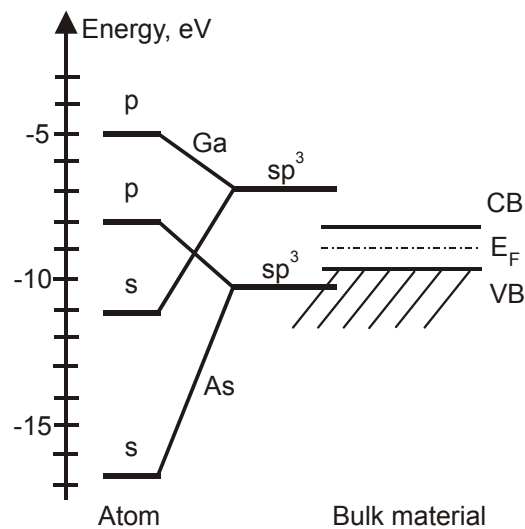


Figure 2.1 [Har79] The energy state diagram for a GaAs surface. The energy states for the sp^3 hybrids are derived from the energies of the s and p orbitals of Ga and As atoms. The dangling bond energies are above the conduction band (CB) minimum for Ga and below the valence band (VB) maximum for As.

The electronic states of As and Ga atoms become sp^3 hybridised in GaAs bulk material as shown in Fig. 2.1. Two hybridised orbitals, sp^3 from Ga and As atoms, combine to form bonding and antibonding orbitals, which are spread out to the conduction (CB) and valence

(VB) bands in the solid state GaAs. When a surface forms, some hybrid orbitals cannot form bonds. Without a reconstruction, partially filled sp^3 dangling bonds (DB) would remain on the surface. The energy states of the Ga and As DBs derived from the energies of the s and p atomic states are compared with the CB minimum and VB maximum in Fig. 2.1. A semiconductor exhibits a completely filled VB and an empty CB, and no states in-between. The energy state of the As DB is placed in the VB and should therefore be filled; that of the Ga DB is in the CB and should be empty. In order to achieve this, electrons should transfer from the Ga DBs to the As DBs. This is the principle of the electron-counting rule (ECR) [Har79, Pas89]. It requires that the number of available electrons in the surface states fill exactly all DB states in the VB, leaving those in the CB empty. If this condition is satisfied, the surface is semiconducting; otherwise, partially filled DBs may lead to a metallic surface. Note, that the ECR is just only a “rule” but not a law. The law is the minimisation of the surface free energy.

2.2 Atomic structure of low-index GaAs surfaces

We will now apply the ECR to some low-index surfaces, which reconstructions will appear on InAs QD facets, as described in chapters 3-6. Figure 2.2(a) shows a top and side view of the non-polar (110) cleavage plane of the GaAs crystal. It is the only one known GaAs surface, which reaches a new equilibrium low-energy configuration through a pure motion of atoms in the surface normal direction. This process is called surface relaxation [see, e.g., Duke96 and references therein]. The unit cell of GaAs(110) exhibits one As and one Ga DB. The Ga DB supplies $3/4$ of electron but needs zero electron (excess charge $+3/4$ el); the As DB supplies $5/4$ of electron, but needs $8/4$ (a charge deficit of $-3/4$ el). Therefore, the electrons from Ga DBs transfer to As DBs and the ECR is fulfilled. As a consequence, the Ga atoms adopt an sp^2 planar configuration and is moved onto the surface plane; the As atoms adopt an s^2p^3 configuration and expand out from the Ga atom by about 0.69 \AA as shown in Fig. 2.2(a). The length of the unit cell vectors for (110) is equal to 5.65 \AA (6.06 \AA) and 4.0 \AA (4.29 \AA) for GaAs (InAs) along $[001]$ and $[\bar{1}\bar{1}0]$ directions, respectively.

In contrast to GaAs(110), the GaAs $\{111\}$ surfaces are polar. A surface with threefold coordinated Ga atoms on top is assigned to (111)A; that with threefold coordinated As atoms is (111)B. On the A face only the Ga-vacancy-buckling model is found at both As and Ga-rich preparation conditions. It is shown in Fig. 2.2(b). The bulk-truncated unit cell,

marked by a dotted line, exhibits a rhombic shape with a vector length of 4.0 \AA (4.29 \AA) along $[0\bar{1}1]$ and $[1\bar{1}0]$ directions and comprises one single Ga DB, i.e., it violates the ECR and is unstable. A $(111)A$ - (2×2) unit cell [Ton84, Cha84] is four times larger and exhibits one missing Ga atom, which sets three As DBs free. This atomic rearrangement, that introduces a change in the surface periodicity with the simultaneous atom relaxation, is called surface reconstruction. The three As and Ga DBs yield charge neutrality and make the surface semiconducting. Note that the Ga atoms are moved onto the surface and the reconstruction reveals to be flat, see the side view in Fig. 2.2(b). The unit cell vectors of the $(111)A$ - (2×2) reconstruction are both equal to 8.0 \AA (8.58 \AA).

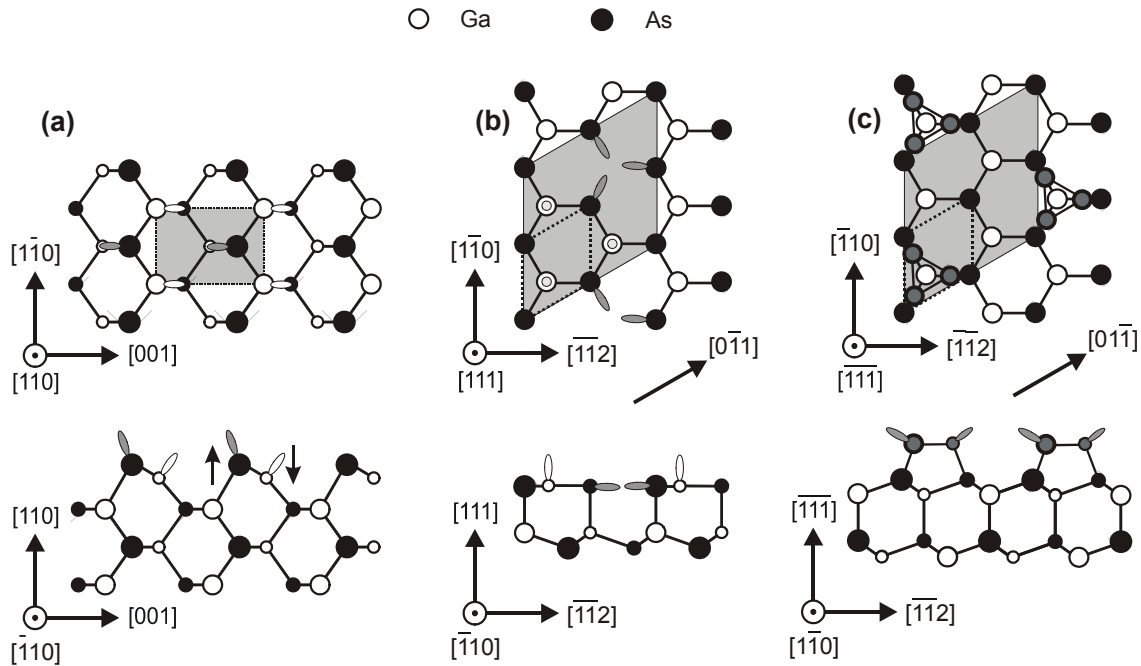


Figure 2.2 Top (above) and side (below) views of the structural models of reconstructed (relaxed) (a) $GaAs(110)$, (b) $GaAs(111)A$ and (c) $GaAs(111)B$ surfaces. Atoms below the figure plane are depicted with smaller circles. Shaded parallelograms and dotted lines mark the unit cells of the reconstructed (relaxed) and the bulk-truncated surfaces, respectively. The As DBs are depicted by gray (filled) ovals, those of Ga - by open (empty) ovals.

Two stable reconstructions are found on the $GaAs(111)B$ surface. At the As-rich conditions a (2×2) reconstruction occurs, consisting of As trimers as shown in Fig. 2.2(c) [Tho94, Set98]. Since the bulk-truncated surface is terminated by the threefold coordinated As atoms, which do not move onto the surface to get a planar configuration, the (2×2) reconstruction is more complex than that on $GaAs(111)A$. The unit cell of the reconstructed surface is four times as large as that of the bulk-truncated surface and

exhibits three adsorbed As atoms sitting on three As DBs underneath. The As atoms in the trimers are connected to each other. The GaAs(111)B - (2x2) unit cell exhibits 4 As DBs (-3 e) and 6 As-As bonds (each As-As bond requires two electrons, but supplies 10/4 of electrons, therefore 6 As-As bonds yield a excess charge of +3 e). Thus, the ECR is fulfilled. A ($\sqrt{19} - \sqrt{19}$) reconstruction develops on GaAs(111)B at the Ga-rich conditions [Ran77, Bie90]. This remarkable structure fails to fulfil the ECR, but nevertheless does appear not only on the nominal GaAs(111)B surface, but also on the facets on InAs QDs as we will show in chapter 3. The model for this complex reconstruction is given in [Bie90].

2.3 Step bunching

Growing crystal surfaces always exhibit atomic step systems or steps of multiple heights as a natural consequence of the growth process and an off-orientation of the surface that is never equal to zero. Schwoebel [Sch66] pointed out that the atomic steps on a surface might interact repulsively or attractively depending on the manner in which adsorbed atoms are captured at steps. A barrier might form at the step-edge on the GaAs surface, hindering either the As and Ga atoms from the lower terrace to attach at the step and making it easier for the atoms arriving from the upper terrace or vice versa. The former case corresponds to a negative Schwoebel barrier and is shown in Fig. 2.3. Let us assume a GaAs surface with a sinusoidally distributed atomic potential on upper and lower terraces (see Fig. 2.3(a)). This potential may be lowered at the step-edge due to, e.g., sp^2 planar relaxation of Ga atoms. It will result in the incorporation of the atoms at the step-edge from the upper terrace rather than from lower one. It results in the steps moving with different velocities over the surface: The steps on the larger terraces collect more atoms and move faster catching up the steps on the smaller ones. The morphology of such a surface consists of large extended terraces with multiatomic steps in-between. The effect of steps, bunching together in the multiatomic steps, is called step bunching.

Being a kind of step-flow growth, the step bunching requires a fulfillment of two conditions: the large diffusion length of the cations and the existence of the negative Schwoebel barrier at the step-edges. Since the diffusion length of Ga atoms by usual MBE conditions ($T=560\text{ }^\circ\text{C}$) is reported to be about $1\text{ }\mu\text{m}$ [Hat90], the steps should bunch on, e.g., GaAs(001) surface already at an off-orientation angle of 0.15° , which is close to a limit, provided by wafer manufacturers (0.1°). Therefore, the second condition is more important, and is dependent on the direction of the step, i.e., its atomic structure.

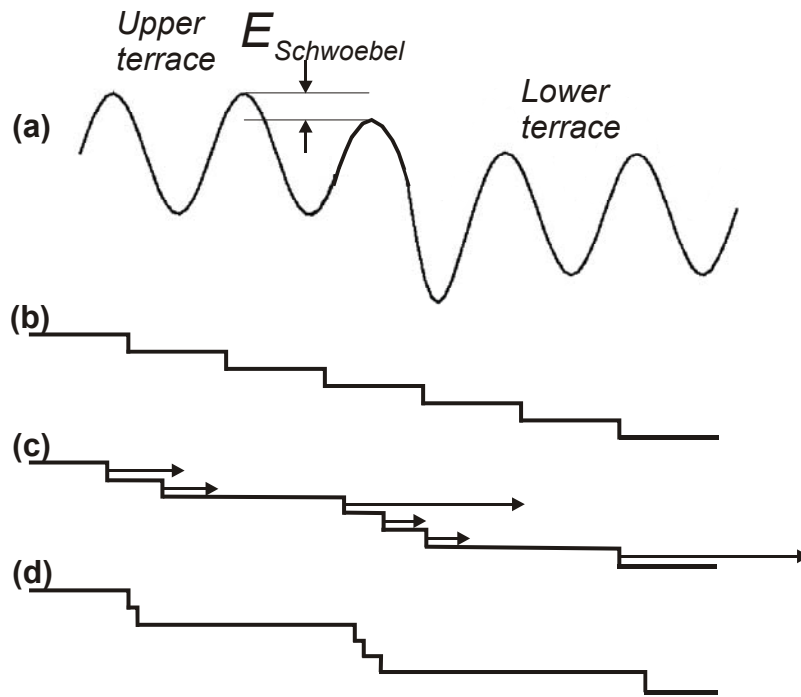


Figure 2.3 (a) The diffusion potential with a negative Schwoebel barrier at the step-edge between upper and low terraces. (b-d) The development of step bunching: (b) the initial surface before the growth process; (c) the fluctuations of the terrace width (the arrows show different growth velocities of the steps); (d) the formation of multiatomic steps.

Figure 2.3(b-d) shows schematically the development of the step bunching. The initial surface before the GaAs growth consists of equally spaced steps with a monatomic height, see Fig. 2.3(b). When the growth is initiated, small fluctuations of the terrace width may appear due to a random distribution of atoms. The larger terraces may now get more atoms which will result in a faster enlargement of the terraces, because the step velocity is proportional to the number of collected atoms, and thus to the terrace width, see Fig. 2.3(c). Finally, the steps of large terraces will catch up those of the small terraces, and will bunch together, producing multiatomic steps, see Fig. 2.3(d). Note, that the topography of the surfaces, on which steps are bunched, is usually similar to faceted surfaces [see, e.g., Noe94]. However the underlying mechanism is completely different. Step bunching is a result of anisotropic diffusion over the step-edges, while faceting is driven by differences of the surface free energies of the substrate and facets.

2.4 Growth modes

The QDs belong to semiconductor objects that are acquired by self-organisation through the heteroepitaxial growth. In general, there are three modes of the heteroepitaxial growth from the vapor phase: Frank-van der Merwe (FM) [Fra49, published in 1949], Volmer-Weber [Vol26, 1926) and Stranski-Krastanow [Str37, 1937]. They represent two-dimensional (2D) layer-by-layer growth (FM), 3D islanding (VW), and an intermediate growth mode, at which firstly 2D layer-by-layer growth is realised, and then after a certain critical thickness of the deposited material, the 3D island start to grow on the remained 2D layer (see Fig. 2.4).

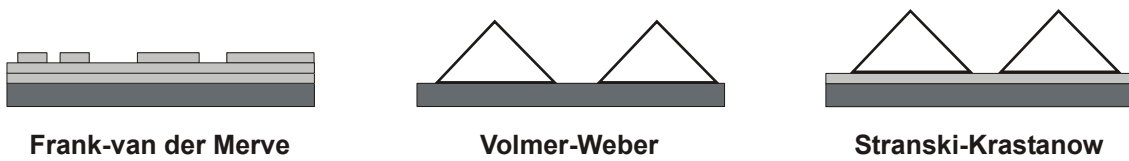


Figure 2.4 The three growth modes observed by the heteroepitaxial deposition of material (light gray and white) onto a substrate (dark gray).

If lattice constants of the deposited material A and substrate B are equal (or near equal, as for AlAs and GaAs), the growth mode is determined by the relation between the surface energies of γ_A and γ_B and the energy of their interface γ_{AB} . Thereby, if $\gamma_A + \gamma_{AB} < \gamma_B$, the deposited material B wets the substrate and grows in the FM mode (Fig. 2.4). An opposite relation $\gamma_A + \gamma_{AB} > \gamma_B$ results in the VW growth mode, where 3D islands made from the material A are directly formed on the substrate B.

In the heteroepitaxial systems with lattice constants $i > g$ as shown in Fig. 2.5(a) and the lattice mismatch $\frac{(i-g)}{g} \cdot 100 \% > 2 \%$ (e.g., InAs/GaAs (7.2%) or Ge/Si (4.2%)) the deposition of the material with a smaller surface energy (InAs upon GaAs, or Ge upon Si) initially proceeds in the FM growth mode. The epilayer grows pseudomorphic with compressive strain, i.e., it is stressed in the horizontal plane. A thicker layer accumulates larger strain energy and can lower it by forming isolated islands (see Fig. 2.5(b)), in which strain can partially be relaxed inside the islands. Thus, the SK growth mode occurs. In the InAs/GaAs system, explored in the present thesis, this scenario is realised on GaAs(001) [Leo94, Bim99], GaAs(113)A, B [Hen97, For98] and GaAs(114)A, B [For98] substrates. However, there is also another way to reduce the compressive strain without formation of

3D islands – incorporation of dislocations at the interface between the materials A and B, as shown in Fig. 2.5(c). 1D crystalline line defects, which often form a 2D network, appear somewhere at the interface and the depositing material A continues to grow in the FM mode further. This scenario occurs on the GaAs(110) [Bel97], GaAs(111)A [Yam96] and GaAs(111)B [Hoo93] substrates. So far, an atomistic explanation of this remarkable difference is not found. It should be related to a different cation diffusion length on the substrate reconstructions and, therefore, to a different size of a critical nucleus, whose formation allows the growth of a stable island. The evidence for this may be found in a recent paper from Wasserman et al. [Was03] that showed the appearance of the InAs QDs on GaAs(110) covered with a thin film of AlAs prior to the InAs deposition. AlAs decreases the cation diffusion length [Vor00], and the InAs QDs appear, although with a very small density.

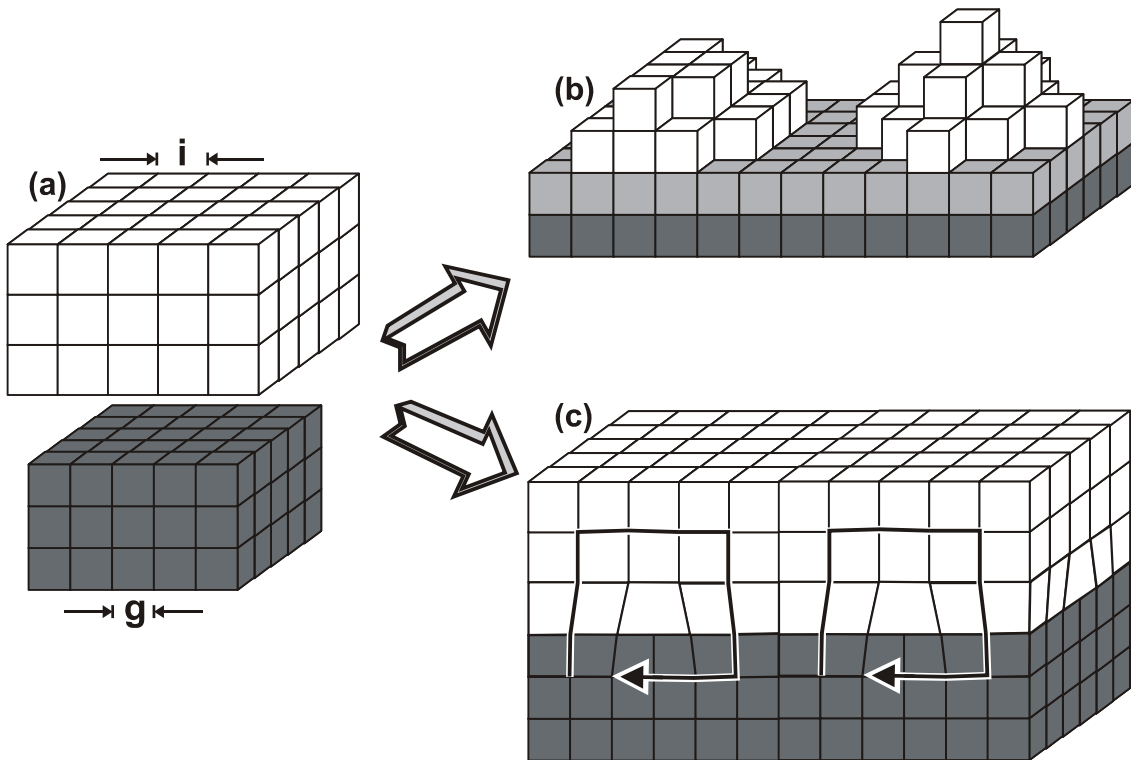


Figure 2.5 Two different ways of the reduction of compressive strain by the epitaxial deposition of mismatched materials with lattice constants i for a deposit (light gray and white) and g for a substrate (dark gray). (a) Materials in solid state before the growth. (b) Stranski-Krastanow transition: white - 3D islands, dark gray - substrate, light gray - wetting layer (WL). (c) Layer-by-layer growth mode with introduction of dislocations, which are surrounded with translation vectors.

2.5 Coherent and incoherent islands

It was for a long time believed that the islands formed in the SK growth mode are dislocated (incoherent), i.e., a dislocation line or even network is incorporated at the interface between the island and WL, of the WL and substrate (see Fig. 2.6). However, the pioneer experiments on InAs/GaAs(001) [Gol85] and on Ge/Si(001) [Moy90] have demonstrated the formation of coherent (dislocation-free) strained islands due to the strain relieve in their volume and at their step-edges.

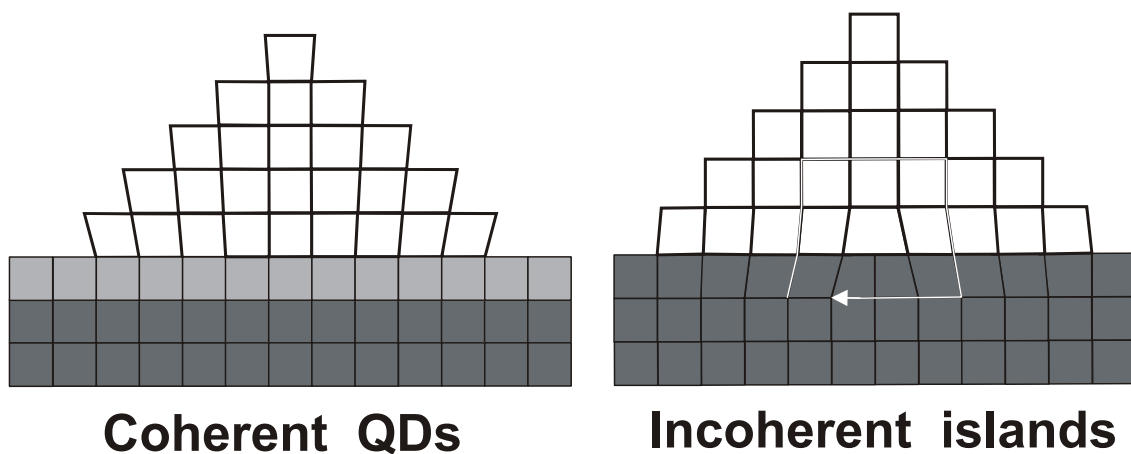


Figure 2.6 Dislocation-free (coherent) and dislocated (incoherent) islands, appeared after the SK transition on the substrate.

The absence of the dislocations in the QDs is particularly important for applications, as the dislocations are good traps for charge carriers and can suppress radiative recombination that produces lasing light. The nature, forming the QDs through self-organisation, offers another surprise: a narrow size distribution for the coherent QDs that allows them to emit the light with almost one certain energy. As has been shown for the Ge/Si system [see, e.g., Jes98, Sha99] and the InAs/GaAs system [Leo93, Nab95, Suz03, Tem03], strain energy, produced by lattice mismatch, acts to reduce the QD size, to increase the density of islands, and to significantly narrow their size distribution to nearly uniformly sized QDs. After the islands have relaxed by misfit dislocations, the island sizes increase (without limitation) and the island size distribution becomes broader [Sha99]. This results in a bimodal size distribution with a very narrow and intense peak for the coherent QDs, and the broad and low peak for the incoherent islands^{*}. Since both types of islands appear mainly in a faceted

^{*} We generally speak about islands (coherent and incoherent) and about QDs, if the islands are coherent.

form, the self-limitation is associated with coherently strained growth of QD facets that we now consider in detail (after Jesson et al. [Jes98], deduced mainly from the Ge/Si system).

The model of facet growth is shown in Fig. 2.7(a-b). We assume a QD to have a pyramidal shape with a half base length s and four bounding facets inclined at an angle θ to the substrate. The 3D island grows via the nucleation of a 2D embryo of height a on the facet surfaces (see Fig. 2.7(b)). The embryo starts growing at the bottom left hand corner of the facet in Fig. 2.7(a). We assume that the embryo shape is dominated by surface energy considerations such that the step energy γ_β is a minimum for a direction in the facet plane, inclined at an angle φ to the base of the island.

If the adatom diffusion length is large on the scale of the spatial extent of the island strain field then the energy to form an embryo with length at the base l , is:

$$\Delta G = a \cdot l \cdot \Gamma + a \cdot \int_{\text{embryo}} \zeta(\mathbf{R}) \cdot d\mathbf{R}, \quad (1)$$

where $\Gamma = \gamma_f \cdot \sin \varphi \cdot \csc \delta + \gamma_\beta \cdot \sin \eta \cdot \csc \delta + \gamma_f \cdot \cot \theta - \gamma_s \cdot \csc \theta$, if $l \gg a$. The surface energies γ_f and γ_s correspond to the island facet and substrate (or the WL) energies, so that the first term in (1) simply reflects the additional surface energy created. The second term involves the elastic relaxation of the material comprising the embryo where $\zeta(\mathbf{R})$ is the elastic energy density at the surface of the embryo minus the elastic energy density of the planar strained WL. \mathbf{R} is a 2D vector in the facet plane as shown in Fig. 2.7(a).

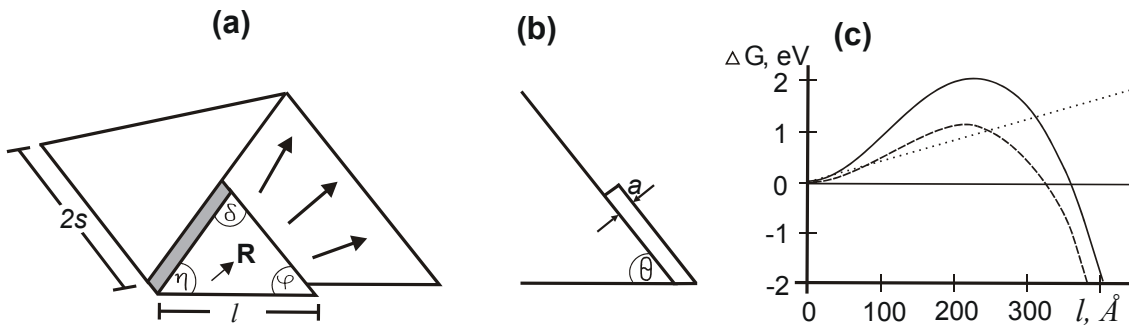


Figure 2.7 [Jes98] (a) Schematic view of the strained facet growth. An embryo emerges from the bottom left hand corner of the facet and expands across the facet. (b) The embryo of height a increases the basal dimension of the island as shown in cross section. (c) Formation energy of the embryo ΔG as a function of its size l (solid line) for the geometry shown in (a). The first and second terms of equation (1) are represented with the dotted and dashed lines, respectively. The misfit is 2% and $s=400 \text{ \AA}$. Elastic constants used in the calculations are: Young's modulus $E=102 \text{ GJ/m}^3$ and Poisson's ratio $\nu=0.27$. $\{105\}$ facets were assumed to bound the QDs with $\theta=11.3^\circ$, $\varphi=51.5^\circ$, $a \cdot \csc \theta = 5.54 \text{ \AA}$, and $\Gamma=3.8 \text{ meV/\AA}^2$.

The elastic energy density at the surface of a pyramidal island can be calculated by finite element analysis (FEA). The elastic energy density $\zeta(\mathbf{R})$ can be integrated over the surface of the embryo and evaluated the total energy change ΔG using equation (1) as a function of the embryo dimension l , as shown in Fig. 2.7(c). Clearly, the energy increases initially and reaches a maximum value of ΔG^* at a critical nucleus size l^* . Hence, there is an energy barrier to complete the strained facet.

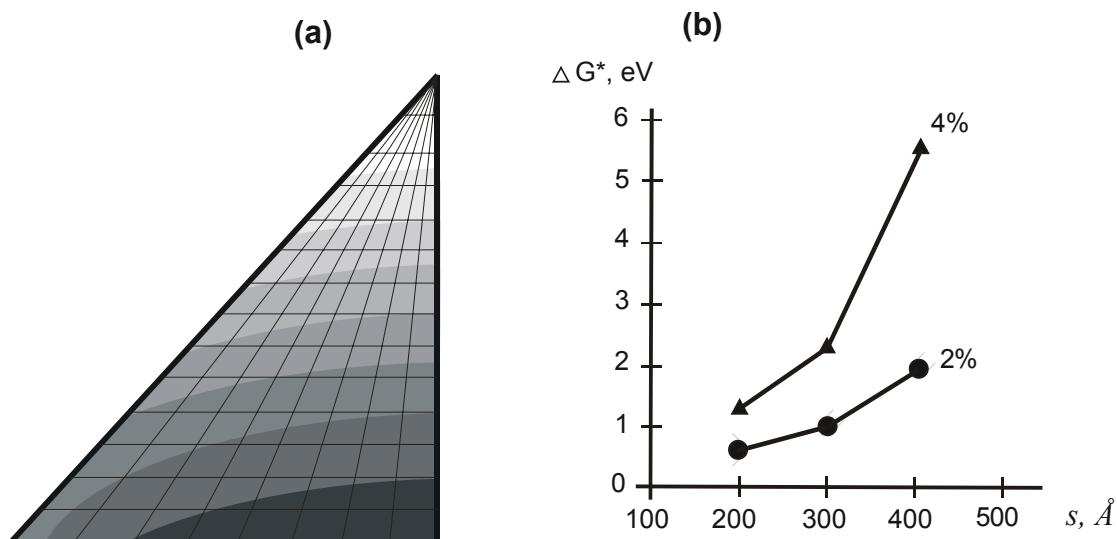


Figure 2.8 [Jes98] (a) Elastic energy density associated with half the triangular facet of a pyramidal island ($s=400 \text{ \AA}$) at 2% misfit. Different grey scales represent the elastic energy density, which decreases from 96 MJ/m^3 (dark scale) at the base to 18 MJ/m^3 (white scale) close to the peak. The calculation involves one-quarter of an island containing a nonuniform mesh of 5600 elements. The island is situated 100 \AA from the sidewall of the substrate which is 200 \AA deep. The substrate is vertically constrained at the bottom and the side facets are compressed to the appropriate displacement for the misfit. (b) Energy barrier to complete the facet ΔG^* as a function of island size s and misfit strain.

The physical origin of this barrier can be deduced from the FEA of the elastic energy density displayed in Fig. 2.8(a). The elastic energy density of the WL corresponds to the third gray scale starting from the island bottom in the figure. Material in the proximity of the island peak is therefore relaxed relative to the WL, but a significant stress concentration occurs at the base of the pyramid. To grow the facet it is necessary to cover the surface with a monolayer of material, which is initially strained as the WL. In order to cover the

highly strained levels close to the base, this material has to be further compressed to values between the first and second gray scale starting from the island bottom. This will initially cost energy until the embryo can expand into more relaxed regions of the surface. Eventually, this reduction in elastic energy dominates the positive surface energy contribution in equation (1), as shown in Fig. 2.7(c), which is the physical origin of the energy barrier.

The magnitude of the stress concentration at the base of the island increases with increasing misfit strain. Furthermore, the spatial extent of the stress concentration increases, as the islands grow larger. The energy barrier to complete the facet will therefore also increase with increasing s and misfit strain as shown in Fig. 2.8(b). Since the island growth rate $R \sim \exp(-\Delta G^*/kT)$, this implies a strong self-limiting growth effect in which *large islands will grow more slowly than smaller islands*. Smaller islands must then catch up to the larger islands in size, which will narrow the island size distribution. Such models are particularly applicable to high misfit systems $> 4\%$.

We now turn to the remarkable phenomenon of island shape elongation during strained layer epitaxy, which was reported for Ge island on Si(001) [Moy90] or for InAs islands on GaAs(113)A [Hen98]. Ge islands were found to elongate along elastically soft $[100]$ giving rise to a so-called “hut cluster shape”, those of InAs were elongated along $[3\bar{3}2]$ and revealed a more complicated arrowhead like shape. If the growth of a square-based pyramidal island shown in Fig. 2.7(a) is limited by the nucleation of new layers on the facets, elastic interaction with neighboring islands or steps will produce a variation in energy barrier across the islands. It will result in a difference in the elastic energy distribution of some facets, leading to an anisotropic growth. Once an island is elongated, the time for a freshly nucleated layer to complete extended facets becomes increasingly significant compared with the time between nucleation events. This is because the basal stress concentration, which acts as a barrier for adatom diffusion, restricts the growth of extended facets more than for short ones. Therefore, the diffusion-limited growth will contribute to the further elongation. The islands will adopt a clearly elongated shape.

It is also clear that incorporation of a dislocation at the interface will completely disturb the distribution of elastic energy density shown in Fig. 2.8(a). The basal stress located near the interface and produced the diffusion barrier to complete the facet will relax to the value of the island peak. The embryo will expand on the whole facet even faster than on the small coherently strained QDs. It will significantly increase the growth rate of incoherent islands,

which can now act as a sink for adatoms attracting the atoms from the QDs too. Since the appearance of dislocated islands through, e.g., coalescence of some QDs, is a local dependent event, they start to grow on the surface at different time and grow without limitation caused by elastic strain. This leads to the reported broad size distribution with the low intense peak.

2.6 Experimental setup

The ultra-high vacuum (UHV) facility used in this work has been designed and built in the Prof. Dr. K. Jacobi group by technician Peter Geng and two generations of PhD students: Juan Márquez, Lutz Geelhaar and Jutta Platen, Carsten Setzer. The instrument is described in more detail in [Gen00] as well as in the PhD theses (in German) available in our homepage under <http://w3.rz-berlin.mpg.de/pc/ElecSpec>. Our task has mainly been in performing the maintenance work consisted of installations and repairs of the Knudsen cell evaporators, RHEED screens, etc. We briefly recall main units of our facility, which are MBE, STM and analysis chambers. All the chambers are connected with an UHV transfer mechanisms as shown in Fig. 2.9 that allows the preparation and investigation *in situ*.

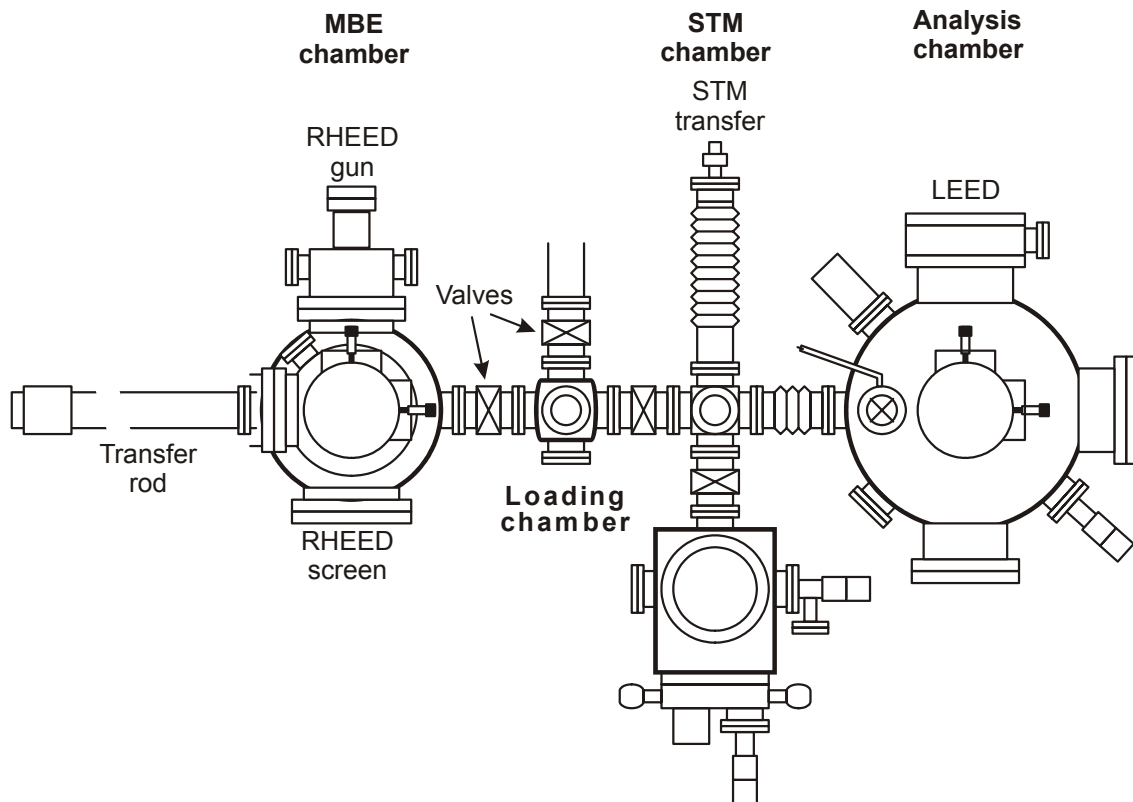


Figure 2.9 [Gen00] Schematic view of the UHV facility. Samples are introduced via the loading chamber, prepared with MBE and investigated *in situ* by STM, RHEED and LEED.

The compact MBE growth chamber, shown schematically on the left hand side of Fig. 2.9, is equipped with three solid state evaporation Knudsen cells loaded with As, Ga, and In. The capacities of the crucibles are 250 cc for the As cell (DCA, Valved Cracker MBS-250-35-11 As), 2 cc for the In cell (DCA, Hot Lip Crucible Miniature K-cell 2CC-3-00), and 0.5 cc for the Ga cell (Oxford Instruments, Miniature K-Cell). The sample is held facing downwards by a manipulator allowing motion in x , y , and z direction as well as 270° rotation about the axis normal to the sample surface. Sample heating is made by thermal radiation from a filament that is mounted on the sample manipulator above the backside of the sample. The sample temperature is monitored with an IR-pyrometer (Kleiber, Pyroskop 202). Temperatures up to 620°C are reachable with this arrangement. The growth rate and the surface quality during growth are monitored with a 15 kV RHEED system. Epitaxial layers of $20\text{--}4000\text{ \AA}$ are typically grown at growth rates between 0.1 and 1.5 \AA/s as can be calibrated with oscillations of the specular spot acquired from the RHEED screen. The pressure produced by the evaporation cells at the sample position is measured with a movable ion gauge. The chamber has a base pressure of $\sim 10^{-10}$ mbar achieved with an ion-getter pump (MECA 2000, PID 200, 200 l/s) and a Ti sublimation pump (Balzers, USP 034). In addition, there are cryopanelled installed, which are filled with liquid nitrogen during MBE growth to keep the background pressure below $5 \cdot 10^{-9}$ mbar.

The surface analysis chamber houses a low-energy electron diffraction (LEED) system (VSI, ErLEED). In addition, there are a $0.5\text{--}2\text{ keV}$ sputtering ion gun for sample cleaning and a mass spectrometer. The latter is used for leak checking in the entire system after bake out procedure. A pressure below $5 \cdot 10^{-11}$ mbar is established in this chamber by a magnetically suspended turbomolecular pump (Balzers, TPU 180, 170 l/s).

The scanning probe microscope is mounted in a small chamber with a 140 mm view port on top in order to have free vision towards the STM. The chamber is pumped by an ion-getter pump (Varian, Noble Diode, 135 l/s), which provides a base pressure below $1 \cdot 10^{-10}$ mbar. The UHV-STM/AFM (atomic force microscope) machine was manufactured by Park Scientific Instruments (Autoprobe VP2). The vibration isolation in this STM is achieved by a two-stage coil-spring suspension with eddy current dampers. The weight of the sample carrier (55g) made from tantalum produce, on the other hand, an additional fixing of the sample unnecessary. It is held just by its own weight on a U-shaped stainless steel holder, which is insulated against the sample stage. There is a tip storage facility for six tips in the STM chamber. Since STM tip contamination occurs quite often when measuring GaAs, the application of the STM is limited by the lifetime of the tips that are available.

Our STM tips were clipped from 0.5 mm thick tungsten wire. The tip handling linear-rotary feed through line was in vacuum used to position the tip in front of a filament. The tip was connected to ground and the filament was biased negatively. Electrons flowed towards the tip and heated it, yielding the sublimation of the tungsten oxide. The removal of the oxide layer was indicated by a pressure increase. This procedure provides good tips and can also be used when the tip was contaminated by arsenic.

The transfer between the MBE and the analysis chamber is performed by a 1.4 m long magnetically coupled linear rotary transfer rod (Huntington, VFC-169-36). It is driven with two direct-current motors, allowing precise and fast sample movement. Moreover, the motors are remote controlled and thus only one person can operate the transfer. After growth the samples can be moved out of the growth chamber within 30 s and afterwards cooled down to room temperature in another chamber.

2.7 STM

Scanning tunneling microscopy (STM) is a powerful technique for imaging surfaces with extremely high resolution (below 0.1 Å). This technique was invented in 1981 by two researchers in Zurich, Switzerland - Gerd Binnig and Heinrich Rohrer [Bin82]. In 1986, they were awarded a Nobel Prize for their invention. To understand why their instrument was so good, we have to think about how people imaged surfaces before that time. Conventional optical microscopes, which are still in use today, use light and lenses to magnify a tiny piece of a surface. With stronger lenses, it is possible to see smaller features. However, there is a limit to how small one can get - namely, the wavelength of the light we see - which is about 500 nm. Features smaller than the wavelength of light cannot be seen. 500 nm may seem small, but even the big QDs are more than one order of magnitude lower. The distance between the atoms is only about 0.5 nm, i.e., three orders of magnitude lower than the resolution of the optical microscopes. To image individual atoms, one needs a microscope which operates on an entirely different principle. This is where the STM comes into play.

The principle of the STM technique is shown in Fig. 2.10(a). STM uses a sharpened, conducting tip with a bias voltage applied between the tip and the sample. Both the tip and the sample must be conductors or semiconductors. When the tip and the sample are brought within 10 Å, their electron wave functions can overlap, and the electrons from the sample begin to tunnel through the 10 Å gap into the tip or vice versa, depending upon the sign of the bias voltage. The resulting tunneling current I varies with the tip-to-sample spacing d as

following: $I \propto \frac{U}{d} \cdot \exp(-Kd\sqrt{\phi})$, see, e.g., [Fow28], where K is a constant, ϕ is the average work function of the tip and sample. So, the tunneling current is an exponential function of distance. If the separation between the tip and the sample changes by 10% (on the order of 1 Å), the tunneling current changes by an order of magnitude. This exponential dependence gives the STM technique its remarkable sensitivity. Taking into account, that 90% of the current flow inside the lateral dimension of the downmost tip atom (see Fig. 2.10(a)), STM can image surfaces with sub-angstrom precision vertically and atomic resolution laterally.

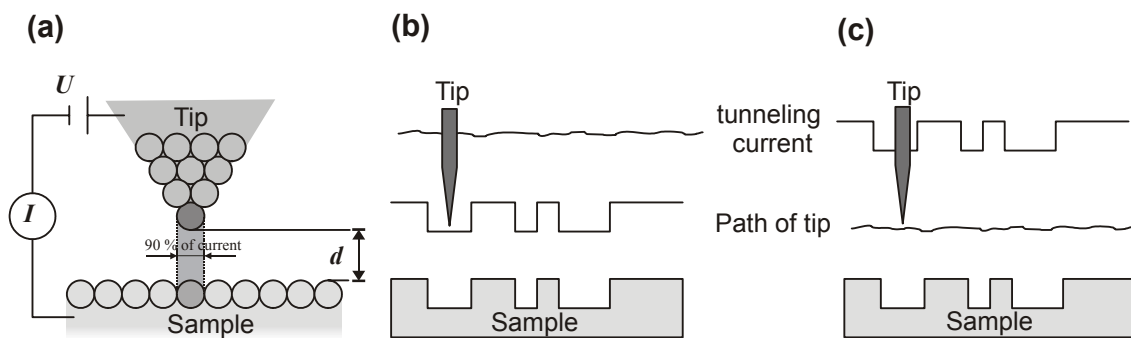


Figure 2.10 (a) Schematic of the tip and sample interaction for STM; (b-c) Comparison between the constant-current and constant-height mode for STM.

The STM technique can scan a sample in either of two modes: constant-current mode (see Fig. 2.10(b)) or constant-height mode (see Fig. 2.10(c)). In constant-current mode, STM uses feedback to keep the tunneling current constant by adjusting the height of the scanner at each measurement point. When the system detects an increase in tunneling current, it adjusts the voltage applied to the piezoelectric scanner to increase the distance between the tip and sample, and the current remains constant. In this mode, the motion of the scanner reproduces the data set, e.g., the surface topography. If the system keeps the tunneling current constant to within a few percent, the tip-to-sample distance will be constant to within a few hundredths of an angstrom.

In constant-height mode, the tip moves in a horizontal plane and the tunneling current varies depending on topography and the local surface electronic properties of the sample. The tunneling current measured at each location on the surface reproduces the data set.

The constant-height mode is applicable only for smooth surfaces; its big advantage is a fast scanning velocity. Constant-current mode allows to measure corrugated surfaces, e.g.,

with 3D QDs. Therefore, we always apply this mode to acquire topography and error signals of our samples containing large 3D objects, e.g., InAs QDs.

The topography signal generates an image of the sample's electronic states using the voltage signal that is applied to the scanner when the feedback is enabled. The voltage signal causes the scanner to extend or retract in response to a change in tunneling current.

The error signal generates an image using the error signal of the feedback loop. With feedback enabled, an image acquired using this option represents the error signal that is sent to the feedback loop at each point in a scan. This type of image gives a measure of how well the feedback loop is tracking topography. A large error excursion indicates poor surface tracking, where edges are accentuated in the image. Depending on the tip sharpness, both topography and error signal can be used for representation of sample surface features.

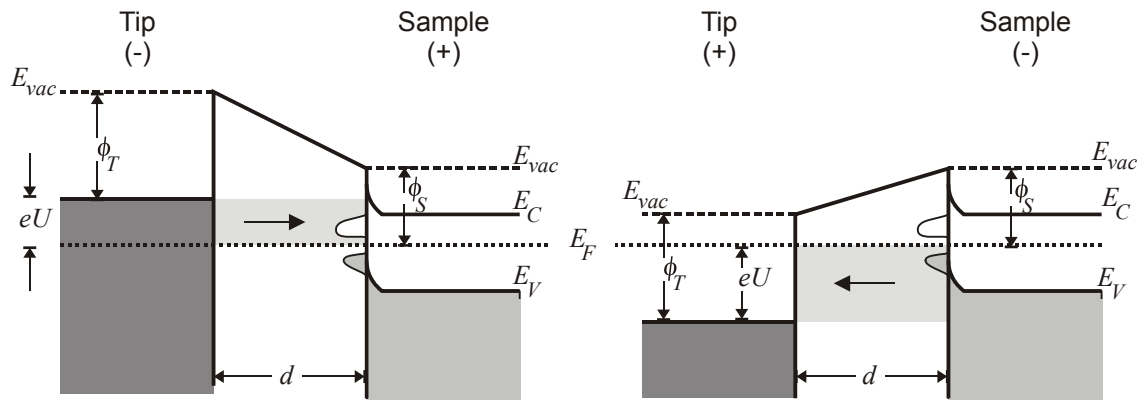


Figure 2.11 Schematic of quantum-mechanical tunneling between a metal tip and a semiconductor surface a distance d apart. The tunneling barrier is determined by work functions of the surface and the tip ϕ_S and ϕ_T , respectively, and the bias voltage applied between the both, eU . For the left-hand side of the figure, surface positive with respect to the tip, electrons tunnel from bands below the Fermi level of the tip to those above the Fermi level of the surface. An opposite case is shown on the right-hand side. E_{vac} , E_C and E_V are energy states for the vacuum level, conduction band minimum and valence band maximum, respectively.

The tunneling current depends not only on the separation between the tip and the sample, but also on their surface electronic states that overlap within the energy range eU for which tunneling can occur (see Fig. 2.11). When a positive bias voltage is applied to the sample (or a negative voltage to the tip, see the left-hand side of Fig. 2.11) electrons in

occupied states on the tip can elastically (without losing energy) tunnel in the empty states of InAs or GaAs surfaces. As has been shown in chapter 2.1 the Ga (or In) derived DBs will be imaged in this case. An opposite sample bias (see the right-hand side of Fig. 2.11) allows electrons occupying filled states on the semiconductor surfaces to tunnel into empty states of the tip. This will image the As derived DBs. Therefore, for the GaAs (InAs) surfaces the electronic structure should be taken into account in order to correctly interpret the surface topography.

2.8 Photoluminescence of InAs QDs

Photoluminescence (PL) is one of the most commonly used methods to investigate the optical properties of the heteroepitaxial nanostructures, like InAs QDs. The basics of the PL can be explained with Fig. 2.12, where a simplified band structure of the GaAs bulk material as well as discrete energy levels for electrons and holes of the capped InAs QDs are shown.

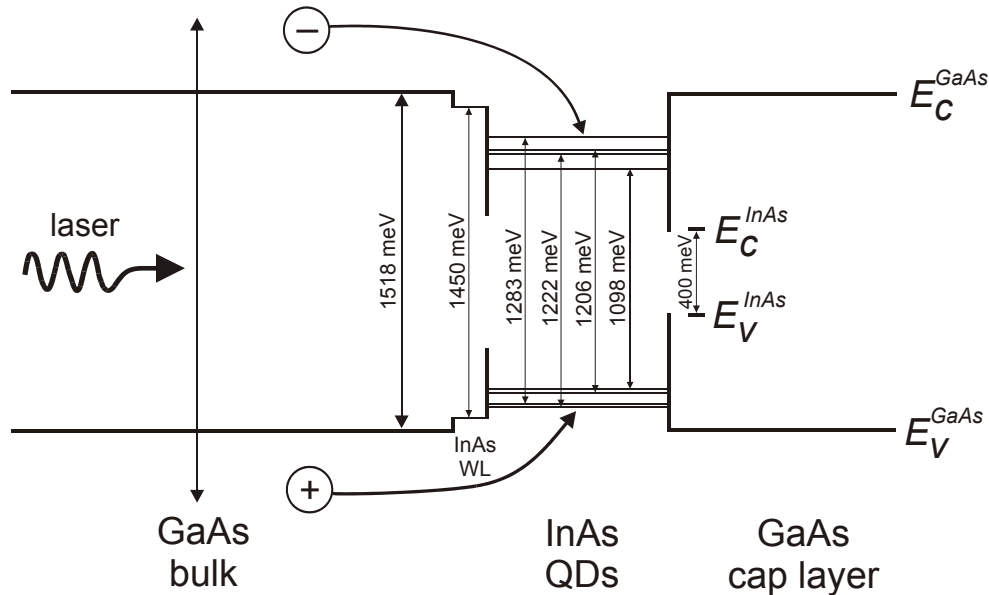


Figure 2.12 Schematic representation of the photoluminescence technique on the example of InAs QDs embedded in a GaAs matrix. The level structure of the InAs QDs is calculated with eight-band $k\cdot p$ theory for the InAs pyramid islands on GaAs(001) with $\{110\}$ facets and a 136 Å long base. Energies are given in millielectronvolts. The band gap of unstrained GaAs and InAs materials is equal to 1518 and 400 meV, respectively. 1098 meV corresponds to the ground state electron-hole recombination. 1206, 1222 and 1283 meV is the allowed recombination of the excited states, which only appears when charge carriers saturate the ground state. The 1450 meV is energy for 1ML thick InAs wetting layer (after [Bim99] and [Hei97a]).

The PL technique involves three stages. First one is called generation of charge carriers. An incident photon with an energy originating from the excitation source (e.g., laser light) hits an electron in the GaAs valence band. The photon is annihilated and transfers its energy to the electron that is excited to the GaAs conduction band. Due to energy conservation, the photon energy has to be equal or larger than the band gap for the unstrained GaAs material (1518 meV) in order to ensure light absorption. Note that electron excitation is vertical in \bar{k} -space since the momentum of a photon is negligible and thus only optical transitions with $\Delta k \cong 0$ are allowed. Electron excitation leaves an empty state in the valence band that is called hole, having a positive charge. The second stage is called thermalisation of charge carriers. The electrons and holes in the conduction and valence bands undergo an energy relaxation due to non-radiative phonon scattering. This process takes time of few tens of picoseconds. As a result, the excited electrons and holes reach lowest energy levels (ground state) in the InAs QDs. Since both band extremes are at the same point in the Brillouin zone for the direct semiconductors like InAs or GaAs, i.e., $\bar{k}=0$, optical recombination can occur in which the conduction band electrons annihilates the valence band hole. This is the third stage of the PL. The recombination time is usually some orders of magnitude larger than the thermalisation time. For the same reason as for the excitation process, the recombination is vertical in \bar{k} -space according to $\Delta k \cong 0$ and produces photons with energies corresponding to the ground and excited states in the InAs QDs, as shown in Fig. 2.12. The emitted photons are collected by a spectrometer and thus the electronic structure of the QDs can be detected.

2.9 Sample preparation

All samples used in this work were cut from single crystal GaAs wafers (500 μm thick and 2" in diameter, Si-doped, n-type, double polished). The main properties of the GaAs substrates are listed in Table 2.1. A typical size of the samples, investigated by STM and PL, was about $10 \times 10 \text{ mm}^2$. They were glued on a massive (55g) Ta sample holder with liquid In and cleaned with He gas. After oxide desorption at a temperature $T \sim 600 \text{ }^\circ\text{C}$, the samples were treated with several ion-bombardment and annealing (IBA) cycles. The annealing was carried out under As_2 flux at 530-580 $^\circ\text{C}$. The temperature was measured by a pyrometer that was calibrated against the GaAs(001)-c(4 \times 4) to β 2(2 \times 4) transition at $465 \pm 10 \text{ }^\circ\text{C}$. Subsequently, GaAs buffer layers 200-4000 \AA (see Table 2.1) were grown by MBE at the rates between 0.1 and 1.5 $\text{\AA}/\text{s}$ as was calibrated with RHEED oscillations of the

specular spot acquired during epitaxial growth of GaAs on GaAs(001). During annealing and growth, the surface periodicity and quality was monitored by RHEED. An As₂ : Ga beam equivalent pressure (BEP) ratio was set to 7 - 20.

Orientation of GaAs substrate	Carrier concentration, x 10 ¹⁸ cm ⁻³	Manufacturer / growth method	Off - orientation	GaAs buffer layer, Å
(113)A	1.4 – 4.8	Wafer Technology / VGF*	± 0.2°	500
(113)B	1.4 – 4.8	Wafer Technology / VGF	± 0.2°	500
vicinal (2 5 11)A	1.0 – 4.8	Wafer Technology / VGF	1.0°	200–4000
(2 5 11)A	> 1.0	MaTecK / LEC**	± 0.2°	200–2000
(2 5 11)B	> 1.0	MaTecK / LEC	± 0.2°	200–2000
(001)	undoped	Wafer Technology / VGF	± 0.1°	2000

Table 2.1 Properties of the supplied GaAs wafers as well as the thickness of the MBE grown GaAs buffer layers.

Then the samples were cooled down to a growth temperature between 435 - 490 °C (see Table 2.2) and InAs was deposited at a growth rate of 0.05 - 0.075 Å/s and an As₂ : In BEP ratio of 40 - 50 at an As₂ pressure of 4 - 7×10⁻⁷ mbar. The growth rate of InAs was calibrated with RHEED oscillations of the specular spot acquired during epitaxial growth of InAs on InAs(001). The sample heater, the In- and As-Knudsen cells were shut off immediately, as soon as the RHEED pattern clearly changed from streaky to spotty, indicating an onset of the 3D growth mode. As can be seen from Table 2.2 the SK transition occurs on the GaAs(001) surface at about 1.5 ML, which is slightly below the reported values of 1.6 - 1.8 ML for similar preparation conditions except for the InAs growth rate [see, e.g., Has98, Mar01]. However, the RHEED estimation of the SK transition is fairly rough because it is dependent on the sensitivity of operator eyes. The SK transition on all substrates except GaAs(113)B is circa equal to that on GaAs(001).

* Vertical gradient-freeze method of the growth of GaAs single crystals with an etch pit density (EPD) below 1000 per cm².

** Liquid encapsulated Czochralski method of the growth of GaAs single crystals with an EPD below 50000 per cm².

For the STM measurements, the samples were quickly (within 30 s) transferred to the STM chamber without breaking vacuum (*in situ*) immediately after the onset of the 3D growth. STM images were acquired from unburied InAs islands at room temperature at negative sample biases of -2.5...-4.0 V (filled states were imaged) and tunneling currents of 0.01-0.7 nA.

Orientation of GaAs substrates	Sample temperature, °C	InAs thickness, Å	InAs thickness in ML of GaAs(001)	InAs growth rate, Å / sec
(113)A	450 ±10	4.6 ± 0.6	1.5 ± 0.2	0.075
(113)B	435 ±10	4.6 ± 0.3	1.5 ± 0.1	0.05
(113)B	450 ±10	2.9 ± 0.5	1.0 ± 0.2	0.05
(113)B	470 ±10	3.9 ± 0.3	1.3 ± 0.3	0.05
(113)B	490 ±10	4.4 ± 1.4	1.5 ± 0.5	0.05
vicinal (2 5 11)A	450 ±10	5.0 ± 0.5	1.7 ± 0.2	0.075
(2 5 11)A	450 ±10	5.0 ± 0.5	1.7 ± 0.2	0.075
(2 5 11)B	450 ±20	4.5 ± 0.4	1.5 ± 0.1	0.075
(001)	450 ±20	4.5 ± 0.5	1.5 ± 0.2	0.075

Table 2.2 InAs deposition on different GaAs substrates.

The photoluminescence (PL) measurements were performed at Technical University at Berlin in the group of Prof. Dr. D. Bimberg. PL was conducted on the GaAs(2 5 11)A, B and GaAs(001) substrates. The InAs islands were overgrown with 50 nm of GaAs. The first 10 nm were grown at the sample temperature of 450 °C, and then it was raised to 520 °C in order to improve the quality of the GaAs cap layer. PL was performed in a closed cycle He cryostat at 10 K using the 514.5 nm line of an Ar⁺ laser for excitation and a cooled Ge pin diode for detection. Excitation densities were set between 5 W/cm² (less than one exciton per QD) and 5000 W/cm² (more than one exciton per QD). PL was spectrally dispersed by a 0.3 m monochromator and detected using lock-in techniques. Note, that the STM measurements require highly doped GaAs substrates, whereas for the PL measurements one usually uses semi-insulating GaAs in order to reduce the background signal from the doping levels. Since our group specializes in the STM technique, doped substrates have been mainly in funds, which resulted in high background intensity in the PL spectra.

3 InAs quantum dots on GaAs(113)A*

3.1 Introduction

From all known high-index GaAs surfaces, the (113)A is the "oldest" one: first surface structure investigations on it are dated in the middle of the Eighties. Such a long history can be explained by its rather complicated reconstruction as well as its possibility to serve as a substrate for different low-dimensional heterostructures. Low defect and dislocation density for InAs/GaAs(113)A interfaces has already been reported from photoluminescence measurements [Xuh99, For98, San98]. The structural properties of the QDs were investigated using atomic force microscopy (AFM) [Xuh99] or *ex situ* STM from decapped samples [Hen98]. An arrowhead-like shape has been observed and attributed to faceting of the GaAs(113)A surface [Hen98]. However, the Miller indices of the QD bounding facets have not yet been determined, and there was no report on any *in situ* STM investigations for QDs on GaAs(113)A. Here we prepared InAs QDs on GaAs(113)A by molecular beam epitaxy (MBE) and acquired *in situ* atomically resolved STM images of the QDs. A motivation for this work was to show the evolution of the InAs QDs with atomic resolution and to find another explanation for the observed nonconventional shape of the islands, because recent experiments of our group [Gee99, Jac02] had demonstrated the stability of the GaAs(113)A substrate.

3.2 Geometry of the bulk-truncated GaAs(113)A surface

The top view of the bulk-truncated (113)A surface is shown in Fig.3.1(a). The surface exhibits twofold-coordinated As atoms and threefold-coordinated Ga atoms in the topmost layer. A primitive unit cell is rhombic. However, experimental findings are better described with a rectangular unit cell that is twice as large as the rhombic one. The lengths of the unit cell vectors for the latter are given for the GaAs (InAs) (113)A surface as 4.0 Å (4.3 Å) along $[\bar{1}10]$ and 13.3 Å (14.3 Å) along $[\bar{3}\bar{3}2]$. The ideal (bulk-truncated) (113)A surface also exhibits a $(\bar{1}10)$ symmetry plane. The side view of the model is shown in Fig.3.1(b). The spacing between (113) planes for GaAs (InAs) is equal to 1.70 Å (1.82 Å). (The

* Generally, our definition of the *A* and *B* faces will be: A surface in the vicinity of (111)A (with threefold coordinated Ga atoms) is an *A* face, and a surface in the vicinity of (111)B (with threefold coordinated As atoms) is a *B* face.

GaAs(113)B surface has the same geometry with exchanged positions of Ga and As atoms.)

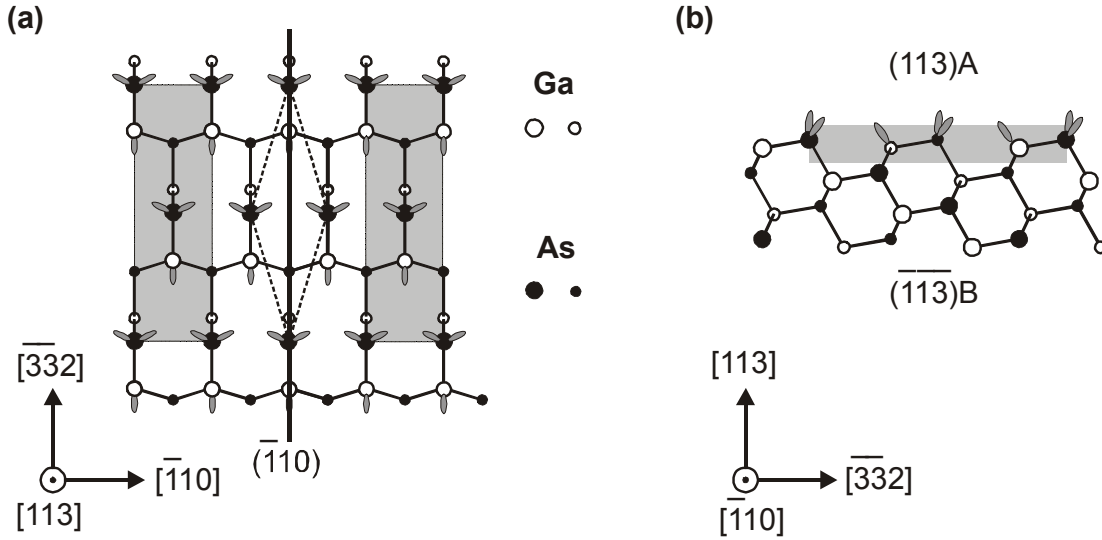


Figure 3.1: Structural ball and stick model of the ideal GaAs(113)A surface viewed from (a) top, and (b) side. The dashed rhombus indicates the primitive unit cell and shaded rectangles the rectangular unit cell used in this work. The $(-1,1,0)$ plane running perpendicular to the figure plane divides the surface into two symmetrical parts, i.e., is a surface mirror plane.

Interestingly, each As surface atom has one Ga neighbor. Since the atoms are differently coordinated, the ECR yields a charge deficit of $-3/4$ electrons per unit cell. Chadi [Cha85] calculated the atomic and electronic structures of the relaxed GaAs(113)A-(1x1) surface using the tight binding approximation and found that its surface structure is metallic with partially filled surface bands. Also a simple dimerization of the twofold-coordinated As atoms would result in an excess charge of +1 electron per unit cell, which is expected to be of high surface free energy and not stable as well. Therefore, the GaAs(113)A surface should find another more complicated reconstruction to reach a minimization of the total surface energy.

3.3 The reconstructed GaAs(113)A surface: a literature survey

According to the available publications, the following very contradictory results on GaAs(113)A prepared under typical MBE growth conditions have been reported: 1) The GaAs(113)A surface is faceted with a period of 32 Å and a height of 10.2 Å; 2) the GaAs(113)A surface and the AlAs/GaAs(113)A interface are flat; 3) the GaAs(113)A

surface exhibits an (8x1) reconstruction with a period of 32 Å and a height of only 3.4 Å; and 4) no long-range ordered reconstruction is observed.

1) Based on the results mostly derived from the RHEED measurement Nötzel et al. claimed the formation of macrosteps on the GaAs(113)A surface comprised of two sets of {331} facets oriented along the $[33\bar{2}]$ direction [Noe91, Noe95, Noe00, Led03]. The lateral periodicity of 32 Å (8 times the length of the unit cell along $[\bar{1}10]$, cf. Fig.3.1(a)) was determined from the splitting of the zeroth-order streak observed along $[33\bar{2}]$ into sharp satellites and the height of the steps of 10.2 Å from the splitting along its length. The GaAs(113)A surface was composed of periodical short (113) terraces (4 Å width) and the two sets of $(3\bar{1}3)$ and $(1\bar{3}\bar{3})$ facets corresponding to upwards and downwards steps of 10.2 Å height, which the authors claimed to confirm by cross section high resolution transmission electron microscopy (HRTEM) [Noe92]. The breaking of the flat GaAs(113)A surface was used for the synthesis of corrugated AlAs/GaAs(113)A superlattices, which exhibit optical properties characteristic for quantum wires. The strong optical anisotropy shown by means of photoluminescence (PL) and photoluminescence excitation (PLE) spectra was claimed to be induced by the interface corrugation.

2) The RHEED and HRTEM measurements performed by Brandt et al. [Bra93] showed no corrugation on GaAs(113)A. The authors did not find the vertical splitting of the main streak in the RHEED pattern and observed a growth mode different from layer-by-layer growth mode of GaAs and AlAs reported by [Noe91]. The PL spectra were also found to be unpolarized with respect to a rotation in the surface plane. Hsu et al. [Hsu94] confirmed the results by Brandt et al. and showed with RHEED and cross section TEM a smooth two-dimensional crystal growth, realized on GaAs(113)A, and sharp and flat heterointerfaces. The authors supposed that the appearance of Nötzel corrugations might stem from the arsenic deficiency during the growth process. However, any model for the stable, smooth GaAs(113)A surface that would obey the ECR, was not proposed in both referred papers.

3) A new structural model that fulfils the ECR, was proposed by Wassermeier et al. [Was95] using *in situ* RHEED and STM (the latter was really a brilliant instrument in that case that could solve such a complicated task.) The first-order bulk diffraction spot showed up the shadow edge of the 16th diffraction streak with a lateral periodicity of 32 Å perpendicular to the $[33\bar{2}]$ direction. In contrast to the Nötzel observation, no clear splitting along the streaks was found. An STM filled-state image revealed a (8x1)

reconstruction with a corrugation of only 3.4 Å and with zigzag chains of As dimers on the upper layers. Many other publications confirmed the Wassermeier model, e.g., the kinematical RHEED simulation of different structures on GaAs(113)A performed by Braun et al. [Bra96]. Platen et al. [Pla99] reported on the *ab initio*-total energy calculation for the (8x1) reconstruction and extracted a very low value for the surface energy of 47 meV/Å², which is well comparable with the known low-index surfaces [cf. appendix 1.1]. By means of LEED and surface core-level spectroscopy, Setzer et al. [Set99] found good agreement of the results with the Wassermeier model and no agreement with the Nötzel model. Vorob'ev et al. [Vor00] also confirmed the occurrence of (113)A-(8x1) on both GaAs and AlAs surfaces by RHEED and found, by HRTEM, a strong modulation in the thickness, related to a wavy morphology of GaAs(113)A. We will return to this point later.

4) Moriarty et al. [Mor97] investigated the decapped GaAs(113)A surface using both STM and synchrotron radiation photoemission. Core-level photoelectron spectra supported the As dimers to be the main part of the reconstruction. The STM results revealed the unbroken As dimer rows extended over much shorter length scales than reported by Wassermeier et al., though. A (8x1) reconstruction was not observed. Instead, the local-ordered 3x, 5x, and 2x periodicity along $[\bar{1}10]$, failing to confirm the ECR, was reported. Periodic faceting of the GaAs(113)A did not also occur. Interestingly, Lubishev et al. [Lub98] investigated the *InAs(113)A* surface (grown as a thick buffer layer on GaAs(113)A) and found, by *in situ* RHEED, two stable structure, namely (2x15) and (1x5). *Ex situ* LEED and STM measurements revealed the surface consisting of the As dimer rows with the above-mentioned periodicity. Neither a Wassermeier nor a Nötzel reconstruction was observed.

Being rather complicated on the microscopic scale the GaAs(113)A surface also shows unusual anisotropic roughness on mesoscopic areas. Nötzel et al. [Noe94] observed by scanning electron microscopy controlled step bunching during MOVPE growth. This led to a one-dimensional array of facets oriented along $[3\bar{3}\bar{2}]$ with a lateral periodicity tunable upon growth temperature and layer thickness. The facets were built up from asymmetric quasiperiodic step arrays. The phenomenon of step bunching was attributed to differences in the incorporation of adatoms at the step edges. On MBE prepared GaAs(113)A Wassermeier et al. [Was95] found by large-scale STM images that the highly anisotropic surface roughness of 5 monolayers was actually typical for this surface. This might give rise to an anisotropy in the exciton confinement and interface roughness scattering,

reported by Nötzel et al. [Noe91]. Pristovsek et al. [Pri98] observed on the MOVPE prepared GaAs(113)A surface by AFM a wavy morphology with the average lateral distances between the waves in the $[\bar{1}10]$ direction of about 400 Å after the IBA treatment of samples to the 800 Å after buffer layer growth. The waves, pointed along $[33\bar{2}]$, exhibited a tilt angle to the substrate of 1° to 10°. Geelhaar et al. [Gee99] found by STM one-dimensional islands extended along $[33\bar{2}]$ that also fulfill the ECR by propagation. The authors suggested that the growth on GaAs(113)A-(8x1) took place mostly by the propagation along $[33\bar{2}]$ which was in agreement with the strong azimuthal dependence of RHEED oscillations on InAs(113)A, reported by Lubishev et al. [Lub98]. Finally, Jacobi et al. [Jac02] found by STM a remarkable waviness along $[\bar{1}10]$ direction on GaAs(113)A. After growth of about 1800 Å of GaAs buffer layer the surface consisted of arrowhead-like depressions pointed along $[33\bar{2}]$, which were 20 Å deep and ~3000 Å long. The walls of the depressions were built up from a (3 7 15)A surface identical to staggered zigzag chains of the (8x1) Wassermeier reconstruction.

3.4 The reconstructed GaAs(113)A surface: our own results

After the deposition of the 500 Å thick GaAs buffer layer as described in chapter 2.9, the GaAs(113)A surface shows the (8x1) reconstruction reported in reference [Was95]. The variation of temperature from 400 °C to 600 °C for samples under As₂ flux does not affect the surface structure. Characteristic RHEED patterns of this reconstruction during preparation (in the annealing stage) are shown in Fig.3.2(a, b). The electron beam is incident along $[\bar{1}10]$ and $[33\bar{2}]$, reflecting the periodicity of the rectangular unit cell in perpendicular directions in real space. The RHEED pattern in the $[\bar{1}10]$ direction yields a period equivalent to ~6.6 Å in real space, which corresponds to a half of the length of the bulk-truncated unit cell along $[33\bar{2}]$. Note that due to the face-centered unit cell only the even reciprocal-lattice-rods contribute to the RHEED pattern [Set99, Mar02]. Therefore, the reconstruction exhibits a 1x periodicity along $[33\bar{2}]$ in real space. A 8x periodicity (32 Å) can be measured from Fig.3.2(b). However the super structure reflexes there are rather weak. The images acquired at room temperature after preparation (without As₂ supply) are shown in Fig.3.2(c, d). The splitting of the zeroth-order streak along $[33\bar{2}]$ is not observed in both cases. The RHEED patterns during and after preparation are identical,

except for the background intensity. This clearly indicates that the (8x1) reconstruction does not change during quenching process, and the subsequent growth of heterostructures occurs on the same surface that can be viewed by room temperature STM. It is evident that GaAs(113)A is much better ordered along $[\bar{3}\bar{3}\bar{2}]$ than along $[\bar{1}10]$, and exhibits many periodicity interruptions (e. g. steps) along $[\bar{1}10]$. However, the RHEED measurements clearly show only one reconstruction, that is (8x1).

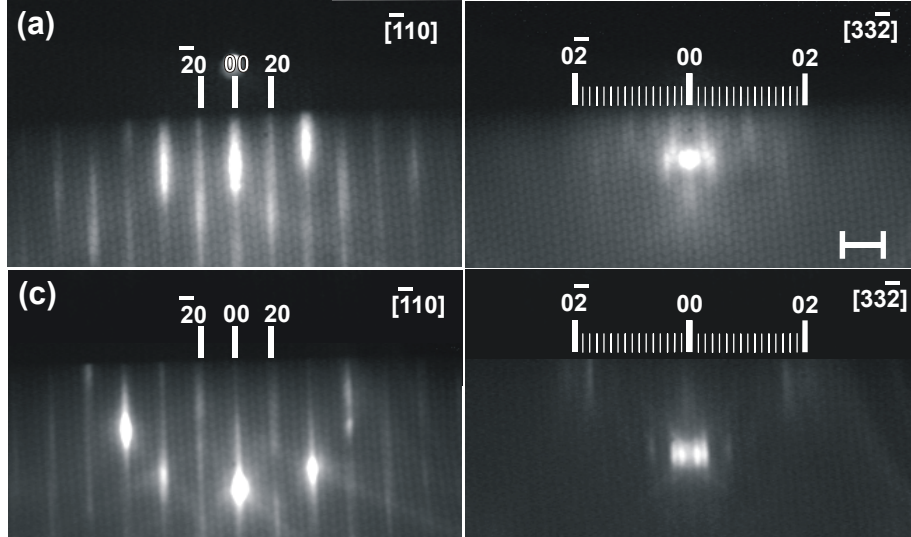


Figure 3.2: RHEED patterns of the GaAs(113)A-(8x1) reconstruction acquired (a),(b) during preparation at a sample temperature of 450 °C and As_2 flux and (c),(d) after preparation at room temperature without As_2 supply. The vertical lines at the top of the images indicate the diffraction streaks of the zero-ordered Laue circle. The specular spot is numbered as 00. The angle of electron incidence is smaller for the RHEED pattern during preparation. The length of the marker in Fig. 3.2(b) corresponds to the reciprocal lattice constant of bulk GaAs. The acceleration voltage is 10 kV.

Zigzag chains of As dimers extending along $[\bar{3}\bar{3}\bar{2}]$ are characteristic elements of the GaAs(113)A-(8x1) Wassermeier reconstruction as depicted schematically in Fig.3.3(a). The reconstruction comprises three atomic layers with an overall corrugation of 3.4 Å and exhibits the largest unit cell among the known GaAs reconstructions: 32.0 Å along $[\bar{1}10]$ and 13.3 Å along $[\bar{3}\bar{3}\bar{2}]$. The zigzag chains in the top and the middle layer are phase shifted by a quarter of the unit cell in the $[\bar{3}\bar{3}\bar{2}]$ direction. Between the middle zigzag chains in the (8x1) unit cell there is a trench containing As and Ga dangling bonds (DBs) from the third layer. The ECR applied to GaAs(113)A-(8x1) yields 16 Ga DBs, corresponding to an excess charge of +12 el, 20 As DBs (-15 el), and 6 As-As dimer bonds (+3 el). The sum is equal to zero. Thus, the structural model fulfills the ECR, and the

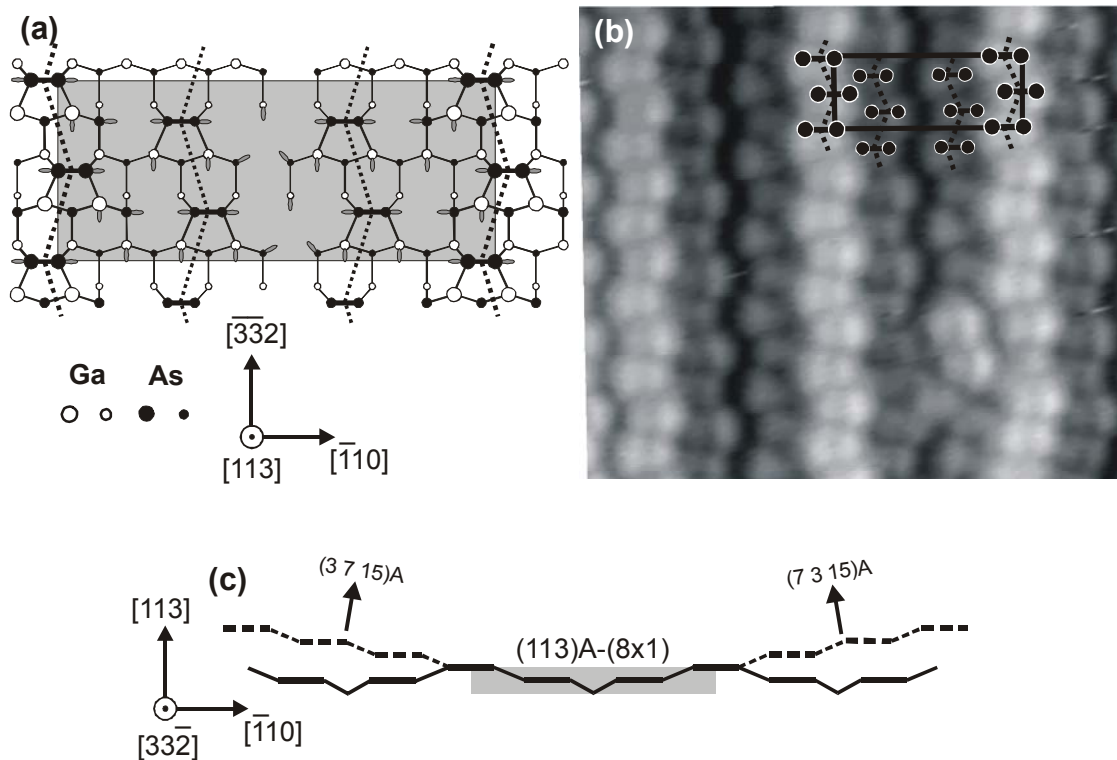


Figure 3.3 [Tem03b]: (a) Top view of the structural model for GaAs(113)A-(8 × 1). Atoms in the second and third layers are depicted with smaller circles. The As atoms in dimers are connected with black bars. The zigzag chains of As dimers are depicted with dotted lines; (b) atomically resolved STM image of GaAs(113)A-(8 × 1): the size of the image is (90 × 80) Å², sample bias voltage $U = -2.5$ V, sample current $I = 0.24$ nA. In the overlay As dimers are depicted with black circles and connected by dotted lines in accord with the structural model; (c) side view sketch of the structural model with {3 7 15}A surfaces arising on both sides of the (8x1) reconstruction. The horizontal black thick bars are assumed to contain both As dimers and Ga DBs from the same atomic layer.

surface has a semiconducting ground state. The bulk-truncated (113) surface exhibits $(\bar{1}10)$ as symmetry plane, but the (8x1) reconstruction suspends this symmetry. A small area STM image of GaAs(113)A is presented in Fig.3.3(b). We succeeded at the first time in atomically resolving the As dimers in the zigzag chains, i.e., the As dimers are imaged as two separated white clouds*. The overall corrugation measured from STM images is 3.0 ± 0.4 Å and the length of unit cell vectors is 32.5 ± 0.5 Å and 13.0 ± 0.5 Å, which nicely confirms the (8x1) reconstruction. Note that the surface, formed by continuously stacking of zigzag chains from middle to top to next top and so on, results in a (3 7 15)A surface [Gee02], two of which are schematically shown in Fig.3.3(c). Thus, not {331} surfaces tilted by 40.5° to (113)A but flatter {3 7 15}A surfaces tilted by only 9.7° contribute to the

* Because of the filled state STM imaging As derived features appear bright.

surface reconstruction. The $(3 \times 7 \times 15)_A$ -(1x1) reconstruction as well as its flat wafer will be considered in more detail in chapter 5.

In reference [Jac02] it has been shown that $\text{GaAs}(3 \times 7 \times 15)_A$ and $\text{GaAs}(2 \times 5 \times 11)_A$ surfaces appear as side facets of arrowhead-like depressions, surrounded by the (8×1) reconstruction. This could not be reproduced in the present study. (The difference may be due to the buffer layer that was 1800 Å in the former studies compared to 500 Å in this work.) Under the preparation conditions used here the surface consists of fairly small (8×1) terraces with many islands 8 ± 4 Å in height and $(120 \pm 50 \text{ Å}) \times (400 \pm 200 \text{ Å})$ in lateral dimensions, which are seen in Fig.3.4(a) as large white hills elongated in the $[\bar{3} \bar{3} 2]$ direction (one of them is marked by a black arrow). The stripes along $[\bar{3} \bar{3} 2]$ are due to the As-dimer zigzag chains. The density of the hills is $(3.7 \pm 1.5) \times 10^{10} \text{ cm}^{-2}$, which is of the same order of magnitude as the density of subsequently grown InAs QDs. Thus, these GaAs islands may act as nucleation centers for the InAs QDs: For the first few layers of InAs overgrowing the GaAs islands, strain relaxation on top of the island is more efficient than in a homogeneous InAs layer. This effect is similar to the strain-induced vertical stacking of InAs QDs on $\text{GaAs}(001)$ surface [Eis99], where the lattice of the embedding material is expanded around the buried dot. Therefore, the QDs in the next layer of the stack prefer to form at these areas of expanded substrate lattice.

A magnified STM image of a typical GaAs island is shown in Fig.3.4(b). On both sides of the island, $\{3 \times 7 \times 15\}_A$ facets develop along $[\bar{3} \bar{3} 2]$ by stacking of (8×1) As-dimer zigzag chains. A high-resolution STM image of one of the facets is shown in Fig.3.4(c). The facet is inclined to the $(113)_A$ substrate by $9 \pm 3^\circ$ and exhibits the unit cell vectors $a_1 = 13.2 \pm 0.3 \text{ Å}$ and $a_2 = 11.0 \pm 0.5 \text{ Å}$. (The geometrical values for the $\text{GaAs}(3 \times 7 \times 15)_A$ -(1x1) reconstruction projected onto the (113) plane are 9.7° , 13.3 Å and 10.5 Å , respectively.) The size of each facet is up to 100 unit cells. As the islands have a triangular shape, facets other than $(3 \times 7 \times 15)_A$ should develop as bounding facets. The $\{137\}_A^*$ and $\{2 \times 5 \times 11\}_A^{**}$ surfaces, whose intersection lines with the $(113)_A$ surface are tilted against $[\bar{3} \bar{3} 2]$ by 16.8° and 5.7° , fulfil this requirement and were actually found in this region, as shown in Fig.3.4(d). However, no long-range ordered areas of these surfaces were observed.

* The reader can find the model for this surface in [Mar01] and its surface free energy calculation in appendix 1.1 and 1.2.

** In chapter 5 we will consider this recently discovered surface [Gee01] in detail.

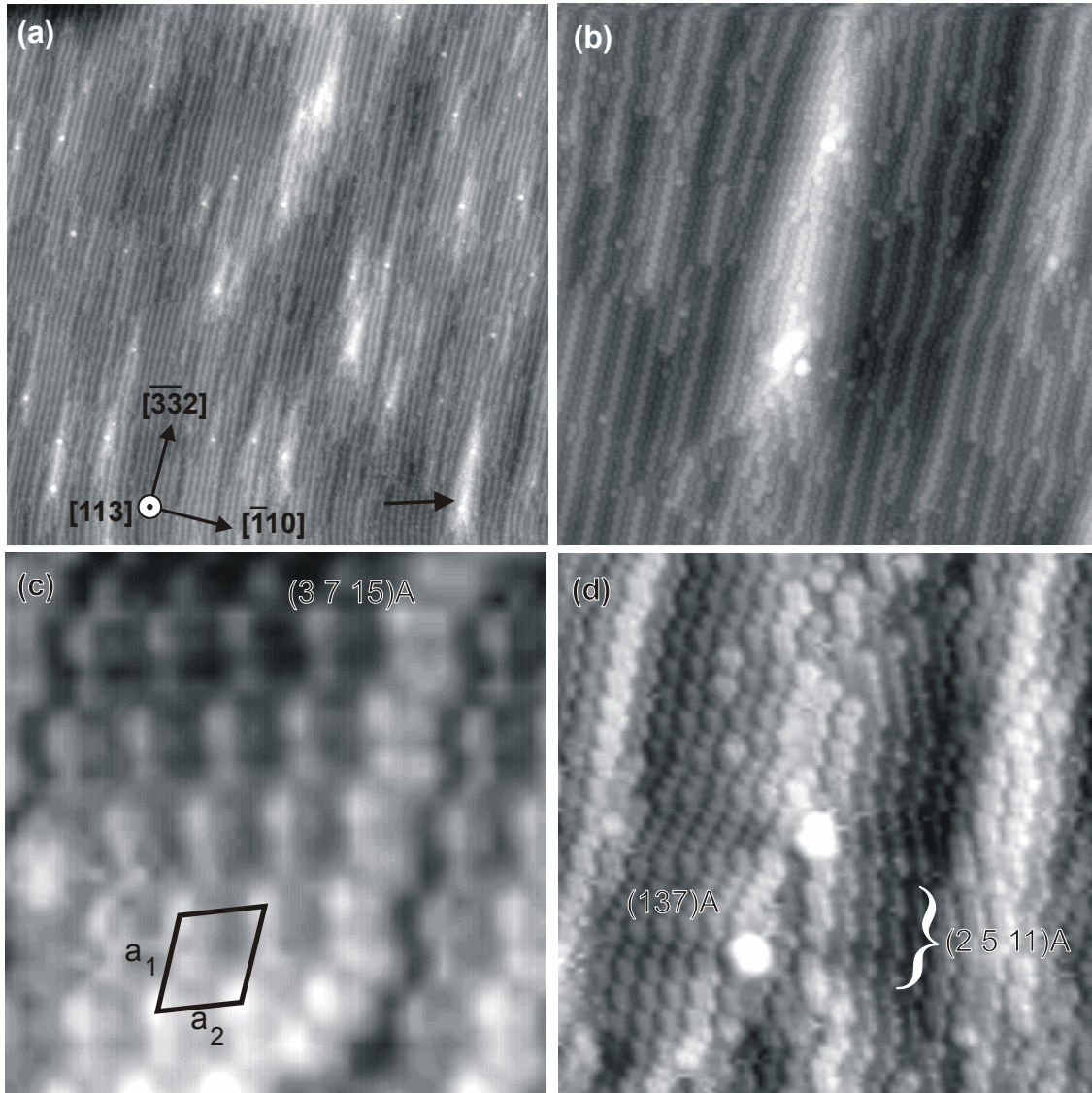


Figure 3.4 [Tem03b]: (a) Overview STM image of GaAs(113)A-(8×1): $(2620 \times 2620) \text{ \AA}^2$, $U = -2.5 \text{ V}$, $I = 0.16 \text{ nA}$; (b) High-resolution STM image of GaAs(113)A-(8×1) with a 3D GaAs island: $(685 \times 685) \text{ \AA}^2$, $U = -2.5 \text{ V}$, $I = 0.16 \text{ nA}$; (c) High-resolution STM image of the GaAs(3 7 15)A-(1×1) facet on the GaAs islands with the unit cell vectors: $(74 \times 74) \text{ \AA}^2$, $U = -2.5 \text{ V}$, $I = 0.16 \text{ nA}$; (d) High-resolution STM image of the spike of a GaAs island on GaAs(113)A-(8×1): $(230 \times 230) \text{ \AA}^2$, $U = -2.7 \text{ V}$, $I = 0.2 \text{ nA}$.

The appearance of high-index GaAs{3 7 15}A, {137}A, and {2 5 11}A surfaces on GaAs(113)A can not be explained by the surface free energy, because under As-rich conditions the respective values of 55 meV/ \AA^2 , 56 meV/ \AA^2 and 52 meV/ \AA^2 [cf. appendix 1.2] are greater than the value of 47 meV/ \AA^2 , which was calculated for the GaAs(113)A-(8×1) reconstruction [Pla99]. Probably, the shape of the GaAs islands is influenced by growth kinetics that was found to be very anisotropic on {113} surfaces [Was95, Gee99,

Lub98]. Finally, STM images in Fig.3.4 can account for the observed RHEED patterns in Fig.3.2. The periodicity of the As dimers in the zigzag chains along $[33\bar{2}]$ in Fig.3.4(b) extends over several hundred of angstrom, whereas it is difficult to find the unperturbed $8x$ periodicity on the scale up to 100 \AA . It is reflected in the much better order of RHEED pattern along $[\bar{1}10]$ than along $[33\bar{2}]$. Also, the small 3D GaAs islands may contribute to the additional dispersion of electron beam, giving rise to rather diffusive GaAs(113)A patterns. The 3D GaAs islands are considered to be small in size to cause the appearance of clearly spotty RHEED pattern that is characteristic for mature large QDs.

3.5 InAs (or $\text{In}_x\text{Ga}_{1-x}\text{As}$) QDs on GaAs(113)A grown by MBE: a literature survey

The initial stage of InAs growth on GaAs(113)A was studied by Ilg et al. [Ilg93]. *In situ* RHEED showed the morphology of the surface to transform from corrugated (reported by the same group [Noe91]) to flat during InAs deposition of only 0.06 monolayer (ML) of InAs(001). Thereby, the satellite peaks (splitting) of the zeroth-order streak were no longer visible, only the bulk streaks remained. From that study the authors assigned GaAs(113)A to be a very appropriate substrate for the production of low-dimensional heterostructures: if one deposits AlAs, the surface remains corrugated, resulting in the quantum wires; but if one deposits InAs, the surface becomes flat and can be used for self-organized In-containing structures, like QDs. Contrary to that result, an increasing roughness of GaAs(113)A appeared by $\text{In}_{0.5}\text{Ga}_{0.5}\text{As}$ deposition as reported by Vaccaro et al. [Vac96, Vac97]. The surface observed by AFM showed corrugated nanostructures like quantum wires along the $[33\bar{2}]$ direction with a period of 350 \AA . However, the temperature dependence of the radiative recombination time indicated that excitons were confined not in a 1D but in a 0D potential (QDs). The authors attributed this to the lack of uniformity along the wire-like structure that might produce a potential modulation large enough to confine carriers in zero dimensions. In addition, a delay of the SK transition (beyond which 3D QDs appeared) on GaAs(113)A as compared to the (001)-oriented samples by the deposition of the same amount of $\text{In}_{0.5}\text{Ga}_{0.5}\text{As}$ was reported.

$\text{In}_{0.5}\text{Ga}_{0.5}\text{As}$ QDs of superior quality with a full width at half maximum (FWHM) of the photoluminescence signal of only 13 meV were observed in references [Hay98, Pol98, Sto98]. The dot size was between 50 and 80 \AA with a dot density of $4 \cdot 10^{11} \text{ cm}^{-2}$ as measured by AFM.

Henini et al. [Hen97] noticed a very broad InAs island size distribution by deposition of 1.7 ML of InAs on GaAs(113)A. Multimodal sizes with a mean value of 358 Å and a deviation of 97 Å was observed using *ex situ* STM and was reflected in the structured PL spectrum, whose integrated intensity was comparable with the QDs on commonly used GaAs(001). In contrast, Fortina et al. [For98] showed a very narrow (~25 meV) FWHM by the 1.7 ML InAs QDs. The emission energy of such QDs was higher than for (001) reference dots, reflecting the smaller QD size. As the amount of deposited InAs was increased to 2.2-2.7 ML, the PL efficiency dropped by as much as 100 times with simultaneous broadening of PL spectra. It was assumed, that the QDs could reach a maximum size before the onset of coalescence between dots with formation of grain boundaries and dislocations able to reduce the number of luminescent dots.

Henini et al. [Hen98] found that 1.7 ML InAs QDs exhibited a nonconventional, faceted, arrowhead-like shape, aligned in the $[33\bar{2}]$ direction (however without determination of this shape). A scenario of QD formation was proposed in the same paper based on the corrugated model for GaAs(113)A reported by [Noe91]. By measuring the polarization dependence of the optical transitions the authors showed that the QDs acted as polarized emitters with a ~13 % fraction of the total intensity polarized along $[33\bar{2}]$. Such an effect made the InAs QDs on GaAs(113)A promising candidates for polarization sensitive applications as magneto-optic disc memory devices.

On the contrary to almost all above-mentioned papers Lobo and Leon [Lob98] reported on InAs QDs with a low density of only $7.4 \cdot 10^8 \text{ cm}^{-2}$ after deposition of 18 Å (6 ML) of $\text{In}_{0.6}\text{Ga}_{0.4}\text{As}$. By means of AFM the small islands were determined to be lens shaped, while the large ones were faceted and elongated along $[33\bar{2}]$. The authors concluded that both types of islands might be incoherent. In contrast to this, Xu et al. [Xuh98] demonstrated, not only by means of AFM but also by the linear dependence of PL intensity on the excitation power, high crystal quality and defect-free nature of InAs QDs on GaAs(113)A. Opposite to the QD ensemble reported in reference [For98], Xu et al. showed a quite broad size distribution for 1.5 ML InAs QDs, which was actually bimodal.

Important information was provided by Sanguinetti et al. [San99] by means of *ex situ* STM and PL. The authors showed that a stable and reproducible polarization of the emission from InAs/GaAs QDs could be obtained only using (113)A oriented substrates. On others surfaces polarization fluctuation, both in magnitude and direction, had been observed. Moreover, on (113)A, the polarization ratio and direction was independent on the

coverage, i.e., on the dot size. An estimate of the mean size of 1.7 ML InAs QDs gave a length of 300 Å along $[3\bar{3}\bar{2}]$, a height of 50 Å, and a width of 100 Å along $[\bar{1}10]$. These data clearly indicated, that the observed polarization ratio $\rho=(I_1-I_2)/(I_1+I_2)=0.12\pm 0.03$, where I_1 and I_2 corresponded to the PL intensity along $[3\bar{3}\bar{2}]$ and $[\bar{1}10]$, respectively, was only possible on the QDs with a significant larger length than a width. In a later paper [San00] this group did not observe the SK transition using AFM and *ex situ* STM following $\text{In}_{0.5}\text{Ga}_{0.5}\text{As}$ deposition on GaAs(113)A, which disagreed from earlier results [Vac96, Vac97, Hay98, Pol98, Sto98].

As can be seen from this literature survey, the faceted shape of the InAs (or $\text{In}_x\text{Ga}_{1-x}\text{As}$) QDs has not been discovered, because nobody has used for this purpose *in situ* STM. The elongation, observed by several groups, is explained mainly with the Nötzel model for GaAs(113)A [Noe91], that was shown in the chapter 3.4 to be incorrect, at least under the preparation conditions, used in this study. We note that nearly simultaneously with our paper [Tem03] (but a month later) the group of G. Salamo (USA) [Wan03] submitted a paper to Applied Physics Letters, whose results on the shape of InAs QDs were in broad agreement with ours, presented in the next section.

3.6 InAs QDs on GaAs(113)A : our own results

Preparation conditions for the InAs deposition are described in chapter 2.9. In contrast to [Ilg93] we state that the GaAs(113)A surface becomes more corrugated and even disordered when depositing InAs. The large-area STM image of the InAs wetting layer (WL) on GaAs(113)A in Fig.3.5(a) reveals that the large white hills elongated along $[\bar{3}\bar{3}\bar{2}]$ still remain, but that the density decreases to $< 10^{10} \text{ cm}^{-2}$ and the height and lateral dimensions are less well defined. An atomically resolved STM image in Fig. 3.5(b), acquired from the WL between the white hills, shows the disappearance of any flat region on the surface. Poorly ordered small 3D arrowhead-like hills develop instead of the original (8×1) reconstruction. The large and small 3D hills are pointing along $[\bar{3}\bar{3}\bar{2}]$ with walls built up from a mixture of $\{3\bar{7}15\}\text{A}$, $\{2\bar{5}11\}\text{A}$, and $\{137\}\text{A}$ surfaces.* (In Fig.3.5(c) a $(137)\text{A}$ facet is shown.) The reason for the strong undulation of the WL is probably that the strain in InAs is partially relaxed at the 3D hills so that a surface rich of hills may be

* A similar behavior of the WL was observed by depositing $\text{In}_{0.5}\text{Ga}_{0.5}\text{As}$ onto GaAs(113)A [Vac96]. The QD like 0D potential reported there might be caused by these large hills since the arrowhead shape limits them.

favorable for the growth of an InAs adlayer. Also, from the surface-energy point of view, covering the GaAs surface by InAs is favorable since the surface free energy of InAs(3 7 15)A, (2 5 11)A, and (137)A is 42, 41, and 44 meV/ Å², respectively, i.e., lower than the respective values for GaAs [cf. appendix 1.2 and 1.3]. This property certainly favors, at least at the beginning, a smoothly following of every substrate roughness. However, no long-range ordered areas of these surfaces were observed after InAs deposition. Overall, the WL exhibits a rather chaotic morphology.

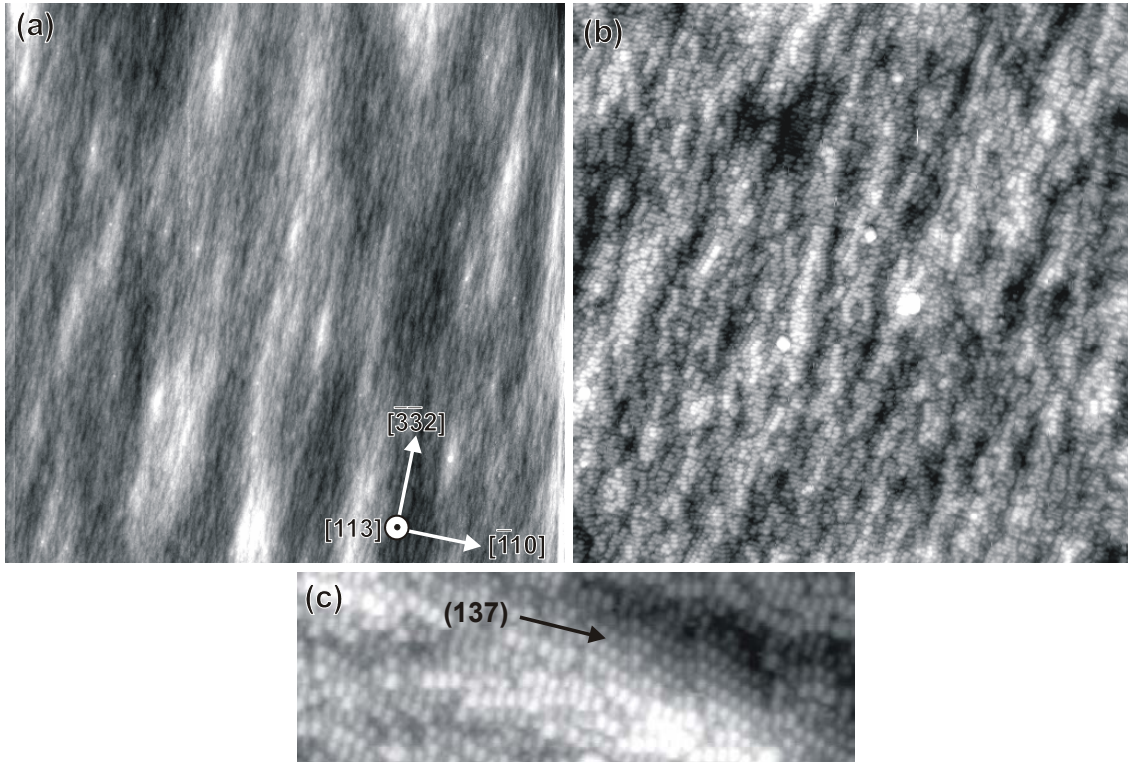


Figure 3.5 [Tem03b]: STM images of the InAs WL on GaAs(113)A. The thickness of deposited InAs is 1.1 ML; (a) (4000 × 4000) Å², U = -3.0 V, I = 0.5 nA; (b) (1000 × 1000) Å², U = -3.0 V, I = 0.2 nA; (c) turned by 90° with respect to (a) and (b) (480 × 165) Å², U = -3.0 V, I = 0.2 nA.

Fig. 3.6(a) shows an STM image with InAs QDs grown on GaAs(113)A. The critical thickness at which the 3D QDs are formed (established with RHEED) at 450 °C is 1.5 ± 0.2 ML. The fairly broad size distribution (shown in Fig. 3.6(b)), the arrowhead-like shape of many islands, and the large number of nuclei are apparent. The measured QD length along $[33\bar{2}]$ lies between 300 and 600 Å, with a peak of 35 % at 375 ± 25 Å. The mean height is 60 Å and the overall number density is 9.5×10^9 cm⁻². The highly disordered, undulating morphology on the (113)A surface before the SK transition exhibits a very inhomogeneous

strain distribution. The large hills protruding from the WL, observed in Fig. 3.5(a), can be considered as QD nucleation places since in the 3D structures InAs can better relax than in such a 2D film. As these hills exhibit largely varying lateral dimensions, the strain relieve may be different, implying different times for nuclei formation. This is evidently seen in Fig. 3.6(a), where side by side with mature QDs small nuclei emerge. In addition to that, the QD growth process may proceed with different rates on different places, because of the non-uniform strain and therefore, non-uniform flux of InAs from the WL to the islands. Thus, the morphology of the bare GaAs substrate and subsequently grown InAs the WL may account for the observed broad size distribution of QDs. Since the nucleation and growth processes occur inhomogeneously, the GaAs(113)A substrate offers a unique opportunity to retrace the kinetics of the QD growth from the nucleus through an intermediate size to the final elongated QDs.

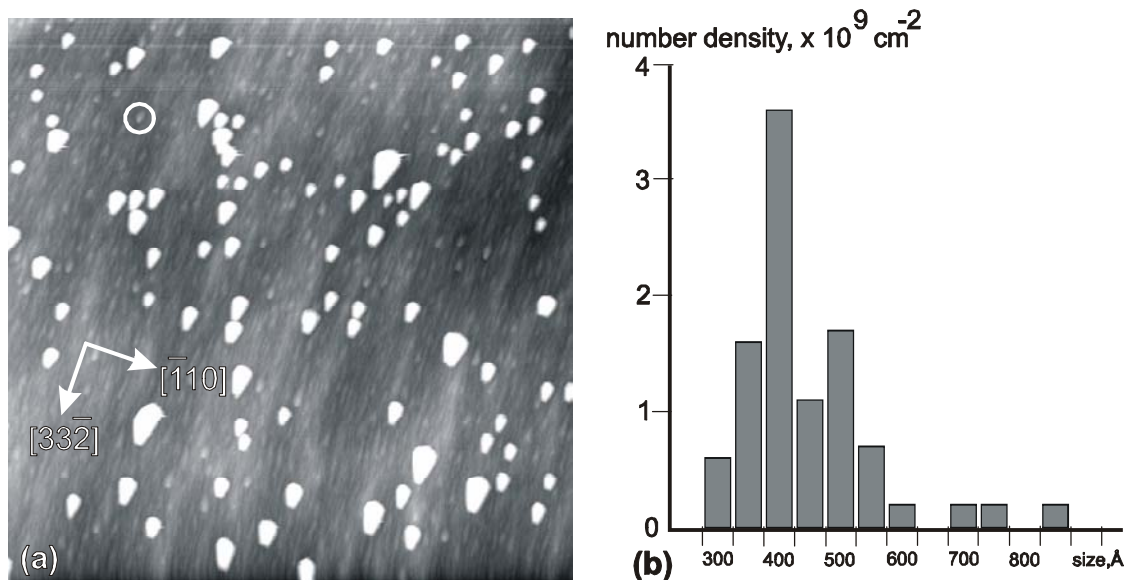


Figure 3.6 [Tem03] (a) Overview STM image with InAs QDs grown on GaAs(113)A. White circle indicates a nucleus. The size is $1 \mu\text{m} \times 1 \mu\text{m}$. $U = -3 \text{ V}$, $I = 0.1 \text{ nA}$; (b) Column diagram of the length of the InAs QDs along $[3,3, -2]$ distributed to different QD number densities.

Figure 3.7(a) shows an STM image of a typical nucleus (its 2D version is presented in Fig. 3.7(b)). The exact azimuthal directions on the substrate were determined from the atomically resolved wetting layer as well as from wafer manufacturer data. The nuclei have a triangular shape elongated towards $[\bar{3}\bar{3}2]$ with the height up to 13 \AA . The bounding facets are inclined to the substrate by $8 \pm 4^\circ$ and exhibit the stripe-like structure with the width of three As dimers, that is characteristic for the $\{2\ 5\ 11\}$ A surfaces [Gee01] (the

geometric angle between $\{2\ 5\ 11\}$ and (113) planes is 10.0°). However, the $\{2\ 5\ 11\}$ A facets coexists with the (137) A areas, as wider stripes up to six As dimers are also seen on the nucleus in Fig. 3.7(a). Thus, the QDs start to grow with very flat, low-energy surfaces, e.g., $\{2\ 5\ 11\}$ A or (137) A. Since the later developing QDs are elongated along the opposite $[3\bar{3}\bar{2}]$ direction a shape transition should occur with appearance of facets different from that on the nuclei.

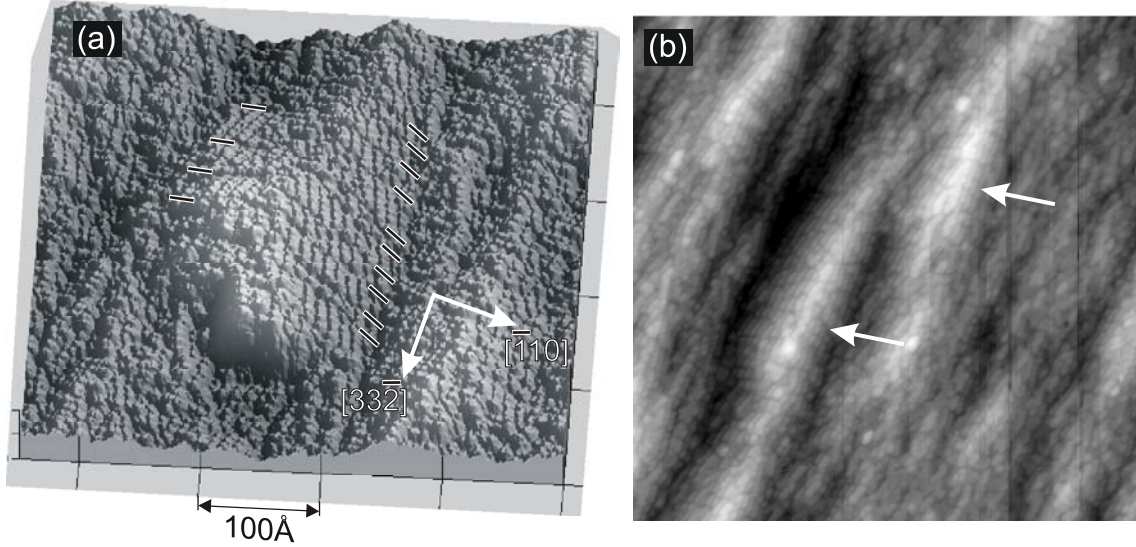


Figure 3.7 [Tem03b] (a) 3D STM image of a QD nucleus grown on GaAs(113)A: $(440 \times 440) \text{ \AA}^2$, $U = -3.0 \text{ V}$, $I = 0.1 \text{ nA}$. The stripes of $\{2\ 5\ 11\}$ A facets are indicated by the bars at the nucleus foot; (b) 2D version with two nuclei, indicated by white arrows: $(750 \times 750) \text{ \AA}^2$, $U = -3.0 \text{ V}$, $I = 0.184 \text{ nA}$.

It is fascinating, how perfect crystalline islands form on a disordered WL on the GaAs(113)A surface shown in Fig. 3.5(b). Figure 3.8(a) presents an STM image of a typical InAs QD with a height of 45 \AA . This QD adopts an intermediate size between the nucleus and the elongated island in the final growth state (see below). The QD exhibits mirror symmetry with respect to the $(\bar{1}10)$ plane perpendicular to the (113) A substrate plane along $[3\bar{3}\bar{2}]$ as the bulk-truncated substrate. The island comprises two symmetrical facets 1, a frontal facet 2, two small facets 3 on the summit and a rounded region 4.

The facets 1 shown in Fig. 3.8(b) are identified to be $\{110\}$ planes from following STM measurements: The facets are inclined to the (113) A substrate by $29 \pm 4^\circ$ and exhibit the unit cell vectors $u_1 = 3.8 \pm 0.2 \text{ \AA}$ and $u_2 = 5.5 \pm 0.2 \text{ \AA}$. The geometrical values for the InAs(GaAs) $\{110\}$ surface projected to (113) are 31.5° , $u_1=3.9 (3.6) \text{ \AA}$ and $u_2=5.8 (5.4) \text{ \AA}$,

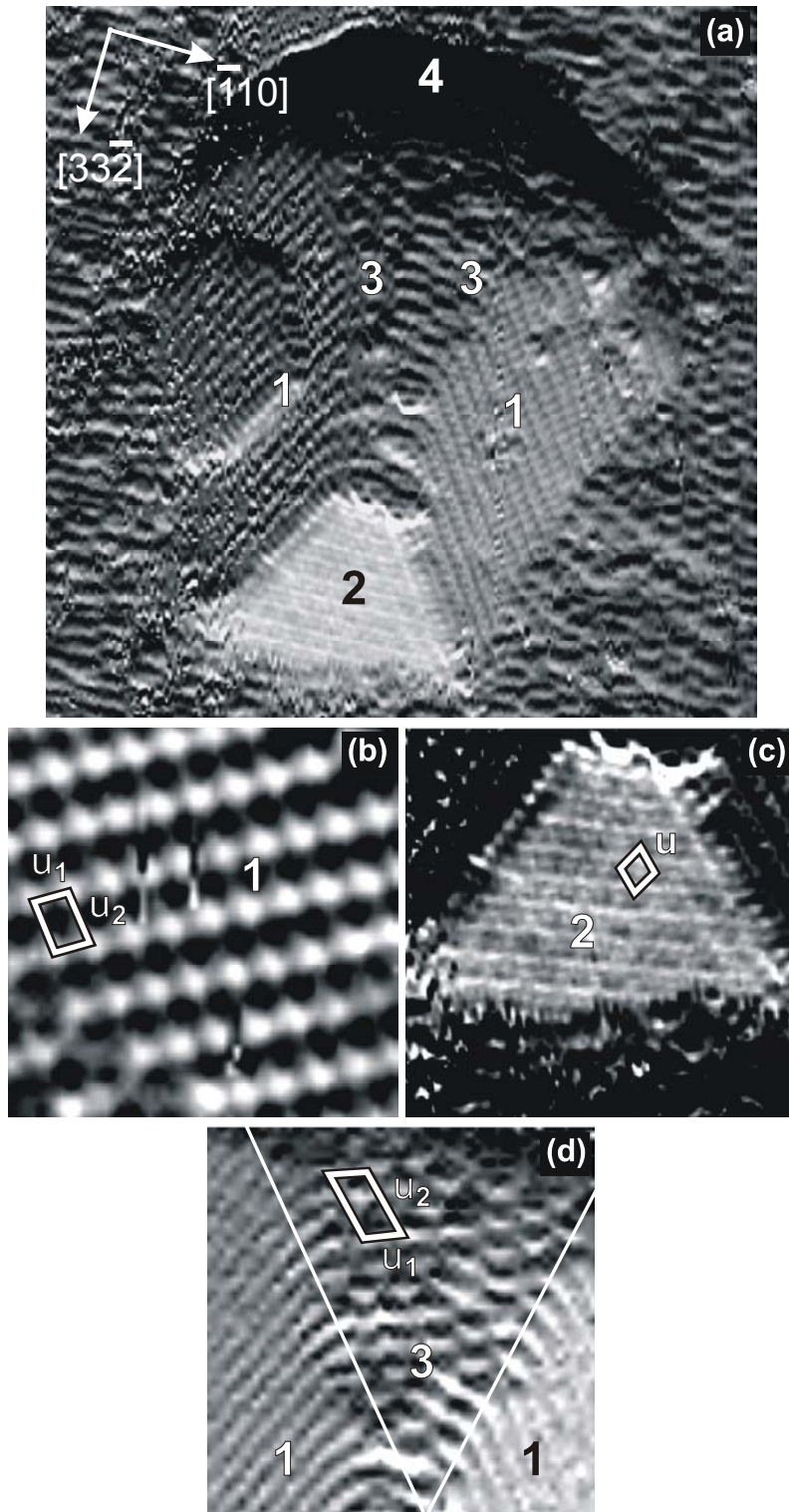


Figure 3.8 [Tem03] Atomically-resolved STM images (error signal \equiv constant height mode) of (a) a QD on GaAs(113)A with four characteristic regions: $(283 \times 283) \text{ \AA}^2$, $U = -3V$, $I = 0.322 \text{ nA}$; (b) the (011) or (101) facet: $(37 \times 37) \text{ \AA}^2$, $U = -3.1 V$, $I = 0.135 \text{ nA}$; (c) the (111)A-(2x2) reconstructed facet: $(98 \times 98) \text{ \AA}^2$, $U = -3V$, $I = 0.322 \text{ nA}$, and (d) $\{2 \ 5 \ 11\}$ A-(1 \times 1) reconstructed facets on the summit of the QD: $(110 \times 110) \text{ \AA}^2$, $U = -2.5V$, $I = 0.33 \text{ nA}$.

respectively. It is interesting to note that on the left facet 1 in Fig. 3.8(a) (on the (101) surface) a 2D embryo one ML high expands from the middle of the facet to the bottom. A nucleation site at the bottom edge was calculated to be of the highest strain energy, so that the InAs material must be strongly compressed before incorporation into the QD crystal [Jes98, Mol98]. This quite general model obviously does not apply here. The observation of such an island further indicates that the (110) facets grow rather slowly otherwise a full facet layer would have been developed during shutting off the Knudsen cells.

The triangular facet 2 shown in Fig. 3.8(c) is a (111)A-(2×2) reconstructed surface as derived from following measurements: It is inclined to (113)A by $26\pm 4^\circ$ and exhibits a rhombic unit cell with the vector $u=8.0\pm 0.4 \text{ \AA}$. Geometrical values for the In(Ga) vacancy buckling model of the (111)A-(2×2) reconstruction [Ton84, Cha84] are 29.5° and $u=8.6$ and 7.8 \AA ($8.2\pm 0.4 \text{ \AA}$ in the following) ($7.6\pm 0.4 \text{ \AA}$, GaAs). The filled state STM image in Fig.3.8(c) is also very similar to that acquired from the planar GaAs(111)A-(2×2) surface [Oht01]. The facets 3 on the summit of the island (Fig.3.8(d)) are $\{2\ 5\ 11\}$ A reconstructed surfaces as extracted from the following measurements: The angle to the substrate and the lengths of the unit cell vectors are $7\pm 3^\circ$, $u_1=11.5\pm 0.5 \text{ \AA}$ and $u_2=21.7\pm 1.0 \text{ \AA}$, respectively. The geometrical values for the InAs(GaAs) $\{2\ 5\ 11\}$ A-(1×1) reconstruction [Gee01, Gee02] are 10.0° , $u_1=11.3$ (10.5) \AA and $u_2=20.2$ (18.8) \AA . The small $\{2\ 5\ 11\}$ A facets are residual elements that vanish when the QD achieves the final elongated shape.

The region 4 in Fig. 3.8(a) exhibits a complex structure that on the intermediate-size islands appears to be rounded. From geometrical considerations, the (001) surface, that is inclined to (113)A by 25° , should develop in this area. The sphere-like shape of the region 4 may be caused by the preferential migration of In atoms from all directions, i.e., from the slower growing $\{110\}$ and (111)A facets and the (113)A substrate to the faster growing (001) surface [Yam99, She95, Noe96] that might develop at some initial moment during the formation of the island. Then the (001) surface transforms into the symmetrical vicinal (001) stacking giving rise to the round shape, that prevents us from acquiring atomically resolved STM images.

Sanguinetti et al. [San98, San99] concluded by the measurement of the PL polarization emission that the InAs QDs retained the same length/width ratio (about 3) while changing the size. This could not be reproduced in our study. Figure 3.9(a) shows a length/width ratio distribution of the InAs QDs measured from STM images with atomic resolution. The quite broad distribution exhibits a maximum of $\sim 34\%$ for the ratio equal to 1.3. This peak

we assigned to the intermediate size of the QDs (one of them is shown in Fig. 3.8(a)). All other islands tend to be elongated, achieving the length/width ratio of 1.4-2.4 and adopting a final shape shown in Fig. 3.9(c) (with ratio equal to 2.3). In comparison to the intermediate size QDs there is a drastic reduction in size of the (111)A facet (the length of the edge between (111)A and (113)A decreases from (116 ± 30) Å for the intermediate size QD to (60 ± 20) Å for the elongated QDs). The islands with the atomically resolved rounded region 4 undergo in addition a partial flattening with appearance of (113)B facets. Such a development means that – from one moment on – In and As are incorporated mainly at (111)A so that (111)A becomes smaller owing to geometrical reasons while long $\{110\}$ surfaces are formed on both sides of the island. Also, the $\{2\ 5\ 11\}$ A facets expected at the summit are largely reduced in size. Note that our elongated islands did not reach a ratio of 3, reported for the coherent QDs in [San99], i.e., they are expected to be coherent as well.

Why is an elongation scenario realized instead of proportional growth of the intermediate shape shown in Fig. 3.8(a)? We believe that generally the (001) facet grows with the largest rate as reported in experiments of simultaneous growth of low-index surfaces on patterned GaAs substrates [Yam99, She95, Hir99, Kis00], whereas other facets on the QDs on GaAs(113)A grow rather slowly. The growth rate of the rounded region is certainly further increased by the high step density on the vicinal (001) surface*. When the islands adopt the final shape elongated along $[3\bar{3}\bar{2}]$ (Fig. 3.9(c)), the vicinal (001) region partially transforms in two flat surfaces, that were identified to be $(\bar{1}\bar{1}3)B$ and $(1\bar{1}\bar{3})B$. They are well connected with the $\{110\}$ facets as shown in Fig. 3.9(b). The $(\bar{1}\bar{1}3)B$ or $(1\bar{1}\bar{3})B$ surface is inclined to (113)A by $40\pm 5^\circ$ and exhibits the unit cell vectors $u_1=4.1\pm 0.2$ Å and $u_2=13.0\pm 0.3$ Å. The geometrical values are 35.1° , $u_1=3.9$ (3.6) Å and $u_2=13.7$ (12.8) Å. Note that these values correspond to the bulk-truncated InAs(GaAs) $(\bar{1}\bar{1}\bar{3})B-(1\times 1)$ surface (with respect to the face-centered rectangular unit cell). However, the (2×1) reconstruction with In dimers on the surface instead of the (1×1) reconstruction cannot be excluded, because the In dimers should be invisible in filled-state images.

* Actually, the elongation of the QDs (beyond the ratio 1.3) can also proceed by the growth of only (001) region but in that case the size of the (111)A facet would not diminish.

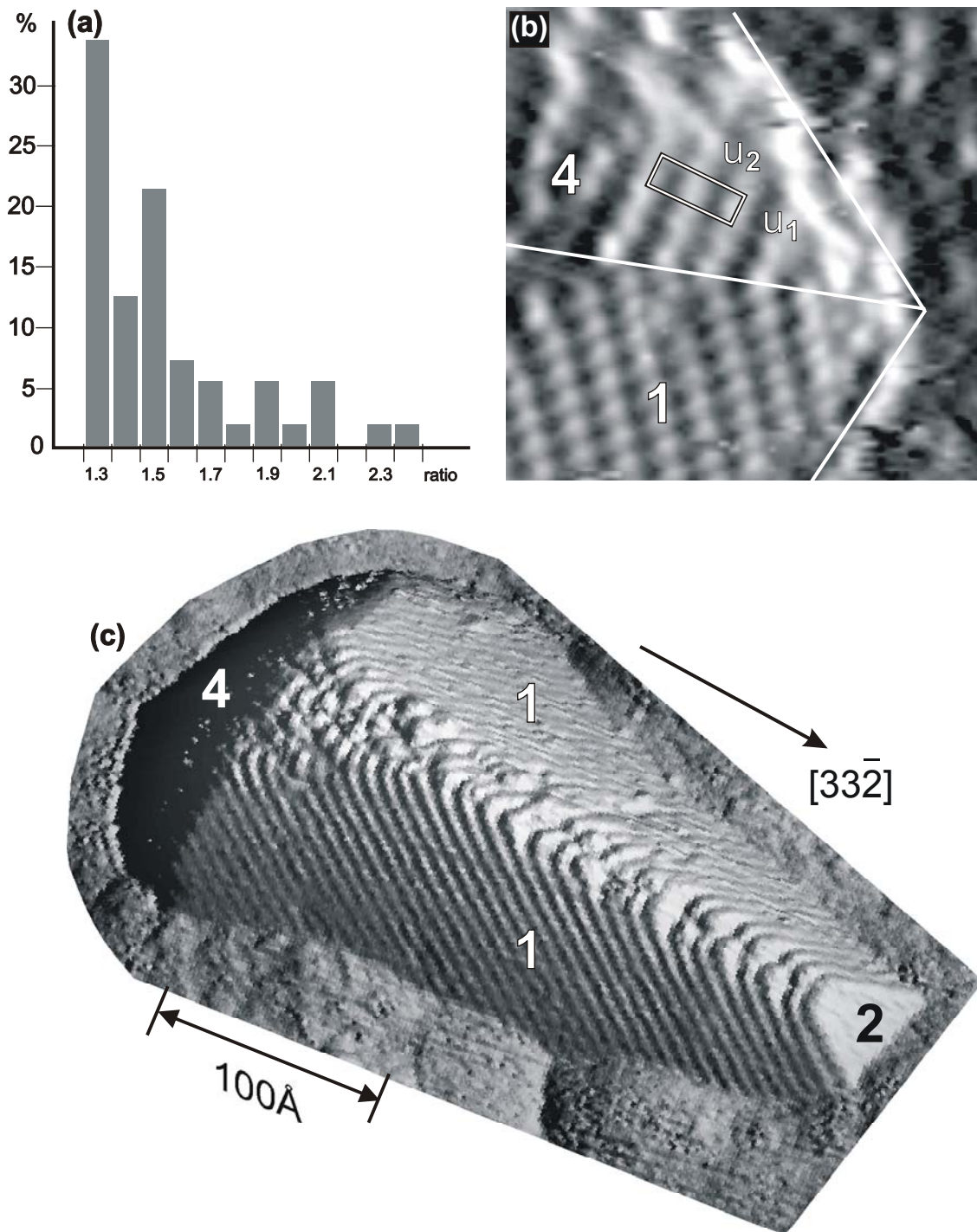


Figure 3.9 [Tem03] (a) Column diagram for the ratio of the length along $[3,3,-2]$ divided to the width along $[-1,1,0]$ in percent of all measured InAs QDs on GaAs(113)A; (b) the border between the (011) and the $(-1,1,3)B-(1 \times 1)$ facet: $(63 \times 63) \text{ \AA}^2$, $U = -3.1 \text{ V}$, $I = 0.135 \text{ nA}$; (c) 3D STM image of an elongated InAs QD grown on GaAs(113)A: $U = -2.5 \text{ V}$, $I = 0.33 \text{ nA}$.

Opposite to the epitaxy on GaAs(001), where the As₂ molecules can adsorb without being dissociated, i.e., can be incorporated as As dimer [Kra02], for the growth of GaAs(113)B, the As₂ molecules must always be dissociated [Suz02]. Very likely, the occurrence of (113)B facets decreases the growth rate at the rounded region strongly since breaking As-As bonds requires some additional energy. Furthermore, the {110} and (113)B surfaces seem to fit very smoothly at the edge between them (see Fig.3.9(b)) that may decrease the probability to form an embryo in this region and therefore, may also decrease the growth rate of the {110} facets. Owing to the – with respect to $[\bar{1}10]$ – larger diffusion length in the $[3\bar{3}\bar{2}]$ direction [Noe97] the In atoms are then incorporated mainly at the (111)A facet whose edge with the (113)A substrate also allows the incorporation of As₂ molecules without dissociation. This is indicated schematically in Fig. 3.10: In our model two In atoms are adsorbed at the edge whereby an As-dimer bond is broken. These two In atoms together with two In atoms from the (111)A facet can bond an As₂ molecule without dissociation as a new dimer. This dimer may be broken up by further In atoms and a new layer on the (111)A facet starts to grow. During further growth the (111)A facet decreases in size and induces even faster growth rate due to the reduction of energy barrier to complete the facet [Jes98]: As shorter the length of the edge between (113)A and (111)A as smaller is the strain and as easier is the growth of the next layer of the (111)A facet. The QD adopts the elongated shape*.

We note that very large $\{2\ 5\ 11\}$ A facets were observed on top of the InAs QDs on GaAs(113)A by Wang et al. [Wan03]. We believe that this only difference with our results is in the different As₂ pressure, which was larger by an order of magnitude in [Wan03]. The surface free energy of the InAs(110) cleavage plane (41 meV/ Å², cf. [Wan99]) is independent of the chemical potential of As₂ whereas the surface energy of the GaAs(2 5 11)A-(1x1) reconstruction increases towards Ga-rich conditions (cf. appendix 1.3). This means that — similar to the GaAs surfaces — the difference between energies of both surfaces was larger in the present study and therefore, the InAs(2 5 11)A facets vanished from the QDs leaving behind the InAs{110} facets. Our results support the idea that both kinetics and thermodynamic energetics control the growth of the QDs.

* Note that this mechanism may account only for the elongation of the QDs but not for the broad size distribution. After the island becomes elongated it can further grow with the rates depending on the inhomogeneous strain distribution in WL, which then results in the broad size distribution.

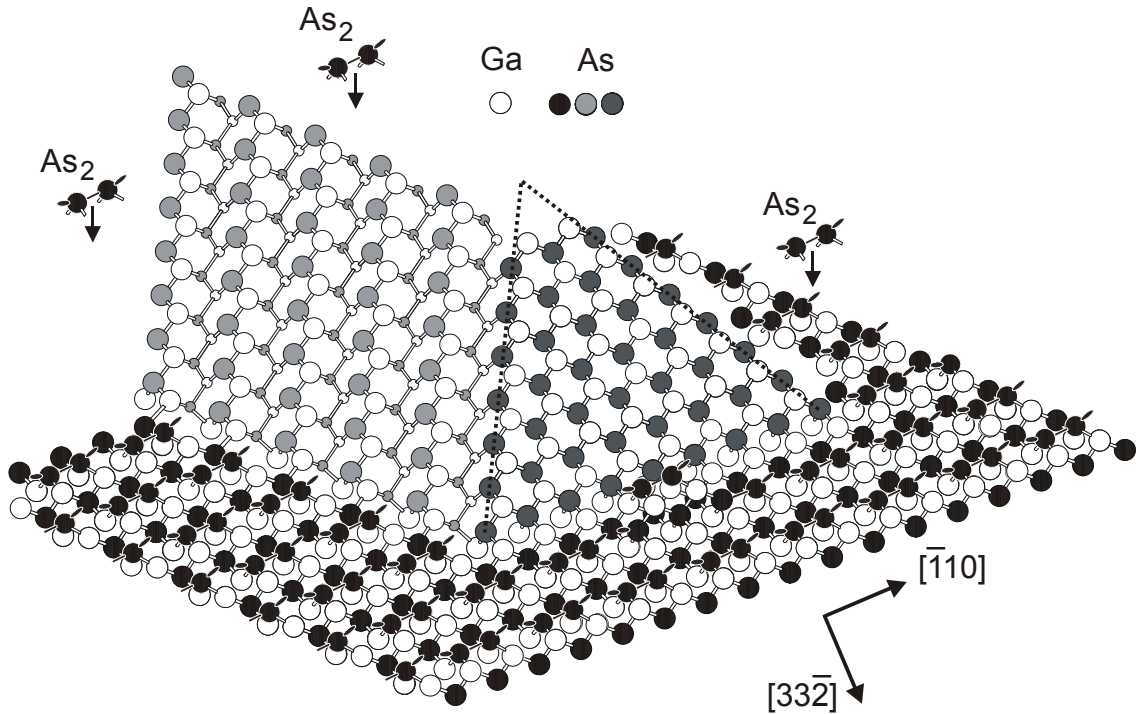


Figure 3.10 [Tem03b] Ball-and-stick model of one corner of the InAs QD grown on GaAs(113)A. The As atoms are marked in different gray scales: black for the (113)A substrate, dark gray for the (111)A facet of the QD and light gray for the (101) facet of the QD. A first growth nucleus at the edge between the (113)A substrate and the (111)A facet is drawn. The edges between (111)A and $\{110\}$ facets are depicted by dotted lines.

3.7 Conclusion

Our results are summarized in Fig.3.11. Depending on growth stage, we observe two QD shapes, which differ in relative facet sizes but not in symmetry and azimuthal orientation. In the early stage of the growth, the shape of the InAs QDs is given by $\{110\}$ and (111)A bounding facets, $\{2\ 5\ 11\}$ A facets at the summit and a rounded region, probably due to a stacking of vicinal (001) surfaces (see solid line). Later in the growth, the QDs become elongated along $[33\bar{2}]$ with a size reduction of the (111)A facet induced by a partially flattening of the rounded region (see dotted line) by (113)B facets which obviously slow down the growth rate in this region. Thus, we do not attribute the arrowhead-like shape to faceting of the GaAs(113)A surface [Hen98] but to facet growth kinetics.

The morphology and atomic structure of the wetting layer seems to have an important influence on the QD formation process. The intrinsic undulation of the GaAs(113)A surface becomes much more pronounced with depositing InAs. As the roughness exhibits largely varying lateral dimensions, the strain relieve is different implying different times

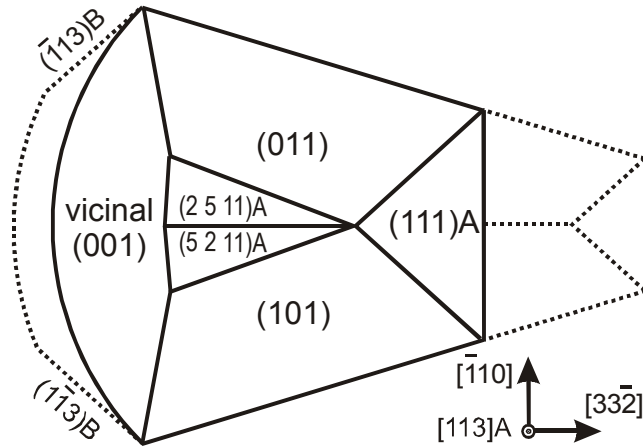


Figure 3.11 [Tem03] Shape of InAs QDs on GaAs(113)A derived from STM measurements. The solid line represents the QD shape briefly after the SK transition; the dotted line shows elongated QDs after further growth.

for nuclei formation. The QD growth process after the SK transition may also proceed with different rates on different places, because of the non-uniform strain and therefore, non-uniform flux of InAs from the WL onto the islands. Thus the morphology of the bare GaAs substrate and the subsequently grown InAs WL is responsible for the observed broad size distribution of QDs. Since the nucleation and growth processes occur inhomogeneously on GaAs(113)A we can retrace the elongation kinetics of the QDs as well as show that the islands start to grow with the very flat $\{2\ 5\ 11\}$ A and (137) A facets.

Generally, it is interesting to note that low-index facets develop on high-index GaAs(113)A and vice versa on low-index GaAs(001) [Mar01]. Also, the symmetry of the QDs derives directly from the ideal unreconstructed substrate, which unambiguously proves epitaxial growth. Taken at all, the GaAs(113)A is not an excellent substrate for producing of the QDs because of their broad size distribution and a simple turn of the (113) wafer from the A-to the B-side can yield much better QD ensembles as will be shown in next chapter.

4 InAs quantum dots on GaAs(113)B

4.1 Introduction

Early publications of our group based on *in situ* STM observations have shown that the GaAs(113)B surface is not a simple mirroring of the surface structure known from GaAs(113)A [Mar00, Mar02, Jac02]. Firstly, for the B face one should distinguish between As and Ga rich reconstructions; secondly, the morphology of GaAs(113)B is rather smooth for both reconstructions and differs largely from those on the A face, shown, e.g., in 3.4. The latter means that GaAs(113)B is a suitable substrate for QD growth. Indeed, the community has reported on InAs (or $\text{In}_x\text{Ga}_{1-x}\text{As}$) QDs grown on GaAs(113)B with even better optical properties than on the commonly used GaAs(001) substrate, e.g., with smaller PL linewidth (FWHM) and larger integrated intensity [Nis96, Pol98a, For98]. In addition, an ordering alignment of $\text{In}_x\text{Ga}_{1-x}\text{As}$ QDs with In content $x < 0.5$ occurs only on GaAs(113)B but not on other stable surfaces [Xuh99, Kaw99]. All these facts make an attempt to study QD formation on the B face very important. InAs QDs have been investigated using atomic force microscopy [Nis96, Guo98, Guo99] or *ex situ* STM from decapped samples [Hen97, San99]. A more or less rounded shape has always been observed. Thus, the intrinsic faceting of the QDs that occurs on all substrates has not been established for this system, and Miller indices of single bounding facets of the InAs QDs on GaAs(113)B have not been reported before our paper. Also, to our knowledge there is no report on any *in situ* STM investigation for (113)B substrates until now. We prepared here InAs QDs on GaAs(113)B MBE and acquired *in situ* atomically resolved STM images of the QDs. A motivation for this work was to compare the development of islands on A and B faces with atomic resolution and to obtain an important information, that is still missing in the literature, namely the dependence of the shape, size and size distribution of InAs/GaAs(113)B QDs on sample temperature. Note that the leading author for this investigation has been Dr. Takayuki Suzuki.

4.2 The bare GaAs(113)B surface and InAs (or $\text{In}_x\text{Ga}_{1-x}\text{As}$) QDs on it: a literature survey

The atomic structure of the B-polar (113) GaAs surface prepared by ion bombardment and annealing (IBA) was investigated by Stiles and Kahn [Sti85] with LEED. The B face was found to be stable at about 600 °C and exhibited a (1x1) atomic geometry. The authors chose the simple primitive unit cell to explain the experimental findings. Chadi [Cha85]

concluded that the surface electronic structure of the relaxed (1x1) surface was metallic with the Fermi level located above the bulk valence band minimum. Using IBA as well as MBE from a single GaAs Knudsen cell Scholz et al. [Sch94] confirmed for GaAs(113)B the (1x1) LEED pattern at the preparation conditions reported in [Sti85]. Platen et al. [Pla99] prepared GaAs(113)B by MBE and reported also on a (1x1) surface stabilized for As-rich conditions by means of spot-profile analysis LEED, AFM and scanning electron microscopy. The energy calculation revealed a very low value of only 43 meV/Å² for the As terminated (1x1) bulk-truncated structure that became greater at more Ga-rich conditions. Setzer et al. [Set99] showed by means of LEED and photoelectron spectroscopy that (113)B decayed onto (111)B and (110) facets after MBE treatment.

To the contrary to all above-mentioned papers Márquez et al. [Mar00] found a well-ordered (8x1) reconstructed (113)B surface under Ga-rich preparation, and proposed a model by simple exchanging of Ga and As atoms in the model for GaAs(113)A [Was95]. *In situ* atomically resolved STM and LEED revealed the surface composed of Ga dimers forming zigzag chains in two atomic levels. The morphology of the GaAs(113)B-(8x1) surface was rather smooth and did not show the typical roughness known for the GaAs(113)A-(8x1) surface. In the later work [Mar02] the authors considered in detail an important As-rich GaAs(113)B surface structure, because the InAs QDs evolve mainly at As-rich preparation conditions. By means of *in situ* RHEED and STM the As-rich structure represented a remarkable case intermediate between a stable singular and an unstable faceted surface: locally As adatoms and dimers created a 1x and 2x periodicity but long-range order did not exist. Nevertheless, the surface comprised large terraces that were separated by well-developed monatomic steps. Finally, we reported on the growth kinetics of the stable Ga-rich (8x1) reconstruction based on the STM analysis of the surface defects [Suz02].

Let us consider the most important publications of InAs heteroepitaxy on GaAs(113)B. Nötzel et al. [Noe94, Noe94a] described the self-organized formation of box-like microstructures during an interrupted epitaxial growth of strained InGaAs/AlGaAs multilayer structures. The samples grown at 800 °C in a MOVPE reactor revealed arrays of well-ordered microcrystals, composed of In_xGa_{1-x}As islands. Increasing the nominal In content x and decreasing the nominal In_xGa_{1-x}As layer thickness d allowed to alter the average size of the islands from 1500 Å for $x=0.2$ and $d=100$ Å down to 300 Å for $x=0.5$ and $d=30$ Å as measured by scanning electron microscopy. Despite of the rather large lateral dimensions the islands exhibited excellent crystal quality as well as 3D exciton

confinement as indirectly concluded from the measured integrated PL intensity in comparison to the $\text{In}_x\text{Ga}_{1-x}\text{As}$ quantum well grown on GaAs(001).

In(Ga)As self-assembled QDs on GaAs(113)B were prepared by Nishi et al. [Nis96] using MBE. Improved uniformity of islands on the (113)B face relative to those on GaAs(001) was confirmed by AFM observation. PL measurement showed a reduced linewidth (by a factor of 3) from (113)B samples, that even at room temperature was as small as 41meV. The reason for the narrowed width was concluded to stem from the improved uniformity of QD ensemble, which might have been achieved by the high surface adatom mobility. PL integrated intensities were comparable for the QDs on GaAs(113)B and (001), while the PL peak for the later substrate was red shifted indicating a larger average QD size. From RHEED and AFM observation, the authors could not derive any bounding facets on the islands except for the flat (001) facet inclined by 25.2° to (113)B.

Fortina et al. [For98] also reported on the PL peak shift of about 0.2 eV for InAs QDs on GaAs(113)B compared to those on GaAs(001) due to the smaller size on the former substrate. In contrast to InAs QDs on GaAs(113)A there was almost no drop in the PL efficiency for the 1.7, 2.2 and 2.7 ML of deposited InAs. This fact indicated an absence of QD degradation due the introduction of grain boundary dislocations and the possibility to tune the QD emission energy from 1.3 eV for 1.7 ML to 1.2 eV for 2.7 ML of InAs.

Polimeni et al. [Pol98, Pol98a] measured for 11.3 Å of $\text{In}_{0.5}\text{Ga}_{0.5}\text{As}$ a narrowest reported FWHM of about 11.4 meV at 4.2 °K, which was explained in terms of an in plain coupling of the islands. The QD size on the B face was larger than on the A face prepared under the same conditions. The authors also showed a bright room temperature electroluminescence signal from a p-i-n device with the intrinsic region containing $\text{In}_{0.5}\text{Ga}_{0.5}\text{As}$ QDs on GaAs(113)B emitting light with energy ~ 1.27 eV.

Lobo and Leon [Lob98] observed by AFM nonfaceted lens-shaped islands by MOCVD deposition of $\text{In}_{0.5}\text{Ga}_{0.5}\text{As}$. The SK transition took place up to a thickness of 15 Å (5 ML), beyond which the density of QDs decreased due to the coalescence.

Spontaneously alignment of MBE grown $\text{In}_x\text{Ga}_{1-x}\text{As}$ QDs with low In content $x\sim 0.3$ has been observed by Xu et al. [Xuh99, Xuh99a] with AFM. The ordering alignment became significantly deteriorated by increasing the In content to above 0.5 or by using (001) and (113)A substrates. Similar results with ordered $\text{In}_{0.4}\text{Ga}_{0.6}\text{As}$ QDs with the density of 10^9 - 10^{11} cm^{-2} , fabricated by atomic-hydrogen assisted MBE, were reported by Kawabe et al. [Kaw99]. The growth temperature between 460 °C and 520 °C largely changed the density and the dot size. In sharp contrast to InAs deposition, where no ordering was detected and

coalescence of the dots occurred beyond a thickness of 2.4 ML, the $\text{In}_{0.4}\text{Ga}_{0.6}\text{As}$ QDs were in contact with each other covering almost 100 % of the WL. It implied the existence of a lateral coupling between the dots, that was thought to stem from the inhomogeneous vertical distribution of In and Ga in the islands.

Jiang et al. [Jia00, Jia01] concluded from AFM images and from PL spectra that $\text{In}_{0.5}\text{Ga}_{0.5}\text{As}$ QDs grown with MBE on high-index surfaces (including (113)B) were smaller in size than those on the (001) substrate. In contrast to reference [Nis96] the reason proposed by Jiang et al. was an expected high density of steps on (n11) surfaces* ($n=3,5$), implying small adatom mobility compared to the atomically flat (001) surface. This explanation in turn contradicted the STM observation from Márquez et al. [Mar02] that showed atomically smooth but disordered As-rich GaAs(113)B. The authors also found a smaller FWHM for the QDs grown on (113)B than on the (113)A, indicating a more homogeneous QD ensemble. Finally, Gong et al. [Gon03] showed by means of AFM that the morphology of the (113)B surface remained flat before island nucleation by MBE deposition of $\text{In}_{0.35}\text{Ga}_{0.65}\text{As}$. Beyond the SK transition the (113)B surface developed a matrix of cells with average height modulation of 10 Å. Upon further growth the height of the cells increased gradually from 15 Å to 25 Å. The area density of the cells remained unchanged indicating a transition of the QDs from flat to steep shapes, which was also confirmed by the continuous shift of the PL peak from 1.43 eV to 1.32 eV corresponding to the flat and steep islands.

4.3 Shape, size, and number density of InAs QDs grown on the GaAs(113)B surface at different temperatures: our own results

The GaAs(113)B substrate, prepared as described in chapter 2.9, exhibits a well-ordered (8×1) reconstruction (8×1 with respect to the face-centered unit cell) consisting of zigzag chains of Ga dimers in the top and middle layers [Mar02], obviously in an identical arrangement as the As dimers on the (113)A face for the As-rich (8×1) reconstruction**. The GaAs(113)B-(8×1) surface is prepared by keeping the sample at the growth temperature of 500 °C for 15 min with the As_2 Knudsen cell shut off, i.e., under Ga-rich conditions. It can be recognized from Fig. 4.1(a), that the mesoscopic morphology of the

* This is a typical make-believe of many authors, used for years, that high-index surfaces are not stable but decayed into stepped low-index ones.

** The ECR applied to GaAs(113)B-(8×1) yields 16 As DBs (-12e), 20 Ga DBs (+15e), and 6 Ga-Ga dimer bonds (-3 e). Thus, the ECR is fulfilled.

GaAs(113)B-(8×1) surface differs strongly from that on the A face (cf. Fig.3.4), as large terraces are observed and not any tendency to form other high-index facets is seen. This may be related to a presumably high energies of (3 7 15)B, (2 5 11)B, and (137)B surfaces which have, however, not been calculated up to now.

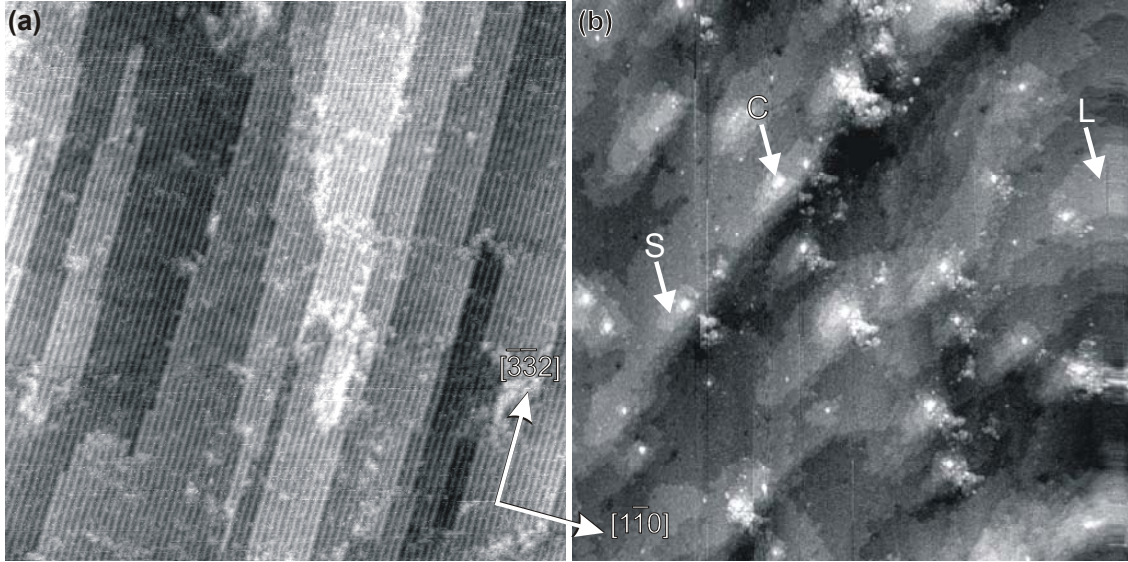


Figure 4.1 [Tem03b] (a) Overview STM image of GaAs(113)B-(8 × 1): $(2500 \times 2500)\text{\AA}^2$, $U = -2.8$ V, $I = 0.15$ nA; (b) Overview STM image of the InAs wetting layer on GaAs(113)B before the SK transition: $(4000 \times 4000)\text{\AA}^2$, $U = -2.55$ V, $I = 0.1$ nA. The thickness of deposited InAs is 0.8 ML.

At ~ 490 °C under As_2 flux, the GaAs(113)B surface undergoes a transition to the less-ordered $(2\times 1)+(1\times 1)$ structure by incorporating As atoms and rearranging Ga dimers, thus filling up the trenches [Mar02, Suz03]. So, at 435-490 °C – the growth temperature of the InAs QDs – the GaAs(113)B surface exhibits this mixed $(2\times 1)+(1\times 1)$ structure consisting of locally ordered As ad-atoms and dimers on the bulk-truncated (113)B surface. Thus, the surface reconstruction on the GaAs(113)A and GaAs(113)B substrates is not the same before the InAs deposition. Furthermore, with the transition to the As-rich phase, the GaAs(113)B surface does not change its morphology [Mar02]. STM images of the InAs WL (cf. one example in Fig. 4.1(b)) exhibit terraces up to 1000 Å wide and separated by mostly monatomic steps, i.e., the (113)B substrate remains very flat before the growth of InAs QDs starts. Moreover, near to the SK transition, the morphology is very similar to that on (001) [Hei97]: small (S) and large (L) 2D monatomic islands and small 3D clusters (C) up to 4 ML_{113} in height (potential precursors for the InAs QDs) are seen in the STM image.

One may suppose that a very large similarity of the wetting layers and a rather homogeneous SK growth may be mirrored in the similarly favorable optical properties found for InAs QDs grown on GaAs(001) and GaAs(113)B substrates [Nis96, Jia00].

As has been shown in chapter 3.6 the InAs QDs on GaAs(113)A are observed in different growth states. The behavior of the QDs on the B face prepared at the same conditions is remarkably different. The wetting layer is much more smooth and the ensemble of dots much more uniform as seen from Fig. 4.2(a). Besides the normal QDs, only a small number of elongated islands is observed. One of them is marked with an arrow in Fig. 4.2(a). Above all, the absence of any nuclei on the B face is remarkable, implying the simultaneous SK transition because of the flat WL. Also, any alignment of the islands is not seen; they are statistically arranged on the surface.

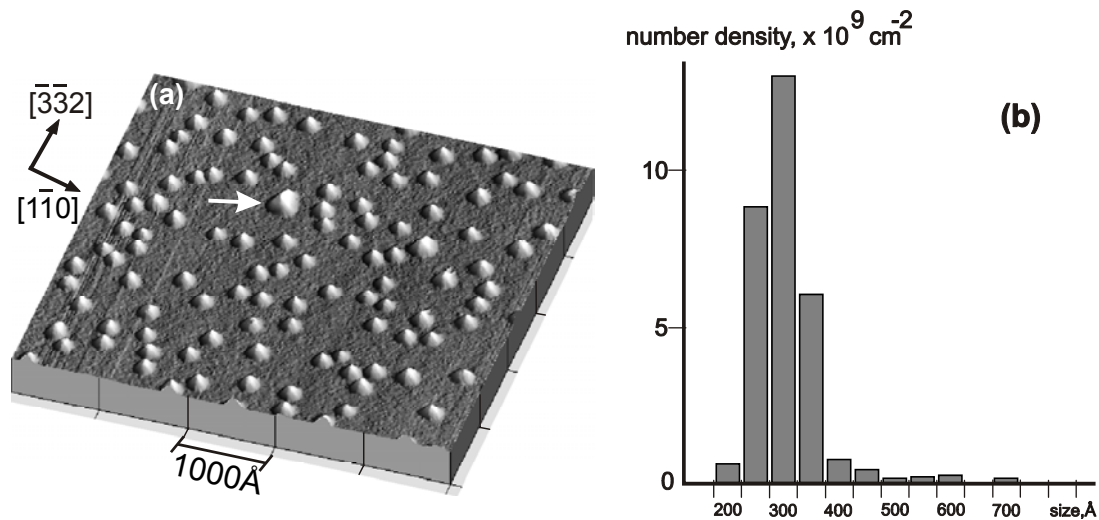


Figure 4.2 [Tem03b] (a) 3D overview STM image with InAs QDs grown on GaAs(113)B. The white arrow indicates a large elongated island. The size is $(5000 \times 5000) \text{ \AA}^2$, $U = -3 \text{ V}$, $I = 0.1 \text{ nA}$; the sample temperature was $450 \text{ }^\circ\text{C}$ and the InAs thickness 1.0 ML ; (b) Column diagram of the length of the InAs QDs along $[3,3,-2]$ distributed to different QD number densities.

The critical thickness at which the 3D QDs are formed at $450 \text{ }^\circ\text{C}$ (established with RHEED) is $1.5 \pm 0.2 \text{ ML}$ for the A face and $1.0 \pm 0.2 \text{ ML}$ for the B face. The delay in the SK transition on the A face can be explained by the partial relaxation of InAs at the 3D hills observed already on the wetting layer, because in the 3D structures InAs can better relax than in the 2D film. A similar delay of QD formation was found for $\text{In}_{0.5}\text{Ga}_{0.5}\text{As}$ grown by the MBE on GaAs(113)A compared to GaAs(001) under otherwise identical preparation conditions [Vac96].

The difference in the size distribution can be seen from comparison between Fig. 3.6(b) and Fig. 4.2(b). On the (113)A surface, the measured lengths at the base along $[3\bar{3}\bar{2}]$ are distributed between 300 to 600 Å with the peak of 35 % at 400 Å whereas on the (113)B surface values between 200 to 400 Å with the peak of 45 % at 300 Å are found. The large elongated islands on GaAs(113)B contribute to a second broad peak starting for lengths above 400 Å. Therefore, we assign these islands to be incoherent with dislocations at the interfaces, i.e., their size development is not restricted by strain. The number density on GaAs(113)B of $3 \times 10^{10} \text{ cm}^{-2}$ is higher than the one of $9.5 \times 10^9 \text{ cm}^{-2}$ on GaAs(113)A. Thus, the InAs QDs on the GaAs(113)B surface are smaller in size and larger in density than those on GaAs(113)A and GaAs(001) [For98, Jia00].

Let us now consider the atomic structure of the presumably coherent islands. Figure 4.3 exhibits 3D STM images of a typical QD viewed along (a) $[3\bar{3}\bar{2}]$ and (b) $[\bar{3}\bar{3}\bar{2}]$. Since we have atomically resolved the WL, we can determine the azimuthal orientation of the dot. Similar to the (113)A case the QD is mirror symmetric with respect to the $(\bar{1}10)$ plane normal to the surface. (The $(\bar{1}10)$ plane is also a plane of mirror symmetry on the bulk-truncated (113)B surface.) The QD comprises a steep main part terminated by regions 1, 2, and 3, and a flat base consisting of the facets 4 and 5. The flat base, that was not observed on the InAs QDs on GaAs(113)A, is an intrinsic part of the InAs QDs on GaAs(113)B, that appears not only during growth, but still exists after annealing treatment of the samples.

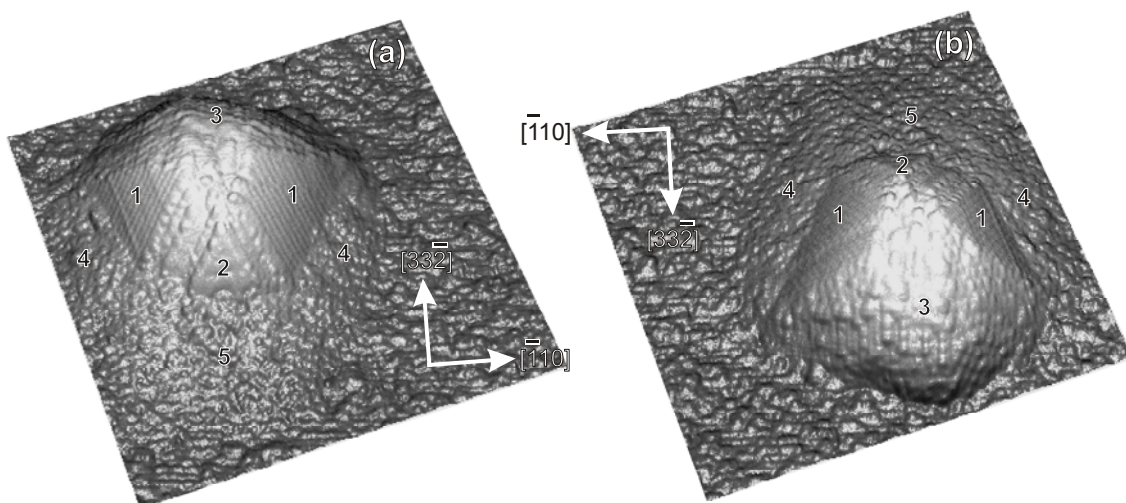


Figure 4.3 [Suz02] 3D STM images of an InAs QD; $(420 \times 420) \text{ \AA}^2$, $U = -3 \text{ V}$, $I = 0.1 \text{ nA}$. The bounding facets are numbered.

Figure 4.4(a-d) shows high-resolution STM images of QD facets. The facets 1 are $\{110\}$ planes as derived from the following facts: Each facet is inclined to the $(113)B$ surface by $29 \pm 2^\circ$ and the lengths of the unit-cell vectors on the facet are $u_1 = 5.6 \pm 0.1 \text{ \AA}$ and $u_2 = 3.9 \pm 0.2 \text{ \AA}$; these values agree with the geometric angle of 31.5° between the $(0\bar{1}\bar{1})$ or $(\bar{1}0\bar{1})$ and $(113)B$ planes and with the lengths of the InAs (GaAs) $(0\bar{1}\bar{1})$ unit-cell vectors projected onto $(113)B$ which are $u_1 = 5.8$ (5.4) \AA and $u_2 = 3.9$ (3.6) \AA . The STM image in Fig. 4.4(a) is also very similar to that acquired on a GaAs(110) surface [Fee87].

The facet 2 is $(111)B$ oriented as concluded from the following facts: It is of triangular shape which is a structural feature of the $\{111\}$ surface; also, it is inclined to $(113)B$ by $28 \pm 1^\circ$ which agrees with the geometric angle of 29.5° between $(111)B$ and $(113)B$. Rings of $8.6 \pm 0.8 \text{ \AA}$ in diameter, indicated by arrowheads in Fig. 4.4(b), are observed on the facet 2, which is considered to be the same kind of structural feature observed on the GaAs $(111)B(\sqrt{19} \times \sqrt{19})$ surface [Bie90, Tho98]. Although the rings are not ordered with respect to the $(\sqrt{19} \times \sqrt{19})$ unit cell, this is not necessarily excluding our interpretation, since such a disordered array of rings was also reported on the flat GaAs $(111)B$ surface (for example cf. Fig. 3 in [Tho98]) and well ordered $\sqrt{19} \times \sqrt{19}$ domains may not easily form on a small facet.

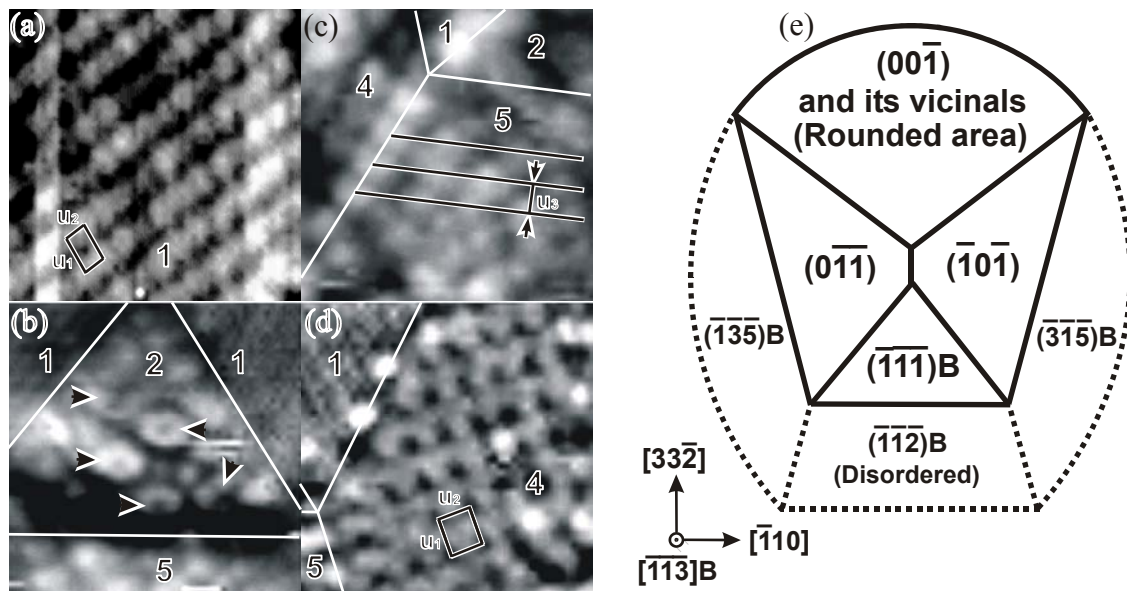


Figure 4.4 [Suz02] (a-d) Atomically-resolved STM images of the four facets ($U = -3 \text{ V}$, $I = 0.1 \text{ nA}$). The image sizes are (a) $(43 \times 43) \text{ \AA}^2$, (b) $(96 \times 96) \text{ \AA}^2$, (c) $(86 \times 86) \text{ \AA}^2$ and (d) $(78 \times 7.8) \text{ \AA}^2$. (e) Schematic drawing of the InAs QD shape on GaAs $(113)B$. The solid line is a contour of the steep part, the dotted line of the flat base.

The facet 5 on the base of the QD is the (112)B orientation from the following facts (see Fig. 4.4(c)): The intersection lines of facet 5 with (113)B and also with (111)B are parallel to $[\bar{1}10]$ which indicates that the facet 5 has Miller index $(\bar{h}\bar{h}\bar{k})$ with $1 < k/h < 3$; also, the facet 5 is inclined to (113)B by $11 \pm 2^\circ$ which agrees with the geometric angle of 10.0° between (112)B and (113)B. Although it is difficult to recognize the exact unit cell, rows of humps are seen which can be connected by lines of a given separation $u_3 = 9.2 \pm 0.3 \text{ \AA}$ in accordance with $10.3 (9.6) \text{ \AA}$, the geometric length of a (112)B unit-cell vector perpendicular to $[\bar{1}10]$ and projected onto (113)B. However, it has been reported that the GaAs(112)B surface on a flat wafer is not stable and is faceted into other low-index surfaces [Pla97, Gee99]. Therefore, the assignment of the (112)B facet is fairly doubtful.

The facets 4 enlarged in Fig. 4.4(d) are considered to be of (135)B orientation from the following facts: These facets are inclined to (113)B by $13 \pm 1^\circ$, the lengths of the unit-cell vectors are $u_1 = 10.1 \pm 0.4 \text{ \AA}$ and $u_2 = 9.4 \pm 0.4 \text{ \AA}$, and the angle between u_1 and u_2 is $89 \pm 2^\circ$. These values agree with the geometric angle of 14.5° between (135)B and (113)B, with the unit-cell vectors of the (135)B-c(2x2) surface projected onto (113)B that are $u_1 = 11.2 (10.5) \text{ \AA}$ and $u_2 = 10.7 (10.0) \text{ \AA}$, and with the angle of 92° between the (135)B unit-cell vectors projected onto (113)B. Moreover, an angle between $[\bar{1}10]$ and an intersection line of the facet 4 with the facet 5 is $67 \pm 1^\circ$. This value agrees with the geometric angle of 67.5° between $[\bar{1}10]$ and $[13\bar{3}5\bar{1}6]$, the intersection line between (135)B and (112)B, projected onto (113)B. The intersection line is parallel to the unit vector u_1 on the facet 4 as seen in Fig. 4.4(c), or 4(d) also in accordance with a feature of the (135)B surface. Our recent experiments on the flat GaAs(135)B surface have shown that the surface is not stable and faceted onto stable $(2\ 5\ 11)B$ and $(\bar{1}0\bar{1})$ surfaces, but becomes flat and stable by the InAs deposition, i.e., under tensile strain on the GaAs substrate [Suz04a].

From pure geometrical considerations, the center part of the rounded region 3 in Fig. 4.3 consists of $(00\bar{1})$ which is inclined to (113)B by 25° . The rounded region 3, which is not shown in detail here, does not exhibit an ordered surface structure. Similar to the QDs on GaAs(113)A the sphere-like shape may stem from migration of In atoms from all directions, i.e., from the slower growing $\{0\bar{1}\bar{1}\}$ and (111)B facets to the faster growing stepped $(00\bar{1})$ surface. In addition, the only region of InAs QDs on GaAs(113)B where the

As₂ molecules can be incorporated without being dissociated is $(00\bar{1})^*$, therefore, its growth is further accelerated. We believe that the $(00\bar{1})$ region overgrows the flat base, which does not exist between the rounded region and (113)B substrate. More generally, difficulties with the incorporation of As₂ molecules may also be responsible for the observed small size of the QDs on the GaAs(113)B substrate as well as for the absence of the elongation through the growth of (111)B facets which edge with the (112)B (or (113)B) surface does not supply As₂ incorporation sites.

The shape determination is summarized in Fig. 4.4(e). The main part of the QD sits on the flat base composed of (135)B, (315)B, and probably (112)B high-index surfaces. Note that on the coherent QDs we do not observe straight edges between {135}B facets and (113)B substrate. Together with the $(00\bar{1})$ region it fashions the rounded overall shape, observed by the community with AFM [Nis96, Lob98]. The shape of the main part of the QD is given by $(0\bar{1}\bar{1})$, $(\bar{1}0\bar{1})$, and (111)B facets and a rounded region that is considered to be composed of $(00\bar{1})$ and its vicinal surfaces. If we assume that the growth of In_{0.35}Ga_{0.65}As and InAs QDs is identical, then, following Gong et al. [Gon03], the flat base comprised {135}B and (112)B facets should rise at first. It may remain unchanged whereas the main steep part evolves on the top of the base. However, due to the rather simultaneous SK transition, the (113)B substrate does not leave any trace of growth and, on the contrary to (113)A, we could not retrace the QD growth kinetics.

Because the InAs QDs on GaAs(113)B yield a dense and uniform ensemble, i.e., could be used equally with those on GaAs(001) as active layer in laser diodes, we have performed some additional experiments on the influence of sample temperature on QD size and density. Fig. 4.5(a-d) shows overview STM images of InAs QDs grown at different temperatures between 435–490 °C. The number densities are 6×10^{10} , 3×10^{10} , 1×10^{10} and 3×10^9 cm⁻² for 435, 450, 470 and 490 °C, respectively. However, as the deposited amount of InAs is not the same for all four growth temperatures, the number densities are considered to be only a rough measure^{**}. Two types of 3D islands are clearly seen in all STM images. There are many relatively small islands of remarkably uniform size

* Because of the high-symmetry the (001) surface can actually be either an A or B face depending on the preparation conditions. Since the QDs are deposited at As-rich conditions, the (0,0,-1) surface is equivalent to (001).

** The InAs deposition was stopped as soon as the change from 2D to 3D RHEED pattern was recognized by eye on the fluorescent screen. The nominal amount of deposited InAs could not be kept accurately constant in the present study. This variation is considered to be in part due to differences of the 2D to 3D transition on growth temperature and in part also to the sensitivity of the operator.

(presumably coherent QDs) and some larger islands that vary significantly in size (presumably incoherent islands). The QDs seem to be more round at the interface, while the larger islands exhibit some elongation along $[\bar{3}\bar{3}2]$. The size and the height distributions of the QDs and the larger islands will be discussed in detail below. However, from the overview STM images it is already obvious that the size of the QDs increases and the number density decreases, as the growth temperature increases.

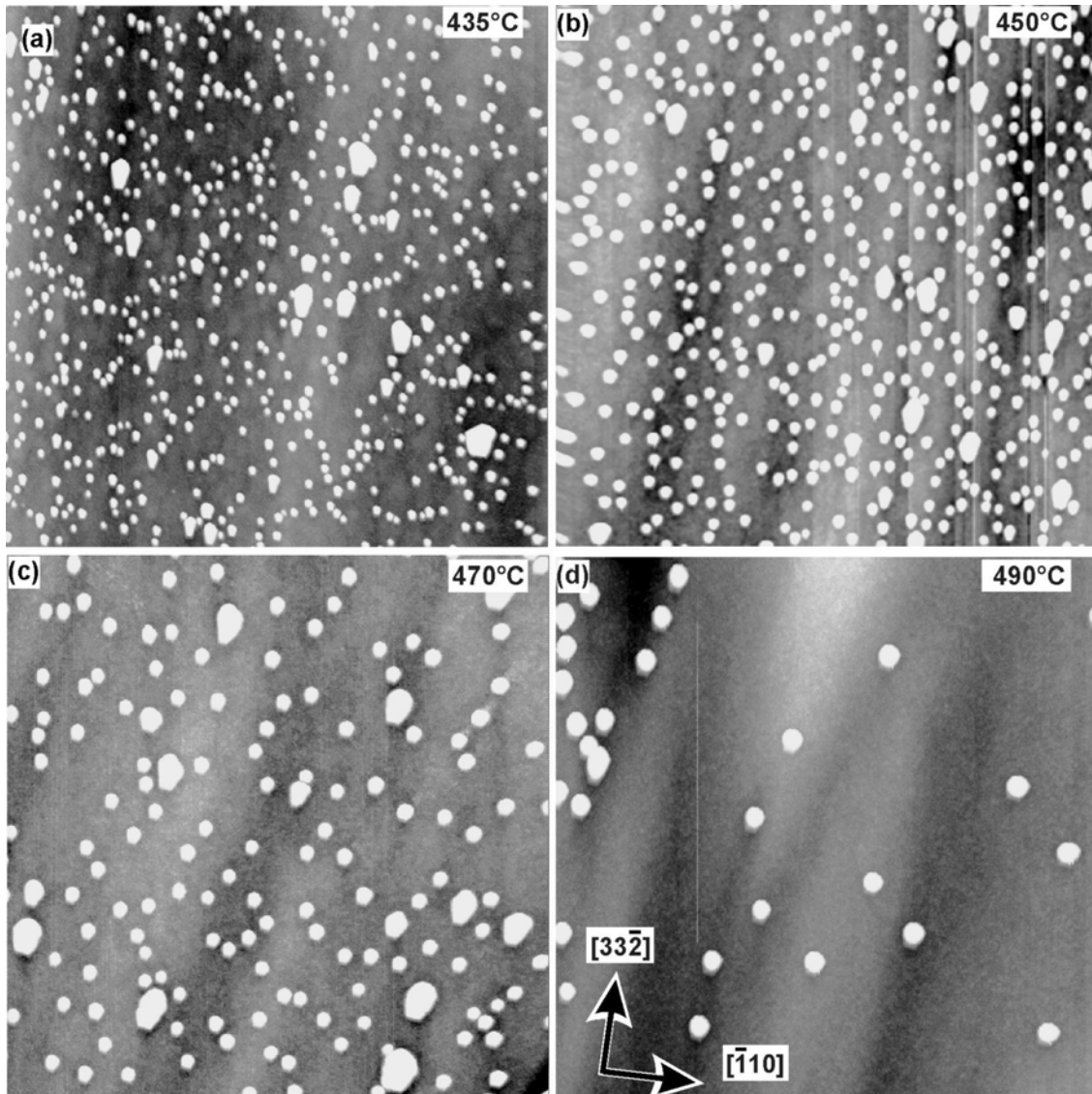


Figure 4.5 [Suz03] Overview STM images of InAs QDs grown on the GaAs(113)B surface at (a) 435 °C, (b) 450 °C, (c) 470 °C and (d) 490 °C (the size is $(1 \times 1) \mu\text{m}^2$, $U = -3 \text{ V}$, $I = 0.1 \text{ nA}$). The nominal amount of deposited InAs is (a) 1.5 ML, (b) 1.0 ML (c) 1.3 ML and (d) 1.9 ML.

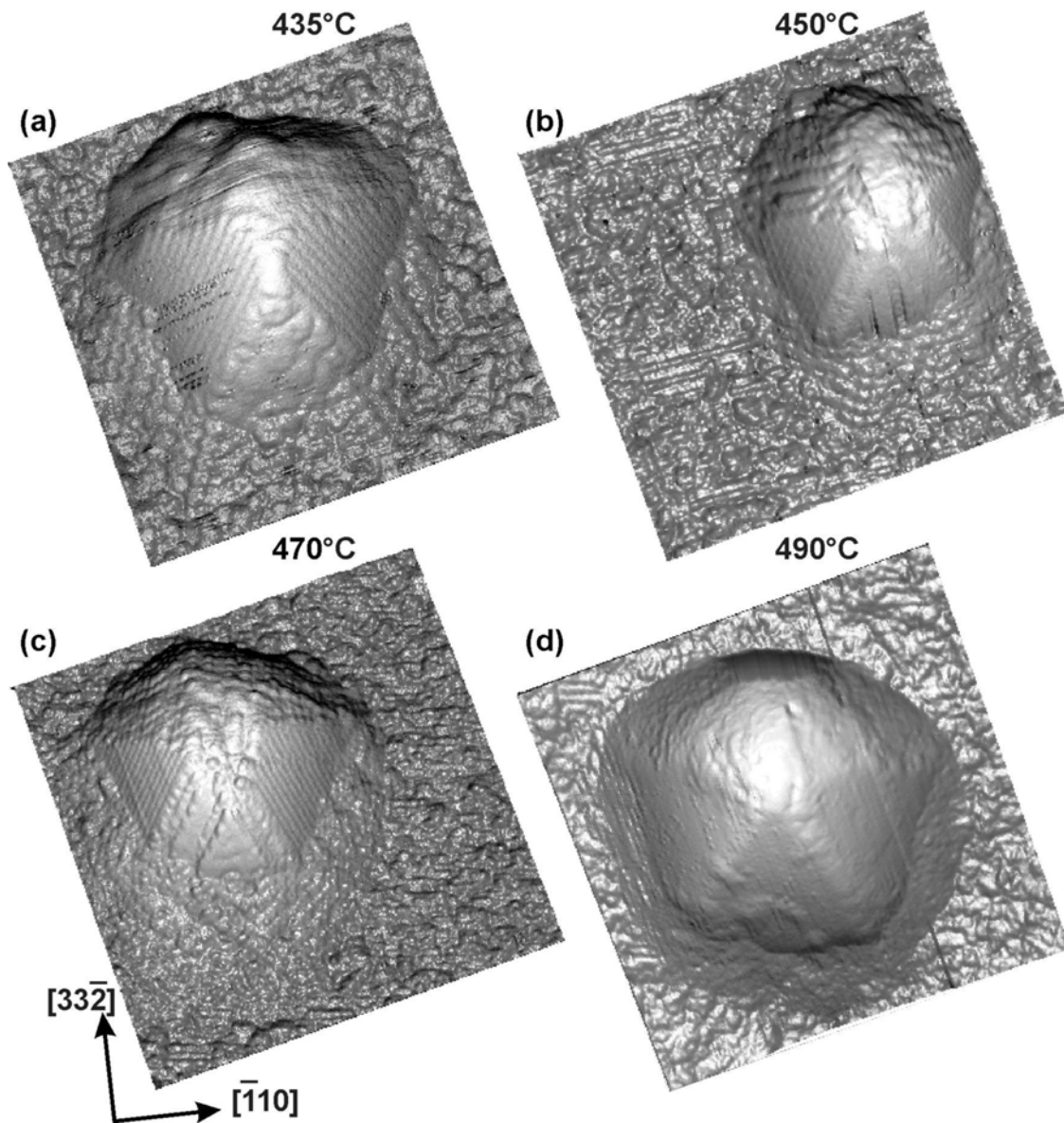


Figure 4.6 [Suz03] High-resolution 3D STM images of InAs QDs grown on GaAs(113)B at different temperatures ($U = -3$ V, $I = 0.1$ nA). The size is (a) $(280 \times 280) \text{ \AA}^2$, (b) $(360 \times 360) \text{ \AA}^2$, (c) $(420 \times 420) \text{ \AA}^2$, (d) $(650 \times 650) \text{ \AA}^2$.

Large-magnification 3D STM images of the QDs grown at indicated temperatures are shown in Fig. 4.6(a-d). For all images except (d), atomic resolution is achieved which allows determining the orientation of the bounding facets. It is obvious from these images that the shape of all four QDs is the same: A main part with steeper facets sits on a flat base with flatter facets. From the images, it is evident that the shape of the QDs does not change significantly for growth temperatures between 435 and 490 °C.

One may ask whether the flat base is stable or induced by growth kinetics. In order to answer this question we performed post-annealing experiments for InAs QDs grown at 435 °C. Fig. 4.7(a) shows an overview STM image and Fig. 4.7(b) a 3D STM image of a single QD post-annealed for 1 minute. Comparing the overview STM image with Fig. 4.5(a) one recognizes that there is no significant change: there are many QDs and some larger islands. However, the size of the QDs increases slightly and the number density ($2 \times 10^{10} \text{ cm}^{-2}$) decreases which is considered to be due to creation of additional large islands by coalescence and little growth of the QDs at the expense of some of them [Ren97]. Also the shape of the QDs does not change significantly as seen in Fig. 4.7(b). The flat base composed of the high-index facets still exists as well as the main part which suggests that the flat base is not a frozen-in transitory structure appearing only during growth, but is an intrinsic part of the InAs QDs on GaAs(113)B.

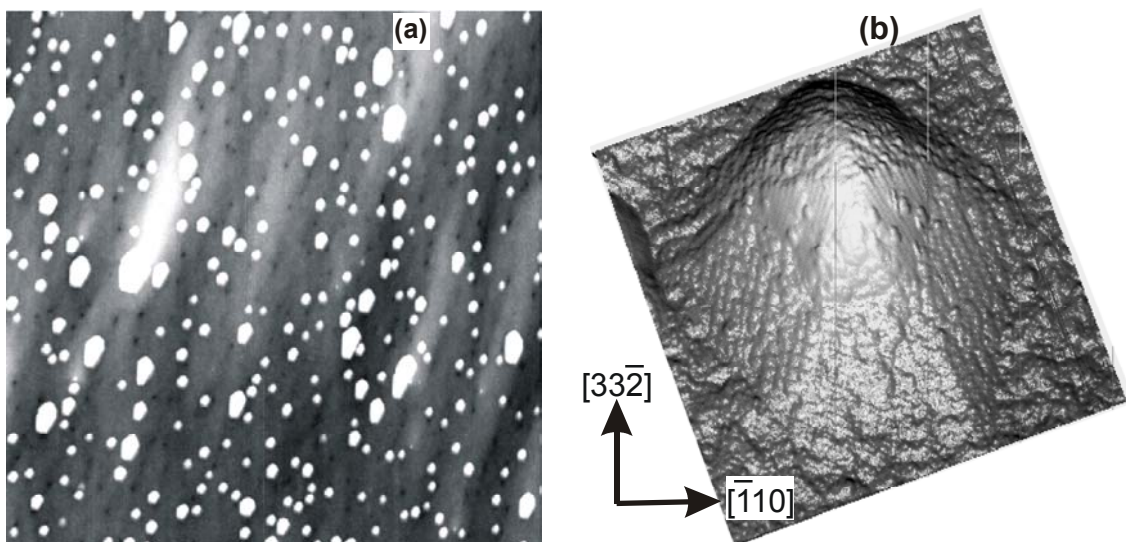


Figure 4.7 [Suz03] (a) STM image of InAs QDs after growth at 435 °C ($U = -3 \text{ V}$, $I = 0.1 \text{ nA}$), post-annealed by 1 min., and (b) 3D STM image of a single QD after the same procedure. The nominal amount of deposited InAs is 1.6 ML. The size is (a) $(1 \times 1) \mu\text{m}^2$ and (b) $(370 \times 370) \text{ \AA}^2$.

Only 4 % of all islands on GaAs(113)B adopt a somewhat elongated shape shown in Fig. 4.8(a). Contrary to the elongated QDs on GaAs(113)A there is no reduction of the GaAs(111)B facet size. The length of the edge between the (111)B and (112)B facets even increases from $105 \pm 15 \text{ \AA}$ for the QDs to $120 \pm 15 \text{ \AA}$ for the elongated islands. This behaviour indicates that the elongation probably proceeds by the growth of the $(00\bar{1})$ rounded region in the $[33\bar{2}]$ direction. Similar to the QDs on the A face, the $\{113\}$ A facets

should develop on the $(00\bar{1})$ vicinal region. Since these facets can grow with the introduction of As_2 , the $\{113\}\text{A}$ facets may not (strongly) decrease the growth rate at the rounded region. With this scenario the elongation could be explained as consequent development of some rounded QDs to the elongated QDs similar to the $(113)\text{A}$ case. However, no flattening of the rounded region was observed in the STM images of the elongated islands. In addition, owing to the geometric reasons the growing $(00\bar{1})$ region should increase in size and may, therefore, induce the lower growth rate [Jes98] that should limit the elongation. We observed the very broad size distribution of the elongated islands with the lengths along $[33\bar{2}]$ from 400 up to 850 Å (e.g., in Fig. 4.2(b) for the QDs grown at 450 °C). There is also no report about the polarization anisotropy from the elongated QDs on $\text{GaAs}(113)\text{B}$. These facts suggest that these islands are incoherent, i.e., have one or several dislocations incorporated at the substrate interface which relieve the strain.

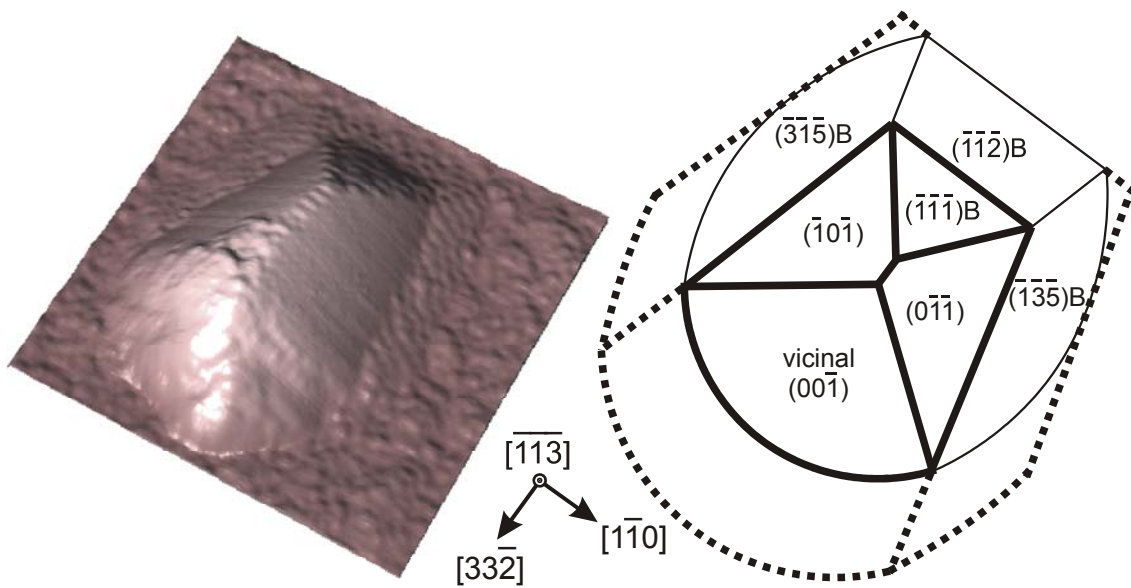


Figure 4.8 [Tem03b] (a) 3D STM image of an elongated InAs QD grown on $\text{GaAs}(113)\text{B}$: $(420 \times 420) \text{ \AA}^2$, $U = -3V$, $I = 0.1 \text{ nA}$; (b) shape of presumably coherent (solid line) and incoherent (dotted line) InAs islands on $\text{GaAs}(113)\text{B}$ derived from STM measurements.

Incorporation of a dislocation requires surmounting an energetic barrier and is achieved only in few cases (for 4 % of all islands). After the dislocation has been formed, the $(00\bar{1})$ region grows with the largest rate without limitation caused by elastic strain present in the QDs, as reported for simultaneously growing low-index surfaces on patterned GaAs

substrate [Yam99, Hir99]. The islands become elongated along $[3\bar{3}2]$. In Fig. 4.8(b) the model for the QDs and elongated islands on GaAs(113)B is sketched. Note that the shape for incoherent and coherent islands is largely similar. This is quite different from GaAs(001) substrates, for which the incoherent islands exhibit irregular shapes [Moi94, Leo94, Joy01].

Figure 4.9 shows the growth-temperature dependence of (a) the size and (b) the height of the QDs. Triangles at 435 °C in (a) and (b) indicate those values measured from samples post-annealed for 1 min. The size and the height increase with temperature monotonously from 250 to 540 Å and from 35 to 98 Å, respectively. The post-annealing increases the size and the height by about 30 %. A similar dependence on growth temperature has been found for the growth of InAs QDs on GaAs(001) [Mad94, Sol95, Guo98, Chu99, Kis00].

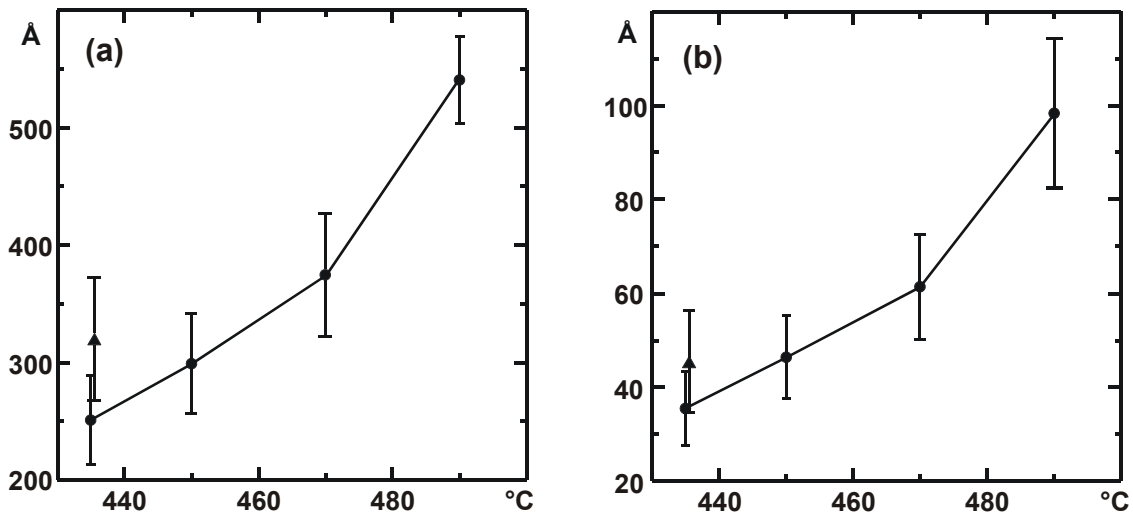


Figure 4.9 [Suz03] Temperature dependence of QD size (a) and height (b). Triangles at 435 °C in (a) and (b) indicate size and height, measured from samples, post-annealed by 1 min. Error bars are given.

The dependence of the QD size and number density on the growth temperature has been explained so far by kinetics. The QDs are formed when a critical thickness of the deposited InAs layer is achieved. After the nucleation, larger strain concentration at the edge of the larger QDs makes it more difficult for the incoming adatoms to be attached to the larger QDs than to the smaller ones, which explains the rather uniform size distribution in terms of kinetics [Che96, Bar97, Jes98]. In this scheme, one nucleation site collects InAs material from a circular area whose radius is proportional to the diffusion length of the In atoms. Therefore, when the growth temperature (and the diffusion length of the In atom) increases,

the average size of the QDs increases and the density of the QDs decreases. In kinetics, the shape of the QDs is mainly determined by the growth speed of each bounding facet [Che63, Jes98]. However, no theoretical calculation or confirmation of the shape of the QDs in kinetics has been reported so far. This explanation seems to be quite straightforward, but a closer look reveals a severe problem: As recognized from Fig. 4.5 the mutual distances between the QDs exhibit a rather large distribution. This indicates that the distance between the QDs is not dominated by a diffusion zone, out of which the material is collected for each dot. Instead, our observation makes it likely that the site distribution of the islands is governed by the statistics in developing growth nuclei. The increase in QD size with temperature may, therefore, indicate a decrease of the number density of critical nuclei, in line with well-known fact that the size of the critical nucleus increases with temperature. The amount of material in the second InAs layer is then distributed quite equally among the given nuclei including some probability for the growth of larger incoherent islands.

Meanwhile, the QD formation was also modeled on thermodynamic ground [Peh97, Wan99]. Here, the QDs are supposed to be in thermal equilibrium. The QD size is calculated from a balance between reduced strain energy and enhanced surface energy, which explains the uniform size of the QDs. The shape of the QDs could also be derived by energetics. It was found that mainly the surface energy of each bounding facet determines the shape [Peh97]. However, we note that the shape of the QDs on the GaAs(001) surface calculated in energetics was composed largely of the $\{011\}$ and the $\{111\}$ facets [Mol96], which is inconsistent with a recent experimental result of our group in which $\{137\}$ bounding facets were observed [Mar01]. Moreover, the average QD size, calculated by energetics, decreases as the growth temperature increases due to entropy contribution [Mei01]. It was shown by the same authors that the size distribution, immediately after growth, is controlled by kinetics, whereas the size distribution changes to thermal equilibrium after long-time annealing [Mei01]. However, the authors considered a 2D islands at submonolayer coverage which is far away from the real 3D QDs. We note, that the real situation in the experiment is even more complex as post-annealing usually induces decomposition of the QDs. Whether the growth mechanism is governed by kinetics or energetics is still an open question. The discussion of further results concerning this topic can be found in a recent paper [Pol00]. From the present and other experimental results described above we believe that both kinetics and thermodynamic energetics contribute to the growth mechanism.

4.4 Conclusion

Comparison between the InAs QDs on GaAs(113)A and GaAs(113)B yields remarkable similarities and differences. The symmetry of the islands and orientation of the main bounding facets are found to be equal on both GaAs(113)A and B surfaces. The QDs on GaAs(113)A exhibit $(\bar{1}10)$ as symmetry plane, $\{110\}$ and $(111)A$ bounding facets, and a rounded region of the vicinal (001) surfaces. The latter region becomes steeper with the appearance of the $(113)B$ surfaces in a later growth state giving rise to a shape elongated along $[33\bar{2}]$. The QDs on GaAs(113)B also exhibit the $(\bar{1}10)$ symmetry plane, $\{\bar{1}\bar{1}0\}$ and $(111)B$ bounding facets, and a rounded region of vicinal $\{00\bar{1}\}$ surfaces, which does not have flat parts. Contrary to the QDs on GaAs(113)A, a flat base of the high-index $(112)B$ and $\{135\}B$ surfaces develops at the foot of the QDs on GaAs(113)B. The differences in shape are attributed to facet growth kinetics associated with As_2 dissociation.

The morphology and atomic structure of the wetting layer also seem to have an important influence on the QD formation process. The undulation of the GaAs(113)A surface becomes much more pronounced with depositing InAs. The result is also a very inhomogeneous strain distribution that may inhibit a simultaneous SK transition on the whole surface. It induces a broad size distribution of the InAs QDs.

The behaviour on the GaAs(113)B surface is quite different. The flatness of the GaAs(113)B surface also remains after InAs deposition. Therefore, the QD growth starts simultaneously at the SK transition and the QDs grow with equal rates resulting in a homogeneous size distribution. Since the SK transition is rather short in time, we are unable to observe any nuclei. Additional experiments also reveal that the shape of the QDs does not change significantly for the growth temperature between 435 and 490 °C. Post-annealing increases the size and the height by about 30 % and decreases the number density, but does not change the QD shape. The incoherent islands have a similar shape as the QDs. The size and the height of the QDs increase monotonously from 250 to 540 Å and from 35 to 98 Å, respectively, whereas the number density decreases, as temperature increases. This is attributed to a decreasing number density of critical QD nuclei with temperature.

Taken at all, the InAs QDs on GaAs(113)B are interesting for possible application in optoelectronics since they yields a uniform and dense QD ensemble with tuneable upon the temperature QD size (and therefore, tuneable emission wavelength); those on GaAs(113)A are interesting for basic understanding of the QD growth kinetics.

5 InAs quantum dots on vicinal and nominal GaAs(2 5 11)A

5.1 Introduction

One of the most important results of our group has been a discovery of a new hitherto unknown stable GaAs atomic geometry - (2 5 11) [Gee01, Jac02, Gee02]. First, there are only few stable GaAs (or InAs) orientations found in material science, actually only five: (001), (110), (111), (113) and (114); therefore, each new orientation will significantly contribute to a deeper understanding of the stability of zinc-blende-type surfaces verifying common principles, such as the ECR or the minimisation of dangling bond density. Furthermore, facets of (2 5 11)A orientation have been observed to form naturally on InAs QDs grown on GaAs(113)A [Tem03] and GaAs(315)B [Suz04], that is GaAs (or InAs) (2 5 11)A and B may play an important role in crystal growth and epitaxy. The third motivation for the study of these high-index surfaces is their potential as substrate for growth of heteroepitaxial low-dimensional semiconductor devices, like InAs QDs*. A number of questions arises here right away, among which first is the morphology change by the mismatch epitaxy, e.g., does the SK transition occur by InAs deposition on GaAs(2 5 11)A and B similar to other high-index GaAs substrates. Also, conclusions about the symmetry of the QDs, the form modification like elongation due to the facet growth kinetics, or narrower size distribution of islands on the B face than on the A face shown in chapters 3 and 4 can be verified by using GaAs(2 5 11)A or B substrates. All above-mentioned issues have been the motivation to study the atomic and morphologic structure of bare GaAs(2 5 11)A and B surfaces, as well as InAs epitaxy on them.

5.2 Surface structure of GaAs(2 5 11)A

For graphic representation of the location of different GaAs orientations one usually works with a stereographic projection of the orientation vector onto a plane, rather than with the three-dimensional vector itself. Because of the crystallographic symmetry of fcc materials, some orientations are equivalent. Therefore, it is sufficient to restrict this projection to the triangle whose corners are marked by the three low index surfaces (001), (011), and (111) as shown in Fig. 5.1. A physical interpretation of the representation using the stereographic triangle (ST) can be given if we assume that surface atoms remain at their bulk positions. In this case, we can think of a surface of arbitrary orientation as being built

* We assume, that only stable surfaces are appropriate substrates for receiving a homogeneous ensemble of statistically distributed QDs suitable for further applications.

up from atomic-scale units of basic orientations (001), (011), and (111). A surface with orientation at an edge of the ST is composed of the two low-index surfaces at the respective corners. All other surfaces are thought to be composed from all three low-index surfaces, and therefore, are more complex. We will show that for a stable singular surface like GaAs(2 5 11)A the above composition is merely a hypothetical concept.

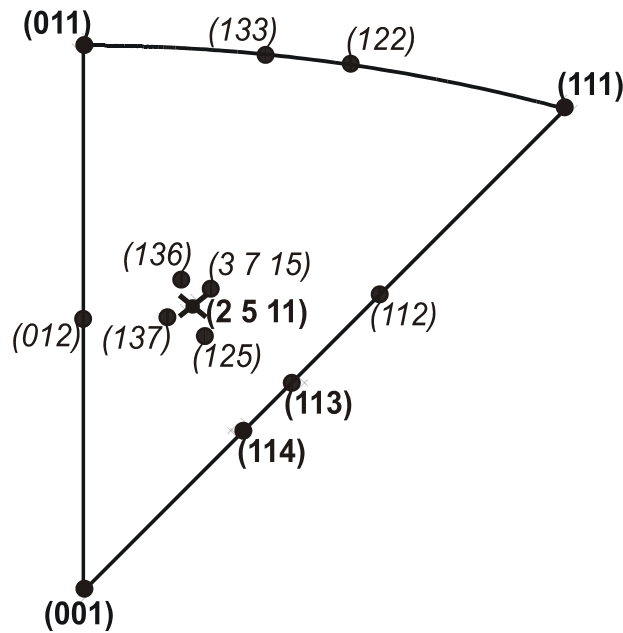


Figure 5.1 [Gee02] Stereographic triangle with the GaAs orientations reported in the literature. Stable surfaces are depicted as bold text. The location of (2 5 11) is shown with a cross.

So far, only few GaAs surfaces on the edges of the ST have been found stable: GaAs(001) [Lab99, Kra02], GaAs(011) [Kah94, Duk96], GaAs(111)A and B [Bie90, Duk96], GaAs(113)A and B [see literature survey in chapters 3 and 4] and GaAs(114)A and B [Shi93, Pla98, Mar01]. Most of the reconstructions on them are confirmed by first-principles energy calculations. GaAs(112)A [Noe91, Pla99], GaAs(112)B [Pla99, Gee99], GaAs(122)A [Wei89], GaAs(133)A and B [Wei89, Noe92, Hor89], GaAs(012)A [Noe92] are unstable. Surfaces that are located within the ST, such as GaAs(137)A [Gee00], GaAs(3 7 15)A [Tem02], GaAs(136)A and GaAs(125)A [Tem04], and GaAs(135)B [Suz04a] have faceted as well. There is up to now only one stable surface within the ST that does not undergo faceting upon annealing or epitaxial growth, that is GaAs(2 5 11)A. This is a rather unexpected result, since such surfaces exhibit no symmetry in contrast to those on the edges, and are thought to be of the high energy and unstable.

A LEED image of the GaAs(2 5 11)A surface, prepared as described in chapter 2.9, is shown in Fig. 5.2(a). The spots are arranged in an oblique net and are sharp, which indicates a high surface quality. In contrast to LEED images of other stable high-index GaAs surfaces [Pla98, Gee99, Mar00], almost all the spots are visible. Two different unit meshes are marked in Fig. 5.2(a). Unit mesh B* fulfils the rigorous crystallographic convention that the basis vectors should be as short as possible. However, in course of the present study it turned out that the surface structure is better described by unit mesh A*. Since the areas of both unit meshes are equal, the two unit meshes are equivalent. Thus in the following we refer mostly to unit mesh A*.

The reciprocal surface net is depicted schematically on the left-hand side of Fig. 5.2(b). The corresponding surface net in real space is constructed on the right-hand side of this figure. Note that none of the real-space basis vectors is parallel to any of the reciprocal space basis vectors, because the surface net is oblique. From the LEED data it was calculated that the lengths of the basis vectors of unit mesh A* are in real space $(11.1 \pm 0.5) \text{ \AA}$ and $(21.0 \pm 1.0) \text{ \AA}$, and the enclosed angle is $(68 \pm 2)^\circ$.

Characteristic RHEED images of GaAs(2 5 11)A are presented in Fig. 5.2(c). These images appear if the electron beam is aligned along the three directions of high crystal symmetry that correspond to the basis vectors of the two unit meshes in real space. Thus one-dimensional cross sections of the reciprocal space surface net are acquired that are oriented perpendicular to the electron beam. The images were collected at room temperature. During growth, RHEED patterns were basically identical but the background intensity was higher. For each direction, two RHEED images are shown that were taken at two different angles of incidence of the electrons. The specular streak is not necessarily the brightest one, and the intensities of the other streaks are not symmetrically distributed with respect to the specular streak. The latter observation indicates that the reconstruction is not symmetrical with respect to the plane defined by the electron beam and the surface normal. The diffraction streaks of the zero-order Laue circle are more pronounced for the greater angle of incidence. However, the relative intensities of the streaks within this circle are different to those in the image for the smaller angle. This is most apparent in direction $[2\bar{3}1]$. At different angles of incidence the Ewald sphere intersects the rods of the reciprocal net at different heights. The change in the relative intensities implies that the intensity varies along different rods perpendicular to the surface in a different way.

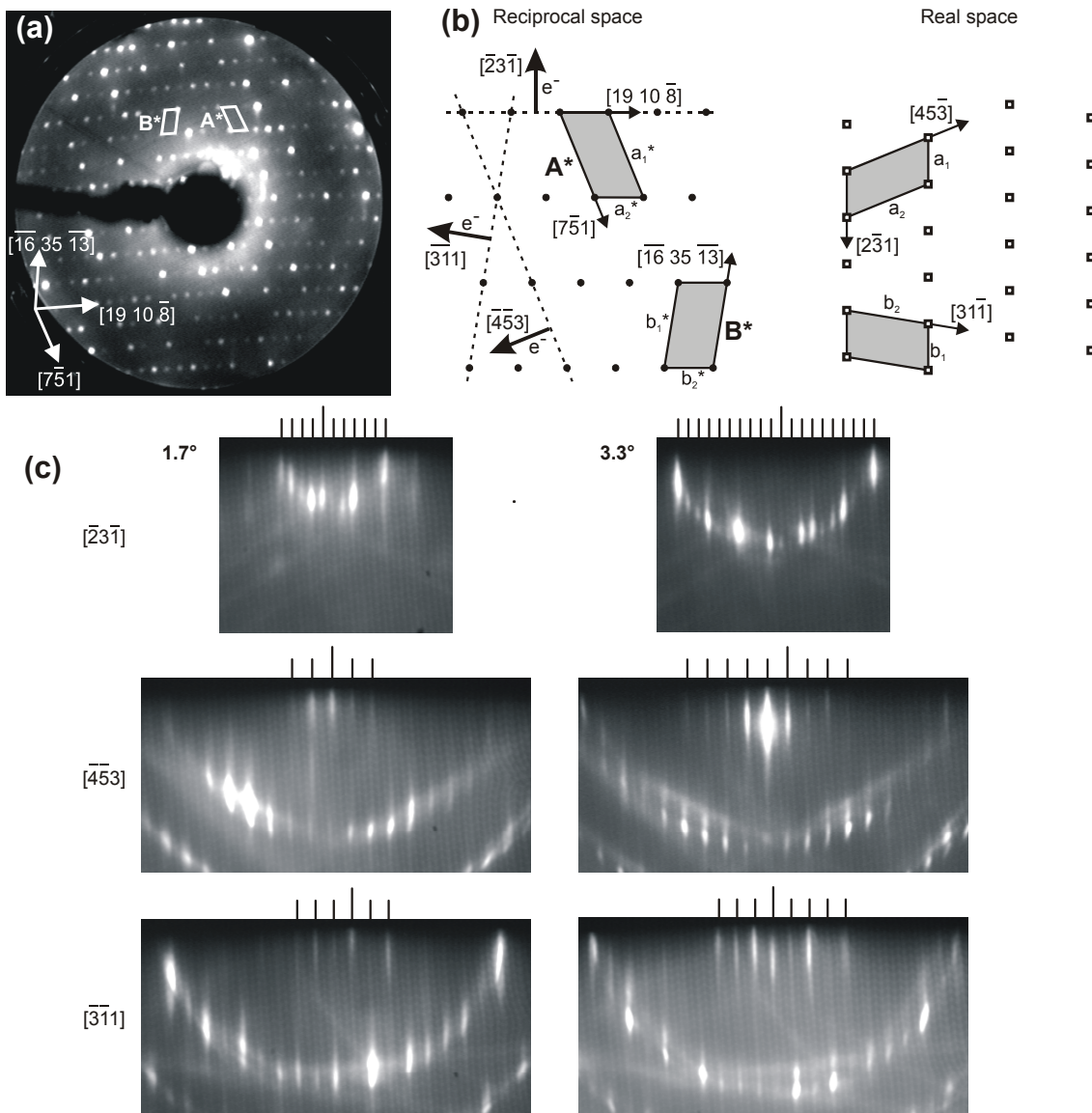


Figure 5.2 [Gee02] (a) LEED image of GaAs(2 5 11)A. $E=121$ eV. (b) Schematic of the surface net in reciprocal space (left-hand side) and in real space (right-hand side). (c) RHEED images of GaAs(2 5 11)A. The vertical lines at the top of the images mark the positions of the diffraction streaks of the zero order Laue circle. The longest line is located for each image above the specular streak. The respective orientations of the electron beam are indicated on the left-hand side of the images. The angles of incidence are specified next to the uppermost images. The acceleration voltage is 10kV.

A high-resolution (200×200) \AA^2 three-dimensional STM image of the GaAs(2 5 11)A surface is shown in Fig.5.3. The surface consists of stripes along $[2\bar{3}1]$ marked by dashed lines on the image border. The stripes are composed of little series made up from three white humps due to As dimers. There are also stripes consisting of series of two humps

(indicated by arrows in Fig. 5.3). This deviation from the periodicity is a typical feature of the GaAs(2 5 11)A surface that we will discuss later. The dimer series in neighbouring stripes are phase shifted, i.e., they are not aligned, but each series in the next stripe is situated between the series in the previous stripe. Narrow dark trenches separate the stripes. Arrows between some of the dashed lines mark two-dimer stripes or a coexistence of two- and three-dimer stripes.

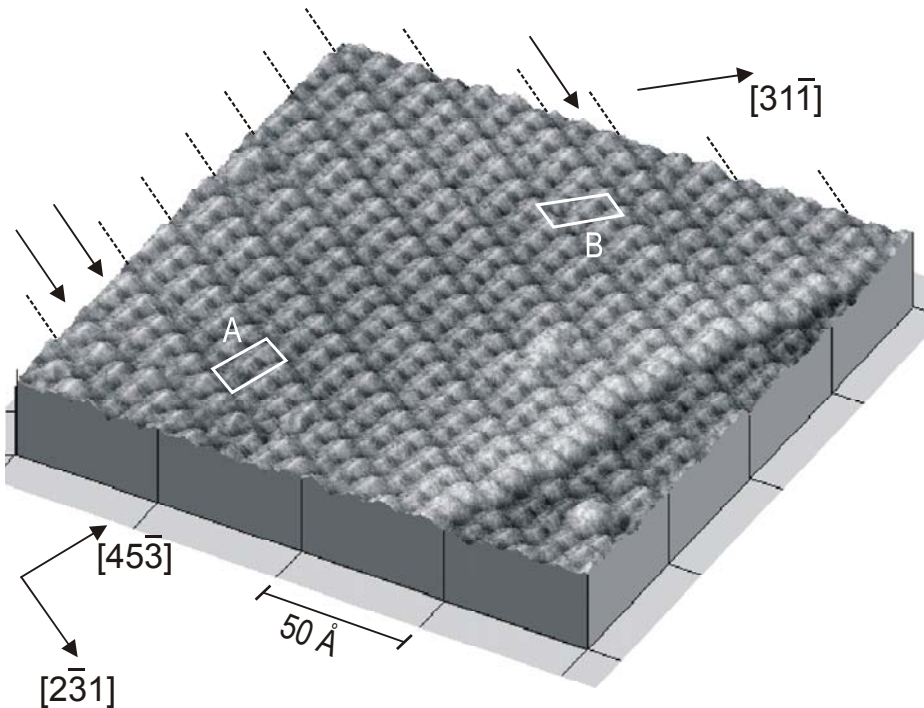


Figure 5.3 [Tem02] High-resolution STM image of the GaAs(2 5 11)A surface presented in three-dimensional form. Dashed lines at the image border indicate the trenches between the dimer stripes. The arrows between some of the dashed lines mark two-dimer stripes or a coexistence of two- and three-dimer stripes. Unit meshes A and B are depicted as white parallelograms. $U = -2.5 \text{ V}$, $I = 0.097 \text{ nA}$.

Quite intuitively two unit meshes can be found which are labelled A and B in Fig.5.3. They correspond to the unit meshes A* and B* in reciprocal space in Fig.5.2. The lengths of the vectors for unit mesh A are 10.6 Å and 20.0 Å, and the enclosed angle is 67.8°, the respective values for mesh B are 10.6 Å, 18.9 Å, and 80.7°. The vectors of mesh A are directed along $[45\bar{3}]$ and $[2\bar{3}1]$; those of mesh B along $[31\bar{1}]$ and $[2\bar{3}1]$. All these directions also play a key role in the morphology of the step structure on the GaAs(2 5 11)A surface.

The STM image of the (2 5 11)A surface depicted in Fig. 5.3 contains two terraces. The step exhibits one kink. The straight parts of the step are directed along $[45\bar{3}]$. The surface

shown in Fig. 5.3 is very perfect and clean: there are only two pieces of contamination likely due to adsorbed As_2 in a $(200 \times 200) \text{ \AA}^2$ area. Vacancies or other defects are not observed. This is different from the well-known $\text{GaAs}(001)$ surface and underlines the very high stability of the $\text{GaAs}(2\ 5\ 11)\text{A}$ surface.

In order to gain more insight into the surface structure a ball-and-stick model is presented in Fig. 5.4. The model has been derived by Geelhaar et al. [Gee01] from STM observations and ab initio total energy electronic structure calculations. Ga atoms are depicted as white, As atoms as black or grey balls. The (1×1) unit meshes A and B are indicated. They correspond to the bulk-truncated surface onto which two As atoms were adsorbed that are depicted as grey balls. The As-As bonds of the As dimers are indicated by black bars. On the filled-states STM image in Fig. 5.3 the dimers are seen as humps. The dimers are arranged in a series along $[12\bar{1}]$ that is inclined with respect to the surface plane such that the right-hand side lies higher than the left-hand side (cf. cross section in Fig. 5.4(b)). The three dimers in the unit mesh form the so-called three-dimer series. Each series is shifted along $[2\bar{3}\ 1]$ with respect to neighbouring one. Between the series there are trenches along $[2\bar{3}\ 1]$ which comprise empty Ga DBs (one of them is marked by number 9 on the right-hand side of Fig. 5.4(a) and therefore, appear as dark lines in the STM images.

For the sake of simplicity we will consider only the unit mesh A whose vectors lie along $[45\bar{3}]$ and $[2\bar{3}\ 1]$. The directions $[31\bar{1}]$ and $[2\bar{3}\ 1]$ form the second unit mesh B that is equivalent to A. The reconstructed (1×1) unit mesh contains 9 As DBs ($-27/4$ electrons), 7 Ga DBs ($+21/4$ electrons) and 3 As-As bonds ($+6/4$ electrons). The structural model fulfils the ECR; i.e., the surface has a semiconducting ground state.

Dimer series, that neighbour in direction $[2\bar{3}\ 1]$, form stripes of the orientation $(137)\text{A}$ (cf. cross section in Fig. 5.4(b)). These stripes are easily recognizable on the STM image in Fig. 5.3. The $(137)\text{A}$ stripes are not the result of nanofaceting, either, as will be explained in the following. First, the spherical depressions studied in [Gee00] also contained regions of the mean orientation $(137)\text{A}$. However, no stable surface was found there. Second, $\text{GaAs}(137)\text{A}$ reconstructed according to the stripes on $\text{GaAs}(2\ 5\ 11)\text{A}$ would violate the ECR (the resulting unit mesh is indicated by the dotted parallelogram in Fig. 5.4(a)). It is reflected in the higher surface energy of $\text{GaAs}(137)\text{A}(1 \times 1)$ compared to the $\text{GaAs}(2\ 5\ 11)\text{A}(1 \times 1)$ reconstruction, as can be seen in appendix 1.2 independent on the As chemical potential. Indeed, the stability of the reconstructed $\text{GaAs}(2\ 5\ 11)\text{A}$ surface is the result of the balance between $\text{GaAs}(137)\text{A}$ stripes of a certain width and the trenches in

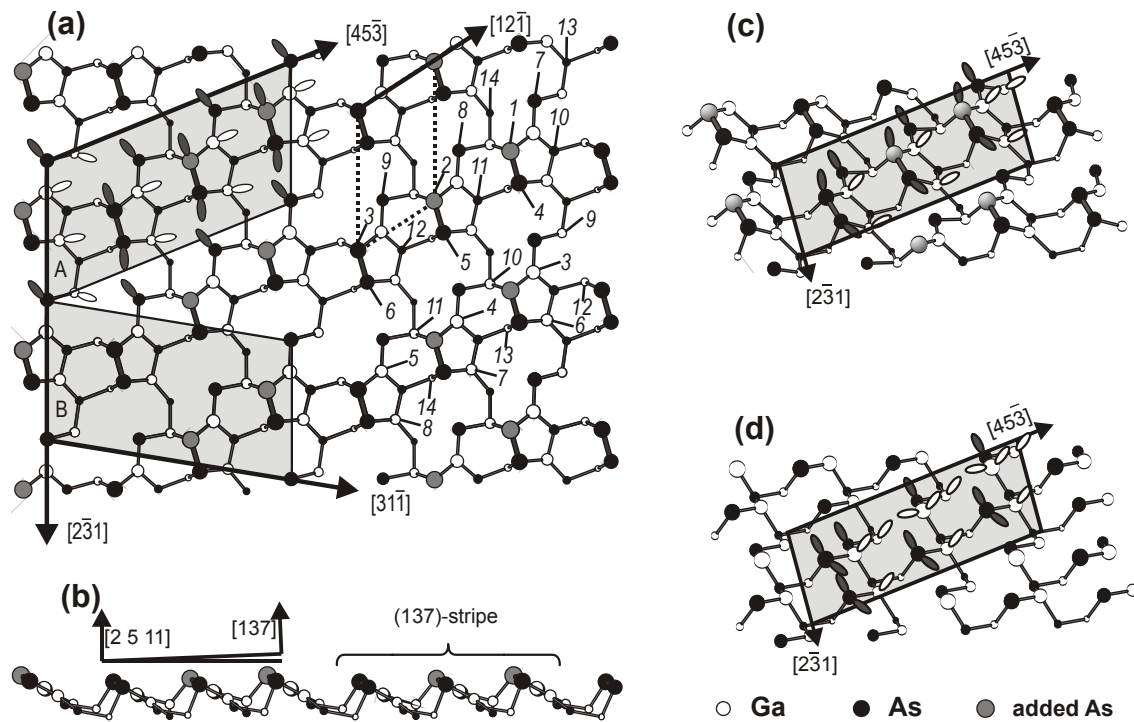


Figure 5.4 [Gee02+Tem02] Ball-and-stick model of the reconstructed $\text{GaAs}(2\ 5\ 11)A$ surface. Shaded parallelograms mark the unit meshes A and B. The size of the circles representing the atoms was chosen according to their vertical distance from the uppermost atom. To arrive at the reconstructed surface, the lighter shaded As atoms have to be added to the bulk-truncated surface. (a) (1×1) reconstruction, top view. The numbers near the As and Ga atoms show which atomic layer they belong to, counting from the top. Within the unit mesh A, the As atoms are depicted with black filled) DBs, the Ga atoms with white (empty) DBs; (b) (1×1) reconstruction, side view; (c) (1×1) reconstruction, perspective view; (d) bulk-truncated $\text{GaAs}(2\ 5\ 11)A$, perspective view.

between: In the trenches there is one Ga DB per unit mesh (labelled with 9 in Fig. 5.4(a)). The charge contributed by this DB is exactly necessary to make the complete structure fulfil the ECR. However, the difference in the surface energy at As-rich conditions is not very large (appendix 1.1): 56 vs. 53 $\text{meV}/\text{\AA}^2$ for $\text{GaAs}(137)A$ and $\text{GaAs}(2\ 5\ 11)A$, respectively. It becomes even smaller for the InAs surfaces: 43 vs. 41 $\text{meV}/\text{\AA}^2$. Furthermore, the surface stresses on coherently strained InAs QDs on GaAs substrates can change the surface energy, as reported by [Mol98] and [Wan00], or as could be seen from $\{135\}B$ facets that appeared as the flat base on InAs QDs on $\text{GaAs}(113)B$ (see chapter 4.2) but do not exist as the planar nominal $\{135\}B$ surface [Suz04a]. All these facts may account for a recent very remarkable result, revealed bounding facets on InAs QDs on $\text{GaAs}(001)$ to be composed of the $(137)A$ - (1×1) reconstructed surface [Mar01]. In addition, the

{137}A facets are often observed on the growth nuclei before the formation of mature QDs on the A substrates.

A model of the bulk-truncated (ideal) GaAs(2 5 11)A surface is shown in Fig. 5.4(d). In every atomic layer there is an equal number of Ga and As atoms. Thus the surface is stoichiometric. All stoichiometric GaAs surfaces automatically fulfil the ECR. However, there are several atoms with two DBs each, which is energetically very unfavourable. Hence it is unlikely that this structure is stable. The differences between the reconstructed surface Fig. 5.4(a-c) and the bulk-truncated surface Fig. 5.4(d) are that two As atoms were added and that the number of DBs was reduced by dimerization of neighbouring As atoms. The addition of two As atoms in the model is in agreement with the fact that the experimental surface preparation was As rich. The dimerization is in accord with the general principle that the number of DBs at a surface should be small. The periodicity of the reconstruction remains (1x1) as observed by LEED and RHEED. (Because of the large bulk-truncated unit mesh, on some high-index surfaces bonds can be created and broken without a change of the periodicity.) Neither bulk-truncated nor (1x1) reconstructed GaAs(2 5 11)A surface exhibits any symmetry plane.

For the following discussion of step structures, the vertical positions of the surface atoms are required. An atom is defined as belonging to the surface if it is in a configuration different from that in the bulk. Because of the high Miller indices, the spacing between the horizontal atomic planes (through lattice points) of the GaAs(2 5 11)A surface is only 0.23 Å. This value is quite small in comparison to those of low-index surfaces (e.g., to 2.00 Å for the GaAs(110) and 2.83 Å for the GaAs(100) surfaces). In the right hand half of Fig. 5.4(a) the GaAs(2 5 11)A surface atoms have been labelled with numbers according to the atomic layers they are part of, starting with the topmost atom (the numbers of different atomic layers are given separately for As and Ga atoms). For this purpose, relaxation from the bulk position has been neglected. The grey As atoms, which are added to form two of the three As dimers in the (1 × 1) reconstruction, occupy the highest positions within the unit mesh. From the third atomic layer on there are one Ga and one As atom in each plane, as the bulk-truncated GaAs(2 5 11)A surface is stoichiometric (cf. also Fig. 5.4(d)). The reconstruction comprises nine atomic layers. Nevertheless, the actual height difference between the top and the bottom surface atom, as calculated in [Gee02], is only 2.1 Å. Beginning from the tenth layer the atoms have bulk-like bonds. If relaxation is considered, the surface structure is even more complex. Note that – both from experiment and from

simulation – the As dimer consisting of As atoms 1 and 4 (dimer 1-4) as marked in Fig. 5.4(a) is higher than the As dimer 2-5 which in turn is higher than the As dimer 3-6. Hence, we will call the As dimer 1-4 the highest dimer, and the one 3-6 the lowest dimer. Since all As (or Ga) atoms are situated in different atomic layers, the height difference between the terraces on GaAs(2 5 11)A must be measured between equivalent elements on each terrace, for example between the highest As dimers. For the construction of step models it is sufficient to refer to the bulk layers that the atoms belong to.

We have been able to improve slightly a resolution of the STM image of GaAs(2 5 11)A presented Fig. 5.3. Two high-resolution (200×200) Å² STM images of the GaAs(2 5 11) surface are shown in Fig. 5.5(a-b). One recognizes that the surface consists of stripes along $[2\bar{3}1]$. Narrow dark trenches, marked by black lines on the image borders, separate the stripes. The stripes are composed of little series made up from three pairs of white dots, two bright pairs and a darker one. The pairs are best identified in the left-hand side of Fig. 5.5(b). From the separation of the dots in the pair and the location of the pair in the unit cell, the two dots of one pair seem to belong to one As dimer. So, each single dimer may be imaged as a pair of well separated dots. The spatial resolution is better than for the image in Fig. 5.3 and is much more clearer than that known for the STM images of GaAs(114)A α 2-(2x1) [Mar01], and GaAs(001) β 2-(2x4) [Bar02], which exhibit rows of As dimers on their reconstructions.

The images in Fig. 5.5(a) and (b) were acquired from the same area of the sample and with the same scanning parameters. Only the scanning direction was rotated at 90° in the image in (b) which can also be recognized by the change in the direction of the noise. These figures are shown in order to demonstrate that we do not have a double tip producing a doubling of structures in one direction.

It is also interesting to note a change in resolution during acquiring the image shown in Fig. 5.5(b). In the left-hand side of the image the surface exhibits very clear dimer constructions made up in perfect ordered stripes along $[2\bar{3}1]$. In the middle part the atomic resolution disappears. The dimers are imaged as whole integral dots that are still ordered in stripes along $[2\bar{3}1]$. This resolution can be most frequently seen in STM images of GaAs surfaces [Gee01, Gee02, Lab99]. In the right hand side of Fig. 5.5(b) the atomic resolution appears again but it is not so clear as in the left hand side. The whole image was acquired with the same sample bias, current and scan rate. It means that the atomic resolution is a matter of tip sharpness that may change during scanning by loosing or picking up of atoms.

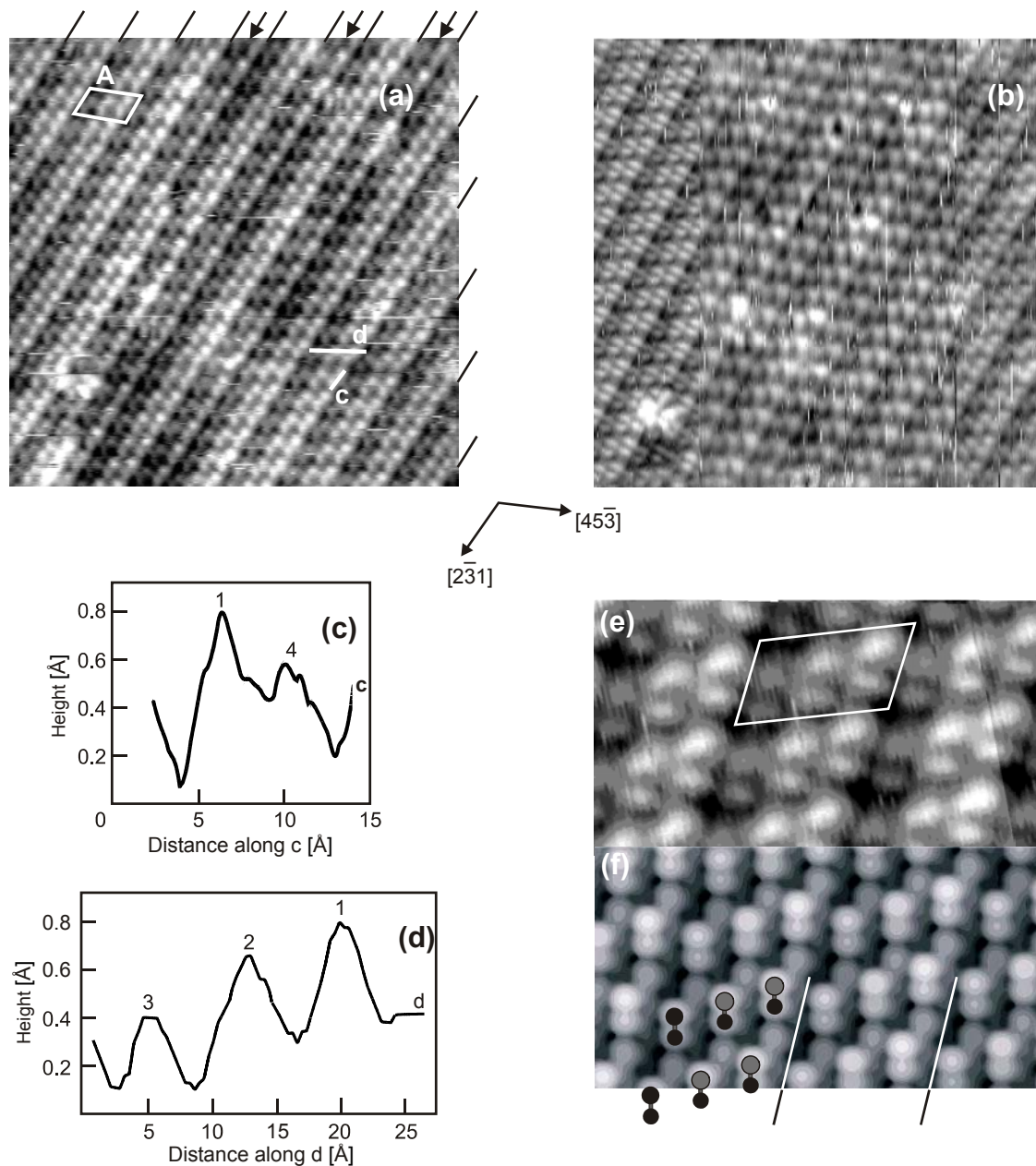


Figure 5.5 (a) Atomically resolved STM image of the GaAs(2 5 11)A surface. $U = -2.5$ V, $I = 0.097$ nA. X scans (fast) in horizontal direction from right to left and Y scans from top to bottom; (b) The same area imaged along the perpendicular direction. $U = -2.5$ V, $I = 0.097$ nA. Fast scan direction is the vertical direction (Y). X scans from right to left and Y scans from bottom to top; (c) Height profile c from top to bottom across two As atoms within one As dimer in (a); (d) Height profile d from left- to right-hand side across three As atoms within one series of As dimers in (a); (e-f) Experimental and simulated STM images of GaAs(2 5 11)A. The white parallelogram indicates the unit mesh, and the white-black lines at the bottom mark the trenches between the three-dimer stripes. The black and gray balls mark the As atoms in the dimer. (a) Experimental, filled states. $U = -2.5$ V, $I = 0.097$ nA. (b) Simulated, filled states. The local density of states was integrated for an energy interval that extended from the valence band top to -2.5 eV below.

The As dimer series are tilted approximately along $[4\bar{5}\bar{3}]$ as can be seen in image depicted in Fig. 5.5(a): The brightness of each of the three As dimer lines within one stripe decreases from the right to the left-hand side. For clarity, two height profiles are depicted in Fig. 5.5(c) and (d) elucidating the height changes of the As atoms. Here the line labelled c in Fig. 5.5(a) is directed along $[2\bar{3}\bar{1}]$ and displays the different heights of As atoms within a single As dimer. The line labelled by d is oriented along $[12\bar{1}]$ and shows the different heights of As dimers within a dimer series with respect to the surface plane. The peaks of the height profiles are numbered according to the labels of the As atoms in Fig. 5.4(a). The mean separation of the As atoms within the dimer was measured as 3.8 Å and the height difference as 0.2 Å. The respective values of the *ab-initio* calculation are 2.5 Å and 0.4 Å [Kra02a]. From measurements similar to the one shown in Fig. 5.5(d) the mean spacing between As dimers within one series (As atoms 1 and 3) was determined as 15.0 Å laterally and 0.4 Å vertically. This compares to the simulated values of 13.5 Å and 0.5 Å, respectively.

In order to understand deviations between distances measured from experimental, filled-state STM images and *ab-initio* calculations, a simulated filled-state STM image was generated using the calculated structure of the GaAs(2 5 11)A surface. Both images are presented in Fig. 5.5(e) and (f). In Fig. 5.5(e) the unit cell comprises six well ordered separated features. The pairs of these features neighboring in direction $[4\bar{5}\bar{3}]$ are separated by the black trenches that run down and connect with excellent agreement the trenches in the simulated image. The series of As dimers neighboring in direction $[2\bar{3}\bar{1}]$ in the simulated image exhibit additional features between the dimers that are not present in the experimental image. These features correspond to the As DBs from the seventh, eighth and ninth atomic planes in Fig. 5.4(a). This fact may indicate that the STM tip has not correctly displayed low-laying As DBs 7-9 and the STM current from them has been probably overlapped with the current from the As DBs 1-3. This has led to a decrease of the height and increase of the separation between the As DBs in the dimers compared to corresponding calculated values. The images in Fig. 5.5 clearly show a gap between the best-resolved structure of the GaAs surfaces and the actual positions of the atoms.

As we have seen, GaAs(2 5 11)A is a stable compound semiconductor surface located within the ST and exhibits a very original (1x1) reconstruction, which is far away from simple faceting or composition of low-index surfaces.

5.3 Step structure on the 1° vicinal GaAs(2 5 11)A surface

Getting ahead of the story, we should tell that the InAs heteroepitaxy is extremely sensitive on the morphology (step structure) of the GaAs(2 5 11)A surface. We will consider firstly the 1° vicinal surface, because historically we have started with this case and in addition, some results on nominal GaAs(2 5 11)A will repeat the results on vicinal GaAs(2 5 11)A.

The nominal orientations of the GaAs wafers (n-type, Si-doped, carrier concentration $1.1\text{--}4.8 \times 10^{18} \text{ cm}^{-3}$, Wafer Technology) were (113)A off-oriented by 9.7° and 10.2° in direction $[\bar{1}10]$ (manufacturer's specification); i.e., (3 7 15)A, and (19 47 99)A (Fig. 5.6(a)), or (2 5 11)A off-oriented by 1.0° in direction $[19\ 10\ \bar{8}]$, and by 1.0° in direction $[21\ 40\ \bar{22}]$, respectively (Fig. 5.6(b)). In contrast to $[2\ 5\ 11]$, the directions $[3\ 7\ 15]$ and $[19\ 47\ 99]$ lie in the plane formed by $[\bar{1}10]$ and $[113]$, i.e., in the $[33\bar{2}]$ zone. The direction $[33\bar{2}]$ was marked on the wafers by the manufacturer. The angle between $[33\bar{2}]$ and (2 5 11)A is about 1°. The projection of $[33\bar{2}]$ onto the (2 5 11)A plane as well as the off-orientation directions are given in Fig. 5.6(b) together with the three unit cell directions $[45\bar{3}]$, $[31\bar{1}]$ and $[2\bar{3}1]$ that are known from the previous chapter. For some STM images shown in the following, $[33\bar{2}]_{\text{proj}}$ is noted which allows to determine the absolute directions on the (2 5 11)A surface. Because of the small angle of 0.6° between (3 7 15)A and (19 47 99)A, their surface morphology exhibits identical step structures.

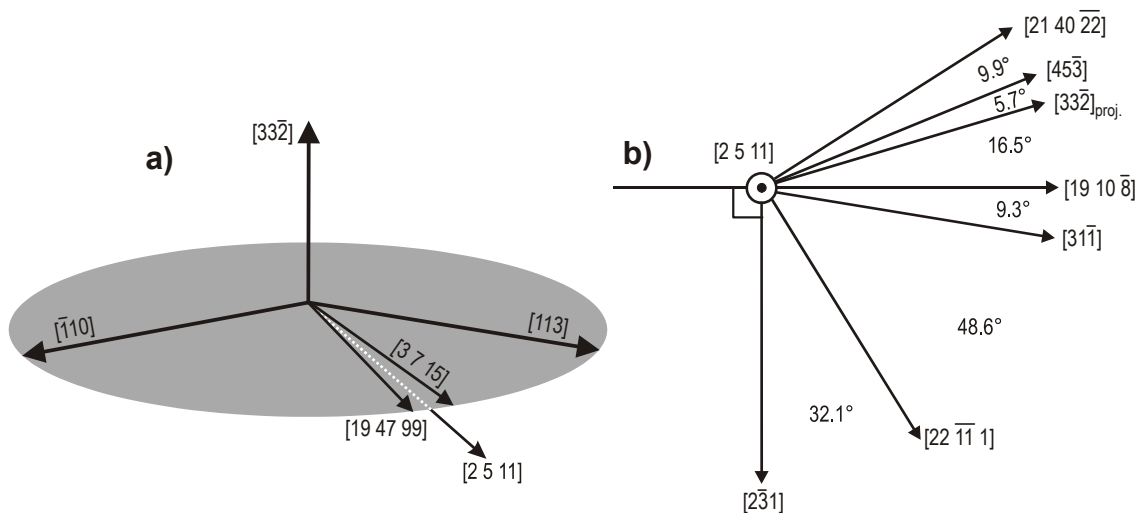


Figure 5.6 [Tem02] (a) Sketch of the $[3,3,-2]$ zone. $[2\ 5\ 11]$ lies about 1° below; (b) Sketch of the $[2\ 5\ 11]$ zone containing the three step directions characteristic for vicinal GaAs(2 5 11)A surfaces.

Therefore, in the following we will not distinguish between these wafer orientations. The majority of the studied samples was of the nominal $(3\ 7\ 15)A$ orientation, however, planar regions of a $(3\ 7\ 15)A$ surface were not observed. This is in accordance with an investigation of a spherical depression, prepared on a $\text{GaAs}(113)A$ wafer, which allowed to investigate GaAs surfaces vicinal to $(113)A$ with a continuous range of off-orientation angles up to 11.5° in all azimuth directions [Gee00]. In addition, $\text{GaAs}(3\ 7\ 15)A$ violates the ECR, and its surface energy was calculated to be greater than that of $\text{GaAs}(2\ 5\ 11)A$ (cf. appendix 1.1+1.2). Thus, $(3\ 7\ 15)A$ is not a stable surface, as opposed to the nearby $(2\ 5\ 11)A$ one. Consequently, in the simplest case one expects the studied samples to form the morphology sketched in Fig. 5.7(a). Steps separate terraces of reconstructed $\text{GaAs}(2\ 5\ 11)A$ (dark grey flats) and continuously decline in one direction in order to compensate the off-orientation. For isotropic step energies, the step edges should extend perpendicular to the direction of the off-orientation $[19\ 10\ \bar{8}]$ and $[21\ 40\ \bar{22}]$, i.e., along $[2\ \bar{3}\ 1]$ and $[21\ 40\ \bar{22}]$ for $(3\ 7\ 15)A$ and $(19\ 47\ 99)A$, respectively.

In order to gain a first overview of the surface morphology, a $(1 \times 1)\ \mu\text{m}^2$ large STM image is shown in Fig. 5.7(b). It is clear that the situation is more complex than sketched in (a). Across the whole image steps decline from the upper left to the lower right. The average direction of the steps, followed across the whole image, is approximately perpendicular to the projected $[33\ \bar{2}]$ direction, which is in agreement with the off-orientation. The image shown in Fig. 5.7(b) looks like typical STM or AFM images of vicinal low-index surfaces with a step structure compensating a slight off-orientation [Hat97, Tej99]. The steps are running along the three characteristic directions marked by dashed white lines and numbers 1 to 3. Steps of type 1 are very straight and extend up to several thousand Å in some areas. This type is similar to step bunch structures with large heights between the terraces. Steps of type 2 are not so straight as steps of type 1. Such steps extend seldom by more than 1000 Å, and their typical height is small. Contrary to steps of type 1 and 2, the steps of type 3 are rough, and occur with small step height only. Note that step of type 3 is close to the simple case shown in Fig. 5.7(a). Steps of type 1 and 2 lie on both sides of steps of type 3 and are straighter and more pronounced. They seem to be energetically more favourable.

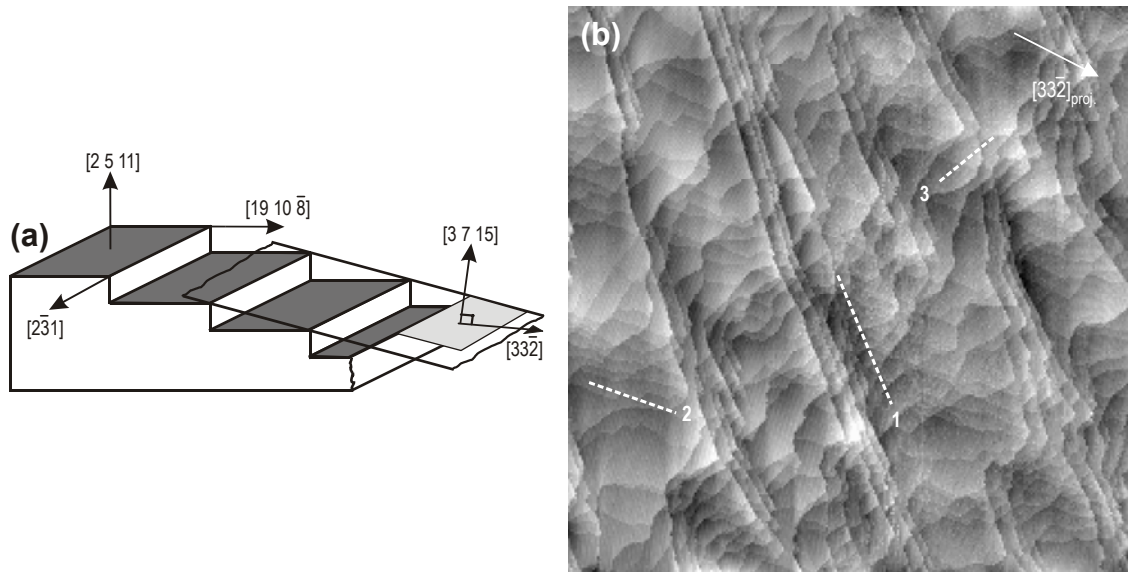


Figure 5.7 [Tem02] (a) Schematic of a step morphology for $\text{GaAs}(3\ 7\ 15)A$. The angle between $[3,3,-2]_{\text{proj}}$ and $[19, 10, -8]$ is 16.5° . The $(2\ 5\ 11)A$ plane is depicted as a dark grey and $(3\ 7\ 15)A$ as a light grey flat; (b) Overview STM image of $\text{GaAs}(2\ 5\ 11)A$. The three characteristic step directions are indicated by dashed lines and labelled 1, 2, and 3. $(1 \times 1)\ \mu\text{m}^2$, $U = -2.5\ \text{V}$, $I = 0.089\ \text{nA}$.

The $(1000 \times 1000)\ \text{\AA}^2$ large STM image shown in Fig. 5.8(a) allows determining the directions of the steps of type 1, 2, and 3. At such a resolution the stripes of the As dimers running from the top right-hand side to the bottom left-hand side are already visible as white rows separated by trenches between the dimers stripes, and even the single dimer series can be recognized. Thus, crystallographic directions can be extracted from the atomic structure and determined with respect to the projected $[33\bar{2}]$ direction. The surface decreases in height from the left lower corner to the right upper one and forms mainly three $(2\ 5\ 11)A$ terraces called as upper, middle and lower. The steps of type 1 form the step bunches running along $[31\bar{1}]$. They extend across the entire image and have few kinks in this area. In Fig. 5.8(a) two neighbouring steps can be seen, a phenomenon, that occurs quite often (see Fig. 5.7(b)). Steps of type 2 run along $[45\bar{3}]$ being sometimes straight, but exhibiting many kinks otherwise. Steps of type 3 run along $[2\bar{3}1]$, are rough, and mostly are not parallel to the trenches between the As dimers rows. Steps of type 2 and 3 usually have the same height. In contrast, steps along $[31\bar{1}]$ are usually of greater and variable height. In spite of the fact that the steps are sometimes rough, all three types can be clearly recognized on the surface for a wide range of preparation conditions. Therefore, we will consider them in more detail.

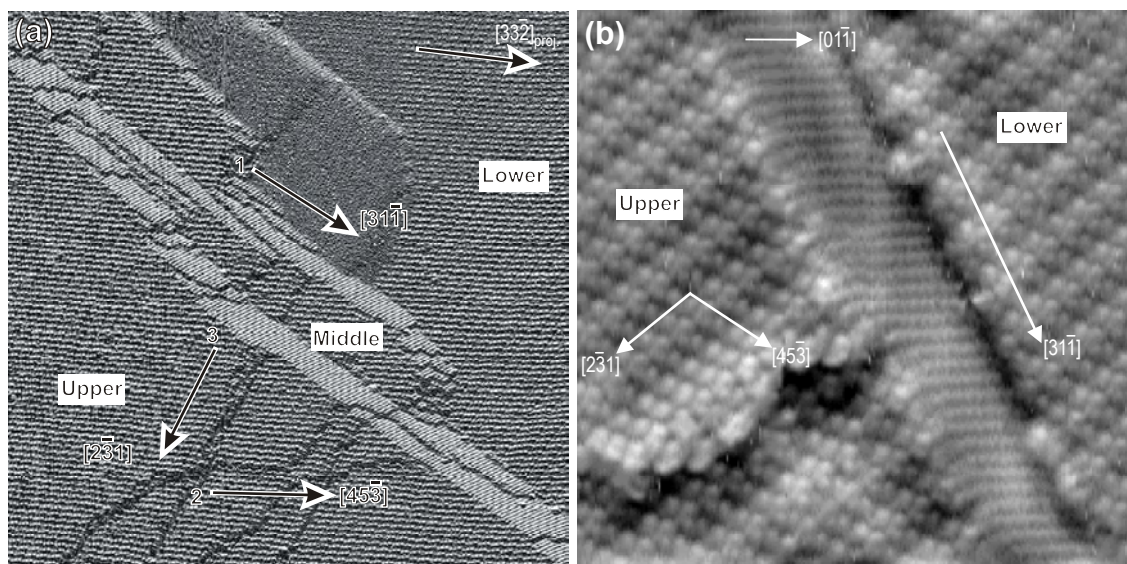


Figure 5.8 [Tem02] (a) High-resolution STM image (error signal=constant height mode) of the 1.0° vicinal $(2\ 5\ 11)A$ surface ($1000 \times 1000 \text{ \AA}^2$, $U = -2.5 \text{ V}$, $I = 0.097 \text{ nA}$); (b) Small area STM image of a $\text{GaAs}(2\ 5\ 11)A$ surface containing a step along $[3,1,-1]$. The upper and lower terraces are labelled U and L, respectively ($200 \times 200 \text{ \AA}^2$, $U = -3.0 \text{ V}$, $I = 0.099 \text{ nA}$).

5.3.1 Steps along $[31\bar{1}]$

A high resolution (200×200) \AA^2 STM image of a step along $[31\bar{1}]$ is presented in Fig. 5.8(b). The upper and the lower $(2\ 5\ 11)A$ terrace exhibit stripes of As dimers imaged as white humps. The step runs across the whole image from the lower left-hand to the upper right-hand side. The step wall consists of well-ordered rows of bright dots, which are most likely due to As-related states because of the negative sample bias (tunneling from filled states) and the As-rich preparation conditions. The distance between the rows is $(5.5 \pm 1.0) \text{ \AA}$ and the separation between the bright dots in each row is $(4.0 \pm 1.0) \text{ \AA}$. These values are in excellent agreement with the unit mesh of the $\text{GaAs}\{110\}$ surface (5.65×4.00) \AA^2 . The angle between the step wall and the $(2\ 5\ 11)A$ terraces as determined from STM images is $(20 \pm 5)^\circ$. This value is in good accord with the geometrical angle of 22.5° between $(2\ 5\ 11)$ and (011) . Also, the intersection line between these planes is along $[31\bar{1}]$. Therefore, we conclude that the walls of the steps along $[31\bar{1}]$ have the orientation (011) , and that each bright dot on the step wall in Fig. 5.8(b) corresponds to one As DB. The appearance of (011) areas as step walls is not surprising because the surface energy of $\text{GaAs}(110)$ is low: It is 52 meV/\AA^2 for the stoichiometric (cleavage) surface and 45 meV/\AA^2 for the highly As-rich surface for which Ga is replaced by As (cf. appendix 1.1). Our STM images indicate that we probably observe the stoichiometric variant.

The upper terrace in Fig. 5.8(b) also exhibits a rough step along $[2\bar{3}1]$ whereas there is not any additional step on the lower terrace. This means that the step along $[31\bar{1}]$ does not have a fixed height. Taking into account all STM observations of steps along $[31\bar{1}]$, the difference in height between the respective $(2\ 5\ 11)A$ terraces varied from 3 Å to 17 Å. These values correspond to lengths on the step wall of about 10 Å and 51 Å (along the $[01\bar{1}]$ direction).

In order to build a structural model of the step we have to know the atomic configuration at the step edges. In general, it is more difficult to resolve lower step edges by STM than upper ones, because at the lower step edge the tunneling current is also influenced by the separation between tip and step wall. Thus, only few STM images have been acquired with clearly resolved lower step edges.

In Fig. 5.9(a) an upper step edge formed by the intersection between the (011) step wall and the $(2\ 5\ 11)A$ terrace is shown. The As dimers on the $(2\ 5\ 11)A$ terrace are imaged as big humps and the As atoms on the (011) step wall as small dots. The upper $(2\ 5\ 11)A$ terrace ends with the highest dimers. At each of these dimers, one of the downward directed rows of As atoms starts on the step wall. Between these rows, there are two additional rows of As atoms. Along the upper step edge, two different features are observed between the highest dimers: in some places there is an extended white cloud (C in Fig. 5.9(a)), on other places there is a black depression (D in Fig. 5.9(a)). These two features may alternate in direction $[31\bar{1}]$, but a long-range periodicity was not found. Thus, there are two different modifications of the structure of the upper step edge.

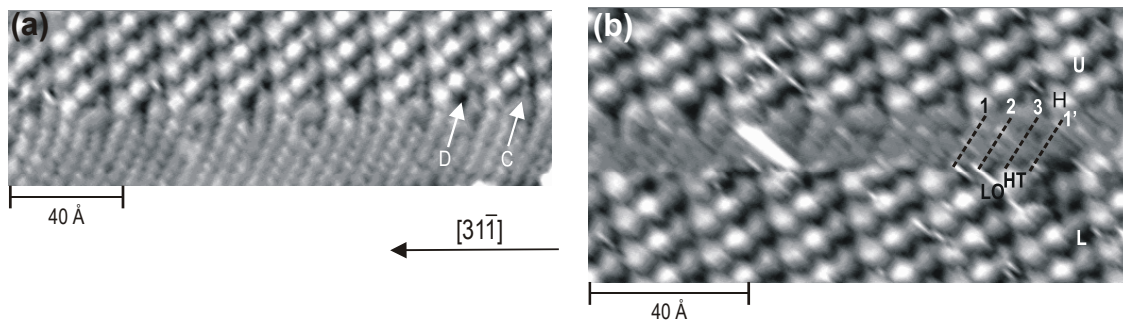


Figure 5.9 [Tem02] (a) $(195 \times 62) \text{ \AA}^2$ cutting out of an STM image of GaAs $(2\ 5\ 11)A$ showing an upper step edge along $[3,1,-1]$ ($U = -2.5 \text{ V}$, $I = 0.097 \text{ nA}$); (b) $(137 \times 69) \text{ \AA}^2$ cutting out of an STM image of GaAs $(2\ 5\ 11)A$ containing the upper and lower step edge along $[3,1,-1]$. The upper and the lower terrace are labelled U and L, respectively. $U = -2.5 \text{ V}$, $I = 0.097 \text{ nA}$.

A lower step edge is presented in Fig. 5.9(b). On this STM image, the upper step edge can also be seen. Here the step height is only $\sim 3 \text{ \AA}$, which is the smallest value observed. At the lower step edge, the highest dimer of the $(2 \ 5 \ 11)\text{A}$ dimer series nearest to the step (labelled as HT) is located between the As atom rows 3 and 1'. The lower dimer at the lower step edge (labelled as LO) is located between the rows 2 and 3 that start from the cloud or depression at the upper step edge. It should be noted that only two lower step edges with an overall length of about 200 \AA could be imaged and that the resolution was not good enough to state different modifications of the step edge.

Based on the STM image in Fig. 5.9(b), we propose in Fig. 5.10 a ball-and-stick model for the step along $[31 \bar{1}]$. In order to better distinguish between the upper and the lower $(2 \ 5 \ 11)\text{A}$ terraces and the (011) step wall, we have decreased the size of the sticks and balls on the step wall from the upper to the lower terrace. The height difference between equivalent As or Ga atoms along the (011) rows, i.e., in direction $[01 \bar{1}]$, is 1.39 \AA , which corresponds to six $\text{GaAs}(2 \ 5 \ 11)\text{A}$ atomic layers. The lower $(2 \ 5 \ 11)\text{A}$ terrace lies fourteen atomic layers lower than the upper terrace. (Compare Ga atoms from thirteenth atomic layer of the upper and of the lower terraces.) The height difference is 3.23 \AA , which is in good accord with the experimental value.

As two different modifications C and D of the upper step edge were observed by STM, two different unit meshes C and D were constructed in the structural model in Fig. 5.10. In both cases, there is one As dimer on the upper terrace corresponding to the lowest dimer of the $\text{GaAs}(2 \ 5 \ 11)\text{A}$ reconstruction in the right-hand corner of the unit meshes. Also, in both cases the (011) zigzag rows 1 and 3 on the step wall end at As dimers, while row 2 ends at a Ga atom that has one DB and that is rebonded to another Ga atom. The length of row 2 is different in unit meshes D and C: there is one extra As and one extra Ga atom in unit mesh C, i.e., in unit mesh C row 2 is longer by one periodicity length of the (011) surface. However, the number and the type of DBs is the same for both configurations. The As and Ga DBs at the upper step edge in unit mesh D, that belong to lower zigzag rows of the (011) surface (elements in dotted circles in Fig. 5.10), are saturated by extra As and Ga atoms with DBs in unit mesh C, that are from the upper zigzag row 2. As in unit mesh C the location of the Ga-Ga bond and of the preceding As DB from row 2 is higher with respect to the $(2 \ 5 \ 11)$ plane than the location of the As DB in the dotted circle and the Ga-Ga bond from row 2 in unit mesh D, these elements in the unit mesh C have to be

imaged brighter. Hence, configuration C corresponds to the white cloud in the STM images, and configuration D to the black depression.

At the lower step edge, the (011) rows 1 and 3 end at the highest and the lowest As dimer, respectively. The row 2 ends with a Ga-Ga bond. The highest and the lowest dimer at the lower step edge are situated between the rows of As DBs 1 and 3, and 3 and 2, respectively. That is in agreement with the STM image in Fig. 5.9(b) where As related states are imaged.

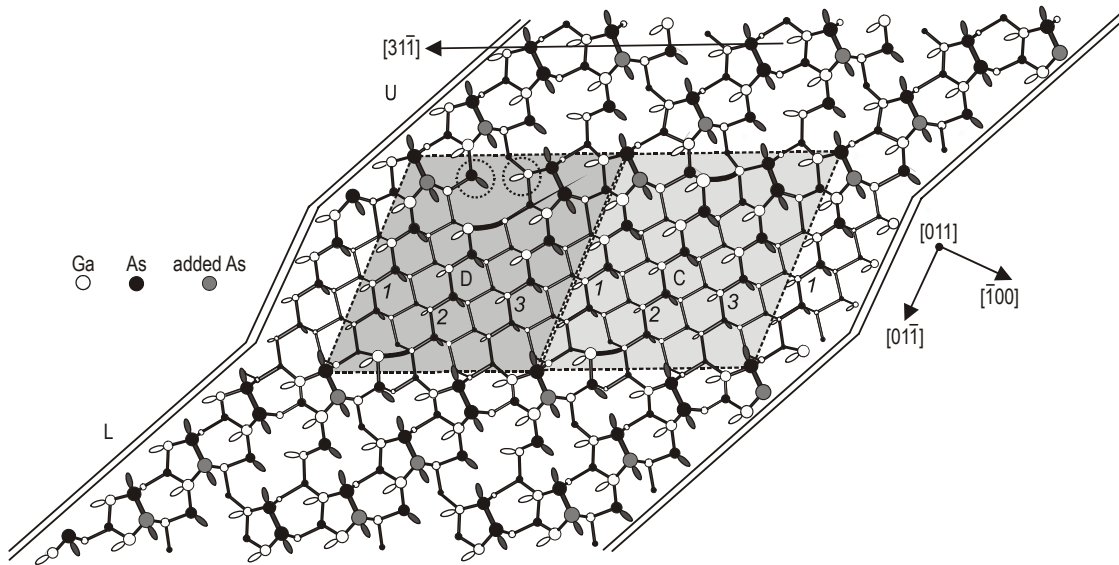


Figure 5.10 *[Tem02]* Ball-and-stick model of the step along $[3,1,-1]$. The upper and the lower terrace are labelled U and L, respectively. The zigzag rows of As and Ga surface atoms in the (011) facet, forming the step wall, are numbered in a sequence from 1 to 3 from left to right. Double lines at model borders outline the position of the terraces and of the step. The balls and sticks of the lower terrace are drawn with the same size as the ones of the upper terrace. Two different unit meshes D and C, corresponding to the different configurations for the upper step edge, are indicated by the dashed parallelograms.

For the analysis of semiconductor surface structures the ECR is of great help. The ECR has also been applied to step structures already before [Pas89, Mcc96, Gee99]. For steps it is problematic to define the area in which the electrons are counted. Unit meshes of the periodicity along the steps are not equal to the unit meshes of the periodicity on the (2 5 11)A terraces. The step unit meshes were chosen such that, if the step is removed, the upper terrace fits to the lower terrace without breaking the periodicity that is characteristic for the (2 5 11)A surface. In this case the ECR can be applied to the steps, since on the

terraces the rule is fulfilled. Note that generally for the construction of models, Ga and As atoms with two DBs were ruled out, since they are energetically unfavourable. Both unit meshes, C and D, fulfil the ECR: They contain 14 As DBs ($-42/4$ electrons), 14 Ga DBs ($+42/4$ electrons), 2 As-As bonds ($+1$ electron), and 2 Ga-Ga bonds (-1 electron). The As-As and the Ga-Ga bonds, which compensate each other, are located at the upper and lower step edge independent of step height. Therefore, the step height can increase stepwise by adding one Ga and one As atom with one DB each to the (011) rows on the step wall without influencing the charge compensation as one Ga and one As DB compensate each other. As mentioned above, adding a pair of Ga and As atoms corresponds to a change in height by 1.39 \AA .

As shown in [Kim01a] the average terrace width and step height of the steps, bunching on the 2° vicinal GaAs(001) surface, strongly depends on the thickness of the grown GaAs buffer layer. Under the preparation conditions used in this study the average terrace width and step height were about 1000 \AA and 8 \AA , respectively, by the minimal buffer layer thickness of 200 \AA . These values are in good agreement with the step bunches observed on vicinal GaAs(001). With increase of the buffer layer thickness, the terrace width and the step height increase on GaAs(2 5 11)A. However this effect is not so much pronounced as in [Kim01a], probably because of the arbitrary off-orientation direction of the vicinal (2 5 11)A surface and therefore, of the existence of the steps running in different from $[3\bar{1}\bar{1}]$ directions.

Although it is a matter of a theoretical study, the presence of many Ga atoms on the upper step edge that move into a surface by a sp^2 planar relaxation, may decrease the surface potential comparing with that away from the step. Therefore, we speculate that the (011) step wall may be formed due to a negative Schwoebel barrier on the step-edges, i.e., due to the preferred attachment of atoms from the higher terrace [Sch66]. As can be seen in Fig. 5.8(a) the steps on the bunched (011) surface run mainly along the zigzag chains (i.e., along the $[0\bar{1}\bar{1}]$ direction). These steps are generally favoured by the homoepitaxial growth on GaAs(110) when As_2 is used [Hol01]. Therefore, we speculate, that the (011) step wall may grow simultaneously and independently, whereas the (2 5 11)A surface may grow through the propagation of other steps, which are not bunched, e.g., steps along $[4\bar{5}\bar{3}]$ or $[2\bar{3}\bar{1}]$. It means, that, if the (011) step wall is once formed, it may not vanish and may increase in size with the increase of the buffer layer thickness.

5.3.2 Steps along $[4\bar{5}\bar{3}]$

The three-dimensional STM image shown in Fig. 5.3 contains a step along $[4\bar{5}\bar{3}]$ with one kink directed along $[2\bar{3}\bar{1}]$. A geometrical consideration reveals that the $(113)A$ plane intersects the $(2\bar{5}11)A$ plane along $[4\bar{5}\bar{3}]$. However, Fig. 5.3 shows that the GaAs $(113)A$ - (8×1) reconstruction with its $(32.0 \times 13.3) \text{ \AA}^2$ wide unit mesh does not form at the step wall. Two steps along $[4\bar{5}\bar{3}]$ can be seen in the high-resolution $(100 \times 100) \text{ \AA}^2$ STM image in Fig. 5.11(a). For clarity, white arrows mark the space between step edges. In contrast to steps along $[3\bar{1}\bar{1}]$, the height of the steps in (a) is fairly small. Most remarkable, in all acquired STM images the same height of $(2.0 \pm 0.5) \text{ \AA}$ was measured for all steps along $[4\bar{5}\bar{3}]$. Thus, the structure of the GaAs $(2\bar{5}11)A$ surface seems to permit only a fixed step height for this step type.

The STM images in figures 5.3 and 5.11(a) reveal that the complete series of three As dimers of the GaAs $(2\bar{5}11)A$ unit mesh A occur at the step edge both on the upper and on the lower terrace. Equivalent dimers on neighbouring terraces, like the ones labelled by 1 and 2 in Fig. 5.11(a), are shifted with respect to each other by $(3.0 \pm 0.5) \text{ \AA}$ in direction $[4\bar{5}\bar{3}]$. This shift is obvious when one looks at the dotted line: The line passes through the uppermost dimers on the middle terrace, but is located between dimers on the upper and the lower terrace. The distance between As dimer 1 and 2 is $(12.2 \pm 1.5) \text{ \AA}$.

On the basis of the experimental data we propose a structure model for the step along $[4\bar{5}\bar{3}]$ as shown in Fig. 5.11(b). When the step is approached from the lower terrace, there is no atom in a configuration other than found in the GaAs $(2\bar{5}11)A$ reconstruction. When the step is approached from the upper terrace, there are additional As and Ga atoms with one DB each below the Ga atoms that the As dimers in the GaAs $(2\bar{5}11)A$ reconstruction are bound to. The height difference between the two terraces is nine atomic layers, i.e., 2.08 \AA . (Along the $[1\bar{1}0]$ direction each atom lies three layers lower than the previous one). The shift in direction $[4\bar{5}\bar{3}]$ and the distance between equivalent dimers is 2.9 and 12.0 \AA , respectively. These values are in good accord with the STM data and support our model. The unit mesh of this step contains 12 As DBs ($-36/4$ electrons), 9 Ga DBs ($+27/4$ electrons) and 3 As-As bonds ($+6/4$ electrons). Hence, there is a charge deficit of $-3/4$ electrons per unit mesh, and the step along $[4\bar{5}\bar{3}]$ violates the ECR.

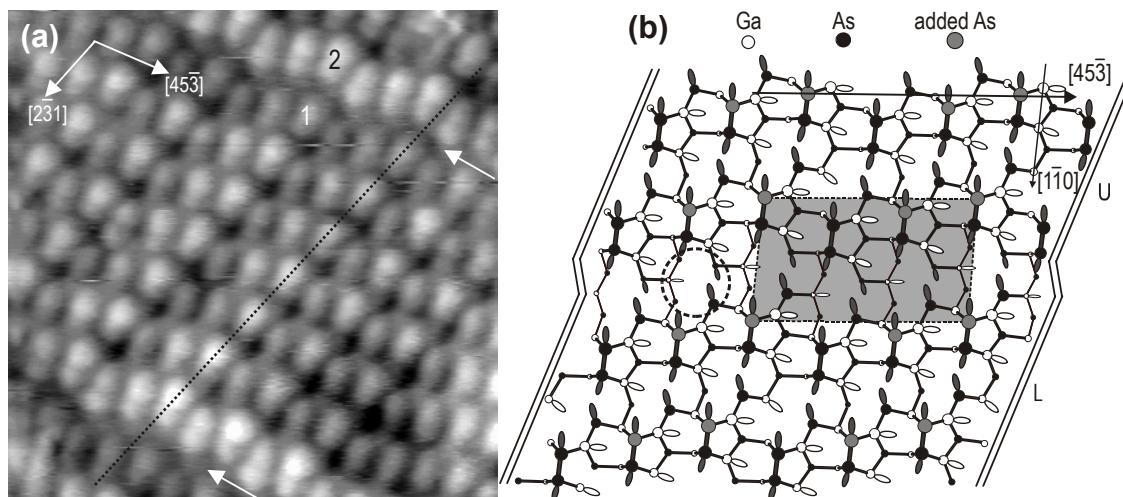


Figure 5.11 [Tem02] (a) Small area STM image of GaAs(2 5 11)A containing three terraces that are separated by steps along $[4,5,-3]$. White arrows near the image border indicate the steps. The dotted line elucidates the shift of equivalent dimers on different terraces, like the ones labelled 1 and 2. $U = -2.5$ V, $I = 0.18$ nA; (b) ball-and-stick model of a step along $[4,5,-3]$. The upper and the lower terrace are labelled U and L, respectively. The balls and sticks of the lower terrace are drawn with the same size as the ones of the upper terrace. The grey parallelogram indicates the unit mesh of the step structure. Double lines at model borders outline the position of the terraces and of the step.

The model presented in Fig. 5.11(b) may be modified by adding one Ga or As adatom at the position marked by the circle. This would decrease the number of DBs by two and would yield an excess charge of only $+1/4$ electron per unit mesh. However, such combinations are not confirmed experimentally. The STM image in Fig. 5.11(a) and its error signal (not shown here) exhibit no additional elements between the step edges. However, it should be noted that also on the (2 5 11)A terraces no element of the reconstruction apart from the dimers is resolved either. Thus, it is unclear whether such an adatom does exist or not.

Although the model for the step along $[4\bar{5}\bar{3}]$ depicted in Fig. 5.11(b) violates the ECR, most likely it does not have an excessively high energy, because there are not any atoms in unfavourable binding configurations (like twofold coordinated atoms), and the overall structure is very similar to that of the reconstructed terrace.

5.3.3 Steps along $[2\bar{3}1]$

Three different types of steps are observed along $[2\bar{3}1]$. The first one corresponds to the already mentioned two-dimer stripe that is visible, e.g., in Fig. 5.3. Such an element coexists with the usual three-dimer stripes. The $(1000 \times 1000) \text{ \AA}^2$ STM image in Fig. 5.12(a) permits to estimate the length and the density of two-dimer stripes. They are imaged as dark rows running from the upper left to the lower right up to a length of 1000 \AA . Sometimes these stripes cross steps along $[4\bar{5}\bar{3}]$ over three or four terraces. Since height measurements from STM images are rather difficult for this step, let us go the opposite way by starting with a model and coming back to the experiment later.

As can be seen in Fig. 5.3, besides the reduced number of dimers, the two-dimer stripe differs from the regular three-dimer stripe only in width. Thus, the construction of the corresponding model is fairly easy on the basis of the known $\text{GaAs}(2\ 5\ 11)\text{A}$ reconstruction. The top view of the model is depicted in Fig. 5.12(b). Starting at the left-hand side with a complete three-dimer series, the upper $(2\ 5\ 11)\text{A}$ terrace U ends with the lowest dimers (4) of the anticipated second three-dimer series which actually is only a two-dimer series. The lower terrace L begins with the lowest dimers (6) of a new three-dimer series shifted one dimer row to the left. In Fig. 5.12(c) the side view of the model is shown, in which the As dimers are depicted in the four uppermost atomic layers. It can be seen that the atoms on the lower $(2\ 5\ 11)\text{A}$ terrace are located one atomic layer lower than the equivalent atoms on the upper terrace.

The model in Fig. 5.12 shows how the two-dimer stripe is located between the three-dimer stripes on the upper and the lower terrace. A step wall is formed that is inclined by only 1.0° with respect to the $(2\ 5\ 11)\text{A}$ plane. On the planar $\text{GaAs}(2\ 5\ 11)\text{A}$ surface, there is a height difference of two atomic layers within a three-dimer stripe between dimers 1 and 3, which is compensated by the same height difference between the dimers 3 and 4 that are located on neighbouring stripes. Within the two-dimer stripe, there is only a height difference of one atomic layer between the dimers 4 and 5 instead of two before the height change of two atomic layers downwards between the dimers 5 and 6. Thus, dimer 6 lies one atomic layer lower than the equivalent dimer 1. Therefore, the two-dimer stripe is connected with a step. It exhibits the smallest possible step height on $\text{GaAs}(2\ 5\ 11)$ of 0.23 \AA , i.e., it is a step by one atomic plane and we call it mono-plane step in the following. The unit mesh of the monoplanes step (dashed parallelogram in Fig. 5.12(b)) contains 6 As DBs

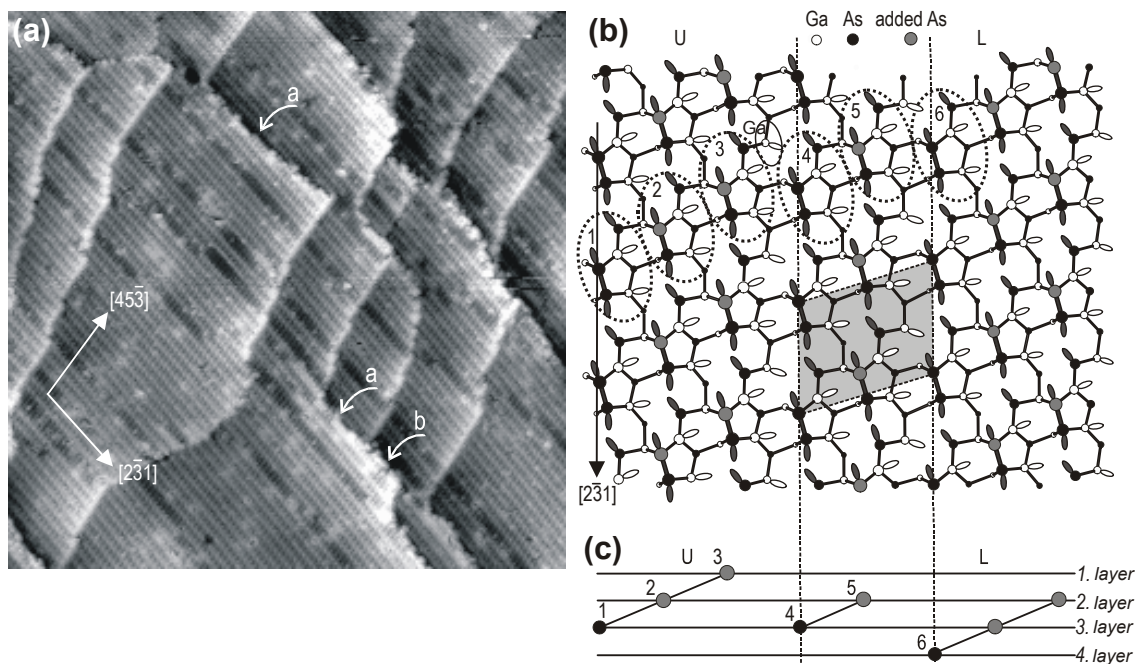


Figure 5.12 [Tem02] (a) Large area STM image of GaAs(2 5 11)A with the steps along $[2, -3, 1]$ ($U = -2.67$ V, $I = 0.1$ nA); (b) ball-and-stick model of the mono-plane step along $[2, -3, 1]$. The upper and the lower terrace are separated with dashed lines and labeled U and L, respectively. The parallelogram indicates the unit mesh of the step structure; (c) side view of the model. The As dimers within the three- or two-dimer stripes are linked with lines. The dimers are numbered according to the elements in the dashed ovals in (b).

(-18/4 el), 5 Ga DBs (+15/4 el) and 2 As-As bonds (+4/4 el). Thus, this unit mesh exhibits a positive excess charge of +1/4 electrons, i.e., this step violates the ECR.

The surface that consisted exclusively of two dimer stripes would be a reconstructed GaAs(3 7 15)A surface (see chapter 3.4), which is the nominal orientation of the samples. A two-dimer stripe is a means by which the macroscopic off-orientation is partly compensated. The analogous mono-plane step in the opposite direction corresponds to a four-dimer stripe. As such a step would induce an even greater deviation from the stable (2 5 11)A orientation, four-dimer stripes are barely found on the samples considered in this study. However, in the spherical depression study [Gee00] such four-dimer stripes were observed in the region near (2 5 11)A, probably induced by the opposite off-orientation.

It is clear from Fig. 5.12(a) that the density of monatomic steps is not sufficient to fully compensate the off-orientation. Indeed, higher steps along $[2\bar{3}1]$ with heights of (2.0 ± 0.5) Å and (4.0 ± 0.7) Å were also observed. The first value corresponds to the steps labelled (a) in Fig. 5.12(a). They separate together with the steps along $[45\bar{3}]$ the same

upper terrace from the same lower one, i.e., both steps have identical heights. Twice as high are the steps labelled (b).

In Fig. 5.13(a) a step of type (a) is shown with higher resolution. The step has a fairly rough structure with many kinks. Only in the about 100 Å long part marked by the white arrow a periodicity is observed. In this place the upper (2 5 11)A terrace ends with a two-dimer stripe and a last row of white features that are shifted along $[2\bar{3}1]$ but do not complete a full three-dimer stripe. The lower terrace starts with a regular three-dimer stripe. The distance between the white features in the shifted row on the upper terrace and the lowest dimers in the first regular three-dimer stripe on the lower terrace is (10.0 ± 1.5) Å.

The model for the straight areas of the steps of type (a) along $[2\bar{3}1]$ is depicted in Fig. 5.13(c). The height difference between two terraces is nine atomic layers, i.e., the same value as for the steps along $[45\bar{3}]$. Along $[01\bar{1}]$ each atom lies six layers lower than the previous one. Dashed lines, indicating the end of the upper and the begin of the lower terrace, pass through the lowest As dimers on the (2 5 11)A reconstruction. There is a two-dimer stripe and a row of shifted As dimers on the step wall. The distance between dimers labelled 1 and 2 in Fig. 5.13(c) is 9.8 Å, which is in good agreement with the measured distance between the white features on the upper terrace and the lowest dimers on the lower terrace. Between the rows of the dimers 1 and 2 a small area of the orientation (111)A is visible. This plane intersects the plane (2 5 11) along the direction $[2\bar{3}1]$. The shaded parallelogram in Fig. 5.13(c) indicates the unit mesh of the step. To avoid a large positive excess charge one Ga atom per unit mesh was removed from the (111)A surface. This is similar to the known vacancy of the reconstructed GaAs(111)A-(2 × 2) surface [Ton84]. However, in this reconstruction the Ga vacancies are not aligned along $[2\bar{3}1]$, as it is the case in Fig. 5.13(c). The unit mesh contains 12 As DBs (-36/4 electrons), 9 Ga DBs (+27/4 electrons) and 3 As-As bonds (+6/4 electrons). Altogether there is a negative excess charge of -3/4 electrons per unit mesh, i.e., the step violates the ECR.

Although the models for the $[2\bar{3}1]$ steps violate the ECR, we suggest a simple consideration based on a local fulfilment of the rule that may yield charge compensation. Starting from the model for the monoplane step in Fig. 5.12(b) let us consider the normal unit mesh of the (2 5 11)A surface containing structural elements 1, 2, and 3 around the As dimers in dashed ovals and the Ga DB in the solid oval next to element 3 (the unit mesh A in Fig. 5.4(a)). Going in direction from the upper to the lower terrace a two-dimer stripe appears because of the off-orientation or kinetic reasons [Gee01]. In order to distribute the

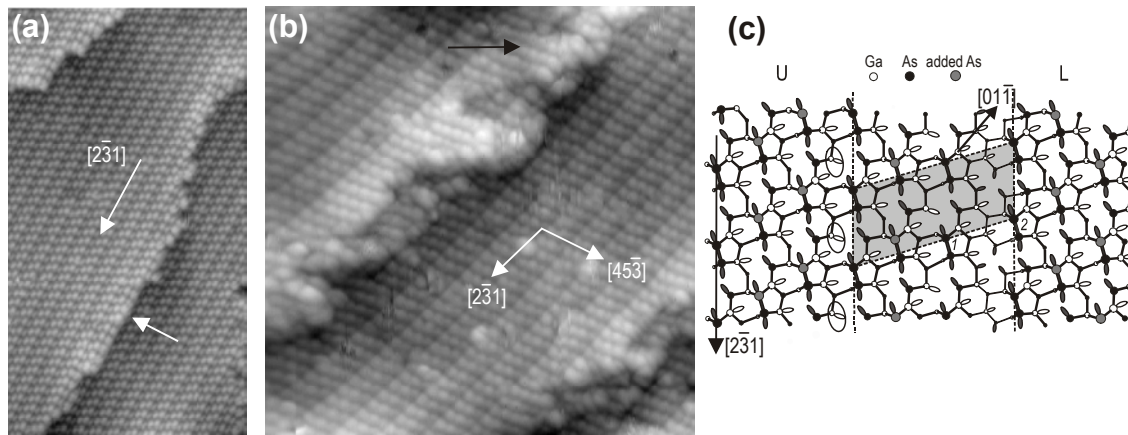


Figure 5.13 [Tem02] (a) $(270 \times 510) \text{ \AA}^2$ cutting out of an STM image of GaAs(2 5 11)A showing a step of type (a) along $[2, -3, 1]$. The straight part of the step is indicated by the white arrow ($U = -2.5 \text{ V}$, $I = 0.097 \text{ nA}$); (b) Small area STM image of GaAs(2 5 11)A containing a step of type (b) along $[2, -3, 1]$. The black arrow indicates a small area of the reconstructed GaAs(137)A surface. $U = -2.5 \text{ V}$, $I = 0.302 \text{ nA}$; (c) ball-and-stick model for a straight area of the step of type (a) along $[2, -3, 1]$. The upper and the lower terrace are separated with dashed lines and labeled U and L, respectively. The parallelogram indicates the unit mesh of the step structure. The balls and sticks of the lower terrace are drawn with the same size as the ones of the upper terrace.

charge in such a way, that all the Ga DBs are emptied and all As DBs are filled, the elements 4 and 5, “confiscate” the element 6 from the neighbouring three-dimer stripe and the Ga atom with a DB between elements 5 and 6. The remaining two As dimers in the three-dimer stripe perform the same operation with the next stripe, etc. Now the form of the unit mesh (but not its content) on the GaAs(2 5 11)A surface is changed: it consists of the elements 4, 5, and 6, and the Ga DB between 5 and 6. In this form the unit mesh exists up to the next two-dimer stripe and thereafter transforms again to include the elements 3, 4, and 5 with the Ga DB situated between 3 and 4. With this form of the unit mesh the GaAs(2 5 11)A terrace can again extend arbitrarily long up to the next two-dimer stripe. After the third two-dimer stripe the unit mesh transforms to the one consisting of elements 1, 2, and 3 with the Ga DB situated before the element 1. A location of the Ga DB inside the unit mesh is reversed but it is not yet far from normal unit mesh A. It means the last terrace can again extend arbitrarily long and can end with the step of type (a) described in Fig. 5.13(c). Thereby, the Ga DBs in solid ovals in Fig. 5.13(c) are superfluous for the upper terrace and they can extinguish the negative excess charge of $-3/4$ electrons that is specific for the straight areas of the step of type (a). The lower terrace beginning after this

step has a normal unit mesh A , and such compensation can be repeated. From Fig. 5.12(a) one can recognize that terraces are separated not only by steps of type (a) (or (b)) along $[2\bar{3}1]$ but also by steps along $[45\bar{3}]$. The full explanation in terms of the ECR would require to take all these steps into consideration what is much more difficult.

More complex is the step labelled (b) in Fig. 5.12(a). It is of double height (about 4 Å) compared to the step of type (a). This step is shown with higher resolution in the $(300 \times 300) \text{ \AA}^2$ STM image in Fig. 5.13(b). In some regions the double-height step is split into two single-height ones. At those positions, where the double-height step is developed, nano-areas are observed (marked by an arrow) consisting of As dimers without any trench along $[2\bar{3}1]$ that is characteristic for the $(2\ 5\ 11)A$ reconstruction. These areas correspond to a $\text{GaAs}(137)A$ surface, which is also the orientation of the three-dimer stripes between the trenches. Any periodicity for the step of type (b) was not observed and a model cannot be offered for this situation.

To summarise the morphology study, three characteristic steps are observed on vicinal $\text{GaAs}(2\ 5\ 11)A$ surfaces which run along $[31\bar{1}]$, $[45\bar{3}]$, and $[2\bar{3}1]$. These directions correspond to the unit cell directions on $\text{GaAs}(2\ 5\ 11)A$ surfaces that were observed also in LEED and RHEED experiments. The directions correspond to the intersections of the (011), (113), and (111) planes with the $(2\ 5\ 11)$ plane, respectively. These steps were atomically resolved what allowed detailed modeling of their structures. Steps along $[31\bar{1}]$ are especially long and straight and often bunch together forming larger (011) facets.

The ECR analysis of the step models indicates that the rule can be fulfilled for steps along $[31\bar{1}]$, but is violated for steps along $[45\bar{3}]$. This holds generally also for steps along $[2\bar{3}1]$ but it may well be that the steps violate the ECR locally but fulfil it within mesoscopic areas for certain step successions. Obviously, the failure in fulfilling the ECR by a charge deficit of $3/4$ electrons for the $[45\bar{3}]$ step (cutting plane (113)) and of a deficit of $3/4$ electrons for the $[2\bar{3}1]$ step (cutting plane (111)) does not introduce a large energetic imbalance. This is concluded as no extended (113)A or (111)A facets with their own reconstructions are formed. The very long and straight steps along $[31\bar{1}]$ could possibly be employed for the ordering alignment of self-organized InAs QDs.

5.4 InAs islands on 1° vicinal GaAs(2 5 11)A

The high performance optical devices based on the InAs QDs require a very homogeneous size distribution and the reduction of the number of incoherent radiationless islands, which usually form due to the coalescence of some QDs [Moi94, Suz03]. Several authors have proposed to use for this purpose vicinal GaAs substrates in order to create dense arrays of the uniform QDs along step-edges [Iko95, Min98]. Such a proposal is based on the experimental fact that the QDs tend to nucleate on the steps even on the nominal oriented GaAs substrate [Leo94, Iko95, Has01], probably on the lower terraces. As shown by Talalaev et al. [Tal00] by means of PL measurements, the QDs become smaller and more uniform in size by increase of the off-orientation angle up to 7° for GaAs(001). This was explained in terms of a lateral confinement of the QD size on terraces by step bunching. An appearance of wirelike InAs QDs at the steps on the 2° off-oriented GaAs(100) substrate was demonstrated in reference [Kim01] using atomic force microscopy (AFM). It was concluded that intervals between these wirelike QDs were significantly affected by the terrace width resulting from the step bunching effect. However, detailed knowledge about the mechanism of the InAs island nucleation at steps as well as the role of the step bunching effect is still missing mainly because of lack of the atomic structure of the steps.

In the previous chapter we have shown, that the 1° vicinal GaAs(2 5 11)A surface exhibits straight step bunches along $[3\bar{1}\bar{1}]$. Hence it is interesting to explore how far these structures can be utilised for the special control of dense arrays of the uniform InAs QDs.

The evolution of the RHEED patterns along the three characteristic directions $[\bar{2}\bar{3}\bar{1}]$, $[\bar{3}\bar{1}\bar{1}]$ and $[\bar{4}\bar{5}\bar{3}]$ during InAs deposition on 1° vicinal GaAs(2 5 11)A is shown in Fig. 5.14(a-f). (For the initial bare GaAs(2 5 11)A surface the RHEED images are depicted in Fig. 5.2(c).) The deposition of InAs up to the transition to the 3D growth mode results in a spreading of the sharp (1x1) periodicity as shown in Fig. 5.14(a-c). It is particularly apparent for the RHEED pattern along $[\bar{2}\bar{3}\bar{1}]$, whereas the diffuse x1 periodicity is still remained for the pattern along $[\bar{4}\bar{5}\bar{3}]$ and $[\bar{3}\bar{1}\bar{1}]$ even beyond the 3D transition (Fig. 5.14(b, e) and Fig. 5.14(c, f)). 3D islands, emerging on the 2D wetting layer after the SK growth mode, give normally rise to the appearance of transition spots on RHEED patterns due to the electrons running through the islands. In the case of InAs islands on the vicinal GaAs(2 5 11)A the change of the RHEED pattern is clearly seen only along $[\bar{2}\bar{3}\bar{1}]$, where the parallel lines of sharp transition spots occur as shown in Fig. 5.14(d).

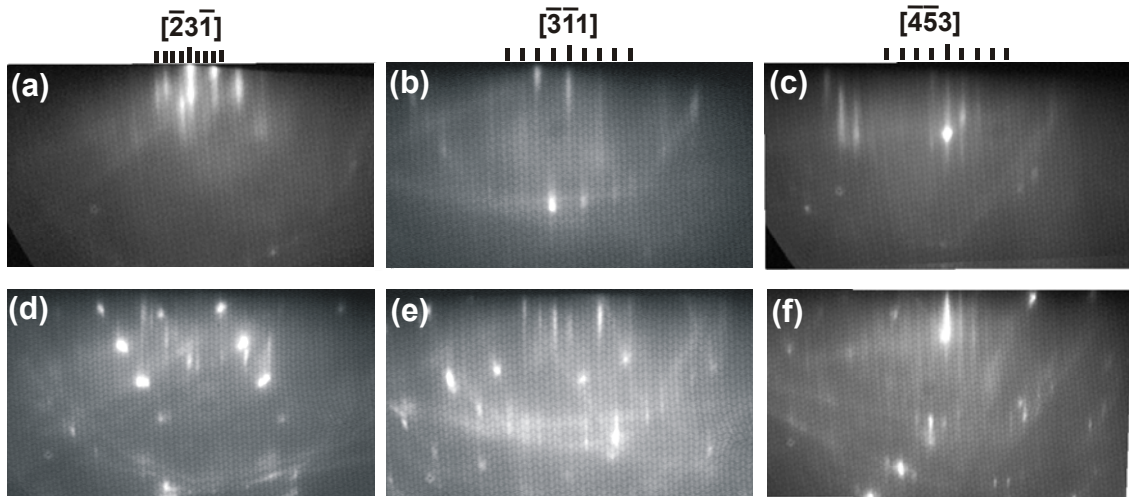


Figure 5.14 [Tem04] Room temperature RHEED pattern ($U=10$ kV) of the InAs wetting layer and InAs islands on the vicinal GaAs(2 5 11)A surface; (a-c) InAs wetting layer (InAs thickness is equal to 3.5 Å); (d-f) RHEED pattern after the 3D transition (InAs thickness is 5.0 Å). The WL or islands have been deposited in the MBE chamber and cooled down in the STM chamber.

The above-mentioned features of the RHEED patterns during InAs deposition can be understood with help of STM images. Figure 5.15(a) shows a large area of the vicinal GaAs(2 5 11)A surface prior to InAs deposition. The long and straight step bunching along $[3\bar{1}\bar{1}]$ as well as large GaAs(2 5 11)A terraces are seen from this image. Figure (b) exhibits an atomically-resolved image of the GaAs(2 5 11)A terrace. Besides the small number of two-dimer stripe perturbations the surface is remarkably well ordered. The deposition of 3.5 Å InAs at 370-500°C, which is below the SK transition, results in morphology, shown in Fig. 5.15(c). The step bunch structures along $[3\bar{1}\bar{1}]$ still persist with similar lengths and step heights as for the bare vicinal GaAs(2 5 11)A. However the atomic structure on the surface becomes quite disordered as shown in Fig. 5.15(d). A fairly long periodicity is remained only along the $[\bar{2}\bar{3}\bar{1}]$ direction on the real space STM image in Fig. 5.15(d), which accounts for the conservation of the diffuse x1 periodicity on the reciprocal space RHEED patterns along $[\bar{3}\bar{1}\bar{1}]$ and $[\bar{4}\bar{5}\bar{3}]$ in Fig. 5.14(b, c).

Figure 5.16(a) exhibits a large area STM image of the 1.0° vicinal (2 5 11)A surface beyond the SK transition. 3D islands, that are very different in size but normally uniform in shape, appear exactly on the step bunches along $[3\bar{1}\bar{1}]$ with a fairly low number density of $7 \cdot 10^9$ cm⁻². The terraces are almost free from the InAs islands. Since the islands are aligned towards the $[3\bar{1}\bar{1}]$ direction, the electron beam along $[\bar{3}\bar{1}\bar{1}]$ and probably along $[\bar{4}\bar{5}\bar{3}]$ (the

angle difference between these directions is 31.5°) cannot pierce through the many large islands. Therefore, the RHEED patterns in Fig. 5.14(e, f) do not clearly reflect the SK transition, which can be only seen with the electrons incident along $[\bar{2}\bar{3}\bar{1}]$.

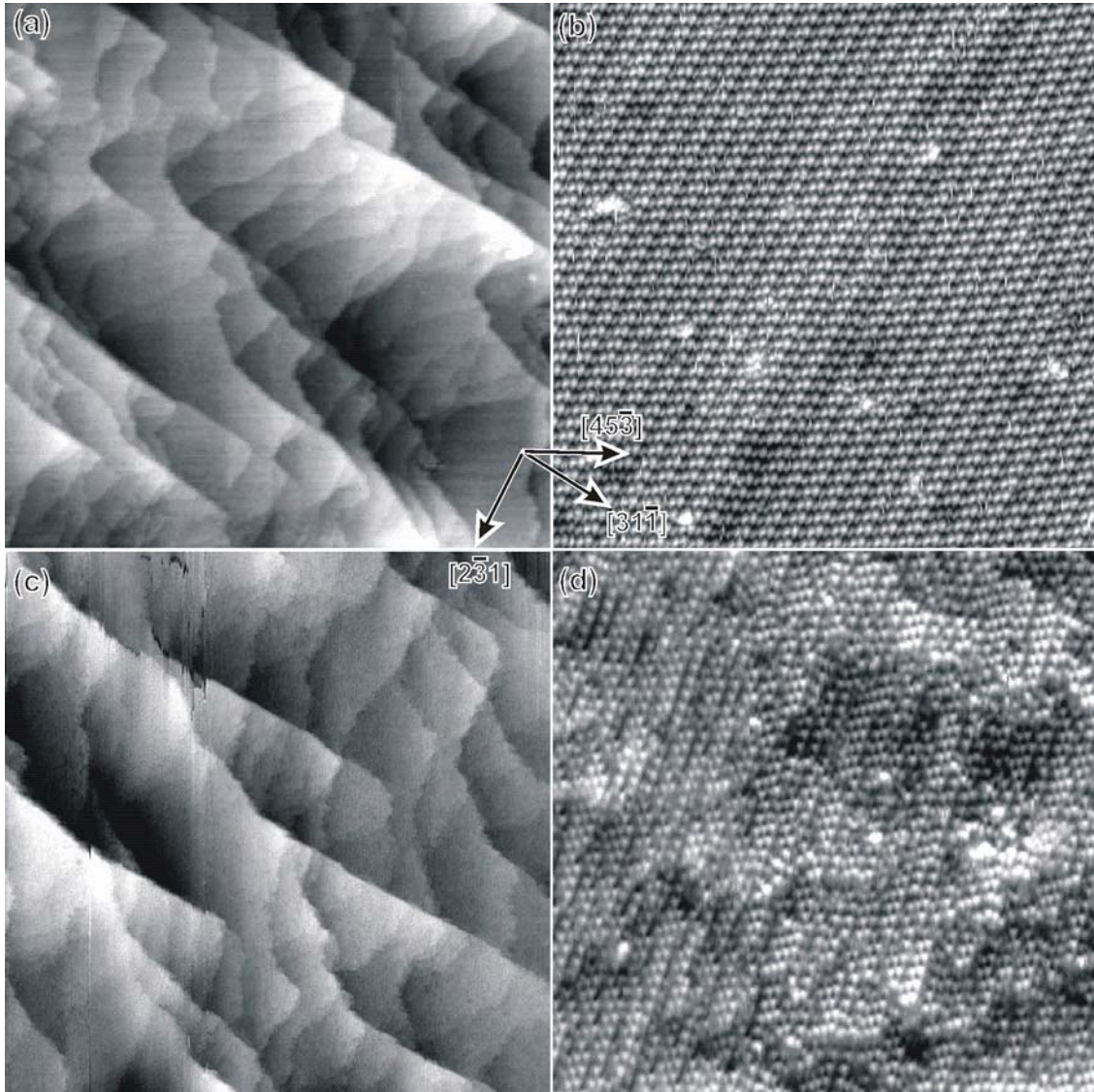


Figure 5.15 [Tem04] (a-b) STM images of the bare vicinal GaAs(2 5 11)A surface: (a) $6000 \times 6000 \text{ \AA}^2$, $U = -2.5 \text{ V}$, $I = 0.1 \text{ nA}$ and (b) $465 \times 465 \text{ \AA}^2$, $U = -2.5 \text{ V}$, $I = 0.097 \text{ nA}$; (c-d) STM images of the InAs WL on the vicinal GaAs(2 5 11)A surface: (c) $6000 \times 6000 \text{ \AA}^2$, $U = -3.0 \text{ V}$, $I = 0.18 \text{ nA}$ and (d) $465 \times 465 \text{ \AA}^2$, $U = -3.0 \text{ V}$, $I = 0.699 \text{ nA}$.

Figures 5.16(b, c) compare the size distribution (the length along the $[31\bar{1}]$ direction) of the InAs islands on vicinal GaAs(2 5 11)A with that of the InAs QDs on GaAs(113)B. InAs was deposited at the same preparation conditions onto both surfaces until the SK transition

occurred. The size distribution of the InAs QDs on GaAs(113)B is very sharp with the peak at about 250 Å running up to 60% of all measured dots. This sharpness is induced by the elastic strain in the QDs that promotes a certain size for the dot at a given temperature (see chapter 4.2). It is obviously not the case for the InAs islands on vicinal GaAs(2 5 11)A. Their size distribution is very broad with the peaks running only up to 15% of all islands. Therefore, we propose a following scenario of the InAs heteroepitaxy on vicinal GaAs(2 5 11)A: InAs may grow simultaneously up to the appearance of 3D islands both on the GaAs(2 5 11)A substrate and on the GaAs(011) step walls in layer-by-layer growth mode. On the latter the misfit dislocations occur in the second InAs layer [Bel97, Joy98].

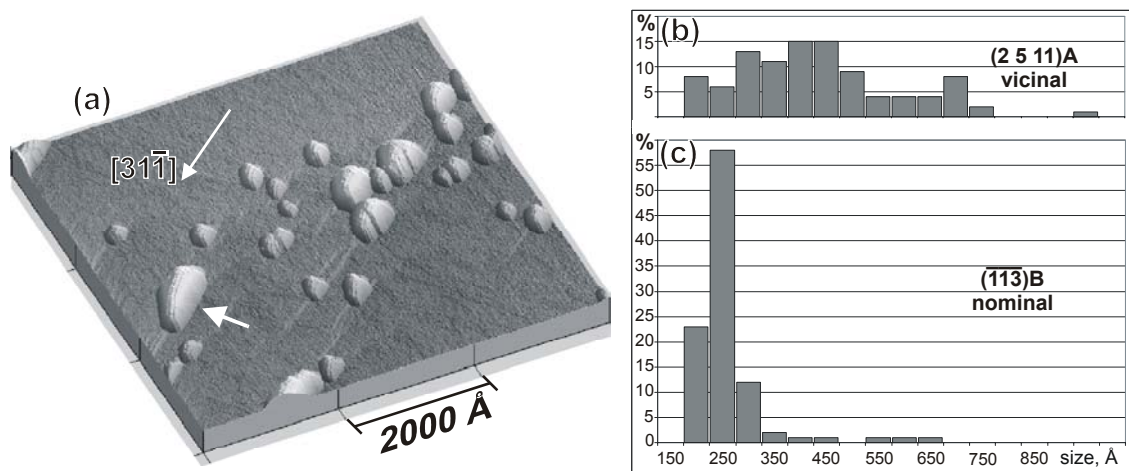


Figure 5.16 [Tem04] (a) 3D STM image of the InAs islands on vicinal GaAs(2 5 11)A (6000x6000 Å², $U = -2.5$ V, $I = 0.15$ nA, InAs thickness was 5.0 Å at sample temperature $T = 440$ °C); (b-c) comparison between the size distribution of the InAs islands on vicinal GaAs(2 5 11)A and of the InAs QDs on nominal GaAs(113)B. (a) InAs thickness was 5.0 Å at $T = 440$ °C; (b) InAs thickness was 4.3 Å at $T = 435$ °C.

After the SK transition on GaAs(2 5 11)A terraces the InAs material may be easily collected on the relaxed (011) step walls and form 3D InAs islands. Since the islands exhibit the misfit dislocations they may grow without limitation caused by the elastic strain that results in the broad size distribution shown in Fig. 5.16(b). Such a broad size distribution can actually be observed also from Fig. 5.16(c) for the InAs islands on GaAs(113)B with the size above 350 Å, but a vast majority of the InAs material is collected in the narrow distributed QDs. This is not the case on vicinal GaAs(2 5 11)A. Note, that the direction of the dislocation appeared on the InAs/GaAs(011) interfaces are

[100] and $[01\bar{1}]$, see, e.g., [Bel97]. As they run oblique to the step wall (see the model in Fig. 5.10), the InAs islands may grow along them, adopting an island-like but not a wire-like shape elongated along $[31\bar{1}]$ that could be expected by dislocations oriented parallel to the same direction.

We have also performed PL measurements in order to support our assumption derived from STM images, that InAs islands on vicinal GaAs(2 5 11)A are incoherent. It is well known that the incoherent (dislocated) QDs are optically dead, because the dislocations are very good traps for charge carriers [Leo98, Gru02]. At the dislocations the excitons can lose their energy through *nonradiative* recombination (without an emission of a photon). As has been shown for quantum wells [Chi01], the nonradiative recombination time is an order of magnitude shorter than the radiative recombination time. In the incoherent QDs the charge carriers are localised in an immediate proximity to the defects, hence the nonradiative recombination time is expected to be even shorter [Fio00]. As a consequence, no light emission should be seen in the PL or electroluminescence spectra of the QDs containing dislocation lines or networks as assumed in our case.

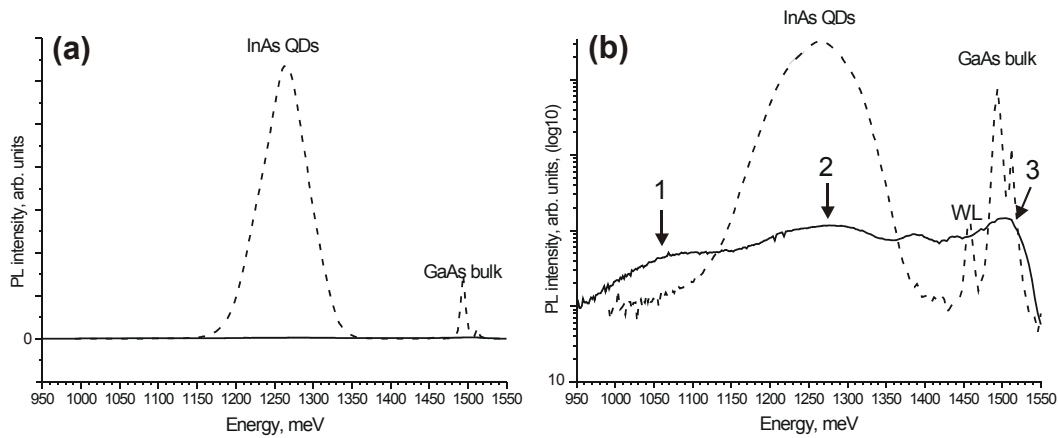


Figure 5.17 [Tem04] PL spectra at 10 K of the InAs QDs grown on GaAs(001) ($T=430^\circ\text{C}$, InAs thickness 4.8 \AA , dashed line) and the InAs islands on 1° vicinal GaAs(2 5 11)A ($T=430^\circ\text{C}$, InAs thickness 5.0 \AA , solid line) presented in (a) linear scale and (b) decimal logarithmic scale. The QDs, WL and GaAs bulk related peaks are labeled. Excitation density was 500 W/cm^2 .

Figure 5.17 shows the PL spectra of the InAs islands on GaAs(001) (dashed line) and on vicinal GaAs(2 5 11)A (solid line) prepared under nearly the same conditions*. The linear

* The GaAs(001) wafers, used for the comparative PL measurements were cut from an undoped, semiinsulating ingot.

presentation of the dependence of PL intensity on the emission energy in (a) reveals for vicinal GaAs(2 5 11)A neither a peak related to the QDs nor a peak related to the GaAs bulk material, which indicates a fairly bad quality of the used GaAs single crystal. In contrast, the spectrum for GaAs(001) shows a single Gaussian-like peak at 1265 meV with a FWHM equal to 78 meV, which is in good agreement with the literature about InAs QDs on GaAs(001) [Bim00, Gru02]. For vicinal GaAs(2 5 11)A, two broad peaks in the QD energy range numbered by 1 and 2 can be seen at very low intensities in the decimal logarithmic scale in (b). Peak 3 is ascribed to the doped GaAs(2 5 11)A substrate, because it is located near to the well resolved double peak of the semiinsulating GaAs bulk material, related to the negatively charged exciton. Note that a peak, centred at 1455 meV, occurs between the peaks for InAs QDs and GaAs bulk exciton on the GaAs(001) sample. It is ascribed to the InAs WL on GaAs(001), since its energy is in excellent agreement with that reported from the PL excitation spectra [~ 1450 meV, Hei97a]. Since the intensity of the solid line for vicinal GaAs(2 5 11)A is about 2.5 orders of magnitude lower than that for GaAs(001), the PL measurements nicely confirm the incoherent nature of the InAs islands on vicinal GaAs(2 5 11)A.

We now turn to structural properties of the InAs islands on vicinal GaAs(2 5 11)A. The shape of the islands undergoes a slight modification from the initial to the final elongated growth stage. At the initial growth stage the islands exhibit three facets and a rounded region as indicated in Fig. 5.18(a). The facet 1 is determined to be of the (111)A orientation from the following measurements: It intersects the (2 5 11)A substrate exactly along the $[2\bar{3}1]$ direction, that can be easily determined from the atomically resolved wetting layer, and is inclined to (2 5 11)A by $28 \pm 4^\circ$ (the (111) plane intersects (2 5 11) along $[2\bar{3}1]$ with an angle of 31.9°). The facet 2 is the (011) surface: It is inclined by $20 \pm 4^\circ$ and exhibits the unit cell vectors $a = 4.3 \pm 0.2 \text{ \AA}$ and $b = 5.8 \pm 0.2 \text{ \AA}$ (see Fig. 5.18(b)). These values agree well with the geometric angle of 22.5° between the (011) and (2 5 11) planes, and with the lengths of the InAs (GaAs) (011) unit cell vectors, projected onto (2 5 11)A, which are $a = 4.0 (3.8) \text{ \AA}$ and $b = 6.0 (5.6) \text{ \AA}$. The intersection line between the (011) facet and the (2 5 11)A substrate runs parallel to the step bunch, i.e., along $[31\bar{1}]$, giving further support for the (011) facet orientation. Facet 3 is considered to exhibit the (317)A-(1x1) reconstruction: It is inclined by $18 \pm 4^\circ$ to (2 5 11)A and exhibits two possible unit cells with the vectors $a = 11.0 \pm 0.5 \text{ \AA}$, $b = 7.5 \pm 0.5 \text{ \AA}$ and $c = 9.2 \pm 0.5 \text{ \AA}$ (see Fig. 5.18(c)). These values are in agreement with the geometric angle of 20.7° between (317) and

(2 5 11) planes, and with the lengths of the InAs(GaAs) unit cell vectors of the (317)A surface, projected onto (2 5 11)A, which are $a = 10.8$ (10.0) Å, $b = 7.4$ (6.9) Å and $c = 8.9$ (8.4) Å. The region 4 on the islands has a rounded shape similar as for the InAs QDs on GaAs(113)A or GaAs(113)B (see Fig.3.11 and 4.4(e)). From geometrical considerations the (001) surface, which is inclined to (2 5 11)A by 26.1° , should develop here. However, instead of the flat surface, the rounded region appear, that is formed probably from vicinal (001) surfaces, which may stem from the preferential migration of cations from slowly growing facets to the quickly growing (001) region.

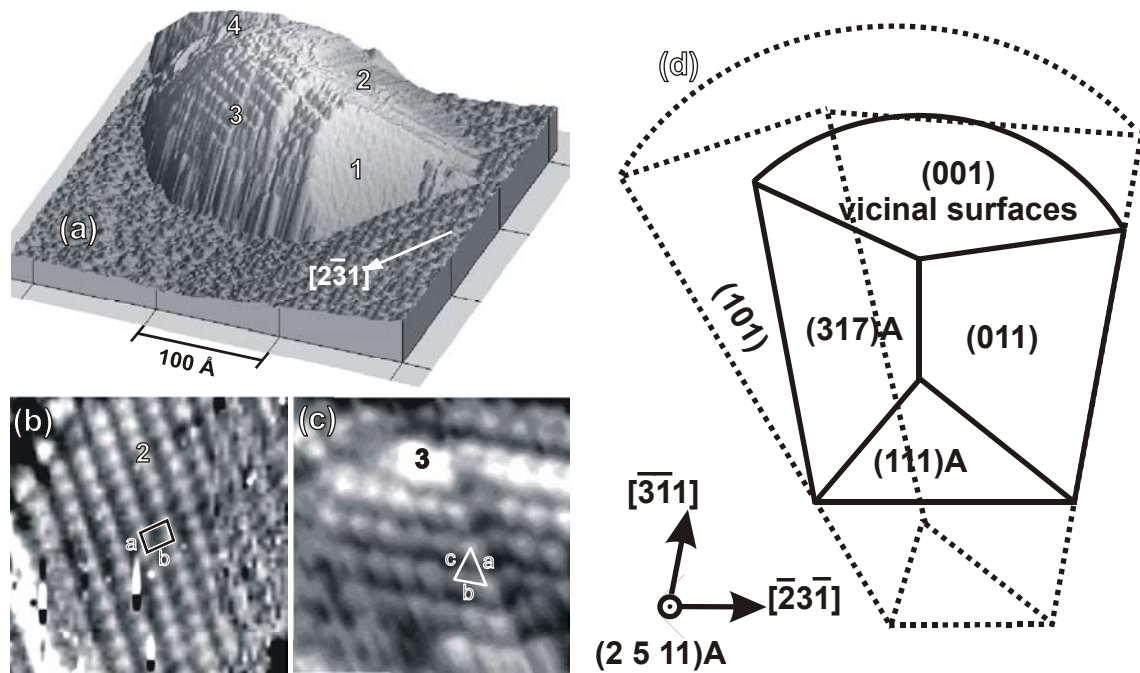


Figure 5.18 [Tem04] (a) 3D STM image of an atomically resolved InAs island on vicinal GaAs(2 5 11)A. The bounding facets and the rounded region are numbered (315×315 Å², $U = -2.5$ V, $I = 0.15$ nA); (b) zoom of (011) facet (numbered with 2 in (a)) with unit cell vectors a and b (error signal \equiv constant height mode, 58×58 Å², $U = -2.45$ V, $I = 0.17$ nA); (c) atomically resolved (317)A facet (numbered with 3 in (a)) with the unit cell vectors a , b and c (70×70 Å², $U = -2.5$ V, $I = 0.15$ nA); (d) schematic drawing of the InAs island shape on vicinal GaAs(2 5 11)A. The solid and dotted lines show the shape at the initial and final growth stages, respectively.

At the final growth stage (see, e.g., an island marked by a white arrow in Fig. 5.16(a)) the (317)A facet partially or completely disappear, and another steeper facet develops on this side of the islands, that is inclined to (2 5 11)A by $39 \pm 4^\circ$. From geometrical

considerations this new facet can be assigned to the (101) surface, that meets the (2 5 11)A at the angle of 41.4°. However atomic-scale features were not resolved from this part, probably because of the high inclination angle. An elongation of the islands proceeds similar to the InAs QDs on GaAs(113)A, i.e., through the disappearance of the (111)A facet. Both growth stages of the InAs islands on the vicinal GaAs(2 5 11)A surface are summarised on a schematic drawing in Fig. 5.18(d). Note, that the shape of the incoherent islands at both growth stages exhibits no symmetry plane, as the (2 5 11)A ideal unreconstructed substrate. Also, the shape in (d) for the incoherent InAs islands is very similar to the shape for the coherent InAs QDs on GaAs(113)A and B. It means, that the strain may not affect the shape of the QDs, but may be only responsible for the size distribution.

To conclude this part, the 1.0° off-oriented GaAs(2 5 11)A surface was used as substrate for the InAs heteroepitaxy. After the deposition of 5.0 ± 0.5 InAs a SK transition occurs at sample temperatures of 370-500°C. Large inhomogeneously distributed InAs islands with very different sizes are formed on the step bunches along $[31\bar{1}]$. The broad size distribution as well as the PL measurements reveals the presence of the misfit dislocations inside of the islands. The dislocation lines may be introduced during the InAs growth on (011) oriented step walls. After the SK transition the InAs material from GaAs(2 5 11)A terraces may easily create nuclei on the relaxed (011) step wall, which develop into the 3D InAs islands. Since the islands grow without limitation caused by the elastic strain, they can achieve arbitrary large sizes, which are actually observed in the experiment.

The shape of the incoherent InAs islands on vicinal GaAs(2 5 11)A is composed mainly of low-index (111)A, (011) and (001), but also of high-index (317)A surfaces. The latter undergoes a transition into the steeper (101) facet, indicating that the flat facets are the pathways by the island developing from the flat substrate to the steep energetically more favorable shape as for the SiGe islands on Si(001) [see, e.g., Mat99]. The shape of the incoherent islands exhibit no symmetry as the GaAs(2 5 11)A ideal unreconstructed substrate.

5.5 InAs islands on nominal GaAs(2 5 11)A

The nominal oriented GaAs(2 5 11)A wafers have been supplied from MaTecK with an 0.2° off-orientation. The preparation procedure is described in chapter 2.9. The surface morphology can be seen from Fig. 5.19(a-b). The actual off-orientation, extracted from many STM images is not equal to 0.2° , but is about 0.5° (0.6° - 0.8° on the image (a) and 0.2° on the image (b)). This indicates a local dependent morphology that may stem from a bad polishing of the wafers by the manufacturer*. The $(5000 \times 5000) \text{ \AA}^2$ large STM image in Fig. 5.19(a) exhibits the already known steps, running mainly along the $[31\bar{1}]$ and $[2\bar{3}1]$ directions, that have been observed on 1° vicinal GaAs(2 5 11)A and described in detail in chapter 5.3. The rough steps along $[2\bar{3}1]$, that are seen on the lower part of Fig. 5.19(a), appear with a height of $\sim 2 \text{ \AA}$. The steps, running along $[31\bar{1}]$ on the upper part, form often bunch structures up to 15 \AA in height and fairly large step walls (up to 40 \AA in length between the terraces) appear similar as on the 1° vicinal GaAs(2 5 11)A surface. Fig. 5.19(b) shows another $(5000 \times 5000) \text{ \AA}^2$ large area of the surface, that exhibits only $\sim 2 \text{ \AA}$ high steps, oriented mainly along $[2\bar{3}1]$. Step bunches are not observed there.

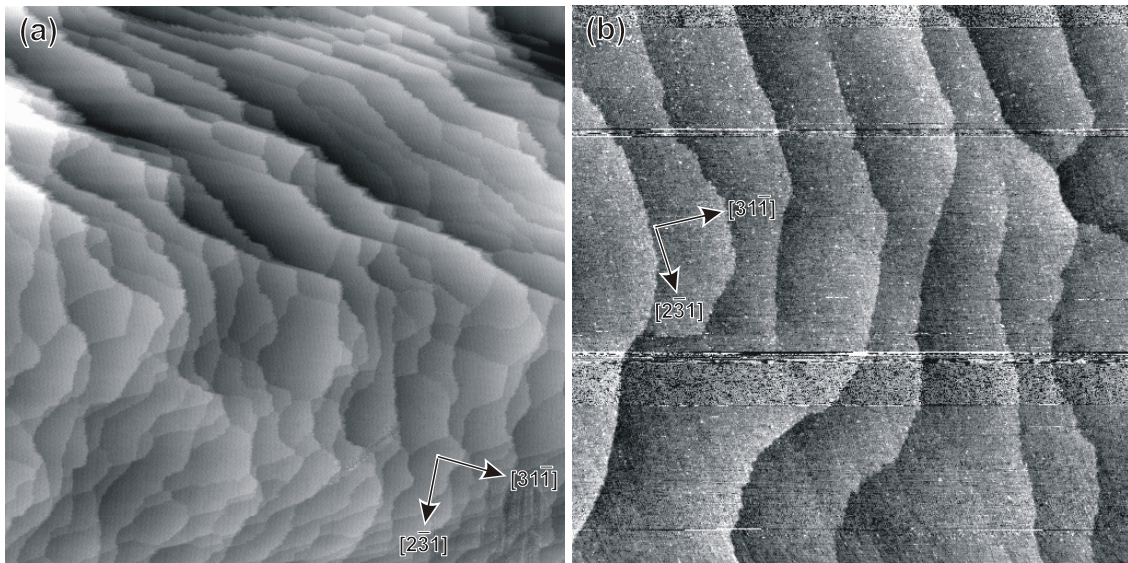


Figure 5.19 [Tem04] (a-b) Overview STM images of nominal GaAs(2 5 11)A from two different position of the wafer ($5000 \times 5000 \text{ \AA}^2$, $U = -2.5 \text{ V}$, $I = 0.15 \text{ nA}$). The extracted off-orientation is (a) 0.6 - 0.8° and (b) 0.2° .

* Note, that no dependence of the morphology on the GaAs buffer layer thickness could be detected.

A high resolution (600×600) \AA^2 STM image in Fig. 5.20(a), acquired from an area like the upper part in Fig. 5.19(a), presents two terraces separated by a step along $[31\bar{1}]$ that is not straight but exhibits many kinks. However, rows of bright dots arranged in a rectangular lattice with the lengths of $(5.5 \pm 1.0) \text{\AA}$ and $(3.9 \pm 1.0) \text{\AA}$ suggest the appearance of the (011) step wall also on the nominal GaAs(2 5 11)A surface. The only difference is that the overall density of these step bunches is roughly a half of the density on the 1° vicinal surface, but significant differences in height and length are not observed.

After the preparation of the bare GaAs(2 5 11)A surface, InAs was deposited under the same preparation conditions as for the 1° vicinal surface (see chapter 2.9). The evolution of the RHEED pattern did not yield remarkable differences from those shown in Fig. 5.14. However, analysing the STM results, two different ways in island developing are found, that usually coexist on the $(1 \times 1) \mu\text{m}^2$ scale. The first one is shown in Fig. 5.20(b). The large islands with a very broad size distribution like the one in Fig. 5.16(b) develop on the steps along $[31\bar{1}]$. Hence, in this case we automatically move to the incoherent islands described in the previous chapter.

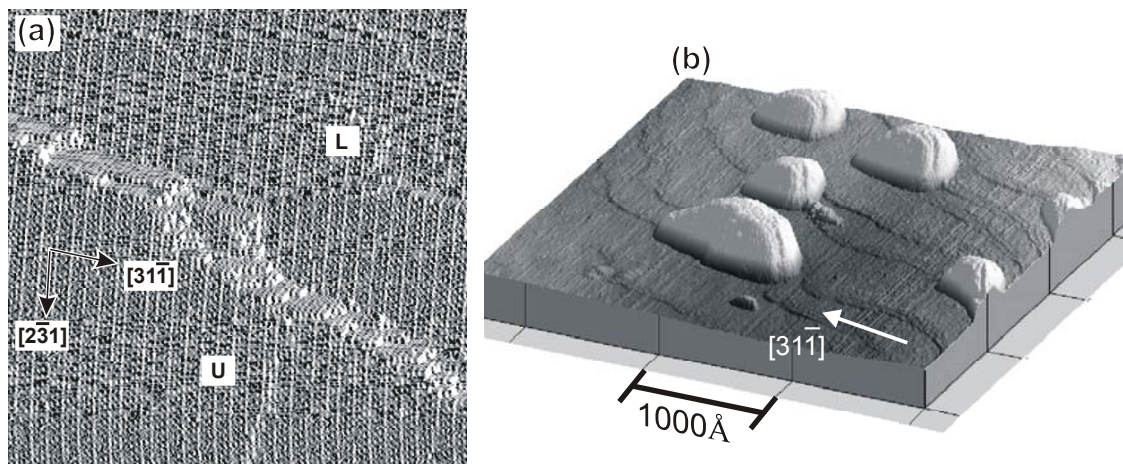


Figure 5.20 [Tem04] (a) High-resolution STM image (error signal=constant height mode) of the nominal GaAs(2 5 11)A surface ($600 \times 600 \text{\AA}^2$, $U = -3.0 \text{ V}$, $I = 0.15 \text{ nA}$). The upper and lower terraces are labelled U and L, respectively; (b) 3D STM image of the InAs islands on nominal GaAs(2 5 11)A grown on the step bunches ($3300 \times 3300 \text{\AA}^2$, $U = -3.0 \text{ V}$, $I = 0.2 \text{ nA}$, InAs thickness was 5.25\AA at sample temperature $T=430^\circ\text{C}$).

The second way in island developing is probably realised on the (2 5 11)A areas with the step structure shown in Fig. 5.19(b). A $(6700 \times 6700) \text{\AA}^2$ large STM image in Fig. 5.21(a)

contains InAs islands that are not aligned along any step. Furthermore, the WL does not exhibit any preferable step directions. The islands are statistically placed on the WL, similar to the InAs QDs on GaAs(113)A or B (see Fig. 3.6 and 4.5). The size distribution shown in Fig. 5.21(b) is much narrower than that of the incoherent islands on the step bunches (cf. Fig. 5.16(b)), which may indicate a coherent nature of these islands. The measured QD length along the $[4\bar{5}3]$ direction lies between 300 and 800 Å with a peak of 43% at 325 ± 25 Å, that is even higher than for the InAs QDs on GaAs(113)A, grown under similar preparation conditions. The mean height is 65 ± 20 Å and the overall number density is $(2 \pm 0.4) \cdot 10^{10} \text{ cm}^{-2}$.

A remarkable feature of the InAs islands shown in Fig. 5.21(a) is that they grow inside holes in the WL, but not at the step-edges on the low terraces as reported on the GaAs(001) substrate [Iko95]. The holes are about 2.2 Å high and present the known steps of nine (2 5 11) atomic layers, like the steps along $[4\bar{5}3]$ or $[2\bar{3}1]$ (type a, see chapter 5.3.3).

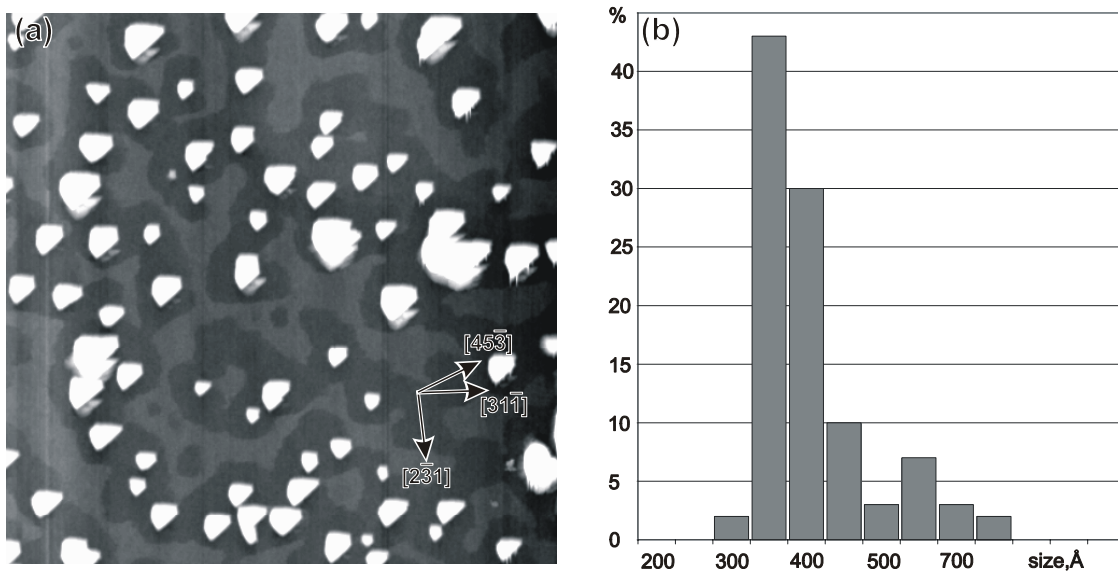


Figure 5.21 [Tem04] (a) Overview STM image with InAs QDs grown on the nominal GaAs(2 5 11)A surface ($6700 \times 6700 \text{ Å}^2$, $U = -2.5 \text{ V}$, $I = 0.15 \text{ nA}$, InAs thickness was 5.25 Å at sample temperature $T=430 \text{ °C}$); (b) Column diagram of the length of the InAs QDs along $[4,5,-3]$ in percents.

On the WL, however, the steps are disordered. Figure 5.22(a) shows a $(1000 \times 1000) \text{ Å}^2$ STM image with the atomically resolved WL, where the QDs are not caught completely into the image frames. The right half of island 1 and the left half of island 2 are quite

symmetrically surrounded by the $\sim 2.2 \text{ \AA}$ deep holes in the WL, as if the QDs grew at the expense of the material from the WL. Indeed, if we assume the InAs QDs on GaAs(2 5 11)A to have a cone pyramid shape with a base radius $R = 162.5 \text{ \AA}^*$ and with a tilt angle $\alpha = 30^\circ$ (see the Fig. 5.23(b) below), the volume of the material in a QD is $V_1 = \pi \cdot R^3 \cdot \text{tg}(\alpha)/3 = 2.6 \cdot 10^6 \text{ \AA}^3$. The volume of the material flowing out by the formation of WL holes is $V_2 = \pi \cdot r^2 \cdot d$, where $d = 9 \cdot 0.25 \text{ \AA} = 2.22 \text{ \AA}$ is the height of the step containing nine InAs(2 5 11) atomic layers, and r is the average radius of the WL holes ($\sim 500 \text{ \AA}$). $V_2 = 1.7 \cdot 10^6 \text{ \AA}^3$ and thus, InAs material from the WL may indeed assemble in the QDs.

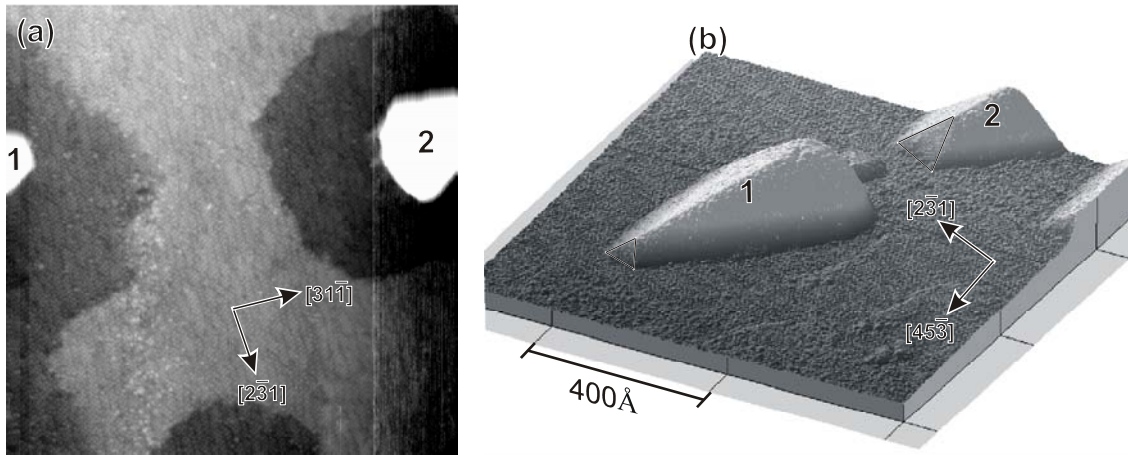


Figure 5.22 [Tem04] (a) STM image with InAs QDs grown on nominal GaAs(2 5 11)A ($1000 \times 1000 \text{ \AA}^2$, $U = -3.0 \text{ V}$, $I = 0.095 \text{ nA}$, InAs thickness was 5.25 \AA at sample temperature $T=430^\circ\text{C}$); (b) 3D STM image of the InAs islands on nominal GaAs(2 5 11)A ($1000 \times 1000 \text{ \AA}^2$, $U = -3.0 \text{ V}$, $I = 0.181 \text{ nA}$, InAs thickness was 5.25 \AA at sample temperature $T=430^\circ\text{C}$).

The island growth on the expense of the WL was reported in a theory paper from Wang et al. (M. Scheffler group, Germany) [Wan99]. A thinning of the WL, acting as a source for InAs material, increased its formation energy and yielded a minimum in the total energy gain curve, that explained a narrow size distribution of coherent QDs. The thinning of the WL with formation of holes has not been reported to our knowledge on any surface, and also not observed in this work on GaAs(113)A, B and vicinal GaAs(2 5 11)A. It would be interesting to explore this phenomenon on the GaAs(2 5 11)A substrate with a very low off-orientation, i.e., without an influence of the step bunching.

* One half of the measured length at the maximum in the size distribution shown in Fig. 5.21(b).

Wang et al. (G. J. Salamo group, USA) [Wan03] have concluded from the shape of the InAs QDs on GaAs(113)A that the occurrence of $\{2\ 5\ 11\}$ A facets indicates a stability of the respective GaAs substrate against the SK transition by the mismatched epitaxial growth, similar to the $\{110\}$ and (111)A facets. We have contrariwise demonstrated that InAs grows on the GaAs(2 5 11)A surface in the SK growth mode, i.e., with the appearance of the 3D islands after the critical thickness at the expense of the material from the WL.

Another remarkable feature of the QD ensemble in Fig. 5.21(a) is that the islands are elongated roughly along the $[4\ 5\ \bar{3}]$ direction*. This is clearly seen in Fig. 5.22(b). The area of the frontal facet on the island 1 is a half of that on the island 2, which indicates that the elongation may proceed through the growth of these facets that consequently vanish. From Fig. 5.21 and 5.22 one can conclude that the islands are not symmetrical and there is no flat base between the steep QD facets and (2 5 11)A substrate as in the case on GaAs(113)B.

Figure 5.23(a) presents an STM image of a typical elongated InAs QD on the flat GaAs(2 5 11)A surface. The QD exhibits no mirror symmetry with respect to any plane perpendicular to the substrate and comprises in an elongated stage six well-pronounced facets numbered in Fig. 5.23(a-b). An early, non-elongated stage (see also the island 2 in Fig. 5.22(b)) is shown in Fig. 5.23(b) by the dotted line and contains only three facets and a rounded region, that is very similar to the shapes of InAs QDs on GaAs(113)A and B (cf. Fig. 3.11 and 4.4(e)). Facet 1 is identified as a (101) surface from the following STM data (see Fig. 5.23(c)): Facet is inclined to the substrate by $38 \pm 5^\circ$ and exhibits unit cell vectors $a = 5.5 \pm 0.4 \text{ \AA}$ and $b = 4.2 \pm 0.8 \text{ \AA}$ (respective geometrical values: 41.4° , 5.2 \AA , 3.9 \AA , with the InAs(101) unit cell projected onto (2 5 11) plane). Facet 2 in Fig. 5.23(a) is the (011) surface as extracted from the following STM measurements: The inclination angle is $19 \pm 3^\circ$, and the unit cell vectors are $a = 5.9 \pm 0.4 \text{ \AA}$ and $b = 3.9 \pm 0.5 \text{ \AA}$ (geometrical values: 22.5° , 6.0 \AA , 4.0 \AA). The atomic resolution of this facet is very similar to that shown in Fig. 5.23(c). The triangular facet 3 consists of the (111)A-2x2 reconstructed surface (see Fig. 5.23(d)): It is inclined to (2 5 11)A by $30 \pm 3^\circ$ and exhibits a rhombic unit cell with a vector $a = 8.0 \pm 0.5 \text{ \AA}$ (geometrical values for the (111)A-2x2 In(Ga) vacancy buckling model [Ton84, Oht01] are 32.0° and $7.7 \pm 0.3 \text{ \AA}$).

The rounded region appears only on the small QDs (with a length up to 350 \AA). The islands in the elongated stage exhibit a completely faceted backside that is inclined by very

* The exact direction of the elongation is $[19, 10, -8]$, that is perpendicular to $[2, -3, 1]$, see Fig. 5.6(b). Since this direction plays no role in the atomic structure of the (2 5 11)A surface, we will use $[4, 5, -3]$.

steep angles to the $(2\ 5\ 11)A$ substrate and therefore, is not acquired with an atomic resolution. However, a tilt angle between a facet and the substrate as well as an azimuthal

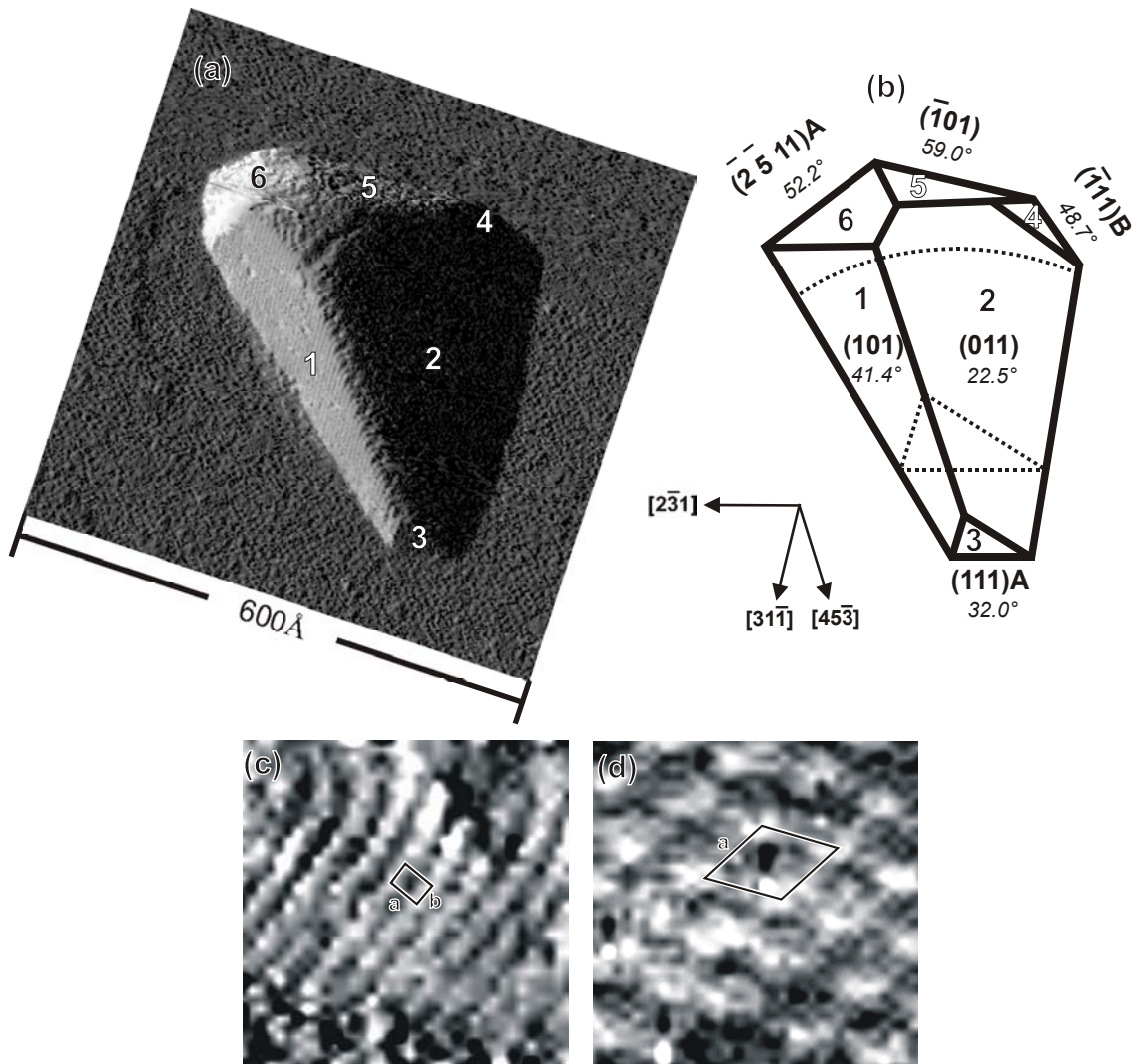


Figure 5.23 [Tem04] (a) Atomically-resolved STM image (error signal \equiv constant height mode) of a QD on GaAs(2 5 11)A with six characteristic regions ($(600 \times 600) \text{ \AA}^2$, $U = -3V$, $I = 0.181 \text{ nA}$); (b) shape of InAs QDs on GaAs(2 5 11)A derived from STM measurements. The solid line represents the elongated QD shape, the dotted line shows QDs briefly after the SK transition; Atomically-resolved STM images (error signal \equiv constant height mode) of the (c) (101) facet ($(65 \times 65) \text{ \AA}^2$, $U = -3V$, $I = 0.181 \text{ nA}$) and (d) (111)A facet ($(35 \times 35) \text{ \AA}^2$, $U = -3V$, $I = 0.181 \text{ nA}$).

angle between the intersection line of a facet with the substrate and, e.g., the $[2\bar{3}1]$ direction have been collected from more than 30 islands and compared with the

geometrical values of the known stable surfaces. This convinces us of the accuracy of this method. According to the STM data, the facet 4 is determined to be of the $(\bar{1}11)B$ orientation: It is inclined by $45 \pm 5^\circ$ and has the azimuthal angle $54 \pm 4^\circ$ (geometrical values are 48.7° and 55.2°). Similarly, the facet 5 is the $(\bar{1}01)$ surface: The inclination angle is $55 \pm 5^\circ$ and the azimuthal angle is $13 \pm 4^\circ$ (geometrical values are 59.0° and 12.8°). The facet 6 is the $(\bar{2} \bar{5} 11)A$ surface due to the facts: The inclination angle is $47 \pm 7^\circ$ and the azimuthal angle is $36 \pm 4^\circ$ (geometrical values are 52.2° and 37.4°). As can be seen, almost all STM measurements are in perfect agreement with the geometrical considerations, however, some deviations for the faceted backside shown in Fig. 5.23(b) are also found, e.g., the facet 6 in (a). The model for the small and elongated InAs QDs on GaAs(2 5 11)A is presented in Fig. 5.23(b). Note, that except for the faceting of the rounded region the shape of the coherent (strained) InAs QDs is similar to the final shape of the incoherent (unstrained, relaxed) islands on the (011) step bunches (cf. Fig. 5.18(d)). This fact confirms our hypothesis, that the strain may affect only the size distribution but not the shape. Both types of islands exhibit no mirror symmetry as the ideal unreconstructed (2 5 11)A substrate (cf. Fig. 5.4(d)), that is also on the line of our observations from all the chapters in this work. Note also, that any nucleus with flat $\{2 \bar{5} 11\}A$ or $\{137\}A$ facets could not be derived from STM images like one shown in Fig. 5.21(a). It may indicate that the SK transition proceeds on GaAs(2 5 11)A without step bunching simultaneous on the whole surface. This is a consequence of the flat WL on GaAs(2 5 11)A, which is free of any undulation.

Another question arises about the elongation of the islands. As has been shown in chapter 3.6, the evolution in shape of InAs QDs on GaAs(113)A may appear due to the faceting of the rounded (001) region into two $\{113\}B$ facets, that could slow down its growth rate. These facets are not identified in Fig. 5.23(b), however the elongation is present. We think, that the $(\bar{1}11)B$ and $(\bar{1}01)$ facets, whose stable reconstructions do not exhibit As dimers as well also can slow down the growth rate of the firstly developed rounded region as the As_2 molecules have to be dissociated prior to incorporation onto these facets. Then the (111)A facet starts to grow and decreases in size for geometrical reasons. Similar to the (113)A case this reduces the strain and thereby the energy barrier for incorporation of further atoms and thus speeds up the growth rate of the (111)A facet. Hence the facet growth kinetics may also be here responsible for the shape elongation.

However, we have not been able to acquire PL spectra with the high emission intensity characteristic for an InAs QD ensemble. For the optical measurements InAs islands on the nominal GaAs(2 5 11)A surface were overgrown with the same preparation procedure as for the 1° vicinal surface (see chapter 2.9). Figure 5.24 shows the PL spectra of the InAs islands on GaAs(001) (dashed line) and on nominal GaAs(2 5 11)A (solid line) prepared under nearly the same conditions. Any qualitative differences between the spectra in Fig. 5.24(a-b) and 5.17(a-b) for the nominal and vicinal (2 5 11)A substrates are not observed. The linear presentation of the PL intensity for GaAs(2 5 11)A in Fig. 5.24(a) reveals no peaks related to the QDs, but a peak related to the GaAs bulk material with an intensity nearly equal to that of the GaAs(001) surface. The dashed line for GaAs(001) shows a single Gaussian-like peak at 1265 meV with the FWHM equal to 78 meV, that is the light from the InAs QDs on GaAs(001). In the decimal logarithmic scale in Fig. 5.24(b) the WL peak of the GaAs(001) sample, centred at 1455 meV, occurs only at the high excitation density (above 500 W/cm²), when the QD levels are completely saturated by the charge carriers.

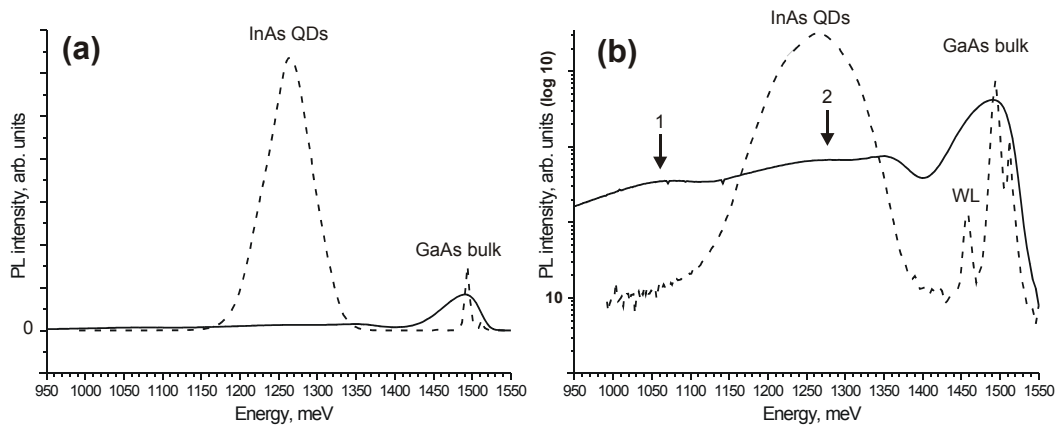


Figure 5.24 [Tem04] PL spectra of the InAs QDs grown on GaAs(001) ($T=430^{\circ}\text{C}$, InAs thickness 4.8\AA , dashed line) and the InAs islands on nominal GaAs(2 5 11)A ($T=430^{\circ}\text{C}$, InAs thickness 5.25\AA , solid line) presented in (a) linear scale and (b) decimal logarithmic scale. The QDs and GaAs bulk related peaks are labeled. Excitation density was 500 W/cm^2 .

Note that the WL peak is clearly resolved and separated from the double peak of the negatively charged exciton only on the GaAs(001) sample because of its undoped nature. The nominal GaAs(2 5 11)A surface has been doped for the STM experiment. On this substrate, the deep lying doping levels together with the WL peak and GaAs bulk exciton have got smeared in a broad peak placed above 1400 meV in Fig. 5.24(b). The broad peaks

in the QD energy range numbered by 1 and 2 can be seen from the GaAs(2 5 11)A sample at a very low intensity in the decimal logarithmic scale in Fig. 5.24(b). The intensity of the peak 2 in Fig. 5.24(b) is about 1.5 orders of magnitude lower than that of the dashed line. This is the only difference to the InAs islands on 1° vicinal GaAs(2 5 11)A, where this relation was equal to 2.5 orders of magnitude.

The reason for the very weak PL from the InAs QDs on nominal GaAs(2 5 11)A shown in Fig. 5.24(a-b) is not clear. Two possible explanations can be proposed. As we have shown in Fig. 5.21(a) and 5.20(b) the InAs islands on nominal GaAs(2 5 11)A may develop with the narrow and broad size distributions, characteristic for the coherent QDs and dislocated islands, respectively. Leon and Fafard (Leo98) have shown, that even a small number of incoherent islands, that appeared in the dense QD ensemble after some critical thickness of InAs deposited onto GaAs(001), can drastically decrease the PL intensity. In our case one incoherent island on the nominal GaAs(2 5 11)A surface coexists with about ten coherent QDs. The dislocation lines or even networks being incorporated in the incoherent islands may trap the charge carriers from the QDs. Hence, no high PL emission would be seen in the spectra. The second explanation is that both islands in Fig. 5.20(b) and 5.21(a) are incoherent, and the InAs growth on the GaAs(011) step walls is not the only possible way to incorporate a dislocation inside the InAs islands. However, this would be opposite to any our understanding of the strain induced narrow size distribution for the coherent QDs shown in Fig. 5.21(b), which has been often observed on different places of the nominal GaAs(2 5 11)A substrate. Therefore, a more systematic investigation on the nominal GaAs(2 5 11)A surface perhaps from the wafers with a really smaller off-orientation and with larger (2 5 11)A areas, unperturbed by the step bunching, are needed to clarify this question.

5.6 Conclusion

GaAs(2 5 11)A is the only one known stable compound semiconductor surface located within the ST with an original (1x1) reconstruction that fulfils the ECR and yields a reduced number of DBs compared with the bulk-truncated GaAs(2 5 11)A surface. A very remarkable feature of the surface is the formation of the bunch structures, resulting in an appearance of fairly large GaAs(011) areas on the straight steps along the $[3\bar{1}\bar{1}]$ direction. This effect is mostly pronounced on slightly vicinal GaAs(2 5 11)A, but still exists also on the nominal oriented surface. The deposition of $5.0 \pm 0.5 \text{ \AA}$ of InAs results in the SK

transition from 2D to 3D growth mode that can be observed in the RHEED pattern only along the $[2\bar{3}1]$ direction. STM images from the 1° vicinal $(2\ 5\ 11)_A$ surface reveal the appearance of 3D InAs islands on the steps along $[31\bar{1}]$ with a very broad size distribution that is characteristic for incoherent islands. The dislocations are thought to be incorporated through the InAs growth on the GaAs(011) step walls. The incoherent nature of the islands is confirmed with the PL measurements. STM images from the nominal $(2\ 5\ 11)_A$ surface show two different ensembles of the InAs islands with narrow and broad size distributions. The latter stems from the islands grown on the (011) step bunches. The narrow size distribution is thought to stem from the coherent dislocation-free QDs that are composed of the $\{110\}$, $(111)_A$ facets and a (001) rounded region (faceted by the elongated islands) similar to the QDs on GaAs(113)_A, but without any symmetry plane. However, the PL measurements from the InAs islands on nominal GaAs(2 5 11) do not exhibit a high emission intensity that would be expected from a coherent InAs QD ensemble. This is explained by the trap of the QD excitons in the dislocations formed in the incoherent islands.

6 InAs quantum dots on nominal GaAs(2 5 11)B

6.1 Introduction

All above-considered substrates in this work, that are GaAs(113)A, B and GaAs(2 5 11)A have already been reported from other authors as being stable surfaces, and our task up to now has been just to use them for the growth of InAs QDs. The GaAs(2 5 11)B surface is an absolute “virgin soil”: it has never been mentioned in any paper as being stable or unstable, although the discovery of stable GaAs(2 5 11)A could imply the stability of GaAs(2 5 11)B, so long as among the GaAs surfaces there is no stable A face without a stable B one. Under this premise three questions arise in the following sequence: a) is GaAs(2 5 11)B a stable surface? If so, then: b) does the SK growth mode occur on it? And if so, then: c) what is the quality of the resulting QDs?

We have learnt from the comparison between InAs QDs on GaAs(113)A and B that the uniform QD ensemble occurs only on the B face. This difference had been attributed to a rough undulating morphology of the bare GaAs(113)A that became even more corrugated after the InAs deposition up to the SK transition in contrast to the flat bare GaAs(113)B surface and the InAs WL on it. Except for the formation of step bunches, the GaAs(2 5 11)A surface and InAs WL on it are free from any undulations. Therefore, one may expect the GaAs(2 5 11)B surface to be an at least not worse substrate than GaAs(113)B by the island evolving. Hence the investigation of the atomic and morphologic structure of the bare GaAs(2 5 11)B surface and the InAs deposition on it has mainly been motivated by the possibility of getting a new suitable substrate for QD growth.

6.2 Surface and step structure of the bare GaAs(2 5 11)B surface

For the graphic representation of the location of GaAs(2 5 11)B one can in principle use Fig. 5.1 (see chapter 5.2) provided the ST is constructed for the B faces, i.e., the $(00\bar{1})$, $(0\bar{1}\bar{1})$ and $(\bar{1}\bar{1}\bar{1})$ B low index surfaces are at the corners. The GaAs(2 5 11)B surface is situated within the ST and surrounded by the respective B faces, in analogy to Fig. 5.1.

Similar to the ST for the A surfaces, stable GaAs B surfaces have been found only on the ST edges: the (111)B [Bie90, Tho98], (113)B (see the literature survey in chapter 4) and (114)B [Pla98]. The GaAs(111)B-(2x2) As trimer [Mol96] and GaAs(113)B-(1x1) As rich reconstructions [Pla99] have been calculated using the density-functional theory. The GaAs(112)B [Pla99, Gee99, Jac99], GaAs(133)B [Hor89] on the ST edges and

GaAs(135)B [Suz04a] inside the ST are found to decompose onto stable GaAs surfaces. We will show that GaAs(2 5 11)B is up to now the only one known stable surface located within the ST for the B faces.

The preparation of the GaAs(2 5 11)B surface is described in chapter 2.9. The diffraction patterns of fairly good quality appeared only after some GaAs growth, therefore, 200-1000 Å thick layers were grown. To get a good quality of the bare surface for STM measurements, the GaAs(2 5 11)B samples were kept at the temperature of 550 °C for 5 min without an As₂ supply from the Knudsen cell, i.e., under less As-rich conditions.

LEED images of GaAs(2 5 11)A and B are compared in Fig. 6.1(a) and (b), respectively. A simple mirroring of a 2D net in reciprocal space on the LEED image in (a) with a subsequent turning in the (2 5 11) plane by 180° leads to a complete superposition with the LEED spots in reciprocal space in (b) (in Fig. 6.1 this mirroring is carried out around the $(19\ 10\ \bar{8})$ plane). The same operation can also be applied in real space, shown in Fig. 6.1(a) and (b) below the respective LEED images. Note that only the mirror operation would also result in the superposed LEED spots from the GaAs(2 5 11)A and B surfaces, because LEED images are invariant to the 180° rotation. However as will be shown by the consideration of the models, one can get the structure of the GaAs(2 5 11)B surface only by the combined mirroring of the A face around any perpendicular plane and by a rotation by 180°.

The spots on the LEED image in Fig. 6.1(b) are very sharp, which indicates a high surface quality and a high degree of order on the surface. Almost all the reflexes are visible which is very different to other stable high-index surfaces [Gee99, Mar00]. A splitting of spots (indicating faceting) in the LEED image in Fig. 6.1(b) is not observed, which is the first evidence for the stability of the GaAs(2 5 11)B surface. Since the spots in (a) are arranged in an oblique net with two different smallest unit cells, two different unit cells A* and B* can also be extracted from the periodicity in (b). As the areas of both unit cells are equal, they both are equivalent. Note, that none of the real-space basis vectors in Fig. 6.1(a) and (b) is parallel to any of the reciprocal space basis vectors because of the oblique surface periodicity. The calculated lengths of the basis vectors of unit cells A* and B* from LEED images, like the one shown in Fig. 6.1(b), are in real space equal to those for the GaAs(2 5 11)A surface (see chapter 5.2). Hence, there is a large similarity for the structure of the GaAs(2 5 11)A and B surfaces.

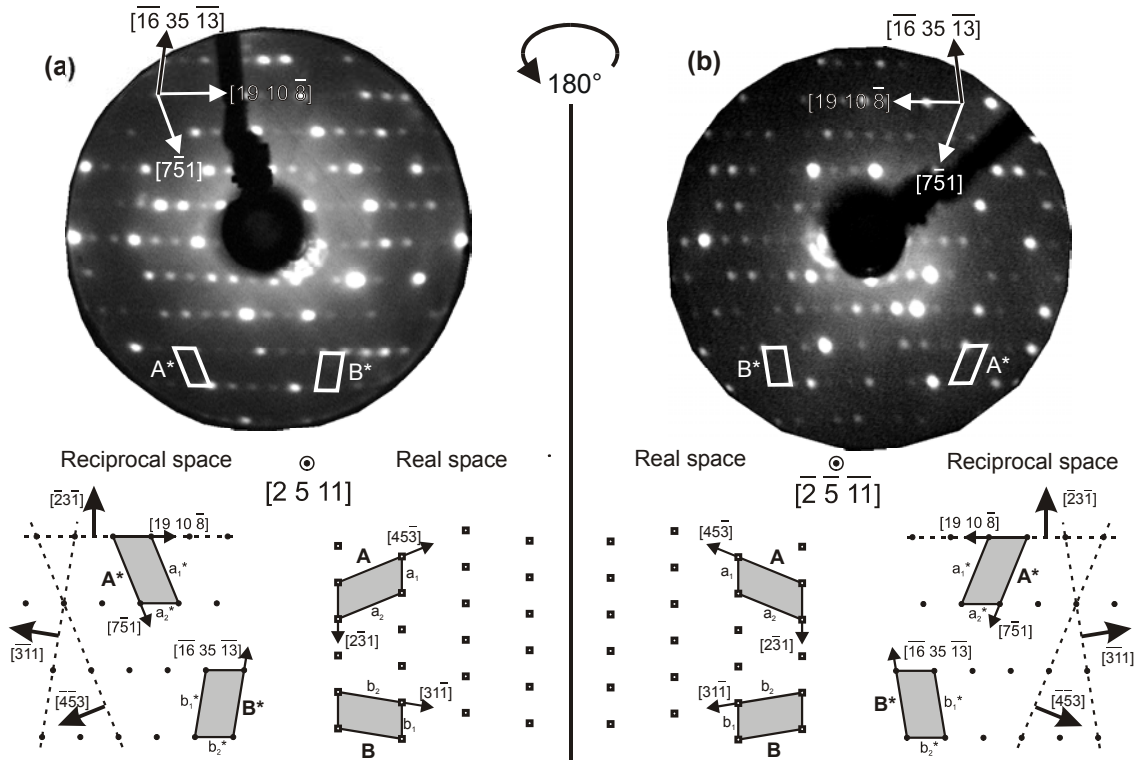


Figure 6.1 [Tem04] (a) LEED image of the GaAs(2 5 11)A surface ($E=59$ eV) with a schematic of the surface net in reciprocal space (left-hand side) and in real space (right-hand side); (b) LEED image of the GaAs(2 5 11)B surface ($E=56$ eV) with a schematic of the surface net in real space (left-hand side) and in reciprocal space (right-hand side). The vertical line between the images (a) and (b) indicates a plane running perpendicular to the GaAs(2 5 11)A or B, around which the mirror operation has been carried out.

The RHEED patterns are not presented here because except for the mirroring they are mainly equal to those shown in Fig. 5.2 for GaAs(2 5 11)A. Note, that in contrast to the GaAs(113)B surface, where a phase transition from Ga-rich (8x1) to As-rich (1x1) reconstructions is measured by RHEED to occur at 470-490 °C [Mar02], the GaAs(2 5 11)B surface exhibit only a (1x1) reconstruction in the temperature range of 400-600 °C under usual MBE preparation conditions.

A high-resolution (120×120) Å² STM image of the GaAs(2 5 11)B surface is shown in Fig. 6.2. The surface consists of stripes along $[2\bar{3}1]$ marked by solid lines on the image border. The stripes contain little series made up from three white humps. These series in neighbouring stripes are phase shifted, i.e., they are not aligned, but each series in the next stripe is located between the series in the previous stripe. As can be seen, the stripes are separated by narrow dark lines.

Two shortest unit meshes labelled by A and B can be constructed from the periodicity in Fig. 6.2. They correspond to the unit cells A* and B* in reciprocal space on the LEED image in Fig. 6.1(b). The lengths of the vectors measured from the STM images are in perfect agreement with those from a model (see below) that for unit mesh A are equal to 10.6 Å and 20.0 Å, and the enclosed angle is 67.8°; the respective values for the mesh B are 10.6 Å, 18.9 Å, and 80.7°. The vectors of mesh A are directed along $[45\bar{3}]$ and $[2\bar{3}1]$; those of mesh B along $[31\bar{1}]$ and $[2\bar{3}1]$.

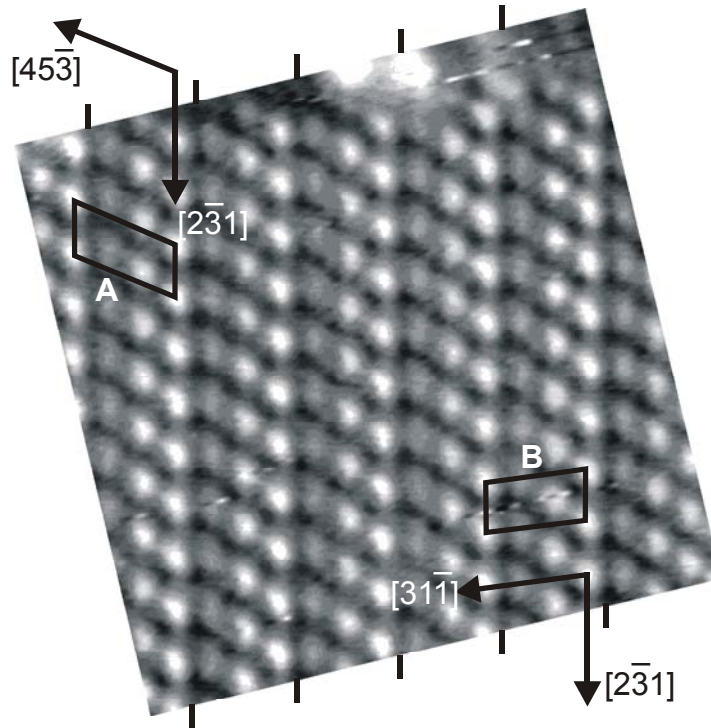


Figure 6.2 [Tem04] High-resolution STM image of the GaAs(2 5 11)B surface. The solid lines at the image border indicate the trenches between the dimer stripes. The unit meshes A and B are depicted as black parallelograms. $(120 \times 120) \text{ \AA}^2$, $U = -2.55 \text{ V}$, $I = 0.1 \text{ nA}$.

A ball-and-stick model for the GaAs(2 5 11)B surface is presented in Fig. 6.3. In order to get a coincidence of this model with the one shown in Fig. 5.4(a) for GaAs(2 5 11)A one should mirror the latter around any plane perpendicular to (2 5 11), then turn the result by 180° and exchange the As and Ga atoms. In contrast to GaAs(2 5 11)A the *ab initio* total energy electronic structure calculation has not been performed for the B face, and precise positions of the As and Ga atoms are unknown. Therefore, Fig. 6.3 shows the atomic structure derived from the STM images provided the relaxation of the atoms is similar to that shown in Fig. 5.4(a) for the A face. Black, white and grey balls depict As, Ga and adsorbed Ga atoms, respectively. The (1x1) unit meshes A and B are shown as shaded

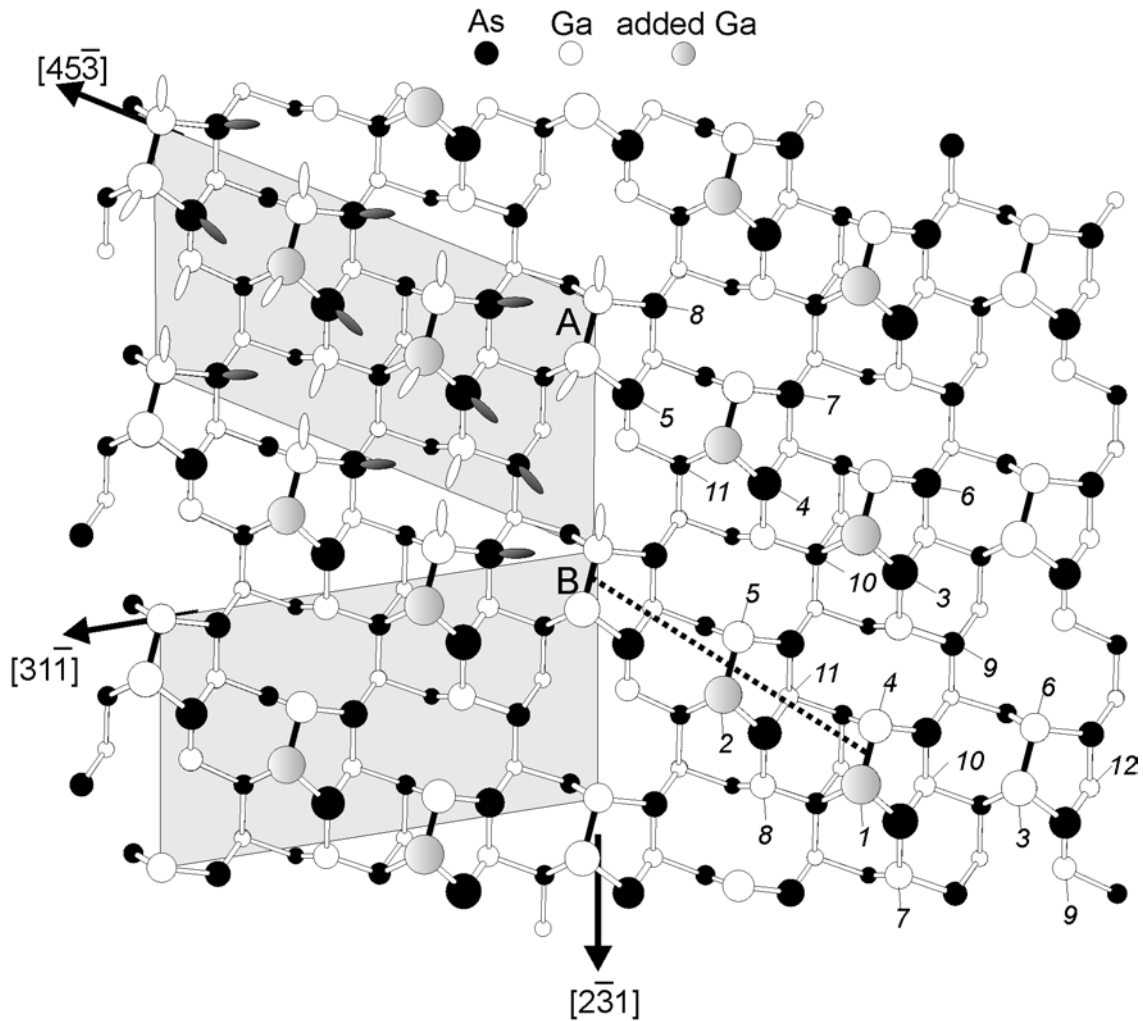


Figure 6.3 [Tem04] Top view of the ball-and-stick model for the (1×1) reconstructed GaAs(2 5 11)B surface. The size of the circles representing the atoms was chosen according to their vertical distance from the uppermost atom. To arrive at the reconstructed surface, the lighter shaded Ga atoms have to be added to the bulk-truncated surface. The numbers near the As and Ga atoms show which atomic layer they belong to, counting from the top. Within unit mesh A, the As atoms are depicted with black (filled) DBs, the Ga atoms with white (empty) DBs.

parallelograms. The vectors of unit mesh A lie along $[4\bar{5}\bar{3}]$ and $[2\bar{3}\bar{1}]$. The directions $[3\bar{1}\bar{1}]$ and $[2\bar{3}\bar{1}]$ form the equivalent unit mesh B. Both meshes correspond to the bulk-truncated GaAs(2 5 11)B surface onto which two Ga atoms were adsorbed that are depicted as grey balls. This conclusion is in agreement with the experimental fact that the surface becomes well ordered only after some GaAs growth and additional annealing without As_2 , i.e., after a supply of additional Ga atoms. Black bars indicate the Ga-Ga bonds in the Ga dimers. The Ga dimers repose on four As atoms, the two uppermost of which exhibit one DB per an atom. According to the autocompensation principle (ECR), each As DB should

be filled with two electrons as well as each Ga-Ga bond of the Ga dimer. Therefore, we assume that on the filled-states STM image in Fig. 6.2 the Ga dimers together with the underneath lying As DBs make up white humps, that are very difficult to resolve into the separated DBs because of the small spacing between these features*. The black troughs on the STM image in Fig. 6.2 may stem from the low lying Ga dimers which Ga atoms are numbered by 3 and 6 in Fig. 6.3. The Ga dimers are arranged in the series along $[12\bar{1}]$ (see the dotted line in Fig. 6.3) that is inclined to the surface plane such, that the right-hand side lies higher than the left-hand side. The three Ga dimers form the above-mentioned series that are shifted along $[2\bar{3}1]$. Between the series there are trenches, which comprise filled As DBs (numbered by 9 on the right-hand side of Fig. 6.3), taking a positive excess charge of $+3/4$ electrons and giving the stability to the whole structure. The reconstructed (1×1) unit meshes A and B contain 9 Ga DBs ($+27/4$ electrons), 7 As DBs ($-21/4$ electrons) and 3 Ga-Ga bonds ($-6/4$ electrons). The structural model fulfils the ECR and the surface is semiconducting.

Because of the large similarity to GaAs(2 5 11)A we do not show the model for the bulk-truncated (ideal) GaAs(2 5 11)B surface. The main points described by the consideration of Fig. 5.4(d) can also be applied here: Neither bulk-truncated nor (1×1) reconstructed GaAs(2 5 11)B surface exhibits any symmetry plane; atoms with two DBs are energetically unfavourable, so the bulk-truncated (1×1) surface does not exist; the Ga dimerisation is in accord with the general principle that the number of DBs at a surface should be as small as possible.

The vertical positions of the atoms, extracted from the bulk-truncated model with an addition of the two adsorbed Ga atoms are depicted in the right hand side of Fig. 6.3. The spacing between the horizontal atomic planes for GaAs(2 5 11)B is the same as for the A face, i.e., only 0.23 Å. The grey Ga atoms occupy the highest positions within the unit meshes. From the third atomic layer on there are one Ga and one As atom in each plane, as the bulk-truncated GaAs(2 5 11)B surface is stoichiometric. The reconstruction comprises nine atomic layers. Beginning from the tenth layer the atoms have bulk-like bonds.

As we have seen from the atomic structure, GaAs(2 5 11)B is a stable compound semiconductor surface located within the ST and exhibits a Ga dimers terminated (1×1) reconstruction, which is not a faceting or a composition of low-index surfaces.

* A similar resolution has been acquired from the (8×1) reconstruction on the GaAs(113)B surface [Suz02a], that is composed of similar Ga dimers with two lower lying As DBs.

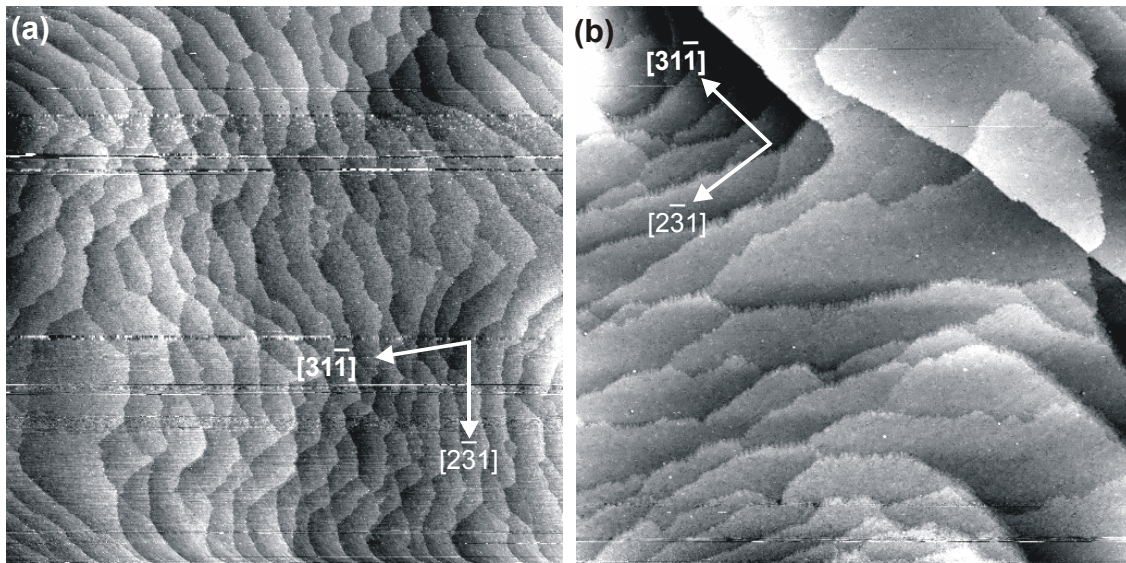


Figure 6.4 [Tem04] Overview STM images from two different locations on the nominal GaAs(2 5 11)B surface; (a) $(1 \times 1) \mu\text{m}^2$, $U = -3.0 \text{ V}$, $I = 0.136 \text{ nA}$, the off-orientation is 0.25° and (b) $5000 \times 5000 \text{ \AA}^2$, $U = -2.5 \text{ V}$, $I = 0.11 \text{ nA}$, the off-orientation is 0.25° .

The surface morphology, playing a central role in the InAs heteroepitaxy on nominal and vicinal GaAs(2 5 11)A surface, is shown for GaAs(2 5 11)B in Fig. 6.4(a-b). Despite of the fact, that the same nominal oriented double side polished (2 5 11) wafers have been prepared with the same conditions for A and B faces, the actual off-orientation extracted from many STM images for GaAs(2 5 11)B has seldom exceeded 0.3° (0.5° for A face, see chapter 5.5). The $(1 \times 1) \mu\text{m}^2$ large STM image in Fig. 6.4(a) exhibits many terraces up to 1000 \AA in width separated by steps, running roughly along the $[2\bar{3}1]$ direction. Across the whole image the steps decline from the left hand to the right hand side. The average direction of the off-orientation is approximately $[\bar{3}\bar{1}1]$. The step height has been measured as $\sim 2 \text{ \AA}$. Therefore, we think that these steps are equal to the steps along $[2\bar{3}1]$, which have been called type “a” and described in chapter 5.3 for the vicinal GaAs(2 5 11)A surface, although they often run with an opposite off-orientation direction $[31\bar{1}]$, see Fig. 6.4(b). This figure shows another $(5000 \times 5000) \text{ \AA}^2$ large area of the surface with two bunch structures running parallel to the $[31\bar{1}]$ direction. The height of the step bunches on GaAs(2 5 11)B has been measured up to 10 \AA with $(0\bar{1}\bar{1})$ step walls up to 30 \AA in length between the terraces, but the frequency of occurrence is very low. Except for the lower

value of the off-orientation angle, the morphology on nominal GaAs(2 5 11)B and A surfaces is very similar (cf. Fig. 6.4(a-b) and 5.19(a-b)).

6.3 Structural properties of InAs QDs on GaAs(2 5 11)B

An ensemble of InAs QDs on the GaAs(2 5 11)B surface grown as described in chapter 2.9 is presented in Fig. 6.5(a). Many small QDs with an average number density of $1.6 \times 10^{11} \text{ cm}^{-2}$ are recognized together with few large islands one of them being marked by an arrow. All islands develop with the same orientation relative to the substrate and exhibit a uniform shape, which does not change for substrate temperatures during preparation between 430 and 470 °C. The uniformity of the QD ensemble is reflected in the size distribution diagram in Fig. 6.5(b). About 70% of the islands exhibit a length between 15 and 20 nm and about 20% of them a length between 10 and 15 nm. The average height of the QDs is $2.2 \pm 0.3 \text{ nm}$. The few large islands contribute to the tail at larger sizes in Fig. 1(b). The large islands do not exhibit a certain size and are probably formed through coalescence of some QDs. They are presumably incoherent, i.e., a dislocation is inserted at the interface. The size distribution is very narrow, even narrower than that found for all reported in this work substrates (cf. Fig. 3.6(a), 4.2(b), 5.16(b) and 5.21(b)).

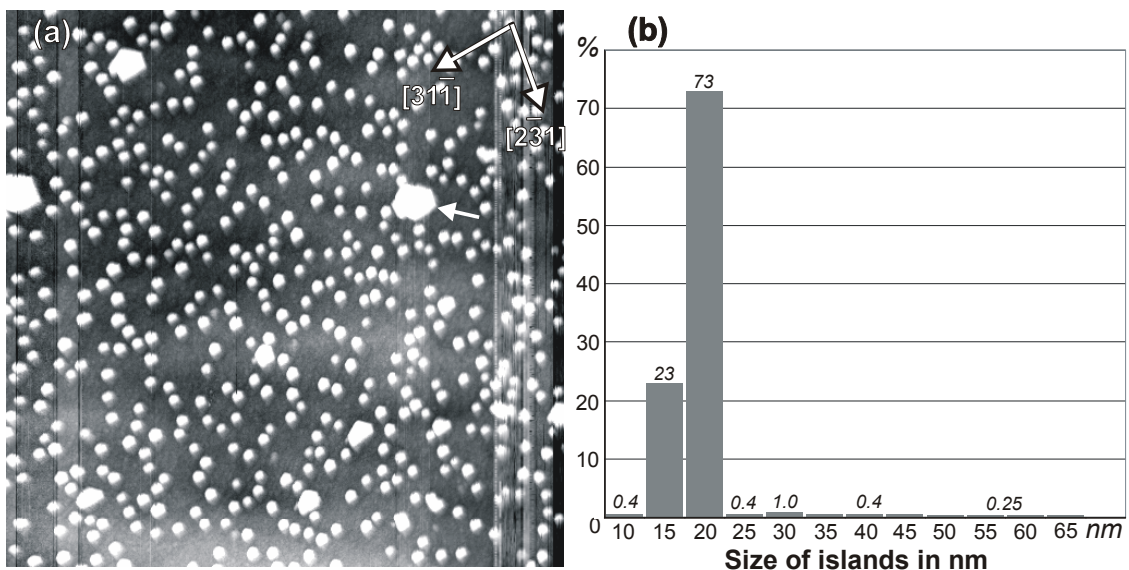


Figure 6.5 [Tem03a] (a) Overview STM image with InAs QDs grown on GaAs(2 5 11)B. White arrow indicates a large incoherent island ($5000 \times 5000 \text{ \AA}^2$, $U = -3.5 \text{ V}$, $I = 0.4 \text{ nA}$, the sample temperature $T=430 \text{ °C}$, InAs thickness is $4.5 (1.5 \text{ ML}) \pm 0.4 \text{ \AA}$); (b) Size distribution derived from 1560 islands in percent (the values are given above the respective columns).

Figure 6.6(a) presents a $(1000 \times 1000) \text{ \AA}^2$ large area of the $(2\ 5\ 11)B$ surface with the InAs QDs. To the contrary to the $(2\ 5\ 11)A$ substrate the WL exhibits no holes around the islands (cf. Fig. 5.22(a)). The WL is absolutely disordered and covered probably with As atoms (because of the As-rich preparation conditions) without any periodicity. That is quite different from the InAs WL on GaAs $(2\ 5\ 11)A$ (see Fig. 5.15(a) and 5.22(a)), where the original stripes made up from As dimers are still aligned along $[2\bar{3}\ 1]$. On the disordered structure one may expect a great number of broken anion bonds, which may catch up the cations to form bulk-like bonds and therefore, may slow down their diffusion length. It may lead to an increase of the nucleation events on the surface, and to an increase of the QD number density, that is usually by one order of magnitude higher on the $(113)B$ or $(2\ 5\ 11)B$ than on $(113)A$ or $(2\ 5\ 11)A$ substrates*. A general problem of As_2 molecule dissociation on the B faces (see chapter 3 and 4) and possible difficulties with the incorporation of these atoms onto the QD facets by the island evolving may yield an effect that the dense array of the QDs grow relatively slow, and In atoms can have enough time to check up many islands before an incorporation event. As the smaller islands are believed to grow faster [Jes98], this would result in a homogeneous uniform QD ensemble. Thus, the B substrates should be generally preferred for the QD application.

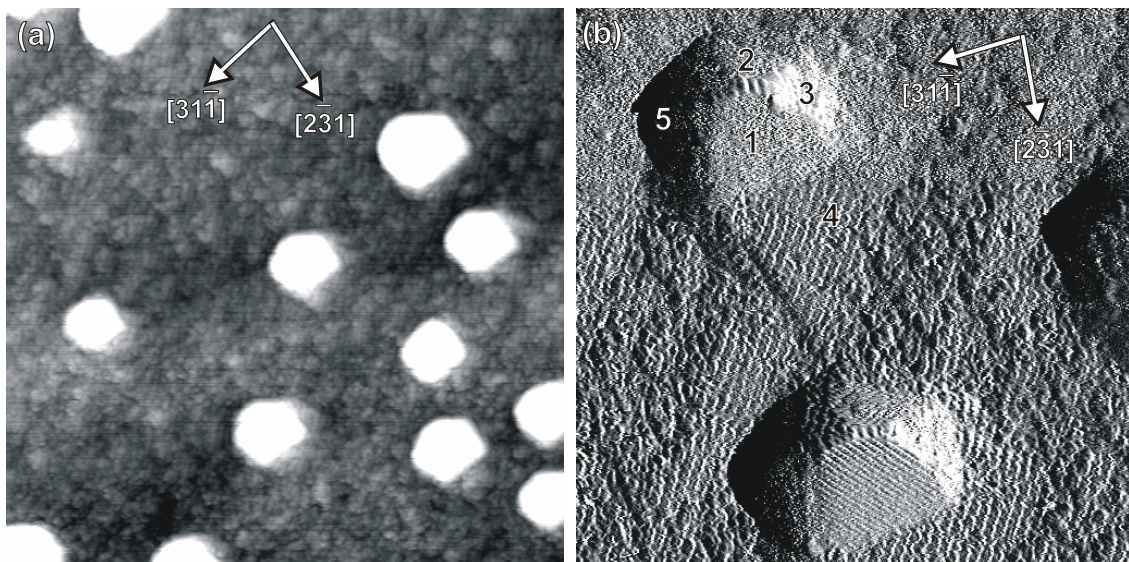


Figure 6.6 [Tem03a] (a) STM image with InAs QDs grown on the $(2\ 5\ 11)B$ WL ($U = -3.0\text{ V}$, $I = 0.1\text{ nA}$, $T=430\text{ }^\circ\text{C}$, 1.5 ML); (b) Atomically-resolved STM image (error signal \equiv constant height mode) of InAs QDs on GaAs $(2\ 5\ 11)B$ prepared at $450\text{ }^\circ\text{C}$ ($U = -3.0\text{ V}$, $I = 0.3\text{ nA}$, $T=450\text{ }^\circ\text{C}$).

* A large diffusion length of In atoms on the $(2\ 5\ 11)A$ WL may result in a disappearance of the QDs on the terraces (or in a decrease of their number density), and the island growth on the (011) step walls, where the InAs material is relaxed due to the dislocation.

Figure 6.6(b) shows an $(600 \times 600) \text{ \AA}^2$ large atomically resolved STM image highlighting the QD shape. The QDs are terminated by several well-developed facets 1 to 4 and a partially rounded region 5. The facet 4 is a flat base extending in front of the facets 1 and 3 on the upper left-hand side of the island in Figure 6.6(b). Interestingly, the QDs do not exhibit any symmetry plane perpendicular to the surface. This mirrors the substrate symmetry and is expected for epitaxial growth. Furthermore, similar to the InAs QDs on GaAs(113)B there is no elongation, in contrast to the respective A faces.

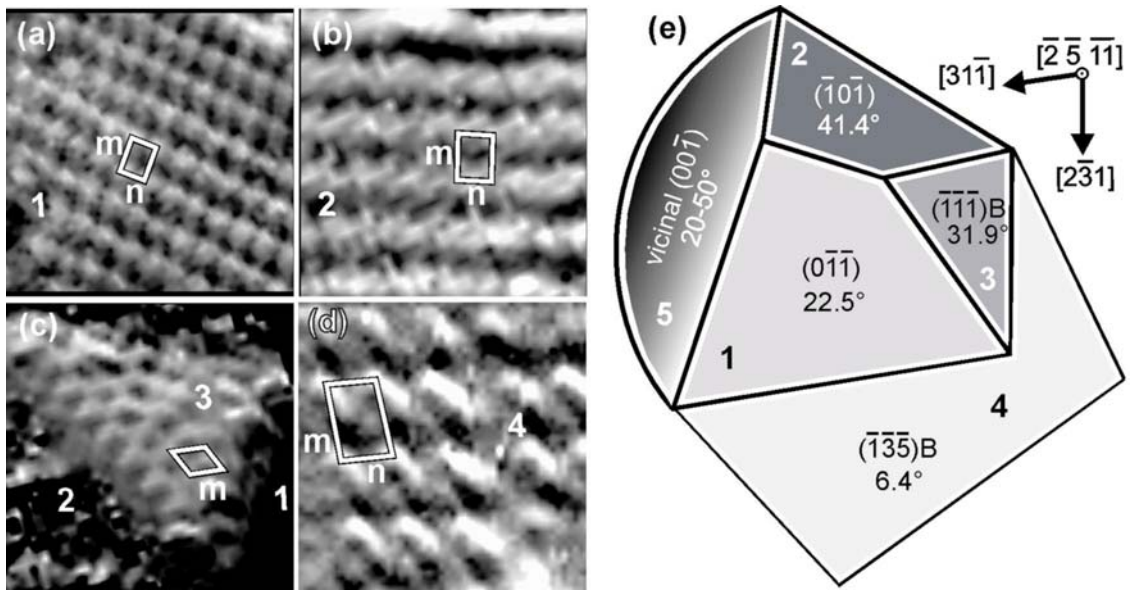


Figure 6.7 [Tem03a] Atomically-resolved STM images (error signal \equiv constant height mode, $U = -3.0 \text{ V}$, $I = 0.1 \text{ nA}$) of (a) the $(0,-1,-1)$ facet (the size is $(47 \times 47) \text{ \AA}^2$), (b) the $(-1,0,-1)$ facet (the size is $(34 \times 34) \text{ \AA}^2$), (c) the $(111)B-(2 \times 2)$ facet (the size is $(78 \times 78) \text{ \AA}^2$), and (d) the $(135)B-c(2 \times 2)$ facet (the size is $(48 \times 48) \text{ \AA}^2$). Letters m and n mark unit cell vectors; (d) schematic model of InAs QDs on GaAs $(2 \ 5 \ 11)B$. Darker grey scales correspond to steeper facets.

In Fig. 6.7(a-d) we show the individual facets with atomic resolution from which the facet orientation could be derived. The facet 1, shown in Fig. 6.7(a), is identified as a $(0\bar{1}\bar{1})$ surface. It is inclined to the substrate by $20 \pm 4^\circ$ and exhibits unit cell vectors $m = 5.9 \pm 0.3 \text{ \AA}$ and $n = 4.3 \pm 0.3 \text{ \AA}$. These values compare perfectly to the geometric values for the InAs $(0\bar{1}\bar{1})$ unit cell projected onto $(2 \ 5 \ 11)B$ of 22.5° , 6.0 \AA , and 4.0 \AA , respectively. The facet 2 in Fig. 6.7(b) is the $(\bar{1}0\bar{1})$ surface as extracted from the following STM measurements: The inclination angle is $38 \pm 4^\circ$, and the lengths of the unit cell vectors are

$m = 5.8 \pm 0.5 \text{ \AA}$ and $n = 4.4 \pm 1.0 \text{ \AA}$ (geometrical values: 41.4° , $m = 5.5$, and $n = 3.7 \text{ \AA}$). The atomic resolution is not as good as in (a) and therefore, the uncertainties in the derived values are larger. The triangular facet 3 in Fig. 6.7(c) consists of the (111)B-(2×2) reconstructed surface: It is inclined to (2 5 11)B by $31 \pm 3^\circ$ and exhibits a rhombic unit cell with vectors of length $m = 8.5 \pm 0.8 \text{ \AA}$ (geometrical values: 31.9° and $m = 8.2 \pm 0.2 \text{ \AA}$ for the As trimer (111)B-(2×2) reconstruction [Bie90]).

The flat facet 4 that extends in front of $(0\bar{1}\bar{1})$ and (111)B is identified as the (135)B-c(2 × 2) surface [Suz04a]: The inclination angle is $6 \pm 3^\circ$ and the lengths of the unit cell vectors are $m = 11.3 \pm 0.5 \text{ \AA}$ and $n = 9.0 \pm 0.5 \text{ \AA}$ (geometrical values: 6.4° , $m = 11.2 \text{ \AA}$, and $n = 9.6 \text{ \AA}$). A similar flat base was observed for InAs QDs on a GaAs(113)B surface (cf. Fig. 4.4(e)). Interestingly, in both cases we observe large and well ordered InAs(135)B facets, that seem to be energetically favourable under tensile strain on the GaAs substrate [Suz04a]. The existence of such flat bases is a new and not understood phenomenon. Together with the main part the facet forms a concave form with respect to the substrate, which is opposite to any understanding of minimization of surface energy since the surface to volume ratio is not minimal in this case.

Finally, the rounded region 5 is not shown in detail in Fig. 6.7 because it does not exhibit an ordered facet. From geometrical considerations, an $(00\bar{1})$ surface, that is inclined to (2 5 11)B by 26.1° , should develop in this area. Why the $\{001\}$ regions are rounded for the InAs QDs on GaAs(113)A, GaAs(113)B, and also here on GaAs(2 5 11)B is unclear. As in the case of GaAs(113), B and GaAs(2 5 11)A substrates, we also presume here that a vicinal $\{001\}$ region is growing with higher speed than regions of $\{110\}$ or $\{111\}$ orientation. The high speed of growth may induce a high degree of disorder and form the observed rounded shape.

The shape of InAs QDs grown on GaAs(2 5 11)B is schematically sketched in Fig. 6.7(e). There is no mirror symmetry on the QDs in agreement with substrate symmetry. Low-index $(0\bar{1}\bar{1})$, $(\bar{1}0\bar{1})$, and (111)B facets and a rounded vicinal $(00\bar{1})$ region for the main part, and a high-index (135)B surface for a flat base, extending in front of the $(0\bar{1}\bar{1})$ and (111)B facets, determine the shape of the QDs. The facets are inclined to the substrate with different angles, which may result in different growth speed that may be higher for the steeper $(\bar{1}0\bar{1})$ and vicinal $(00\bar{1})$ facets yielding a compact QD shape without an elongation into any specific direction. In addition to that there should be difficulties by the

incorporation of As₂ molecules onto all the facets, except for the rounded region (see chapter 3 and 4). This facet growth kinetics (that should be similar to that described for the GaAs(113)A and B substrates) together with the poor ordered InAs WL can account for the very narrow size distribution and high number density of the InAs QDs on GaAs(2 5 11)B.

6.4 Optical properties of InAs QDs on GaAs(2 5 11)B

It is now tempting to look how the uniform QD ensemble can improve the PL spectra. The InAs QDs were overgrown under the same preparation conditions as for InAs islands on GaAs(2 5 11)A*. Figure 6.8(a) shows PL spectra of one single sheet of InAs QDs. The linear presentation of the dependence of PL intensity on the emission energy is taken with four different excitation densities: 5000 W/cm² (solid line), 500 W/cm² (dashed line), 50 W/cm² (dotted line), and 5 W/cm² (dashed-dotted line). The Gaussian-like PL peaks marked by 1 in Fig. 6.8(a) are centred at ~1333 meV with the FWHM values of 58, 50, 44 and 45 meV for the solid, dashed, dotted and dashed-dotted line, respectively. These peaks are intense and cover the energy range expected for the small sized InAs QDs. The broad peaks numbered by 3 stem from the InAs WL and doped GaAs(2 5 11)B substrate, because they are located next to the double peak of the semiinsulating GaAs(001), see, e.g., Fig. 5.24(b). The solid line exhibits an additional peak (numbered by 2 in Fig. 6.8(a)) that is ascribed to stem from the first excited state in the QDs. At the highest excitation density (5000 W/cm²), the excited state peak evolves into a separate peak because the ground state level is completely saturated by the charge carriers. Despite the reduces thermal energy at 10K for the carriers, the very high density of the InAs QDs on GaAs(2 5 11)B (see Fig. 6.5(a)) allows electrons to find an available ground state level in nearby dots, thus suppressing excited state recombination for the excitation densities below 5000 W/cm². No other peaks are found between 2 and 3. It means that the InAs QDs on GaAs(2 5 11)B with the measured diameter of 175 ± 25 Å (see Fig. 6.5(b)) are so small in size, that the only ground and first excited state levels are confined. This is quite different from the recently reported *eight-band k-p calculations* for InAs QDs on GaAs(001) exhibiting a pyramidal shape with {101} facets (45° tilt angle) and a base length of 136 Å [Bim99], from which at least three transition peaks from the ground and excited states should appear in the PL spectra. A flatter shape of our QDs with an average tilt angle of the facets of ~30° as well

* The GaAs overgrowth as well as PL parameter were set equal for all the substrates (i.e., vicinal and nominal GaAs(2 5 11)A and nominal GaAs(2 5 11)B) in order to insure a correct quantitative comparison for the QDs.

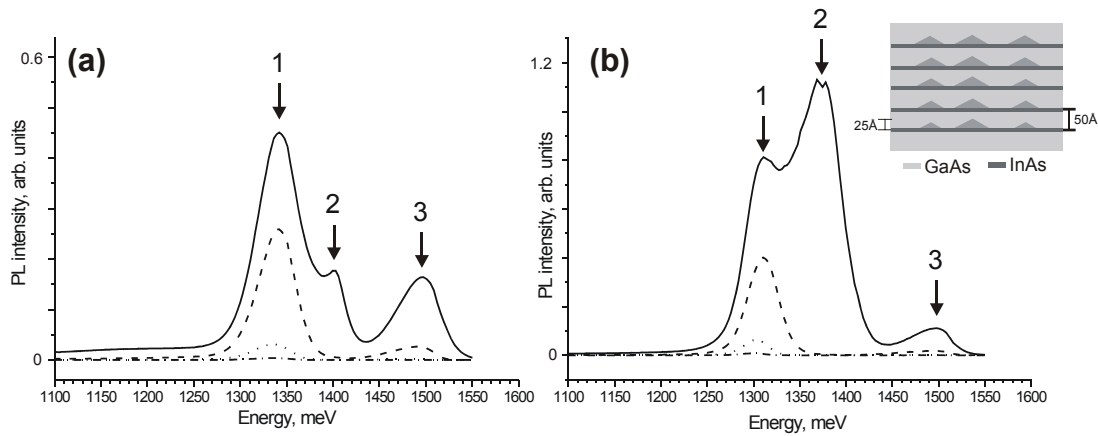


Figure 6.8 [Tem04] PL spectra of InAs QDs grown on GaAs(2 5 11)B ($T=430^{\circ}\text{C}$, 1.5 ML) acquired with different excitation densities and presented in linear scale for (a) a single QD sheet and (b) 5 x vertical stacked QDs. Excitation density was 5000, 500, 50 and 5 W/cm^2 for solid, dashed, dotted and dashed-dotted lines, respectively. 1, 2 and 3 numbers the peaks related to the QDs and GaAs bulk material. The inset in (b) shows the geometry of the 5 QD sheets.

as a possible segregation of In atoms by the overgrowth, that results in a shrinkage of the QD size, may account for this discrepancy.

It is well known that a vertical stacking of the InAs QDs can improve the optical properties of QD lasers and can yield an increase of the active volume, a shift of the emission to longer wavelength (smaller energy), and a decrease of the emission linewidth [Sol96]. This improvement is reported to stem from the strain field of underlying dot sheets that can influence the dot formation in the sheet above as well as from the electronic coupling of all dots, which increases the effective height and therefore, reduces the effect of QD size fluctuations [Lip00]*. Figure 6.8(b) shows the PL spectra of five InAs QD sheets on GaAs(2 5 11)B with a GaAs spacer thickness of 50 Å, which is roughly twice as large as the average QD height (~22-25 Å, see also the inset in (b)). The spectra are mainly similar to those in (a) with the following differences: the intensities of the QD peak with the same excitation densities are higher for the vertical stacking; the QD peaks numbered by 1 are all centred at 1299 meV with the FWHM values of 44, 38, 30 and 29 meV for the lines from solid down to the dashed-dotted; the excited state peak 2 for the solid line in (b) is more intensive than that for the single sheet of the QDs in (a) and even larger than the ground state peak 1. Thus, the desirable shift of the emission energy (~34 meV) and the

* A prerequisite is a thin GaAs spacer thickness between the InAs QD sheets (up to ten QD heights).

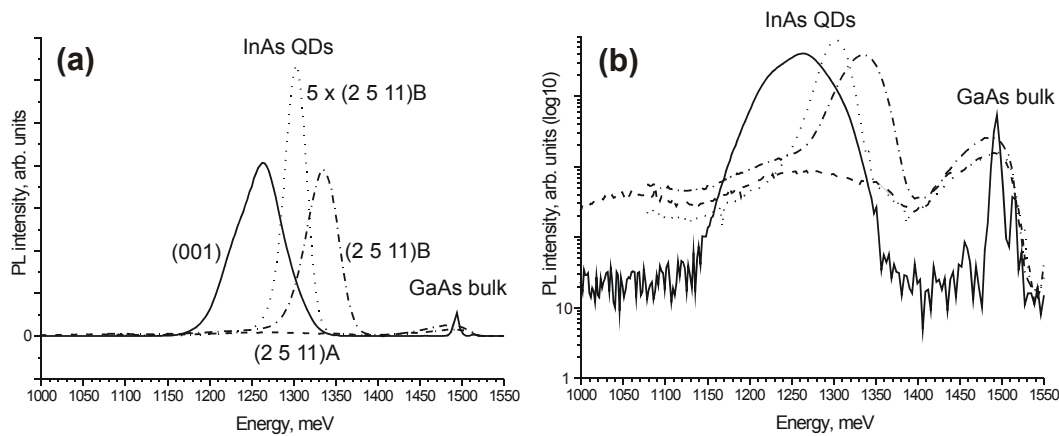


Figure 6.9 [Tem04] PL spectra of the InAs QDs grown on different GaAs substrates presented in (a) linear scale and (b) decimal logarithmic scale. The QDs and GaAs bulk related peaks are labeled. Excitation density was 5 W/cm^2 .

decrease of the linewidth can be clearly detected by using the vertical stacking of the InAs QDs on GaAs(2 5 11)B.

Figure 6.9 shows a quantitative comparison of the PL spectra of InAs QDs on different GaAs substrates. The solid, dashed, dotted and dashed-dotted lines correspond to nominal (001), (2 5 11)A, 5x QD stacking on (2 5 11)B and one single QD sheet on (2 5 11)B, respectively. All the QDs are grown at the same sample temperature $T=430 \text{ }^\circ\text{C}$ with the InAs thickness needed for the onset of the SK transition (1.5 ML for GaAs(001) and GaAs(2 5 11)B, and 1.7 ML for GaAs(2 5 11)A). The linear and logarithmic presentations of PL intensity on the emission energy is shown in Fig. 6.9(a) and (b), respectively. As can be seen, the Gaussian-like PL peaks of the InAs QDs on GaAs(2 5 11)B (dotted and dashed-dotted lines) exhibit the same or even higher intensity than the peak of the QDs on commonly used GaAs(001). To the contrary, the line for the InAs islands on GaAs(2 5 11)A is about two orders of magnitude lower. The PL peaks for the solid, dotted and dashed-dotted lines are centred at 1265, 1299 and 1333 meV, with the FWHM values of 66, 30, and 45 meV, respectively. It means, that the QDs on GaAs(2 5 11)B prepared under the same MBE conditions are smaller and more uniform in size than those on GaAs(001). This should be related to the atomic structure of both substrates, i.e., to the adsorption, desorption and migration of In and As atoms on their reconstructions. The integrated intensity is highest for the GaAs(001) substrate. However, highly doped GaAs(2 5 11)A and B wafers have been used for the PL (the higher background intensity can be seen for all lines except for the solid line in Fig. 6.9(b)), which may result in an

absorption of photons by the substrate doping. Thus, GaAs(2 5 11)B can be used as a substrate for the growth of InAs QDs with an especial narrow size distribution, thus, a small PL linewidth.

There is an interest for the development of InAs-QD-based devices emitting in the datacom wavelength region around 1.3 μm (954 meV). This would allow the realisation of datacom sources cheaper and less temperature sensitive than commonly used InP-based devices [Gru02]. To extend the emission wavelength to 1.3 μm from the single QD sheet one employs usually some special tricks, among which the first one is to embed the InAs QDs into an $\text{In}_x\text{Ga}_{1-x}\text{As}$ matrix (with In content $x < 0.3$). The resulting red shift has been observed even beyond 1.3 μm and attributed to an increase of the dot height caused by spinoidal-activated decomposition and to a reduced strain in the InAs QDs [Max00, Che02]. Another trick is a deposition of more InAs that is needed for the SK transition [Pas03].* As we have seen in chapter 4.2 an increase of the sample temperature from 435 to 490 $^\circ\text{C}$ results in a doubling of the QD size, accompanied however with a decrease of QD number density by an order of magnitude. Being unable to perform a systematic PL study because of the lacking of a PL facility at our permanent disposal, we have tried to employ all these tricks to shift the emission energy of InAs QDs on GaAs(2 5 11)B to the low energy range.

Figure 6.10 shows the PL spectra of one single sheet of InAs QDs on GaAs(2 5 11)B presented in linear (a) and logarithmic (b) scales. The solid line corresponds to a reference sample (=the dotted line in Fig. 6.8(a)): the QDs grown at 430 $^\circ\text{C}$ with an InAs thickness $l = 4.5 \text{ \AA}$ (=1.5 ML₀₀₁) and overgrown with 50 nm pure GaAs as described in chapter 2.9. The dashed line stems from the InAs QDs grown at $T=500 \text{ }^\circ\text{C}$ with $l = 6 \text{ \AA}$ (=2.0 ML) and overgrown at the same temperature with 7 nm of $\text{In}_{0.1}\text{Ga}_{0.9}\text{As}$ and then with 43 nm of pure GaAs. The latter growth sequence has been repeated for the QDs presented by the dashed-dotted line except for $l = 9 \text{ \AA}$ (=3.0 ML). The solid, dashed and dashed-dotted lines are centred at 1333 meV (FWHM=44 meV), 1222 meV (FWHM=62 meV) and 1218 meV (FWHM=105 meV), respectively. Thus, a red shift can be achieved, however by only 111 meV to the value of 1222 meV, which is of course still far away from 954 meV (1.3 μm) needed for the QD applications. The red shift seen at the dashed line is accompanied with a reduction of the integrated PL intensity (by a factor of 4) that is on the line of our STM observations for InAs QDs on GaAs(113)B, where an increased sample temperature yields

* The third way is to make large sized dots by reducing InAs growth rate [Joy00]. However, we use one of the smallest rates, reported in literature (0.07 $\text{\AA}/\text{s}=0.02 \text{ ML}/\text{s}$, more than 60 seconds to achieve the SK transition).

a decrease of the QD number density. The increase of the FWHM value for the dashed line in comparison with the solid one does not agree with literature [see, e.g., Sch02], where the reduced linewidth has been reported by increase of the sample temperature. The dashed-dotted line corresponding to the 3 ML InAs QDs shows a degradation of the single Gaussian-like peak and a high FWHM value. The energy peak is centred at 1218 meV that is next to the 2 ML InAs QDs. It indicates that between 2 and 3 ML of InAs deposition the islands have not increased in size, but have become degraded probably through the incorporation of dislocations after a certain QD size.

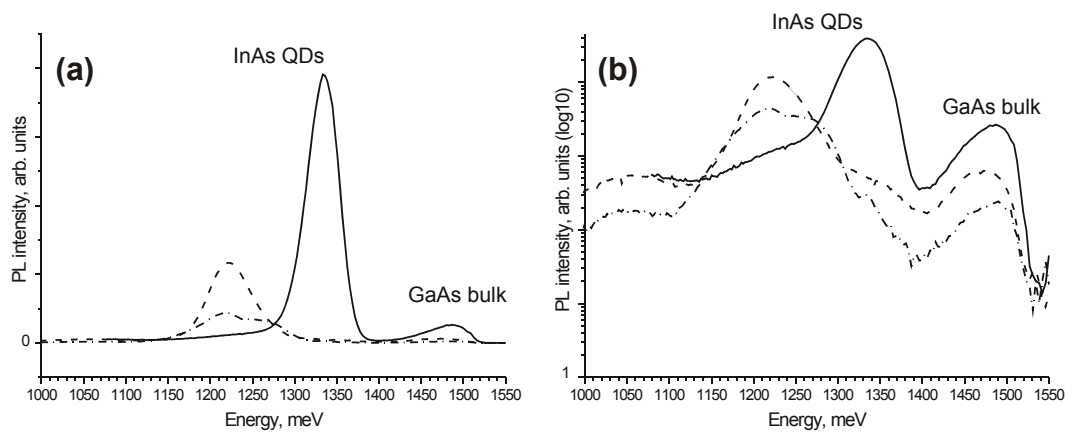


Figure 6.10 [Tem04] PL spectra of the InAs QDs grown on GaAs(2 5 11)B grown with modified conditions and presented in (a) linear scale and (b) decimal logarithmic scale. The solid, dashed and dashed-dotted lines correspond to the InAs thickness of 1.5 ML ($T=430$ °C), 2.0 ML ($T=500$ °C), and 3.0 ML ($T=500$ °C), respectively. The QDs and GaAs bulk related peaks are labeled. Excitation density was 50 W/cm².

As we have shown, it is in principle possible to shift the PL peak of the InAs QDs on GaAs(2 5 11)B to smaller energies. One should probably not use the high sample temperature for the overgrowth procedure, which may reduce the QD size through an In segregation, in order to shift the QD peak further.

6.5 Conclusion

GaAs(2 5 11)B is the only known stable compound semiconductor surface located within the ST for the B faces. One can get the atomic structure of GaAs(2 5 11)B by mirroring the GaAs(2 5 11)A surface around any perpendicular plane, subsequently rotation by 180° and exchanging the As and Ga atoms. The ball-and-stick model of GaAs(2 5 11)B reveals a

(1x1) reconstruction, terminated by Ga dimers, that fulfils the ECR and yields a reduced number of DBs compared with the bulk-truncated surface. No symmetry plane exists on bulk-truncated and reconstructed GaAs(2 5 11)B. The morphology of the nominal GaAs(2 5 11)B surface exhibits a low off-orientation angle of $\sim 0.3^\circ$ and consists of ~ 2 Å high steps running mainly along $[2\bar{3}1]$ with a small number of step bunch structures along $[31\bar{1}]$.

The deposition of 1.5 ML of InAs results in the SK transition. STM images reveal a uniform ensemble of small InAs QDs on GaAs(2 5 11)B with a very narrow size distribution and a high number density. There is no mirror symmetry on the QDs in agreement with the substrate symmetry. Low-index $(0\bar{1}\bar{1})$, $(\bar{1}0\bar{1})$, and (111)B facets and a rounded vicinal $(00\bar{1})$ region for the main part, and a high-index (135)B surface for a flat base, extending in front of the $(0\bar{1}\bar{1})$ and (111)B facets, determine the shape of the QDs. The facets are inclined to the substrate with different angles, which may result in different growth speed that may be higher for the steeper $(\bar{1}0\bar{1})$ and vicinal $(00\bar{1})$ facets yielding a compact QD shape without an elongation into any specific direction. In addition, there should be difficulties by the incorporation of As₂ molecules onto all the facets, except for the rounded region. This facet growth kinetics together with the poor ordered InAs WL, which can reduce the diffusion length of In atoms, can account for the very narrow size distribution and high number density of the InAs QDs on GaAs(2 5 11)B.

The Gaussian-like PL peak of the InAs QDs on GaAs(2 5 11)B exhibits a similar intensity to the peak from the InAs QDs on commonly used GaAs(001), but a higher emission energy and a smaller FWHM, indicating a smaller and more uniform in size QD ensemble. A small red shift of the emission energy has been achieved by using vertical stacked QDs or by increase the sample temperature and InAs thickness of the dots embedded in a In_{0.1}Ga_{0.9}As cap layer.

7 General conclusions

Self-organised InAs QDs grown on four high-index substrates such as GaAs(113)A, B and GaAs(2 5 11)A, B, have been the subject of the present thesis. We have mainly focused our efforts on the QDs evolving in a stage before the overgrowth for the further application. Their development has been followed from the atomic structure of the bare substrates through the InAs WL stage to the bounding facets framing the 3D islands due to the SK transition that occurs on all investigated surfaces. We have collected experimental material in hope that somebody from the theoreticians will use it to answer a fundamental question, namely why InAs grows by usual MBE conditions in the SK growth mode on all known stable GaAs substrates except for low-index (110), (111)A and B [Hoo93, Yam96, Bel97].

From the STM, RHEED, LEED and PL measurements conducted in this work some general points by the QD evolution can be extracted:

- The SK transition is realised on all high-index substrates, where the InAs material grows first in the layer-by-layer growth mode. When the amount of deposited material exceeds a critical thickness of about 1.5-1.8 ML₀₀₁, the 3D islands suddenly appear on top of the WL.
- The symmetry of the QDs derives directly from the ideal (bulk-truncated) substrate that unambiguously proves epitaxial growth by the SK transition.
- The QD ensemble on the B face exhibits a narrower size distribution and a larger number density than that on the respective A face.
- The InAs QDs on the A faces tend to adopt an elongated shape, whereas those on the B face are rather round.
- The QDs start to grow with the flattest facets with respect to the substrate, which are $\{2\ 5\ 11\}$ A or $\{137\}$ A for the GaAs(113)A and GaAs(2 5 11)A, and probably $\{135\}$ B for the GaAs(113)B and GaAs(2 5 11)B. At the mature stage the islands adopt a steeper shape, terminated by the low-index regions. This final shape seems to remain further unchanged, even by incorporation of dislocations onto the QDs, except for small modifications, like a shape elongation or faceting of the rounded $\{001\}$ region. Being unstable as nominal GaAs surfaces, large areas of the (137)A or (135)B facets with their own reconstructions develop on the strained InAs QDs.

Despite of the common similarities, the behavior of each substrate is peculiar. Two shapes are observed for the mature QDs on GaAs(113)A, which both have the same $(\bar{1}10)$ symmetry plane and azimuthal orientation. In the first stage, the shape is given by $\{110\}$,

(111)A and $\{2\ 5\ 11\}$ A bounding facets and a rounded region due to a stacking of vicinal (001) surfaces. The second shape is characterised by an elongation along $[3\ 3\ \bar{2}]$ with a size reduction of the (111)A facet, induced by a partially flattening of the rounded region by $\{113\}$ B facets, which slow down its growth rate.

The morphology of the bare GaAs(113)A surface and of the InAs WL on it influence significantly the size distribution of the QDs. The intrinsic undulation of bare GaAs(113)A becomes larger with depositing InAs. As the WL roughness exhibits varying lateral dimension, the strain relieve is different, and the nuclei do not form simultaneously on the whole surface. It leads to the observed broad size distribution. In addition, the WL still exhibits As dimers aligned along $[3\ 3\ \bar{2}]$, that may not significantly decrease the diffusion length of In atoms, which results in the low QD number density. Because of the inhomogeneous nucleation and growth processes we are able to retrace the QD kinetics, that start to grow with the very flat (2 5 11)A and (137)A facets.

The InAs QDs on GaAs(113)B evolve with $(\bar{1}\ 1\ 0)$ mirror symmetry and with a central steep part sitting on a flat base. The shape of the central part is given by $\{110\}$ and (111)B bounding facets, and a $(00\bar{1})$ rounded region. High-index $\{135\}$ B and (112)B facets are derived for the flat base. An elongation of the shape with a reduction in size of (111)B is not observed. It is attributed to the difficulties with the incorporation of As_2 molecules onto the QD facets, as their edges with the substrate as well as facet reconstructions require the dissociation of As_2 molecules, that is not the case for GaAs(113)A.

The morphology of the bare GaAs(113)B surface preserves its original flatness also after InAs deposition. Thus, the QDs start to grow simultaneously at the SK transition and mature on the whole surface with equal rates, resulting in a narrow size distribution. Furthermore, the disordered WL may decrease the diffusion length of the In atoms that induces a high QD number density. Additional experiments reveal the increase of the size and height of the QDs by more than 100 % and decrease in the number density by an order of magnitude if the sample temperature increases from 435 to 490 °C. Post-annealing also increases the QD size and the height by about 30 % and decreases slightly the number density. However, the shape of the QDs is found to be independent on the sample temperature or post-annealing procedure.

We have also employed the stable GaAs substrates located within the ST and therefore, exhibited no mirror symmetry. The recently discovered in our group GaAs(2 5 11)A surface has been used for the InAs QD growth. The surface exhibits an interesting (1x1)

reconstruction, terminated by As dimers, that fulfils the ECR and has a surface energy comparable with that of the known stable GaAs reconstructions.

A remarkable feature of this substrate is the formation of step bunch structures, resulting in an appearance of large GaAs(011) areas on straight steps along the $[3\bar{1}\bar{1}]$ direction. The morphology of 1° vicinal GaAs(2 5 11)A is mainly determined by these steps, but they still exist also on the nominal-oriented surface.

The deposition of a certain amount of InAs results in the SK transition that can be observed with RHEED measurements. STM images from the vicinal (2 5 11)A surface reveal an appearance of 3D InAs islands sitting exactly on the steps along $[3\bar{1}\bar{1}]$. The measured number density is low and the size distribution is very broad, which is characteristic for the incoherent (dislocated) islands that grow without size limitation caused by the elastic strain as in the coherent QDs. The dislocations are assumed to be incorporated through the InAs growth on the GaAs(011) step walls, as the GaAs(011) surface does not grow in the SK growth mode. The incoherent nature of the islands is confirmed by PL spectra, where the emission in the QD energy range from the (2 5 11)A samples is more than two orders of magnitude lower than that from a reference (001) sample.

STM images from the nominal GaAs(2 5 11)A surface exhibit two different ensembles of InAs islands with narrow and broad size distributions. The latter stems from the islands grown on the (011) bunch structures that also appear on nominal GaAs(2 5 11)A. The narrow size distribution is thought to stem from the coherent, dislocation-free QDs. They are largely similar to the InAs QDs on GaAs(113)A, except for the missing $(\bar{1}10)$ symmetry plane: In the early stage, the shape is given by $\{110\}$, (111)A bounding facets and a rounded region due to a stacking of vicinal (001) surfaces. After some growth the shape is characterised by an elongation along $[4\bar{5}\bar{3}]$ with a size reduction of the (111)A facet, induced by a flattening of the rounded region by $(\bar{2}\bar{5}11)$ A, $(\bar{1}01)$ and $(\bar{1}11)$ B facets, two latter of which slow down its growth rate. However, the PL measurements show mainly identical results from the nominal and vicinal GaAs(2 5 11)A substrates, implying a very low emission intensity from the islands. It is explained by trapping of the QD excitons in the dislocations formed in the incoherent islands.

GaAs(2 5 11)B is another stable substrate located within the ST for the B faces that has been used for the InAs QD growth. The atomic structure of this surface, which has been determined in this work for the first time, can be obtained from the GaAs(2 5 11)A surface

applying a combined mirroring and rotation by 180° , with a subsequent exchange of As and Ga atoms. We propose a model for the GaAs(2 5 11)B surface exhibiting a (1x1) reconstruction, terminated by Ga dimers, that fulfils the ECR and yields a reduced number of DBs compared with the bulk-truncated surface. Together with the (1x1) reconstruction the latter shows no symmetry plane that is also retained in the InAs QDs.

The deposition of a certain amount of InAs onto GaAs(2 5 11)B results in the SK transition. STM images reveal a uniform QD ensemble with a high number density. The size distribution is very narrow strongly evidencing the coherent nature of the islands. Low-index $(0\bar{1}\bar{1})$, $(\bar{1}0\bar{1})$ and (111)B facets and a rounded vicinal $(00\bar{1})$ region for the central steep part, and a high-index $\{135\}$ B surface for the flat base determine the shape of the InAs QDs on GaAs(2 5 11)B, which is similar to that on GaAs(113)B, except for missing mirror symmetry. The WL on GaAs(2 5 11)B is much more disordered than that on the A face. The reason may stem from the surface geometry: the As atoms covering the GaAs surfaces by the As-rich preparation conditions can not form such a stable low-energy elements as As dimers. It may lead to the disordered surface with a great number of As DBs, which may decrease the diffusion length of In atoms during and after the SK transition. It results in an increased QD number density compared with the GaAs(2 5 11)A surface. In addition, the facet growth kinetics, that prohibits the incorporation of As_2 molecules onto the InAs QD facets on GaAs(2 5 11)B, thus decreasing their growth rate, may also delay the incorporation of the In atoms, that may check up many islands before finally being incorporated. This can account for the very narrow size distribution.

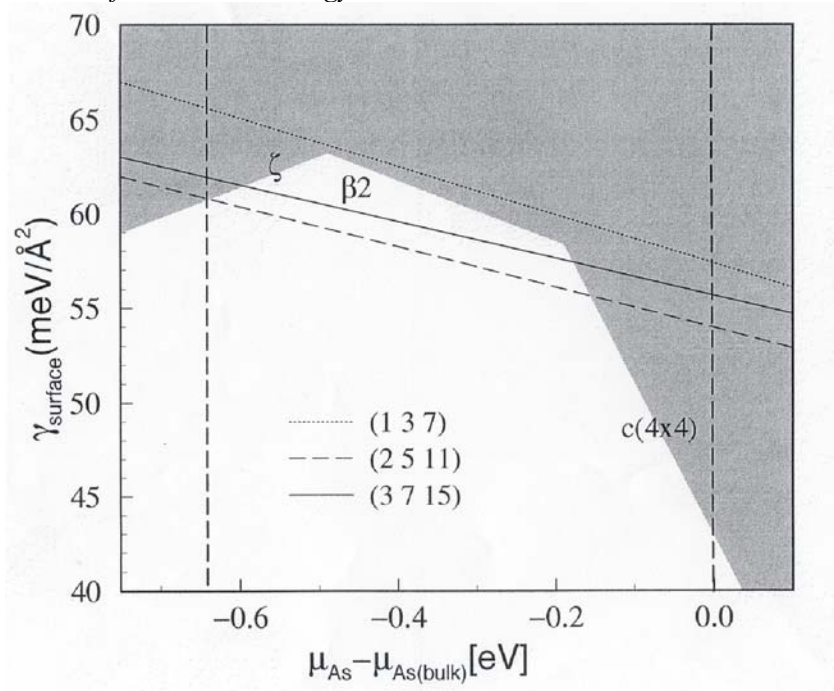
The Gaussian-like PL peak of the InAs QDs on GaAs(2 5 11)B exhibits an intensity similar to that from the InAs QDs on GaAs(001), but higher emission energy and smaller FWHM, indicating a smaller and more uniform QD ensemble. A red shift of the emission energy has been achieved by using vertical stacked QDs or by increase the sample temperature and InAs thickness of the dots embedded in the $In_{0.1}Ga_{0.9}As$ cap layer.

Thus, GaAs(113)B and GaAs(2 5 11)B can be used equally with GaAs(001) as substrates for different QD applications in optoelectronics since they yield a uniform and dense QD ensemble with a tunable upon the temperature QD size and emission wavelength; GaAs(113)A and GaAs(2 5 11)A substrates are interesting for understanding of basic processes by the QD evolving.

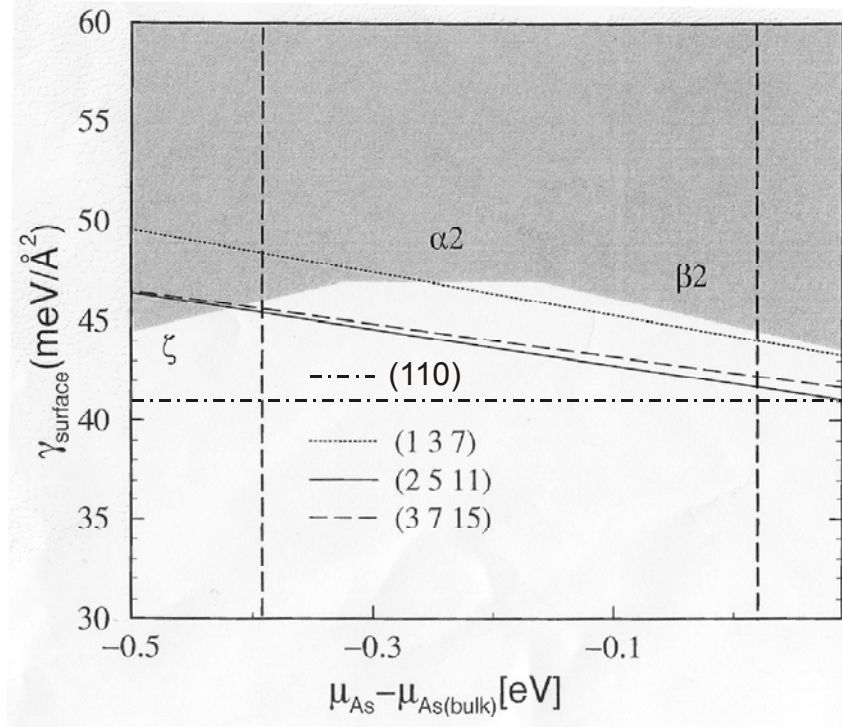
Appendix 1.1: Table with GaAs and InAs surface energies for As rich preparation conditions. The energies are calculated using density-functional theory.

Reconstruction	Energy, meV/Å²	Reference
<i>GaAs(001)-β2(2x4)</i>	55	[Mol96]
<i>GaAs(001)-c(4x4)</i>	45	[Mol96]
<i>GaAs(110) cleavage plane</i>	52	[Mol96]
<i>GaAs(111)A-(2x2) (Ga vacancy)</i>	54	[Mol96]
<i>GaAs(111)B-(2x2) (As trimer)</i>	43	[Mol96]
<i>GaAs(113)A-(8x1)</i>	47	[Pla99]
<i>GaAs(113)B-(1x1) (As double layer)</i>	43	[Pla99]
<i>GaAs(114)A-β2c(2x2)</i>	46	[Kra02a]
<i>GaAs(114)A-α2(2x1)</i>	53	[Mar01a]
<i>GaAs(2 5 11)A-(1x1)</i>	53	[Gee01]
<i>GaAs(3 7 15)A-(1x1)</i>	55	[Gee01]
<i>GaAs(137)A-(1x1)</i>	56	[Kra02a]
<i>InAs(001)-β2(2x4)</i>	44	[Mol98]
<i>InAs(001)-c(4x4)</i>	44	[Mol98]
<i>InAs(110) cleavage plane</i>	41	[Wan99]
<i>InAs(111)A-(2x2) (In vacancy)</i>	42	[Mol98]
<i>InAs(111)B-(2x2) (As trimer)</i>	36	[Mol98]
<i>InAs(114)A-β2(2x1)</i>	43	[Kra02a]
<i>InAs(2 5 11)A-(1x1)</i>	41	[Kra02a]
<i>InAs(3 7 15)A-(1x1)</i>	42	[Kra02a]
<i>InAs(137)A-(1x1)</i>	43	[Kra02a]

Appendix 1.2: GaAs surface energies of the (1x1) reconstructed (137)A, (2 5 11)A and (3 7 15)A surfaces as a function of the As chemical potential. The energies are calculated using density-functional theory. The shaded areas highlight the calculated surface energies of the GaAs(001) reconstructions of lowest total energy.



Appendix 1.3: InAs surface energies of the (1x1) reconstructed (137)A, (2 5 11)A and (3 7 15)A surfaces and of the relaxed (110) cleavage plane as a function of the As chemical potential. The energies are calculated using density-functional theory. The shaded areas highlight the calculated surface energies of the InAs(001) reconstructions of lowest total energy.



Bibliography

- App76** J. A. Appelbaum, G. A. Baraff, D.R. Hamann, Phys. Rev. **B 14**, 1623 (1976).
- Ash96 R. C. Ashoori, Nature **379**, 413 (1996).
- Ave94 A.R. Avery, D. M. Holmes, T. S. Jones, B. A. Joyce, G. A.D. Briggs, Phys. Rev. **B 50**, 8098 (1994).
- Ave96 A.R. Avery, C. M. Goringe, D. M. Holmes, J. L. Sudijono, T. S. Jones, Phys. Rev. Lett. **76**, 3344 (1996).
- Bar97** A.-L. Barabási, Appl. Phys. Lett. **70**, 2565 (1997).
- Bar02 W. Barvosa-Carter, R. S. Ross, C. Ratsch, F. Grosse, J. H. G. Owen, J. J. Zinck, Surf. Sci. **499**, L129 (2002).
- Bas96 A.A. Baski, and L.J. Whitman, J. Vac. Sci. Technol. **B 14**, 992 (1996).
- Bel97 J. G. Belk, J. L. Sudijono, X. M. Zhang, J. M. Neave, T. S. Jones, B. A. Joyce, Phys. Rev. Lett. **78**, 475 (1997).
- Bel99 G. R. Bell, M. Itoh, T. S. Jones, B. A. Joyce, Surf. Sci. **423**, L280 (1999).
- Ber98 E. Bertel, K. Swamy, P. Hanesch, Phys. Rev. Lett. **80**, 2019 (1998).
- Bie90 D. K. Biegelsen, R. D. Bringans, J. E. Northrup, L.-E. Swartz, Phys. Rev. Lett. **65**, 452 (1990).
- Bim99 D. Bimberg, M. Grundmann, N. N. Ledentsov, *Quantum Dot Heterostructures* (Wiley, Chichester, NY, 1999).
- Bim00 D. Bimberg et al., Thin Solid Films **367**, 235 (2000).
- Bin82 G. Binnig, H. Rohrer, Ch. Gerber, E. Weibel, Phys. Rev. Lett. **49**, 57 (1982).
- Bra93 O. Brandt, K. Kanamoto, Y. Tokuda, N. Tsukada, O. Wada, J. Tanimura, Phys. Rev. **B 48**, 17 599 (1993).
- Bra96 W. Braun, O. Brandt, M. Wassermeier, L. Däweritz, K. Ploog, Appl. Surf. Sci. **104**, 35 (1996).
- Bra99 W. Braun, Applied RHEED, Springer Tracts in Modern Physics, Vol. **154** (Springer, Berlin, 1999).
- Cha84** D. J. Chadi, Phys. Rev. Lett. **52**, 1911 (1984).
- Cha85 D. J. Chadi, J. Vac. Sci. Technol. **B 3**, 1167 (1985).
- Cha91 D. J. Chadi, Electron-Hole Counting Rule at III-V Surfaces: Applications to Surface Structure and Passivation in: *The Structure of Surfaces III, Springer Series in Surface Sciences*, Vol. **24**, S. Y. Tong, M. A. Van Hove, D. Takayanagi and X.D. Xie (Edit), (Springer, Berlin, 1991), S. 532.

- Che63 A.A. Chernov, Soviet Physics Crystallography **7**, 728 (1963).
- Che96 Y. Chen and J. Washburn, Phys. Rev. Lett. **77**, 4046 (1996).
- Che02 J. X. Chen et al., J. Appl. Phys. **91**, 6710 (2002).
- Chi01 C. H. Chia, T. Makino, Y. Segawa, M. Kawasaki, A. Ohtomo, K. Tamura, H. Koinuma, J. Appl. Phys. **90**, 3650 (2001).
- Cho99 A. Y. Cho, J. Cryst. Growth **201/202**, 1 (1999).
- Chu96 Y. J. Chun, S. Nakajima, M. Kawabe, Jpn. J. Appl. Phys. **35**, L1075 (1996).
- Chu99 L. Chu, M. Arzberger, G. Böhm, G. Abstreiter, J. Appl. Phys. **85**, 2355 (1999).
- Cor97 E. Corcoran und G. Zorpette, Diminishing Dimensions in: The Solid State Century, Scientific American Special Issue (Oktober 1997).
- Cos03 G. Costantini, C. Manzano, R. Songmuang, O. G. Schmidt, K. Kern, Appl. Phys. Lett. **82**, 3194 (2003).
- Dae90** L. Däweritz and R. Hey, Surf. Sci. **236**, 15 (1990).
- Dar97 I. Daruka and A. –L. Barabasi, Phys. Rev. Lett. **79**, 3708 (1997).
- Dob97 H. T. Dobbs and D. D. Vvedensky, Phys. Rev. Lett. **79**, 897 (1997).
- Dra78 P. Drathen, W. Ranke, K. Jacobi, Surf. Sci. **77**, L162 (1978).
- Duk86 C. B. Duke, C. Mailhiot, A. Paton, A. Kahn, K. Stiles, J. Vac. Sci. Technol. **A 4**, 947 (1986).
- Duk96 C. B. Duke, Chem. Rev. **96**, 1237 (1996).
- Ebe01** Ph. Ebert, Current Opinion in Solid State and Materials Science **5**, 211 (2001).
- Eis99 H. Eisele, O. Flebbe, T. Kalka, C. Preinesberger, F. Heinrichsdorff, A. Krost, D. Bimberg, M. Dähne-Prietsch, Appl. Phys. Lett. **75**, 106 (1999).
- Far87** H. H. Farrell, J.P. Harbison, L.D. Peterson, J. Vac. Sci. Technol. **B 5**, 1482 (1987).
- Fee87 R. M. Feenstra, J. A. Stroscio, J. Tersoff, A.P. Fein, Phys. Rev. Lett. **58**, 1192 (1987).
- Fle99 O. Flebbe, H. Eisele, T. Kalka, F. Heinrichsdorf, A. Krost, D. Bimberg, M. Dähne-Prietsch, J. Vac. Sci. Technol. **B 17**, 1639 (1999).
- Fio00 A. Fiore, P. Borri, W. Langbein, J. M. Hvam, U. Oesterle, R. Houdre, R. P. Stanley, M. Illegems, Appl. Phys. Lett. **76**, 3430 (2000).
- For88 A. Forchel, H. Leier. B. E. Maile, R. Germann, Festkörperprobleme (Advance in Solid State Physics), **28**, 99 (1988).
- For98 S. C. Fortina, S. Sanguinetti, E. Grilli, M. Guzzi, M. Henini, A. Polimeni, L. Eaves, J. Cryst. Growth **187**, 126 (1998).

- Fow28 R. H. Fowler and L. Nordheim, Proc. Roy. Soc. London Ser. A, **119**, 173 (1928).
- Fra49 F. C. Frank and J. H. Van der Merwe, Proc. Roy. Soc. A **189**, 205 (1949).
- Gar97** J. M. García, G. Medeiros-Ribeiro, K. Schmidt, T. Ngo, J. L. Feng, A. Lorke, J. Kotthaus, P. M. Petroff, Appl. Phys. Lett. **71**, 2014 (1997).
- Gee99 L. Geelhaar, J. Márquez, K. Jacobi, A. Kley, P. Ruggerone, M. Scheffler, Microelectr. J. **30**, 393 (1999).
- Gee99a L. Geelhaar, J. Márquez, K. Jacobi, Phys. Rev. **B 60**, 15890 (1999).
- Gee01 L. Geelhaar, J. Márquez, P. Kratzer, K. Jacobi, Phys. Rev. Lett. **86**, 3815 (2001).
- Gee02 L. Geelhaar, Y. Temko, J. Márquez, P. Kratzer, K. Jacobi, Phys. Rev. **B 65**, 155 308 (2002).
- Gen00 P. Geng, J. Márquez, L. Geelhaar, J. Platen, C. Setzer, K. Jacobi, Rev. Sci. Instr. **71**, 504 (2000).
- Gol85 L. Goldstein, F. Glas, J. Y. Marzin, M. N. Charasse, G. Le Roux, Appl. Phys. Lett. **47**, 1099 (1985).
- Gon03 Q. Gong, R. Nötzel, J. H. Wolter, J. Crystal Growth **251**, 150 (1999).
- Gos90 H.-J. Gossmann, F. W. Sinden, L. C. Feldman, J. Appl. Phys. **67**, 744 (2003).
- Gru97 M. Grundmann and D. Bimberg, Phys. **B 53**, 517 (1997).
- Gru00 M. Grundmann, Physica E (Amsterdam) **5**, 167 (2000).
- Gru02 *Nano-optoelectronics: concepts, physics and devices*, edited by M. Grundmann, (Springer, Berlin, 2002).
- Guo98 S. P. Guo, A. Shen, Y. Ohno, H. Ohno, Physica E (Amsterdam) **2**, 672 (1998).
- Guo98a S.P. Guo, H. Ohno, A. Shen, Y. Ohno, F. Matsukura, Jpn. J. Appl. Phys. **37**, 1527 (1998).
- Guo99 S. P. Guo, A. Shen, F. Matsukura, Y. Ohno, H. Ohno, J. Crystal Growth **201/202**, 684 (1999).
- Han97** P. Hanesch and E. Bertel, Phys. Rev. Lett. **79**, 1523 (1997).
- Har79 W. A. Harrison, J. Vac. Sci. Technol. **16**, 1492 (1979).
- Has95 T. Hashizume, Q.-K. Xue, A. Ichimiya, T. Sakurai, Phys. Rev. **B 51**, 4200 (1995).
- Has98 Y. Hasegawa, H. Kiyama, Q. K. Xue, T. Sakurai, Appl. Phys. Lett. **72**, 2265 (1998).
- Has01 S. Hasegawa, K. Arakawa, M. Tanaka, H. Nakashima, J. Cryst. Growth **227-228**, 1029 (2001).
- Hat90 M. Hata, T. Isu, A. Watanabe, Y. Katayama, Appl. Phys. Lett. **56**, 2542 (1990).
- Hat97 K. Hata, H. Shigekawa, T. Ueda, M. Akiyama, T. Okano, J. Vac. Sci. Technol. **A 15**, 1269 (1997).

- Hei97 R. Heitz, T. R. Ramachandran, A. Kalburge, Q. Xie, I. Mukhametzhanov, P. Chen, and A. Madhukar, *Phys. Rev. Lett.* **78**, 4071 (1997).
- Hei97a R. Heitz, M. Veit, N. N. Ledentsov, A. Hoffmann, D. Bimberg, V. M. Ustinov, P. S. Kop'ev, *Zh. I. Alferov, Phys. Rev.* **B 56**, 10435 (1997).
- Hen94 M. Henzler and W. Göpel, *Oberflächenphysik des Festkörpers* (Teubner, Stuttgart, 1994).
- Hen97 M. Henini, S. Sanguinetti, L. Brusaferrri, E. Grilli, M. Guzzi, M.D. Upward, P. Moriarty, P. H. Beton, *Microelectr. J.* **28**, 933 (1997).
- Hen98 M. Henini, S. Sanguinetti, S. C. Fortina, E. Grilli, M. Guzzi, G. Panzarini, L. C. Andreani, M. D. Upward, P. Moriarty, P. H. Beton, L. Eaves, *Phys. Rev.* **B 57**, R6815 (1998).
- Her51 C. Herring, *Phys. Rev.* **B 82**, 87 (1951).
- Her96 M. A. Herman and H. Sitter, *Molecular Beam Epitaxy*, Springer Series in Materials Science, Vol. 7 (Springer, Berlin, 1996).
- Her96a M. A. Herman and H. Sitter, *Microelectronics J.* **27**, 257 (1996).
- Hey00 Ch. Heyn, D. Endler, K. Zhang, W. Hansen, *J. Cryst. Growth* **210**, 421 (2000).
- Hey01 Ch. Heyn and C. Dumas, *J. Cryst. Growth* **227-228**, 990 (2001).
- Hir99 S. Hirose, A. Yoshida, M. Yamaura, H. Munekata, *Appl. Phys. Lett.* **74**, 964 (1999).
- Hol01 D. M. Holmes, E. S. Tok, J. L. Sudijono, T. S. Jones, B. A. Joyce, *J. Cryst. Growth* **192**, 33 (2001).
- Hoo93 S. E. Hooper, D. I. Westwood, D. A. Woolf, S. S. Heghoyan, R. H. Williams, *Semicond. Sci. Technol.* **8**, 1069 (1993).
- Hor89 S. Horng, K. Young, A. Kahn, *J. Vac. Sci. Technol.* **A7**, 2039 (1989).
- How96 R. Howland and L. Benatar, *A Practical Guide to Scanning Probe Microscopy* (Park Scientific Instruments, 1996).
- Hre84 P. Hren, D. W. Tu, A. Kahn, *Surf. Sci.* **146**, 69 (1984).
- Hsu94 Y. Hsu, W. I. Wang, T. S. Kuan, *Phys. Rev.* **B 50**, R4973 (1994).
- Ide92 T. Ide, A. Jamashita, T. Mizutani, *Phys. Rev.* **B 46**, 1905 (1992).
- Iko95 N. Ikoma and S. Ohkouchi, *Jpn. J. Appl. Phys.* **34**, L724 (1995).
- Ilg93 M. Ilg, R. Nötzel, K. H. Ploog, *Appl. Phys. Lett.* **62**, 1472 (1993).
- Ish96 J. -Y. Ishizaki, K. Ohkuri, T. Fukui, *Jpn. J. Appl. Phys.* **35**, 1280 (1996).
- Jac99 K. Jacobi, J. Platen, C. Setzer, J. Márquez, L. Geelhaar, C. Meyne, W. Richter, A. Kley, P. Ruggerone, M. Scheffler, *Surf. Sci.* **439**, 59 (1999).
- Jac00 K. Jacobi, J. Platen, C. Setzer, *phys. stat. sol. (b)* **218**, 329 (2000).

- Jac02 K. Jacobi, L. Geelhaar, J. Márquez, *Appl. Phys.* **A 75**, 113 (2002).
- Jac03 K. Jacobi, *Prog. Surf. Sci.* **71**, 185 (2003).
- Jes98 D. E. Jesson, G. Chen, K. M. Chen, S. J. Pennycook, *Phys. Rev. Lett.* **80**, 5156 (1998).
- Jia01 W. Jiang, H. Xu, B. Xu, W. Zhou, Q. Gong, D. Ding, J. Liang, Z. Wang, *J. Vac. Sci. Technol.* **B 19**, 197 (2001).
- Joy98 B.A. Joyce, T.S. Jones, J.G. Belk, *J. Vac. Sci. Technol.* **B 16(4)**, 2373 (1998).
- Joy98a P. B. Joyce, T. J. Krzyzewski, G. R. Bell, B. A. Joyce, T. S. Jones, *Phys. Rev.* **B 58**, R15 981 (1998).
- Joy01 P.B. Joyce, T.J. Krzyzewski, G.R. Bell, T.S. Jones, E.C. Le Ru, R. Murray, *Phys. Rev.* **B 64**, 235317 (2001).
- Kah94** A. Kahn, *Surf. Sci.* **299/300**, 469 (1994).
- Kam99 T. I. Kamins, G. Medeiros-Ribeiro, D. A. A. Ohlberg, R. S. Williams, *J. Appl. Phys.* **85**, 1159 (1999).
- Kas92 M. Kasu and T. Fukui, *Jpn. J. Appl. Phys.* **31**, L864 (1992).
- Kas93 M. A. Kastner, *Physics Today* **46(1)**, 24 (1993).
- Kaw98 M. Kawase, Y. Ishikawa, T. Fukui, *Appl. Surf. Sci.* **130-132**, 457 (1998).
- Keg00 I. Kegel, T. H. Metzger, A. Lorke, J. Peisl, J. Stangl, G. Bauer, J. M. Garcia, P. M. Petroff, *Phys. Rev. Lett.* **85**, 1694 (2000).
- Kel95 M. J. Kelly, *Low-Dimensional Semiconductors* (Oxford University Press, Oxford, 1995).
- Kim01 H. J. Kim, Y. J. Park, Y. M. Park, E. K. Kim, *Appl. Phys. Lett.* **78**, 3253 (2001).
- Kim01a H. J. Kim, Y. J. Park, B. D. Min, C. K. Hyon, S. K. Park, E. K. Kim, T. W. Kim, *Jpn. J. Appl. Phys.* **40**, 2146 (2001).
- Kir01 S. Kiravittaya, R. Songmuang, P. Changmuang, S. Sopitpan, S. Ratanathammaphan, M. Sawadsaringkarn, S. Panyakeow, *J. Cryst. Growth* **227-228**, 1010 (2001).
- Kis00 D. Kishimoto, T. Nishinaga, S. Naritsuka, T. Noda, Y. Nakamura, H. Sakaki, *J. Cryst. Growth* **212**, 373 (2000).
- Kis00a H. Kissel, U. Müller, C. Walther, W.T. Masselink, Yu.I. Mazur, G.G. Tarasov, M.P. Lisitsa, *Phys. Rev.* **B 62**, 7213 (2000).
- Kra02 P. Kratzer and M. Scheffler, *Phys. Rev. Lett.* **88**, 036102 (2002).
- Kra02a P. Kratzer, privat communication (2002).
- Kra02b P. Kratzer, E. Penev, M. Scheffler, *Appl. Phys.* **A 75**, 79 (2002).

- Lab99** V. P. LaBella, H. Yang, D. W. Bullock, P. M. Thibado, P. Kratzer, M. Scheffler, Phys. Rev. Lett. **83**, 2989 (1999).
- Lee98 H. Lee, R. Lowe-Webb, W. Yang, P. C. Sercel, Appl. Phys. Lett. **72**, 812 (1998).
- Lee99 H. Lee, W. Yang, P. C. Sercel, A. G. Norman, J. Electron. Mater. **28**, 481 (1999).
- Lee00 S. H. Lee, W. Moritz, M. Scheffler, Phys. Rev. Lett. **85**, 3890 (2000).
- Lee00a J.-S. Lee, K. Nishi, Y. Masumoto, J. Cryst. Growth **221**, 586 (2000).
- Leo93 D. Leonard, M. Krishnamurthy, C.M. Reaves, S.P. Denbaars, P.M. Petroff, Appl. Phys. Lett. **63**, 3203 (1993).
- Leo94 D. Leonard, K. Pond, P. M. Petroff, Phys. Rev. **B 50**, 11687 (1994).
- Leo98 R. Leon, S. Fafard, Phys. Rev. **B 58**, R1726 (1998).
- Ley00 M.R. Leys, J. Cryst. Growth **209**, 225 (2000).
- Lip00 M. O. Lipinski, H. Schuler, O. G. Schmidt, K. Eberl, N. Y. Jin-Phillipp, Appl. Phys. Lett. **77**, 1789 (2000).
- Liw92 W. Q. Li, P. K. Bhattacharya, S. H. Kwok, R. Merlin, J. Appl. Phys. **72**, 3129 (1992).
- Lob98 C. Lobo, and R. Leon, J. Appl. Phys. **83**, 4168 (1998).
- Lom99 M. Lomascolo, R. Cingolani, P.O. Vaccaro, K. Fujita, Appl. Phys. Lett. **74**, 676 (1999).
- Lub96 D.I. Lubyshev, P.P. González-Borrero, E. Marega, Jr., E. Petitprez, P. Basmaji, J. Vac. Sci. Technol. **B 14**, 2212 (1996).
- Lub98 D. I. Lubyshev, M. Micovic, D. L. Miller, I. Chizhov, R. F. Willis, J. Vac. Sci. Technol. **B 16**, 1339 (1998).
- Mad94** A. Madhukar, Q. Xie, P. Chen, A. Konkar, Appl. Phys. Lett. **64**, 2727 (1994).
- Mar88 K. Maruyama, M. Yoshikawa, H. Takigawa, J. Cryst. Growth **93**, 761 (1988).
- Mar00 J. Márquez, L. Geelhaar, K. Jacobi, Phys. Rev. **B 62**, 9969 (2000).
- Mar01 J. Márquez, L. Geelhaar, K. Jacobi, Appl. Phys. Lett. **78**, 2309 (2001).
- Mar01a J. Márquez, P. Kratzer, L. Geelhaar, K. Jacobi, M. Scheffler, Phys. Rev. Lett. **86**, 115 (2001).
- Mar02 J. Márquez, L. Geelhaar, K. Jacobi, Phys. Rev. **B 65**, 165320 (2002).
- Mas02 *Semiconductor Quantum Dots*, Y. Masumoto and T. Takagahara (Eds.), (Springer, Berlin, Heidelberg, 2002).
- Mat99 E. Mateeva, P. Sutter, M. G. Lagally, Appl. Phys. Lett. **74**, 567 (1999).
- Max00 M. V. Maximov et al. Physica E (Amsterdam), **7**, 326, (2000).

- Maz84 A. Mazur and J. Pollmann, Phys. Rev. **B 30**, 2084 (1984).
- Mei01 M. Meixner, E. Schöll, V.A. Shchukin, D. Bimberg, Phys. Rev. Lett. **87**, 236101 (2001).
- Moi94 J.M. Moison, F. Houzay, F. Barthe, L. Leprince, W. André, O. Vatel, Appl. Phys. Lett. **64**, 196 (1994).
- Mol96 N. Moll, A. Kley, E. Pehlke, M. Scheffler, Phys. Rev. **B 54**, 8844 (1996).
- Mol98 N. Moll, M. Scheffler, E. Pehlke, Phys. Rev. **B 58**, 4566 (1998).
- Mor97 P. Moriarty et al., Phys. Rev. **B 55**, 15 397 (1997).
- Moy90 Y.-W. Mo, D. E. Savage, B. S. Swartzentruber, M. G. Lagally, Phys. Rev. Lett. **65**, 1020 (1990).
- Min98 B. D. Min, Y. Kim, E. K. Kim, S.-K. Min, M. J. Park, Phys. Rev. **B 57**, 11879 (1998).
- Mir99 S. Mirbt, N. Moll, A. Kley, J.D. Joannopoulos, Surf. Sci. **422**, L177 (1999).
- Mcc96 J.M. McCoy, and J.P. LaFemina, Phys. Rev. **B 54**, 14511 (1996).
- Nab94 Y. Nabetani, T. Ishikawa, S. Noda, A. Sasaki, J. Appl. Phys **76**, 347 (1994).
- Nab95 Y.Nabetani, N. Yamamoto, T. Tokuda, A. Sasaki, J. Cryst. Growth **146**, 363 (1995).
- Ned96 H. Neddermeyer, Rep. Prog. Phys. **59**, 701 (1996).
- Nic65 J. F. Nicholas, *An Atlas of Models of Crystal Surfaces* (Gordon and Breach, New York, 1965).
- Nis96 K. Nishi, R. Mirin, D. Leonard, G. Medeiros-Ribeiro, P.M. Petroff, A.C. Gossard, J. Appl. Phys. **80**, 3466 (1996).
- Nis97 K. Nishi, T. Anan, A. Gomyo, S. Kohmoto, S. Sugou, Appl. Phys. Lett **70**, 3579 (1997).
- Noe91 R. Nötzel, N. N. Ledentsov, L. Däweritz, M. Hohenstein, K. Ploog, Phys. Rev. Lett. **67**, 3812 (1991).
- Noe92 R. Nötzel, L. Däweritz, K. Ploog, Phys. Rev. **B 46**, 4736 (1992).
- Noe94 R. Nötzel, J. Temmyo, T. Tamamura, Appl. Phys. Lett. **64**, 3557 (1994).
- Noe94a R. Nötzel, J. Temmyo, T. Tamamura, Nature **369**, 131 (1994).
- Noe96 R. Nötzel, J. Menniger, M. Ramsteiner, A. Ruiz, H.-P. Schönherr, K. Ploog, Appl. Phys. Lett. **68**, 1132 (1996).
- Noe97 R. Nötzel, J. Menniger, M. Ramsteiner, A. Trampert, H.-P. Schönherr, L. Däweritz, K. H. Ploog, J. Cryst. Growth **175/176**, 1114 (1997).
- Noe99 R. Nötzel, H.-P. Schönherr, Z. Niu, L. Däweritz, K. H. Ploog, J. Cryst. Growth **201/202**, 814 (1999).

- Oht01** A. Ohtake, J. Nakamura, T. Komura, T. Hanada, T. Yao, H. Kuramochi, M. Ozeki, *Phys. Rev. B* **64**, 045318 (2001).
- Oka95 Y. Okada, T. Fujita, M. Kawabe, *Appl. Phys. Lett.* **67**, 676 (1995).
- Pas89** M. D. Pashley, *Phys. Rev. B* **40**, 10 481 (1989).
- Pas91 M. D. Pashley, K. W. Haberern, J. M. Gaines, *Appl. Phys. Lett.* **58**, 406 (1991).
- Pas03 A. Passaseo et al., *Appl. Phys. Lett.* **82**, 3632 (2003).
- Pav95 L. Pavesi, M. Henini, D. Johnston, *Appl. Phys. Lett.* **66**, 2846 (1995).
- Peh97 E. Pehlke, N. Moll, A. Kley, M. Scheffler, *Appl. Phys. A* **65**, 525 (1997).
- Pei55 R. E. Peierls, *Quantum Theory of Solids* (Clarendon Press, Oxford, 1955).
- Pla97 J. Platen, C. Setzer, P. Geng, W. Ranke, K. Jacobi, *Microelectr. J.* **28**, 969 (1997).
- Pla98 J. Platen, C. Setzer, W. Ranke, K. Jacobi, *Appl. Surf. Sci.* **123/124**, 43 (1998).
- Pla99 J. Platen, A. Kley, C. Setzer, K. Jacobi, P. Ruggerone, M. Scheffler, *J. Appl. Phys.* **85**, 3597 (1999).
- Pol98 A. Polimeni, M. Henini, A. Patanè, L. Eaves, P. C. Main, G. Hill, *Appl. Phys. Lett.* **73**, 1415 (1998).
- Pol00 P. Politi, G. Grenet, A. Marty, A. Ponchet, J. Villain, *Physics Reports* **324**, 271 (2000).
- Pri98 M. Pristovsek, H. Menhal, T. Wehnert, J.-T. Zettler, T. Schmidling, N. Esser, W. Richter, C. Setzer, J. Platen, K. Jacobi, *J. Cryst. Growth* **195**, 1 (1998).
- Pri00 M. Pristovsek, H. Menhal, J.-T. Zettler, W. Richter, *Appl. Surf. Sci.* **166**, 433 (2000).
- Puk89 P.R. Pukite, G. S. Petrich, S. Batra, P. I. Cohen, *J. Cryst. Growth* **95**, 269 (1989).
- Ran77** W. Ranke and K. Jacobi, *Surf. Sci.* **63**, 33 (1977).
- Ran83 W. Ranke, *Physica Scripta* **T4**, 100 (1983).
- Ree93 M. A. Reed, *Scientific American* **268(1)**, 98 (1993).
- Ren97 H.W. Ren, K. Nishi, S. Sugou, M. Sugisaki, Y. Masumoto, *Jpn. J. Appl. Phys.* **36**, 4118 (1997).
- Ren98 H.W. Ren, K. Nishi, S. Sugou, Y. Masumoto, *Jpn. J. Appl. Phys.* **37**, 1548 (1998).
- Ros98 F. M. Ross, J. Tersoff, R. M. Tromp, *Phys. Rev. Lett.* **80**, 984 (1998).
- Ros99 F. M. Ross, R. M. Tromp, M. C. Reuter, *Science*, **286**, 1931 (1999).
- Sai99** H. Saito, K. Nishi, S. Sugou, *Appl. Phys. Lett.* **74**, 1224 (1999).
- San98 S. Sanguinetti, S. C. Fortina, A. Miotto, E. Grilli, M. Guzzi, M. Henini, A. Polimeni, L. Eaves, *Thin Solid Films* **336**, 9 (1998).

- San99 S. Sanguinetti, A. Miotto, S. Castiglioni, E. Grilli, M. Guzzi, M. Henini, A. Polimeni, A. Patane, L. Eaves, P. C. Main, *Microelectronic Journal*, **30**, 419 (1999).
- San00 S. Sanguinetti, G. Chiantoni, A. Miotto, E. Grilli, M. Guzzi, M. Henini, A. Polimeni, A. Patane, L. Eaves, P. C. Main, *Micron*, **31**, 309 (2000).
- Sch66 R. L. Schwoebel and E. J. Shipsey, *J. Appl. Phys.* **37**, 3682 (1966).
- Sch86 A. Scherer and H. G. Craighead, *Appl. Phys. Lett.* **49**, 1284 (1986).
- Sch94 S. M. Scholz, M. Morgenstern, K. Jacobi, *Surf. Sci.* **316**, 157 (1994).
- Sch02 O.G. Schmidt, S. Kiravittaya, Y. Nakamura, H. Heidemeyer, R. Songmuang, C. Müller, N.Y. Jin-Phillipp, K. Eberl, H. Wawra, S. Christiansen, H. Gräbeldinger, H. Schweizer, *Surf. Sci.* **514**, 10 (2002).
- Set97 C. Setzer, J. Platen, P. Geng, W. Ranke, K. Jacobi, *Surf. Sci.* **377-379**, 125 (1997).
- Set98 C. Setzer, J. Platen, H. Bludau, M. Gierer, H. Over, K. Jacobi, *Surf. Sci.* **402-404**, 782 (1998).
- Set99 C. Setzer, J. Platen, W. Ranke, K. Jacobi, *Surf. Sci.* **419**, 291 (1999).
- Sha99 X. Shao et al., *J. Appl. Phys.* **85**, 578 (1999).
- She95 X. Q. Shen and T. Nishinaga, *J. Cryst. Growth* **146**, 374 (1995).
- Shi93 S. Shimomura, A. Wakejima, A. Adachi, Y. Okamoto, N. Sano, K. Murase, S. Hiyamizu, *Jpn. J. Appl. Phys.* **32**, L1728 (1993).
- Shi95 M. Shinohara and N. Inoue, *Appl. Phys. Lett.* **66**, 1936 (1995).
- Sol95 G. S. Solomon, J. A. Trezza, J.S. Harris, *Appl. Phys. Lett.* **66**, 991 (1995).
- Sol96 G. S. Solomon, J. A. Trezza, A. F. Marshall, J. S. Harris, *Phys. Rev. Lett.* **76**, 952 (1996).
- Sti85 K. Stiles, A. Kahn, *J. Vac. Sci. Technol.* **B 3**, 1089 (1985).
- Sto98 S. T. Stoddart, A. Polimeni, M. Henini, L. Eaves, P. C. Main, R. K. Hayden, K. Uchida, N. Miura, *Appl. Surf. Sci.* **123/124**, 366 (1998).
- Str37 I. N. Stranski and L. Krastanow, *Sitzungsber. Akad. Wiss. Wien, Math.-Naturwiss. Klasse* **146**, 797 (1937).
- Sub86 S. Subbana, H. Kroemer, J. L. Merz, *J. Appl. Phys.* **59**, 488 (1986).
- Sun91 M. Sundaram, S. A. Chalmers, P. F. Hopkins, A. C. Gossard, *Science* **254**, 1326 (1991).
- Suz02 T. Suzuki, Y. Temko, K. Jacobi, *Appl. Phys. Lett.* **80**, 4744 (2002).
- Suz02a T. Suzuki, Y. Temko, K. Jacobi, *Surf. Sci.* **511**, 13 (2002).
- Suz03 T. Suzuki, Y. Temko, K. Jacobi, *Phys. Rev.* **B 67**, 045 315 (2003).

- Suz04 T. Suzuki, Y. Temko, M. C. Xu, K. Jacobi, submitted to Phys. Rev. B.
- Suz04a T. Suzuki, Y. Temko, M. C. Xu, K. Jacobi, Surf. Sci. **548**, 333 (2004).
- Swa99 K. Swamy, E. Bertel, I. Vilfan, Surf. Sci. **425**, L369 (1999).
- Tak91** T. Takamori, K. Watanabe, T. Fukunaga, Electron. Lett. **27**, 729 (1991).
- Tal00 V. G. Talalaev et al., Semiconductors, **34**, 453 (2000).
- Tej99 P. Tejedor, P. Šmilauer, B.A. Joyce, Surf. Sci. **424**, L309 (1999).
- Tej99a P. Tejedor, P. Šmilauer, C. Roberts, B. A. Joyce, Phys. Rev. **B 59**, 2341 (1999).
- Tem02 Y. Temko, L. Geelhaar, T. Suzuki, K. Jacobi, Surf. Sci. **513**, 328 (2002).
- Tem03 Y. Temko, T. Suzuki, K. Jacobi, Appl. Phys. Lett. **82**, 2142 (2003).
- Tem03a Y. Temko, T. Suzuki, M. C. Xu, K. Jacobi, Appl. Phys. Lett. **83**, 3680 (2003).
- Tem03b Y. Temko, T. Suzuki, P. Kratzer, K. Jacobi, Phys. Rev. **B 68**, 165310 (2003).
- Tem04 Y. Temko, T. Suzuki, M. C. Xu, K. Jacobi, to be submitted to Phys. Rev. B.
- Ter94 J. Tersoff and F. K. LeGoues, Phys. Rev. Lett. **72**, 3570 (1994).
- Ter98 J. Tersov, Phys. Rev. Lett. **80**, 2018 (1998).
- Tho94 J. M. C. Thornton, P. Unsworth, M. D. Jackson, P. Weightman, D. A. Woolf, Surf. Sci. **316**, 231 (1994).
- Tho98 J. M. C. Thornton, D. A. Woolf, P. Weightman, Appl. Surf. Sci. **123/124**, 115 (1998).
- Ton84 S. Y. Tong, G. Xu, W. N. Mei, Phys. Rev. Lett. **52**, 1693 (1984).
- Ton91 X. Tong and P. A. Bennett, Phys. Rev. Lett. **67**, 101 (1991).
- Tso88 T. T. Tsong, D. L. Feng, H. M. Liu, Surf. Sci. **199**, 421 (1988).
- Wan99** L. G. Wang, P. Kratzer, M. Scheffler, N. Moll, Phys. Rev. Lett. **82**, 4042 (1999).
- Wan00 L. G. Wang, P. Kratzer, N. Moll, M. Scheffler, Phys. Rev. **B 62**, 1897 (2000).
- Wan01 Z. M. Wang, L. Däweritz, K. H. Ploog, Appl. Phys. Lett. **78**, 712 (2001).
- Wan03 Z. M. Wang, H. Wen, V.R. Yazdanpanah, J.L. Shultz, G.J. Salamo, Appl. Phys. Lett. **82**, 1688 (2003).
- Was95 M. Wassermeier, J. Sudijono, M. D. Johnson, K. T. Leung, B. G. Orr, L. Däweritz, K. Ploog, Phys. Rev. **B 51**, 14721 (1995).
- Was03 D. Wasserman, S. A. Lyon, M. Hadjipanayi, A. Maciel, J. F. Ryan, Appl. Phys. Lett. **83**, 5050 (2003).
- Wei89 W. Weiss, W. Ranke, D. Schmeisser, W. Göpel, Surf. Sci., **221**, 91 (1989).

- Whi98 L. J. Whitman, Tunneling Microscopy and Spectroscopy in: Encyclopedia of Applied Physics, Vol. 22, G. L. Trigg and E. H. Immergut (Edit), (Wiley-VCH, Weinheim, 1998).
- Vac96 P. O. Vaccaro, M. Hirai, K. Fujita, T. Watanabe, J. Phys. D: Appl. Phys. **29**, 2221 (1996).
- Vac97 P.O. Vaccaro, K. Fujita, T. Watanabe, Jpn. J. Appl. Phys. **36**, 1948 (1997).
- Vac99 P.O. Vaccaro, H. Ohnishi, K. Fujita, Appl. Phys. Lett. **74**, 3854 (1999).
- Vai02 A. Vailionis, B. Cho, G. Glass, P. Desjardins, D. G. Cahill, J. E. Greene, Phys. Rev. Lett. **85**, 3672 (2000).
- Van86 M. A. Van Hove, W. H. Weinberg, C.-M. Chan, Low-Energy Electron Diffraction, Springer Series in Surface Sciences, Vol. 6 (Springer, Berlin, 1986).
- Ver99 C. A. Verschuren, M. R. Ley, R. T. H. Rongen, H. Vonker, J. H. Wolter, J. Crystal Growth **200**, 19 (1999).
- Vol26 M. Volmer and A. Weber, Z. Phys. Chem., **119**, 277 (1926).
- Xue97 Q.-K. Xue, T. Hashizume, T. Sakurai, Progr. Surf. Sci. **56**, 1 (1997).
- Xue99 Q.-K. Xue, T. Hashizume, T. Sakurai, Appl. Surf. Sci. **141**, 244 (1999).
- Xue99a Q.-K. Xue, Y. Hasegawa, H. Kiyama, T. Sakurai, Jpn. J. Appl. Phys. **38**, 500 (1999).
- Xuh99 H. Xu, Q. Gong, B. Xu, W. Jiang, J. Wang, W. Zhou, Z. Wang, J. Cryst. Growth **200**, 70 (1999).
- Xuh01 H.Z. Xu, K. Akahane, H.Z. Song, Y. Okada, M. Kawabe, Appl. Surf. Sci. **185**, 92 (2001).
- Yam95 H. Yamaguchi, T. Yamada, Y. Horikoshi, Jpn. J. Appl. Phys. **34**, L1490 (1995).
- Yam96 H. Yamaguchi, M. R. Fahy, B. A. Joyce, Appl. Phys. Lett. **69**, 776 (1996).
- Yam96a H. Yamaguchi, Y. Horikoshi, Phys. Rev. **B 53**, 4565 (1996).
- Yam99 A. Yamashiki, T. Nishinaga, J. Cryst. Growth **198/199**, 1125 (1999).
- Yam00 K. Yamaguchi, K. Yujobo, T. Kaizu, Jpn. J. Appl. Phys. **39**, L1245 (2000).
- Yan00 W. Yang, H. Lee, T. J. Johnson, P. C. Sercel, A. G. Norman, Phys. Rev. **B 61**, 2784 (2000).
- Yoo99 S. Yoon, Y. Moon, T.-W. Lee, H. Hwang, E. Yoon, Y.D. Kim, Thin Solid Films **357**, 81 (1999).
- Zha97 Z. Zhang and M. G. Lagally, Science **276**, 377 (1997).
- Zou99 J. Zou, X. Z. Liao, D. J. H. Cockayne, R. Leon, Phys. Rev. **B 59**, 12 279 (1999).

Our own papers

First author:

- *Y. Temko, T. Suzuki, P. Kratzer, K. Jacobi* – InAs quantum dots grown on the GaAs(113)A and GaAs($\bar{1}\bar{1}\bar{3}$)B surfaces: A comparative STM study, Phys. Rev. **B 68**, 165310(1)-165310(12) (2003);
- *Y. Temko, T. Suzuki, M. C. Xu, K. Jacobi* – InAs quantum dots on the GaAs($\bar{5}\bar{2}\bar{1}\bar{1}$)B surface, Appl. Phys. Lett. **83**, 3680-3682 (2003);
- *Y. Temko, T. Suzuki, K. Jacobi* – Shape and growth of InAs quantum dots on GaAs(113)A, Appl. Phys. Lett. **82**, 2142-2144 (2003);
- *Y. Temko, L. Geelhaar, T. Suzuki, K. Jacobi* – Step structure on the GaAs(2 5 11)A surface, Surf. Sci. **513**, 328-342 (2002).

Co-author:

- *M. C. Xu, Y. Temko, T. Suzuki, K. Jacobi* – InAs quantum dots on GaAs(114)A at the mature stage, Appl. Phys. Lett. **84**, 2283 (2004);
- *T. Suzuki, Y. Temko, M. C. Xu, K. Jacobi* – Lattice defects in InAs quantum dots on the GaAs($\bar{3}\bar{5}\bar{1}$)B surface, submitted to Phys. Rev. **B** (2004);
- *M. C. Xu, T. Suzuki, Y. Temko, K. Jacobi* – A concept for modeling self-assembled quantum dot growth, submitted to Phys. Rev. **B** (2004);
- *T. Suzuki, Y. Temko, M. C. Xu, K. Jacobi* – Surface morphology and structure of the bare and InAs covered GaAs($\bar{3}\bar{5}\bar{1}$)B surface, Surf. Sci. **548**, 333-341 (2004);
- *T. Suzuki, Y. Temko, K. Jacobi* – Shape, size, and number density of InAs quantum dots grown on the GaAs($\bar{1}\bar{1}\bar{3}$)B surface at various temperatures, Phys. Rev. **B 67**, 045315(1)-045315(7) (2003);
- *T. Suzuki, Y. Temko, K. Jacobi* – Shape of InAs quantum dots grown on the GaAs($\bar{1}\bar{1}\bar{3}$)B surface, Appl. Phys. Lett. **80**, 4744-4746 (2002);
- *T. Suzuki, Y. Temko, K. Jacobi* – Growth nuclei and surface defects on GaAs($\bar{1}\bar{1}\bar{3}$)B, Surf. Sci. **511**, 13-22 (2002);
- *Geelhaar, Y. Temko, J. Márquez, P. Kratzer, K. Jacobi* – Surface structure of GaAs(2 5 11)A, Phys. Rev. **B 65**, 155308(1)-155308(13) (2002).

Thanks to...

Щиро дякую (ukr.)...

... Prof. Dr. G. Ertl, Director of the Department of Physical Chemistry at Fritz-Haber-Institut for the financial support. Not to forget his effort to organise excellent holidays, like Weihnachtsfeste or Betriebsausflüge.

... Prof. Dr. K. Jacobi, who has given me a chance to work in his group. His great joy of getting new STM results as well as his ongoing encouragement in our project have strongly motivated me. Thank you very much also for helping me in improving my papers and lectures.

... Prof. Dr. M. Dähne for the supervision on the part of Technical University (TU) in Berlin and for invitations to some group seminars.

... Dr. Lutz Geelhaar from Infineon Technologies AG (Munich) for his teaching to do the things up to standard „made in Germany“ as well as for many beautiful pieces of advice.

... Dr. Takayuki Suzuki and Dr. Ming Chun Xu for working together in many experiments, for many new ideas and open discussions.

... Our technician Peter Geng for telling as many secrets of the UHV world and for his support not only in technical problems, but also in supplying of provisions, e.g., bananas.

... Konstantin Pötschke and Iliia Kaiander from the Prof. Dr. D. Bimberg group and Cristof Märker from the Prof. Dr. W. Richter group in TU as well as the group leaders for helping me to conduct the PL measurements and for the proof-reading (K.P.).

... Dr. Peter Kratzer for fruitful discussions and theoretical support.

... All the members of the Prof. Dr. K. Jacobi group, especially to the former members Dr. Juan Márquez, Dr. Chaoyang Fan, Dr. Jinghai Wang, but also to the current members Dr. Takayuki Suzuki, Dr. Yuemin Wang, Maria Richard, Dr. Ursula Paulus, Undine Erlekam and other members of our department and institute for a nice and friendly attitude. It was a real pleasure to work together with you!

... And primarily my parents, my brother and my friends, who helped me to live in Germany being far away from here.

Curriculum Vitae

Name	Yevgeniy Temko
Sex	Male
Birthday	22 nd Mai 1975 in Dnipropetrovsk, Ukraine
Nationality	Ukraine
Status	Single
07 / 1981 – 08 / 1983	Learning at the ground school, Dnipropetrovsk.
07 / 1983 – 08 / 1992	Learning at the middle physics-mathematical school, Dnipropetrovsk.
09 / 1992 – 08 / 1997	Study at the Dnipropetrovsk State University, department of radio physics and electronics.
08 / 1997	Finished Diploma in Fundamental Physics (kind of master thesis) with a subject “Electrocrystallisation of the transition metal oxides” .
10 / 1997 – 08 / 2000	Work as an assistant lecturer at the Dnipropetrovsk State University, department of radio physics and electronics.
Since 1 st July 2000	working of the PhD thesis in the Fritz-Haber-Institut of the Max-Planck-Society in the Department of Physical Chemistry at the group of Prof. Dr. K. Jacobi.